



**HAL**  
open science

# ERK-MyD88 interaction inhibition : a novel therapeutic approach in resistant melanoma

Rita Frem

► **To cite this version:**

Rita Frem. ERK-MyD88 interaction inhibition : a novel therapeutic approach in resistant melanoma. Molecular biology. Université Claude Bernard - Lyon I, 2023. English. NNT : 2023LYO10076 . tel-04480270

**HAL Id: tel-04480270**

**<https://theses.hal.science/tel-04480270v1>**

Submitted on 27 Feb 2024

**HAL** is a multi-disciplinary open access archive for the deposit and dissemination of scientific research documents, whether they are published or not. The documents may come from teaching and research institutions in France or abroad, or from public or private research centers.

L'archive ouverte pluridisciplinaire **HAL**, est destinée au dépôt et à la diffusion de documents scientifiques de niveau recherche, publiés ou non, émanant des établissements d'enseignement et de recherche français ou étrangers, des laboratoires publics ou privés.



**THESE de DOCTORAT DE  
L'UNIVERSITE CLAUDE BERNARD LYON 1**

**Ecole Doctorale N° 340  
Biologie Moléculaire Intégrative et Cellulaire**

**Discipline** : Biologie moléculaire et cellulaire

Soutenue publiquement le 23/05/2023, par :

**Rita FREM**

---

**L'inhibition de l'interaction ERK-MyD88,  
une nouvelle approche thérapeutique  
dans les mélanomes résistants**

---

Devant le jury composé de :

LEBECQUE, Serge, PU-PH, UCBL1

CRESPO BARAJA, Piero, Professeur, Universidad de Cantabria  
TARTARE-DECKERT, Sophie, DR1, INSERM  
BUSCA, Roser, CRCN, CNRS

RENNO, Toufic, DR2, INSERM  
COSTE, Isabelle, CRCN, CNRS

Président

Rapporteur  
Rapporteuse  
Examinatrice

Directeur de thèse  
Co-directrice de thèse



---

**ERK-MyD88 interaction inhibition, a  
novel therapeutic approach in resistant  
melanoma**

---



*“Progress lies not in enhancing what is, but in advancing toward what will be.”*

*- Gibran Khalil Gibran*



## Résumé

Le mélanome cutané, une forme maligne et agressive de cancer de la peau qui se développe à partir des mélanocytes producteurs de pigments, est responsable de la plupart des décès dus aux cancers cutanés. Il est relativement rare par rapport aux autres cancers de la peau, mais son incidence a augmenté au cours des dernières années. Si le diagnostic est précoce, la plupart des lésions de mélanome sont excisables et donc curables. Cependant, le traitement des stades métastatiques ultérieurs reste problématique. Plusieurs voies de signalisation sont altérées dans le mélanome. Les mutations les plus fréquentes se trouvent dans la voie MAPK-ERK (mitogen-activated protein kinase - extracellular signal-regulated kinase), également connue sous le nom de voie RAS-RAF-MEK-ERK. Cette voie centrale régule la croissance, la prolifération et l'apoptose des cellules. Plus de 50% des mélanomes cutanés sont porteurs d'un *BRAF* constitutivement actif et plus du quart porte de mutations dans *NRAS*. Au cours de la dernière décennie, une nouvelle ère de thérapies ciblées a changé le sort des patients atteints de mélanome avec la découverte et l'utilisation d'inhibiteurs de kinases (KI) ciblant l'activité de la kinase BRAF ou MEK. Les KI ont permis d'augmenter efficacement le taux de survie chez les patients atteints de mélanome. Cependant, dans la plupart des cas, les patients qui ont initialement répondu aux KI acquièrent une résistance à ces inhibiteurs, ce qui entraîne une progression de la maladie. Une autre avancée dans le traitement du mélanome est la découverte et l'utilisation d'inhibiteurs de points de contrôle immunitaire (ICI). Cependant, seuls 40 % des patients répondent aux ICI pour des raisons qui restent à identifier.

Compte tenu de la résistance innée et acquise aux KI et aux ICI, il y a un besoin urgent de nouveaux traitements. Des travaux antérieurs de notre laboratoire ont montré que MyD88, une molécule adaptatrice dans les voies des récepteurs Toll-Like et des récepteurs de l'interleukine-1 (TLR et IL1-R), interagit avec ERK, empêchant son inactivation par sa phosphatase MKP3. Cette interaction amplifie la voie MAPK, conduisant à une activation MAPK autonome et à une transformation cancéreuse *in vitro* et *in vivo*. Sur la base de ces résultats, nous avons développé un nouvel agent thérapeutique ciblé - EI-52 - qui inhibe l'interaction ERK-MyD88 et perturbe d'autres interactions protéine-protéine (PPI) de ERK plutôt que son activité kinase. Nous avons découvert que, dans de nombreux types de cancer, EI-52 induit la mort des cellules cancéreuses. Étant donné que la plupart des patients atteints de mélanome ont une voie RAS-MAPK trop active et qu'il est urgent de trouver de nouveaux



traitements, l'objectif principal de mes travaux de recherche était d'étudier les effets de l'inhibition de l'interaction ERK-MyD88 dans des modèles de mélanome. Cette étude montre que EI-52 induit une mort cellulaire immunogène et apoptotique dans les cellules de mélanome *BRAF* et *NRAS*, sensibles et résistantes au KI, sans provoquer de résistance après un an de traitement continu *in vitro*. En outre, EI-52 réduit de manière significative la progression tumorale du mélanome muté *NRAS* et agit en synergie avec l'anti-PD1 *in vivo*. Une deuxième partie de ma thèse visait à étudier l'impact de EI-52 sur les interactions entre ERK et ses multiples partenaires, par immunoprécipitation et spectrométrie de masse. Cette partie en est encore au stade préliminaire, mais elle nous a permis jusqu'à présent d'identifier plusieurs partenaires potentiels d'ERK qui sont gagnés ou perdus après un traitement à EI-52. Nous discuterons de ces deux parties dans ce manuscrit.

## Summary

Cutaneous melanoma, a malignant and aggressive form of skin cancer that arises from pigment-producing melanocytes, is responsible for most deaths due to cutaneous cancers. It is relatively rare compared to other skin cancers, but its incidence has recently increased. If diagnosed early, most melanoma lesions are excisable and thus curable. However, the treatment of later metastatic stages remains problematic. Several signaling pathways are altered in melanoma. However, the most frequent mutations are found in the MAPK-ERK pathway (mitogen-activated protein kinase – extracellular signal-regulated kinase), also known as the RAS-RAF-MEK-ERK pathway. This central pathway regulates cell growth, proliferation, and apoptosis. Over 50% of cutaneous melanomas harbor a constitutively active *BRAF*, and 25% carry *NRAS* mutations. In the last decade, a new era of targeted therapies changed the outcome for melanoma patients with the discovery and use of kinase inhibitors (KIs) targeting BRAF or MEK kinase activity. KIs effectively increased the overall survival of melanoma patients. However, in most cases, patients who initially responded to KIs acquire resistance to these inhibitors, leading to further disease progression. Another breakthrough in melanoma treatment is the discovery and use of immune checkpoint inhibitors (ICIs). However, only 40% of patients respond to ICI for yet-to-be-identified reasons.

Given the innate and acquired resistance to KIs and ICIs, there is an urgent need for novel treatments. Previous work from our lab showed that MyD88, an adaptor molecule in Toll-Like Receptor and Interleukin-1 receptor (TLRs and IL1-R) pathways, interacts with ERK, preventing its inactivation by its phosphatase MKP3. This interaction amplifies the MAPK pathway, leading to cell-autonomous MAPK activation and transformation *in vitro* and *in vivo*. Based on these results, we developed a new targeted therapy agent - EI-52 - that inhibits the ERK-MyD88 interaction and perturbs other ERK protein-protein interactions (PPI) rather than its kinase activity. We found that, in many cancer types, EI-52 induces cancer cell death. Considering that most melanoma patients have an overly active RAS-MAPK pathway and the urgent need for new treatments, the central aim of my research was to investigate the effects of ERK-MyD88 interaction inhibition in melanoma models. This study shows that EI-52 induces immunogenic and apoptotic cell death in KI-sensitive and KI-resistant *BRAF* and *NRAS* melanoma cells without causing resistance after up to one year of continuous treatment *in vitro*. In addition, EI-52 significantly reduces tumor progression of *NRAS*-mutated melanoma and synergizes with

anti-PD1 *in vivo*. In another study, I evaluated the impact of EI-52 on ERK interactions with its multiple partners through immunoprecipitation and mass spectrometry. This part is still in the preliminary stages, but it has thus far allowed us to identify several potential partners of ERK that are gained or lost after treatment with EI-52. We will discuss both studies in this manuscript.



## Acknowledgments

I would like to begin by thanking the members of my PhD jury: Piero Crespo-Baraja, Sophie Tartare-Deckert, Roser Busca and Serge Lebecque for accepting to evaluate my work. Also, many thanks to the reviewers for giving me some extra time and for the time spent reading and evaluating my dissertation. I also want to thank la Ligue Nationale Contre le Cancer, Comité de l'Ain, for supporting my research project with a grant.

My PhD journey was full of exciting and enriching moments that taught me many things, most importantly to never give up and to always keep pushing forward. This would not have been possible without my colleagues, friends and family.

I would like to thank Isabelle Coste, my main thesis supervisor, for always being present and caring. You have taught me so many things and guided me all along my journey, all while giving me the necessary push to grow personally as a researcher. Your indispensable advice helped me shape and drive this project, and your encouragement and support were always there when I needed them the most.

I would also like to thank Toufic Renno, my thesis co-supervisor and our team leader, for giving me the chance of doing a PhD in his group, for his wisdom and lessons. You were always there for guidance, you helped steer this project into what it became. Your suggestions and advice were primordial throughout my PhD.

I thank our small (but very efficient!) "Team Coste" for their support. Nader, François and Serge, your advice and suggestions were always helpful and understanding. A more specific shoutout to Nader, not because he is a fellow Lebanese, but because his help was particularly valuable for my experiments (so many immunoprecipitations!), to François for being our "tech" guy in addition to a great scientist, and to Serge for his always interesting advice and discussions. During my PhD, I had the chance to work with many amazing persons in our little team, that ultimately became my friends. Melissa, Maissa, Manon and Aurora, your help and support were vital for me. I will always cherish our moments together: Mel and our "pause kinder", Maissa and our late nights at the lab, Manon and your kindheartedness (and travel

advice haha), and Aurora and your lovely Italian culture. Mel, I wish you the best for your new PhD adventure, I know that your perseverance will get you wherever you would like. Maissa, you're probably the one I shared most of my memories with, I wish you the best, wherever and whatever that may be. Manon, I hope your future will be filled with amazing experiences and travels (with your many van road trips to come!), and that you will always enjoy what you do in life. Aurora, I wish you all the best, I know you're enjoying yourself now that you're back in Palermo! It has been a joy to have you as an M2 intern, and I know that you will do great things in the future.

Of course, I would like to thank all my colleagues from the 6<sup>th</sup> floor of Cheney D, both Team Renno and Team Petrilli. This experience would not have been the same without you all, all your jokes (Stéphane and Nico), all your advice (Anne-laure, Stéphane, Nico, both Cédric (s), Agnès, Joelle, Sabine), all our shared (student) moments (Rouma, P.A., Marie, Helena, Delphine, Léa) and all the delicious cakes we all have shared together (Thanks to Delphine and Léa!!). Every single one of you taught me so many things, even though I will not explicitly talk about them in this section, know that I will always carry our memories in my heart.

I would like to give a special thanks to Stéphane for being the great researcher he is, always present with his enlightening advice. You have helped me throughout my PhD, I learned so many things from you. I will forever remember the words you always tell me: "La peur n'évite pas le danger". Your sense of humor along with that of Nico and Nader fulfilled the ambience with laughter. I will miss the sound of you three bickering just for fun.

Rouma, my desk neighbor/friend, I will always remember our conversations, discussions, motivational speeches (both ways), and mostly our shared snacks. I wish you the best for the rest of your PhD journey, and after.

I thank all my collaborators during my PhD, especially Julie Caramel, Stéphane Dalle and their team.

I thank the members of my thesis committee (CST), Gilles Pagès and Stéphane Dalle, for their valuable suggestions and advice, I could not have had a better committee.

I would also like to express my gratitude to both associations I joined during my PhD. “Les P’tits Génies IHOPe” helped me see a greater picture and the real reason for why I always wanted to be a researcher. “CLYRA” or the CRCL Young Researchers Association, allowed me to meet so many great persons in the research field.

And finally, I would like to thank my family and my friends for their constant support, long talks and motivation. Mom, Dad and Gretta, this would not have been possible without you. You have always supported me through everything, I owe it all to you. Arnaud, your love has kept me sane during the most difficult moments of this thesis, I could not have dreamt of a better partner to spend my life with.

I would like to dedicate this manuscript to my family, to Arnaud, and to my late grandmother Marie, who will always be in our hearts and minds.





## Table of contents

<b>RÉSUMÉ</b> .....	<b>7</b>
<b>SUMMARY</b> .....	<b>9</b>
<b>ACKNOWLEDGMENTS</b> .....	<b>12</b>
<b>TABLE OF CONTENTS</b> .....	<b>16</b>
<b>LIST OF FIGURES</b> .....	<b>18</b>
<b>ABBREVIATIONS</b> .....	<b>19</b>
<b>INTRODUCTION</b> .....	<b>24</b>
<b>I. THE ERK MAPK PATHWAY</b> .....	<b>24</b>
1. MAPK pathways .....	24
2. MAPK-ERK pathway .....	25
3. ERK pathway components .....	25
4. ERK pathway activation .....	26
5. ERK pathway targets .....	27
5.1. ERK pathway nuclear targets .....	27
5.2. ERK pathway cytoplasmic targets .....	28
6. ERK pathway biological functions .....	29
7. ERK pathway regulation .....	31
8. ERK protein .....	33
8.1. ERK structure .....	33
8.2. ERK active and inactive conformations.....	35
8.3. ERK substrate docking and enzyme recruitment sites.....	36
9. ERK scaffolds and anchors .....	37
10. ERK nuclear translocation .....	38
11. ERK dephosphorylation.....	39
<b>II. THE ERK MAPK PATHWAY IN CANCER</b> .....	<b>39</b>
1. ERK pathway and cancer.....	39
2. ERK pathway inhibitors for cancer treatment .....	40
2.1. Kinase Inhibitors .....	40
2.2. Other small-molecule inhibitors .....	42
3. Crosstalk with other pathways .....	43
4. TLR and IL-1R signaling pathways and their adaptor protein MyD88.....	44
5. The ERK-MAPK pathway in cutaneous melanoma.....	47
<b>III. CUTANEOUS MELANOMA: AN AGGRESSIVE TUMOR ON THE RISE</b> .....	<b>48</b>
A. <i>Normal Skin</i> .....	48
1. Skin biology .....	48
2. Melanocyte biology .....	50
3. Melanin synthesis .....	51
4. Melanocyte regulation.....	52
B. <i>Cutaneous Melanoma</i> .....	53
1. Melanocyte transformation to melanoma .....	53
2. Melanoma epidemiology: alarming numbers.....	53
3. Melanoma epidemiology: risk factors .....	54
4. Melanoma: oncogenic mutations .....	55

4.1.	<i>BRAF</i> -mutated melanoma.....	56
4.2.	<i>NRAS</i> -mutated melanoma .....	57
5.	Melanoma: Non-genetic heterogeneity .....	58
6.	Melanoma: Histological subtypes, stage classification, and diagnosis. ....	62
7.	Melanoma: Current treatment options and their obstacles.....	64
7.1.	Previous treatments (pre-TT and -ICI) .....	65
7.2.	Targeted Therapies .....	65
7.3.	Immunotherapy: Immune Checkpoint Inhibitors .....	67
7.4.	Resistance to KIs and ICIs.....	69
7.5.	Adjuvant systemic therapy .....	73
7.6.	Emerging therapies.....	74
8.	Melanoma: conclusion and unanswered questions .....	75
<b>IV.</b>	<b>CONTEXT AND OBJECTIVES OF MY PH.D. RESEARCH.....</b>	<b>77</b>
1.	ERK-MyD88 interaction as a novel target for cancer treatment.....	77
2.	ERK-MyD88 interaction inhibitor: EI-52.....	77
3.	Objectives of my Ph.D. research .....	79
<b>RESULTS</b>	<b>.....</b>	<b>82</b>
Article in preparation:	.....	82
Abstract.....	.....	83
Introduction .....	.....	84
Results.....	.....	86
Discussion and conclusion .....	.....	90
Material and Methods .....	.....	92
Figures.....	.....	97
Figure legends.....	.....	106
<b>DISCUSSION</b>	<b>.....</b>	<b>110</b>
<b>CONCLUSION</b>	<b>.....</b>	<b>118</b>
<b>ANNEXES</b>	<b>.....</b>	<b>120</b>
1.	Additional preliminary results.....	120
2.	Article 1, submitted, in review in Nature Cancer.....	127
3.	Article 2, submitted, in review.....	171
<b>BIBLIOGRAPHY</b>	<b>.....</b>	<b>210</b>

## List of Figures

FIGURE 1: THE ERK, P38, AND JNK MAPK CASCADES.....	25
FIGURE 2: MAPKS' RESPONSES TO DIFFERENT STIMULI .....	30
FIGURE 3: ERK PATHWAY REGULATION.....	32
FIGURE 4: ERK STRUCTURE .....	35
FIGURE 5: MAPK MUTATIONS IN DIFFERENT CANCERS .....	40
FIGURE 6: CROSS-TALKING BETWEEN MAPK AND OTHER TUMOR-PROMOTING SIGNALING PATHWAYS. ....	44
FIGURE 7: TOLL-LIKE RECEPTORS AND INTERLEUKIN-1 RECEPTORS SIGNALING PATHWAYS.....	47
FIGURE 8: ANATOMY OF THE SKIN. ....	49
FIGURE 9: ANATOMY OF THE EPIDERMIS. ....	50
FIGURE 10: MELANOGENESIS THROUGH MC1R SIGNALING AND ITS DOWNSTREAM EFFECTORS. ....	52
FIGURE 11: MUTATION FREQUENCY OF DRIVER GENES OF SKIN MELANOMA BASED ON TCGA DATA.....	56
FIGURE 12: TRANSCRIPTIONAL PROGRAMS AND PLASTICITY IN MELANOMA.....	61
FIGURE 13: THE FOUR STAGES OF MELANOMA.....	63
FIGURE 14: TNM STAGING OF MELANOMA BASED ON THE RECOMMENDATIONS OF THE 8TH AJCC. ....	64
FIGURE 15: FDA-APPROVED TARGETED THERAPIES AND IMMUNOTHERAPIES FOR THE TREATMENT OF MELANOMA IN 2020.....	66
FIGURE 16: OVERALL TWO-YEAR SURVIVAL FOR ADVANCED MELANOMA PATIENTS IN PIVOTAL CLINICAL TRIALS OF CURRENT FDA-APPROVED TREATMENTS. ....	67
FIGURE 17: REPRESENTATION OF IMMUNE CHECKPOINT BLOCKADE.....	69
FIGURE 18: DYNAMIC RESPONSES TO MAPK INHIBITION.....	71
FIGURE 19: EI-52 CHEMICAL STRUCTURE.....	79
FIGURE 20: PROTOCOL FOR GENERATING IN VIVO TUMOR MODELS WITH ACQUIRED RESISTANCE TO ICIS. ....	117
FIGURE 21: ANNEX: EI-52'S IMPACT ON ERK INTERACTIONS. ....	125

## Abbreviations

a.a.: Amino Acid

ASP: Agouti Signaling protein

ACTH: Adrenocorticotrophic Hormone

AXL: AXL receptor tyrosine kinase

Bad: Bcl-2-associated death promoter

BCL2: B-cell lymphoma-2

BIK: Bcl-2-interacting killer

BIM: Bcl-2 Interacting Mediator of cell death

BIRC5: Baculoviral IAP Repeat Containing 5

BRAFi: BRAF kinase inhibitor

BRF1: BRF1 RNA Polymerase III Transcription Initiation Factor Subunit

CCND1: Cyclin D1

CD domain: Common Docking Domain

CDKs: Cyclin-Dependent Kinases

CDKN2A: Cyclin-dependent kinase inhibitor 2A

COX-2: Cyclooxygenase-2

CREB: cAMP response element-binding protein

CTLA-4: Cytotoxic T-lymphocyte antigen -4

D-site: D-docking domain

DAPK: Death-Associated Protein Kinase

DOPA: Dihydroxyphenylalanine

DQ: Dopaquinone

DRS: D-site Recruitment site

DUSP: Dual-specificity phosphatase

ECM: Extracellular Matrix

EGF: Epidermal Growth Factor

eIF4B: Eukaryotic Initiation Factor 4B

Elk1: ETS like-1

Elk1: ETS-Like 1

EMT: Epithelial-Mesenchymal Transition

ER- $\alpha$ : Estrogen Receptor- $\alpha$

ERK: Extracellular signal-Regulated Kinase

F-site: F-docking domain

FAK: Focal Adhesion Kinase

FDA: Food and Drug Administration

FRS: F-site Recruitment site

GAB2: GRB2-associated binding protein

GDP: Guanosine diphosphate

GEFs: Guanine nucleotide Exchange Factors  
GPCRs: G-Protein-Coupled Receptors  
Grb2: Growth factor Receptor-Bound protein  
GTP: Guanosine triphosphate  
HGF: Hepatocyte growth factor  
HIF1- $\alpha$ : Hypoxia Inducible Factor 1 Subunit alpha  
hnRNPK: Heterogeneous Nuclear Ribonucleoprotein K  
ICD: Immunogenic Cell death  
ICI: Immune Checkpoint Inhibitor  
IEGs: Immediate Early Genes  
IGF1: Insulin-like Growth Factor-1  
IL: Interleukin  
JNK: c-Jun N-terminal Kinase  
KIs: Kinase Inhibitors  
KSR: Kinase Suppressor of RAS  
LAG-3: Lymphocyte-activation gene 3  
MAF: Melanoma-associated fibroblasts  
MAP2Ks: MAP kinase kinases  
MAP3Ks: MAP kinase kinases  
MAPK: Mitogen-Activated Protein Kinase  
MAPKAPKs: Mitogen-activated protein kinase-activated protein kinase  
MC1R: Melanocortin 1 receptor  
MCL1: Induced myeloid leukemia cell differentiation  
MEK: Mitogen-activated protein kinase kinase  
MEKi: MEK kinase inhibitor  
MEKK1: MAPK/ERK kinase kinase 1  
MITF: Microphthalmia-associated transcription factor  
MKP: MAP Kinase phosphatases  
MNK: MAPK-interacting protein kinases  
MP1: MEK partner 1  
MRTF: myocardin-related transcription factor  
 $\alpha$ -MSH:  $\alpha$ -Melanocyte Stimulating Hormone  
MSK: Mitogen- and Stress-activated Kinase  
mTORC1: mammalian target of rapamycin complex 1  
mut: Mutant  
MyD88: Myeloid differentiation primary response 88  
NCSC: Neural Crest Stem Cells  
NF- $\kappa$ B: Nuclear Factor- $\kappa$ B  
NF1: Neurofibromin  
NFAT3: Nuclear Factor of Activated T cells 3

NGFR: Neural Growth Factor Receptor  
NLS: Nuclear Localization Signal  
NTS: Nuclear Translocation Signal  
OS: Overall Survival  
PD-1: Programmed Cell death protein -1  
PD-L1: Programmed Cell death protein ligand -1  
PKA: Protein Kinase A  
POMC: Proopiomelanocortin  
PPI: Protein-Protein Interaction  
PTEN: phosphatase and tensin homolog  
Rac1: RAS-related C3 botulinum toxin substrate 1  
RAPTOR: Regulatory-associated protein of mTOR  
rDNA: ribosomal DNA  
rpS6: Ribosomal Protein S6  
RRN3: RNA polymerase I-specific transcription initiation factor  
RSK: p90 ribosomal S6 kinase  
RTKs: Receptor Tyrosine Kinases  
S6K1: p70 ribosomal S6 kinase 1  
SCF: Stem cell factor  
SoS1/2: Son of Sevenless  
SOX: SRY-related HMG-box genes  
SPRED: Sprouty-related, EVH1 domain-containing protein 1  
SPRY: Sprouty  
SRE: Serum response elements  
SRF: Serum response factor  
TCFs: Ternary Complex Factors  
TF: Transcription Factor  
TGF- $\beta$ : Transforming Growth Factor  $\beta$   
TIF1A: Transcription Initiation Factor  
TIM3: T-cell immunoglobulin domain and mucin domain-3  
TLR: Toll-like receptor  
TME: Tumor microenvironment  
TNF- $\alpha$ : Tumor Necrosis Factor  
YP52: Tumor protein 53  
tRNA: transfer RNA  
TRP: Tyrosinase-related protein  
TT: Targeted Therapy  
Tyr: Tyrosinase  
TWIST: Twist Family BHLH Transcription Factor  
UBF1: Nucleolar transcription factor 1

USF1: Upstream transcription factor 1

UV: Ultraviolet

VEGF: Vascular Endothelial Growth Factor

vFGF: Viral fibroblast growth factor

WT: Wild-Type

YAP: yes-associated protein 1

ZEB: Zinc Finger E-Box Binding Homeobox





# Introduction

## I. The ERK MAPK pathway

### 1. MAPK pathways

Mitogen-activated protein kinase (MAPK) pathways are highly conserved three-tier signaling cascades that play critical roles in various cellular processes, including proliferation, differentiation, survival, apoptosis, and stress response. These pathways are activated by diverse extracellular signals, including growth factors, cytokines, and environmental stresses such as UV (Ultraviolet) radiation and oxidative stress. They comprise a series of cytoplasmic kinases required for signal transduction from the surface to the cell's interior. The MAPK pathways consist of different subfamilies, the main four are extracellular signal-regulated kinase 1/2 (ERK1/2), c-Jun N-terminal kinase (JNK), p38, and ERK5. Each of these subfamilies has distinct upstream regulators, downstream effectors, and cellular functions (Figure 1) [1], [2].

The JNK and p38 pathways are activated by a variety of stress signals, including inflammatory cytokines such as tumor necrosis factor (TNF)- $\alpha$  and interleukin (IL)-1 $\beta$ , environmental stresses, and cellular damage. The JNK pathway is involved in the regulation of apoptosis, inflammation, and the development of multiple immune cells. In contrast, the p38 pathway is involved in regulating cell proliferation, angiogenesis, inflammation, and the production of cytokines. The JNK and p38 pathways are activated by a cascade of kinases, including MAP kinase kinase kinases (MAP3Ks), MAP kinase kinases (MAP2Ks), and MAP kinases (MAPKs). The JNK pathway is activated by the upstream kinases MEKK1/4/7, while the p38 pathway is activated by the upstream kinases MEKK3/4/6 and TAK1. Once activated, JNK and p38 phosphorylate a wide variety of substrates, including transcription factors, cytoskeletal proteins, and enzymes, leading to changes in gene expression and cellular behavior. Dysregulation of the JNK and p38 pathways underlies pathologies such as inflammatory disorders, cancer, and neurodegenerative diseases [3].

ERK-5 is ubiquitously expressed and is activated by its only upstream kinase, MEK5, in response to growth factors and stress stimulations. The ERK5 cascade has been associated mainly with stress and proliferation [4].

In this manuscript, we will mainly focus on the ERK1/2 pathway.

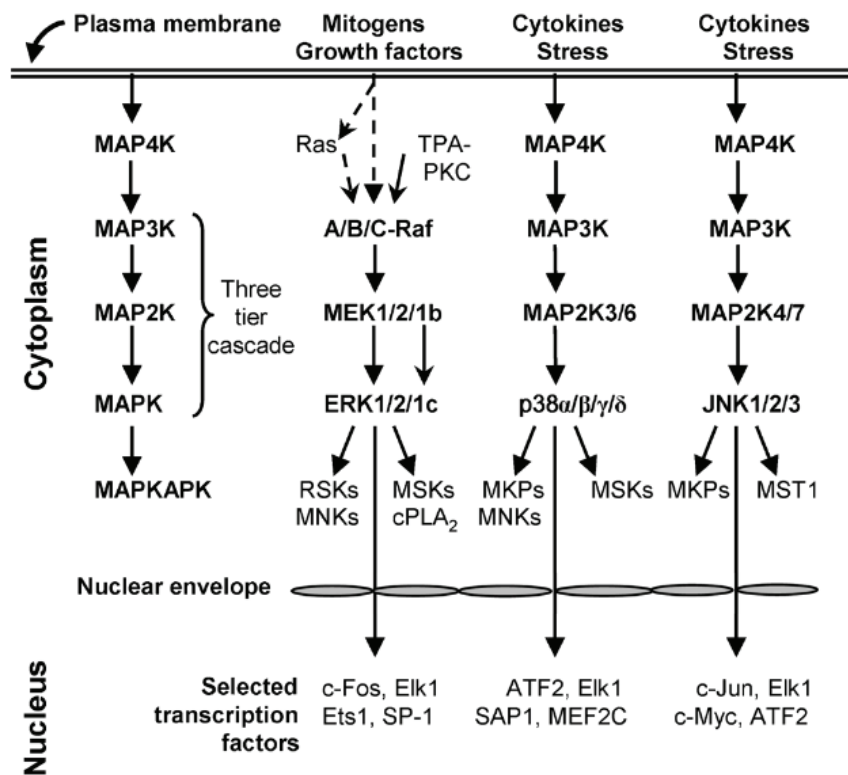


**Figure 1: The ERK, p38, and JNK MAPK cascades.**

The MAP kinases, which occur in the cytoplasm and can be translocated into the nucleus, catalyze the phosphorylation of dozens of cytosolic proteins and numerous nuclear transcription factors. Adapted from Roskoski R, *Pharmacol. Res.* 2012 [5].

## 2. MAPK-ERK pathway

The ERK pathway is a critical signaling pathway that plays a crucial role in cell growth, proliferation, differentiation, survival, and apoptosis. This pathway is activated in response to various extracellular stimuli, including growth factors, cytokines, hormones, and stress, and leads to the activation of downstream transcription factors that regulate gene expression [5]–[7].

## 3. ERK pathway components

The MAPK-ERK pathway, also known as the RAS-RAF-MEK-ERK pathway, is a three-tier cascade of kinases: MAP3K- MAP2K- MAPK. The first component of this pathway is the protein RAS,

whose gene is activated in one-third of all human cancers. RAS is a GTP-binding protein (G protein) with isoforms: HRAS, KRAS, and NRAS and a dozen of downstream effector pathways [8]. The MAP3K, RAF, is a serine/threonine kinase with three isoforms: A, B, and C RAF, and a more restricted substrate specificity. They catalyze the phosphorylation and activation of the mitogen-activated protein kinase kinases MEK1 and MEK2 at S218/222 and S222/226 (respective residues of MEK1/2) [9]. MEK1 and MEK2 are dual-specificity tyrosine/threonine protein kinases that mediate the phosphorylation of ERK-1 and ERK-2, their only known substrates, at Tyr204/187 and then Thr202/185 (respective residues of ERK1/2) [10]. ERK-1 and ERK-2, the final elements of the MAPK pathway, share 84% of their sequence and the majority, if not all, functions [11]. For this reason, they will be referred to in singular as ERK1/2 or ERK in this manuscript. Contrary to the limited substrate specificity of RAF and MEK kinases, ERK1/2 has more than 200 cytoplasmic and nuclear substrates [12].

The activation-induced dimerization of RAS, RAF, MEK, and ERK has been widely described. While all RAS isoforms can dimerize, their exact molecular structures remain poorly defined [13]. RAF can homo- and hetero-dimerize, and the BRAF/BRAF homodimer and BRAF/CRAF heterodimer appear dominant [14]. Activated MEK1 and MEK2 can homo- and hetero-dimerize [15]. Upon phosphorylation, ERK-1 and ERK-2 primarily form homodimers, as ERK1-ERK2 heterodimers are unstable [16]

#### **4. ERK pathway activation**

The ERK pathway is initiated by the binding of extracellular ligands to their cognate receptors on the cell surface, which triggers the activation of receptor tyrosine kinases (RTKs), leading to their dimerization, or G-protein-coupled receptors (GPCRs), leading to changes in their conformation [17], [18]. Multiple stimulants such as growth factors (EGF, VEGF, IGF1, and many more), cytokines, viruses, G-protein-coupled receptor ligands, and oncogenes activate the ERK pathway [19]. Ligand-bound receptors dimerize, leading to their activation by autophosphorylation in *trans*. This creates a binding site for adaptor proteins with a phosphotyrosine binding domain (PTB), an Src homology 2 (SH2) domain, or both, like in Shc proteins [17]. Shc then recruits and activates Grb2 (growth factor receptor-bound protein) and the guanine nucleotide exchange factor (GEF) SoS1/2, which catalyzes the exchange of

GDP for GTP on the small GTPase RAS once recruited to the plasma membrane. Activated RAS then binds and activates RAF leading to its homo- or heterodimerization. RAF dimers then phosphorylate and activate MEK1/2 [9]. In turn, activated MEK1/2 dimers then phosphorylate and activate ERK1/2, the downstream effector of the pathway. Once activated, ERK translocates into the nucleus and phosphorylates various transcription factors, including Elk1, c-Fos, and c-Jun, which regulate the expression of target genes [5]–[7]. ERK has cytoplasmic targets as well, including some of the MAPKAPKs (RSKs, MSKs, ...) that propagate the activation signal to additional targets and many cytoskeletal elements (such as Paxillin) that are necessary for the determination of cellular morphology, as well as protein anchoring [12].

## 5. ERK pathway targets

ERK has more than 200 cytoplasmic and nuclear targets, both direct and indirect, through the activation of other kinases [12], [20], [21]. Here is a summary of some of the most critical targets.

### 5.1. ERK pathway nuclear targets

Stimulated cells need to synthesize new proteins to respond to external stimuli. The first pool of mRNA appears within a few minutes of the trigger, so the genes encoding them are known as immediate early genes (IEGs). IEGs' transcription is rapidly induced by the binding of transcription factors (TFs) (e.g., SRF: serum response factor) that are continuously expressed in cells to specific regions in their promoters (e.g., SRE: serum response elements). Many of these TFs are substrates of the ERK pathway and are swiftly activated once ERK relays the external signal [22]. For more information on ERK nuclear targets, see Maik-Rachline *et al.* [21].

To summarize, some of the most critical targets are TFs such as Elk1, c-Fos, and c-Myc, but it should be noted that not all nuclear effectors of ERK are TFs. Other groups include transcriptional repressors (e.g., Tob and Foxo3a) and protein kinases such as DYRK1B. Elk1, one of the best-characterized ERK targets, is a ternary complex factors (TCFs) family member with a C-terminal transcriptional activation domain containing multiple MAPK phosphorylation sites. Elk1 is expressed in resting and stimulated cells. Elk1 is rapidly

phosphorylated on 6 to 9 residues, although only Ser383 phosphorylation by ERK is necessary for Elk activity. Phosphorylated Elk1 has an enhanced DNA-binding capacity leading to its high transcriptional activity and the recruitment of other factors in the transcriptional complex [12]. Among the targets whose transcription is induced by the binding of Elk1, c-Fos is a TF crucial for the induction of proliferation. When c-Fos protein is expressed, nuclear ERK phosphorylates its Ser374 to enhance its stability, ultimately leading to its transformation activity once accumulated. The accumulation of c-Fos depends entirely on the duration of ERK activity which should be transient in normal cells (<30 minutes), where c-Fos will have limited transcriptional activity without being stabilized. The opposite scenario occurs in cancer cells, where ERK is often continuously activated [21]. Another essential nuclear target of ERK is c-Myc, a TF necessary for cell cycle progression and other fundamental cellular processes. In an oncogenic setting, ERK stabilizes c-Myc by phosphorylation on Ser62, which leads to its accumulation in various RAS- or RAF-driven cancers [21]. Other known nuclear targets of ERK include the TFs c-Jun, SP-1, Ets1, and ATF2 [19].

## 5.2. ERK pathway cytoplasmic targets

Even though ERK's most described activities are in the nuclear compartment, ERK has as many cytoplasmic as nuclear substrates [12]. ERK's first reported cytosolic target is the Phospholipase A2 (PLA<sub>2</sub>), which plays essential roles in diverse cellular responses, including phospholipid digestion and metabolism, host defense, inflammation, and signal transduction. The best characterized cytosolic targets of ERK are part of the mitogen-activated protein kinase-activated protein kinases (MAPKAPKs), a family of kinases that further propagate the signal to other cytosolic and nuclear targets. MAPKAPKs include the families of RSK, MSK and MNK. The RSK family (RSK1-4) is a critical component of ERK signaling, as it participates in both cytoplasmic and nuclear signal extension. RSKs participate in ERK-mediated cellular outcomes such as the induction of the cell cycle and the inhibition of apoptosis. RSKs also play a role in c-Fos' stabilization through phosphorylation on Ser362. RSKs contain two catalytically active kinase domains: The C-terminal domain, necessary for RSK activation, and the N-terminal domain, responsible for the phosphorylation of RSK's targets. In stimulated cells, ERK phosphorylates residues Thr573, Ser363, and Thr359 in RSK's C-terminal kinase domain. These phosphorylations induce the activation of RSK, which then trans-autophosphorylates Ser380,

creating a docking site for PDK1. In turn, PDK1 phosphorylates Ser221 in the N-terminal kinase domain of RSK, leading to its full activation. When the signal is over, the N-terminal kinase domain auto-phosphorylates Ser733, dissociating RSK from ERK and thus allowing the inactivation of RSKs by phosphatases [23]. ERK can also phosphorylate and activate MNK1/2, MSK1/2, and to some extent, MAPKAPK3 and MAPKAPK5. MNKs and MSKs are structurally similar to RSKs, having two distinct kinase domains within the same protein. Their activation process is similar to what we described for RSKs. However, both MNKs and MSKs are not exclusively activated by ERK since they can also be phosphorylated by p38MAPKs after a stress-induced signal. All these kinases help propagate ERK signals to additional targets, thus extending the pathway's specificity [12].

In addition to MAPKAPKs, ERK can phosphorylate cytoskeletal elements. Paxillin, a focal adhesion protein, is essential for integrin and other receptor signaling and regulating proliferation, morphology, and motility [24]. Paxillin can be phosphorylated by ERK and the other MAPKs, JNK, and p38, with different outcomes. ERK phosphorylation of Paxillin induces the recruitment and activation of the focal adhesion kinase FAK, subsequently enhancing adhesion and cell spreading[25]. In addition, Paxillin constitutively associates with MEK and can recruit ERK to the complex, consequently facilitating its activation. Furthermore, ERK phosphorylates several other cytoskeletal elements, such as vinexin, calnexin, tubulin, and vimentin. These are necessary for regulating many cellular activities, including proliferation, differentiation, and oncogenic transformation [12].

## **6. ERK pathway biological functions**

The ERK pathway is vital in many biological processes, including cell proliferation, growth, metabolism, motility, differentiation, and development (Figure 2) [26].

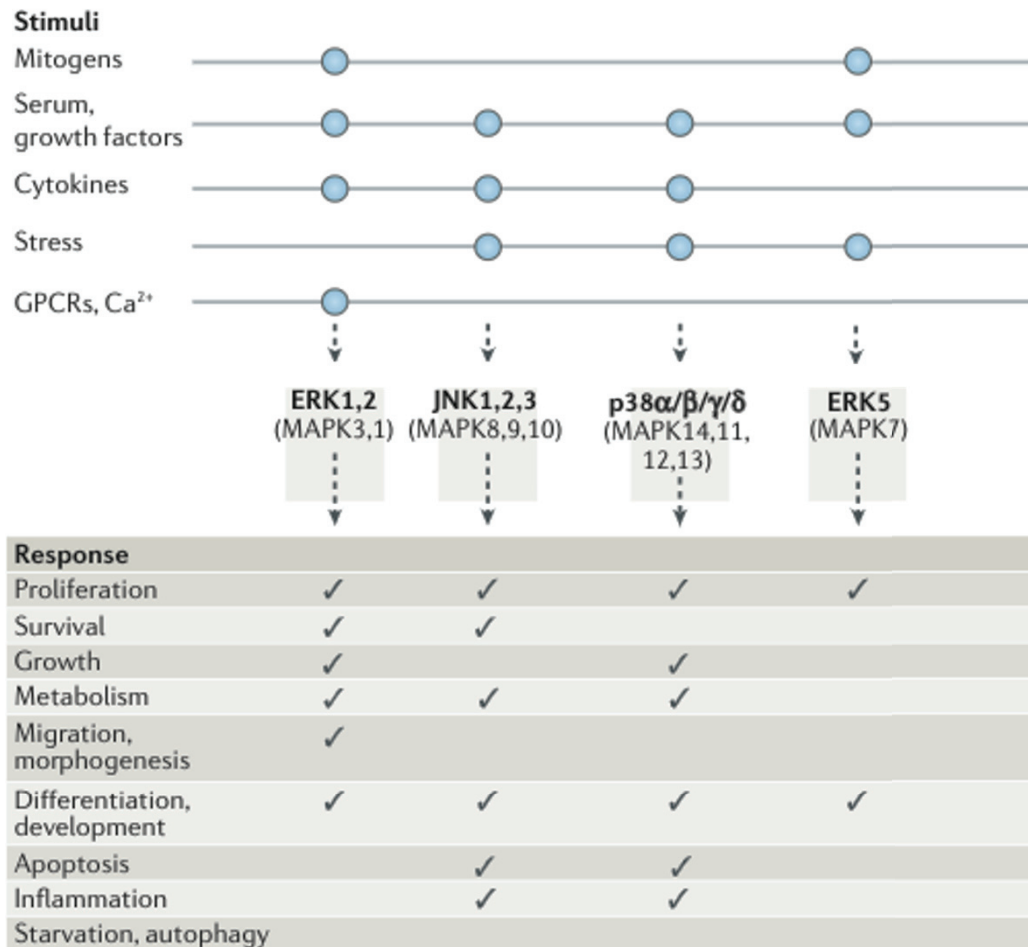


**Figure 2: MAPKs' responses to different stimuli**

Each MAPK family responds in a defined manner to specific external stimuli. Adapted from Lavoie et al. [26]

ERK regulates cell proliferation directly and indirectly via its target kinases. Phosphorylation and activation of Elk1 lead to the expression of IEGs such as c-Fos. ERK then stabilizes c-Fos allowing it to associate with c-Jun to form transcriptionally active AP-1 complexes whose activity is required for the expression of cyclin D1. This protein interacts with cyclin-dependent kinases (CDKs) and initiates the G1/S transition of the cell cycle [7]. In addition, active RSKs regulate transcription by phosphorylating several TFs, including CREB, SRF, estrogen receptor- $\alpha$  (ER- $\alpha$ ), nuclear factor- $\kappa$ B (NF- $\kappa$ B), nuclear factor of activated T cells 3 (NFAT3), and the transcription initiation factor TIF1A. RSKs also activate several ribosome-associated proteins, such as the ribosomal protein S6 (rpS6) and the eukaryotic initiation factor 4B (eIF4B), thus enhancing protein synthesis. RSKs inactivate pro-apoptotic proteins, including Bad (Bcl-2-associated death promoter) and death-associated protein kinase (DAPK), as well as the cyclin-

dependent kinase inhibitor p27<sup>KIP</sup>, thus promoting G1-phase progression [27]. ERK can directly inhibit pro-apoptotic proteins such as BIM and BIK, as well as a Caspase 9 of the intrinsic apoptotic pathway, or activate anti-apoptotic proteins including MCL1, BCL2, BCL2L1, and BIRC5 (also known as surviving) [26].

ERK regulates cell growth by upregulating the transcription of ribosomal DNA (rDNA) by Pol1 through phosphorylation of the nuclear TF UBF1 and that of tRNA by Pol III through activating the TF BRF1. Additionally, c-Myc controls the transcription of many elements of the Pol I machinery, such as RRN3 and UBF1. Activated RSKs and ERK regulate mTORC1 by RAPTOR phosphorylation, increasing protein synthesis. MNKs activate eIF4E, while RSKs activate eIF4B [26].

ERK has a significant role in regulating cell metabolism, primarily in respiration and glucose metabolism, carried out mainly by c-Myc and HIF1- $\alpha$  which are both directly phosphorylated by ERK. ERK signaling stimulates the flux of anabolic pathways connected with glycolysis.

ERK activity is vital for the regulation of cell shape and motility. Motility occurs in single cells or during collective movement or migration. ERK phosphorylates RHO family GTPases (RHO, RAC1, and CDC41), which control cell shape and motility [26].

ERK's extensive impact on cell differentiation and development is well documented. ERK can mediate cell-fate and tissue-fate decisions. Through different effectors, ERK plays a role in embryonic stem cell differentiation, bone development, heart formation, and brain development and functions [26]. Dysregulation of RAS-ERK signaling has been linked to various pathologies collectively known as RASopathies. Patients of RASopathies share similar traits, including facial dysmorphism, cardiac malformations, cutaneous and musculoskeletal anomalies, cognitive impairment, and increased cancer susceptibility, highlighting once again the central role of RAS-ERK signaling [28].

## **7. ERK pathway regulation**

Given its strong impact on various cell functions, ERK pathway signaling is tightly regulated. Once activated, ERK auto-regulates its pathway via direct, RSK-mediated, or transcription-mediated retro-inhibitory loops. ERK directly phosphorylates and inhibits upstream elements of the pathway, including many RTKs and adaptor proteins, RAS' GEF SoS1, RAF (and KSRs), and MEKs. ERK activates RSKs that also play a role in negative pathway regulation. RSKs can



inhibit RAS activation by inhibitory phosphorylation of GAB2 and SoS1. Finally, ERK signaling rapidly induces the transcription of several inhibitory proteins, such as the selective ERK dual-specificity phosphatases DUSPs (DUSP1/2/4/5/6/7/9) and proteins such as SPRY4 and SPREDs that recruit the RAS GTPase-activating protein neurofibromin (NF1) at the plasma membrane, leading to a decrease in the RAS-bound GTP pool (Figure 3) [29].

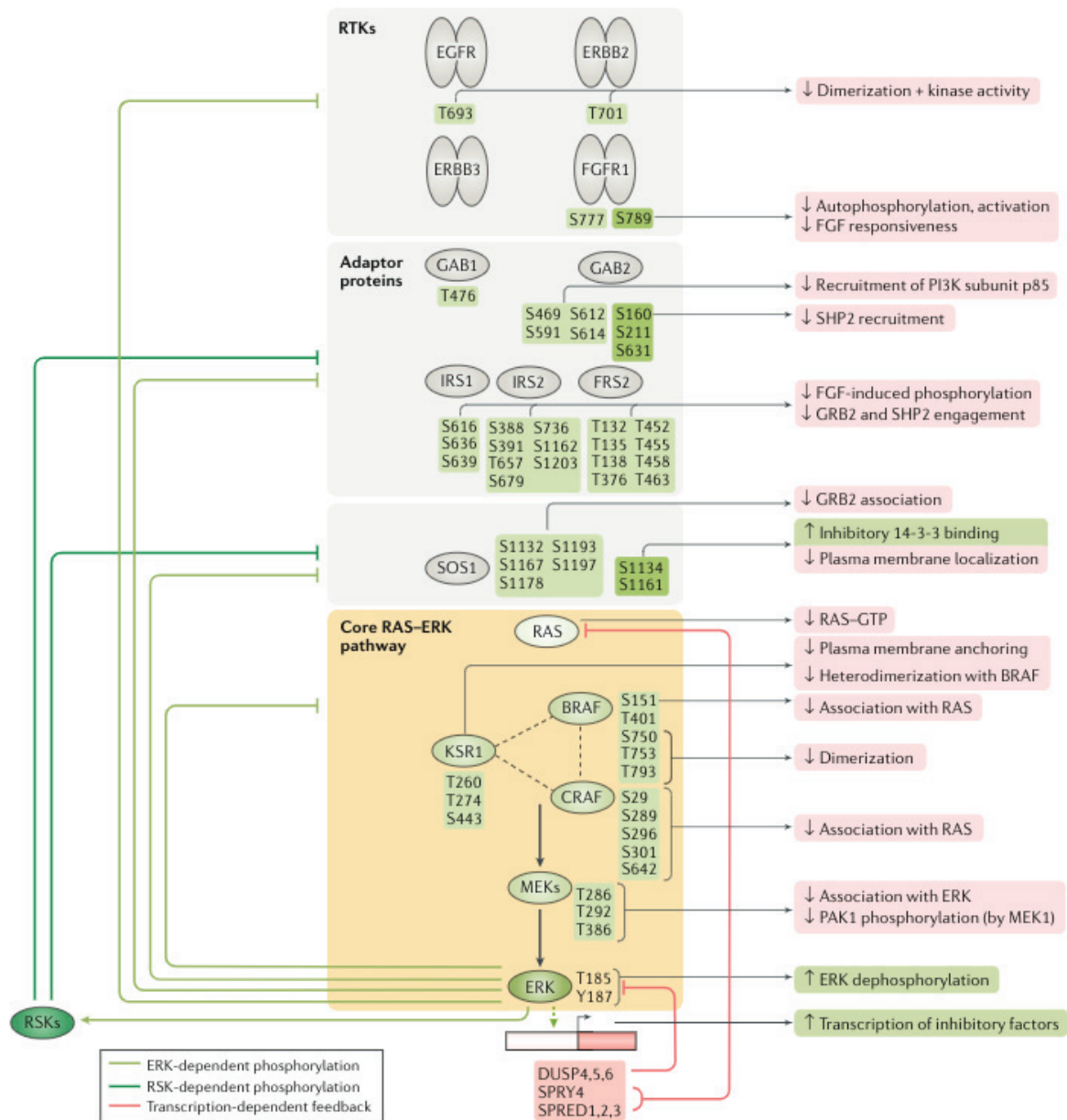


Figure 3: ERK pathway regulation

ERK pathway negative feedback regulation occurs through ERK- or RSK-dependent inhibitory phosphorylations, as well as via transcription-dependent feedback Figure from Lavoie et al. [26]

## 8. ERK protein

### 8.1. ERK structure

ERK-1 and ERK-2 proteins are similar in structure: like virtually all protein kinases, they contain N-terminal and C-terminal extensions responsible for ERK signal specificity. ERK-1 includes a 17 amino-acid (a.a.) residue insertion in its N-terminal extension and two additional a.a. in the C-terminal extension. ERK-1 and ERK-2 have a 31-a.a. insert within the kinase (insert) domain that ensures additional functional specificity. ERK-2 has generally been more studied than ERK-1. Human ERK-1 and ERK-2 consist respectively of 379 and 360 a.a. and are almost identical to mouse/rat ERKs, with only one and two more amino acids in rat/mouse ERK-1 and ERK-2 respectively, the difference being most likely inconsequential. No specific context has been described for activating one ERK isoform but not the other. All known stimulants of the ERK pathway lead to the activation of both ERK-1 and ERK-2 [5].

Like all protein kinases, ERK1/2 has a small amino-terminal lobe and a sizeable carboxyterminal lobe that consist of several conserved  $\alpha$ -helices and  $\beta$ -strands. The small lobe is composed of a five-stranded antiparallel  $\beta$ -sheet ( $\beta$ 1- $\beta$ 5), an essential and conserved  $\alpha$ C-helix, a glycine-rich (GxGxxG) ATP-phosphate-binding loop also known as the P-loop that occurs between  $\beta$ 1- $\beta$ 2 strands, as well as an AxK sequence in the  $\beta$ 3 strands. The glycine-rich loop helps position the ATP for catalysis while the lysine (K71/54 of ERK1/2) from the AxK sequence couples the released phosphates of ATP to a conserved glutamate residue in the  $\alpha$ C-helix (E88/71 in ERK1/2), creating a salt-bridge that is required for the formation of the activated " $\alpha$ C-in" conformation. This conformation is insufficient for total kinase activity; however, its absence indicates an inactive kinase. The large C-terminal lobe, which binds the substrates, is primarily  $\alpha$ -helical (six segments:  $\alpha$ D- $\alpha$ I). It also contains four short conserved  $\beta$ -strands ( $\beta$ 6- $\beta$ 9) that harbor most of the catalytic sites that are implicated in the transfer of the phosphoryl group from ATP to ERK substrates (Figure 4a) [30]. The catalytic core of ERK, like all protein kinases, is made of 12 subdomains with conserved a.a. residue signatures [31]. Three of these, a.a. define the K/D/D (Lys/Asp/Asp) catalytic domain of ERK1/2. A conserved  $\beta$ 3-strand lysine (K88/71 of ERK1/2) forms salt bridges with the  $\alpha$ - and  $\beta$ - phosphates of ATP, while Asp166/149, the first aspartate from the K/D/D catalytic domain, plays a significant role

in catalysis (Figure 4c). The second Asp186/169 is the first residue of the activation segment that begins with DFG and ends with APE, like all protein kinases. This residue binds  $Mg^{2+}$  ions that coordinate the three phosphates of ATP. Other important residues in the catalytic domain are His147, Arg148, Asp149, and Lys151. The activation segment controls both substrate binding and catalytic efficiency. This segment begins with the DFG five-residue magnesium positioning loop, followed by a middle activation lip and a conserved HRD component [5]. Taylor and Kornev [30] describe a hydrophobic skeleton of ERK with two different spines: a regulatory R-spine made of four non-consecutive hydrophobic residues and a catalytic C-spine made of eight hydrophobic residues. Each spine contains residues from the small and large lobes. The R-spine contains residues from the activation segment and the  $\alpha$ C-helix, whose conformations define active and inactive states. The C-spine regulates catalysis by directing ATP binding, while the R-spine directs substrate binding (Figure 4b).

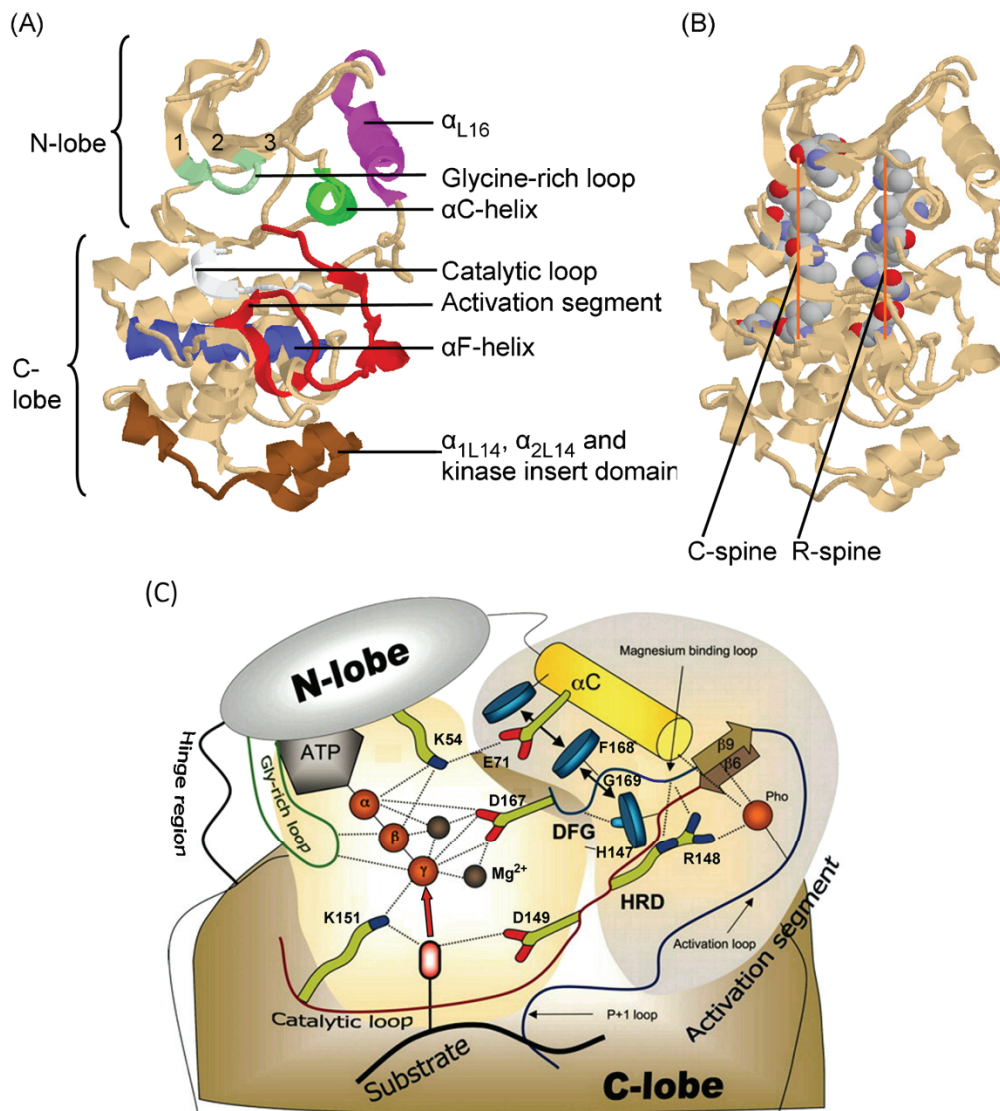


Figure 4: ERK structure

A-B) Ribbon diagrams of human ERK-2 (hERK2) in its inactive form (DFG-aspartate out) but with a  $\alpha$ C-helix is viewed from its N-terminus. C) Representation of the interactions between the hERK2 catalytic core residues, ATP and protein substrates. Figures from Roskoski [5].

## 8.2. ERK active and inactive conformations

ERK catalytic site is located in the cleft between the two lobes. When inactive, the enzyme is in an open conformation where the lobes are tilted away from each other. Once activated, the enzyme takes a closed and catalytically active conformation where the lobes come closer.

The  $\alpha$ -C-helix of the small lobe has active ( $\alpha$ C-helix in) and inactive ( $\alpha$ C-helix out) conformations that are rotated relative to the rest of the lobe, making or breaking ERK active state. In the inactive state, the aspartate D184/167 (of ERK1/2) of the conserved DFG sequence faces away from the active site, giving the “DFG-aspartate out” name for this conformation. In the active state, the aspartate face into the ATP-binding pocket and coordinates  $Mg^{2+}$ . This is called “DFG-aspartate in” conformation. Accordingly, the active form of ERK is DFG-aspartate in/ $\alpha$ C-helix in.

The conversion from inactive to active conformation occurs after the phosphorylation of two residues within the activation lip by MEK1/2. These two residues appear in a Thr-Glu-Tyr sequence. MEK1/2 first phosphorylates ERK at Tyr204/187, leading to the dissociation of the two proteins. Then, ERK reassociates with the same or a different active MEK1/2, inducing the phosphorylation of Thr202/185. Phosphorylation on both residues is required to activate ERK [5].

### 8.3. ERK substrate docking and enzyme recruitment sites

ERK catalyzes the phosphorylation of serine/threonine residues occurring in a Ser/Thr-Pro sequence, where the phosphorylation site is numbered 0, and the proline is at +1. ERK optimal phosphorylation sequence is Pro-Xxx-Ser/Thr-Pro, with two prolines at -2 and +1 [32].

ERK interacts with its protein partners via two independent docking domains, a D-recruitment site (DRS) and an F-recruitment site (FRS). These bind ERK partners via their D-docking (D-site) or F-docking domain (F-site), respectively. ERK partners can have one, both, or neither of the docking domains [33].

The D-site of substrates contains both hydrophobic and positively charged basic residues, allowing its interaction with ERK DRS that also contains a hydrophobic component but negatively charged residues (including the two aspartate residues D318/321 known as the common-docking CD domain). ERK DRS is on the protein's opposite side of the catalytic cleft. Substrates with a D-domain include Elk1, Lin1, TFII, MKP3, also known as DUSP6, MEK1, MNK1, MSK1, and RSK1 – 3. ERK FRS is located near the activation segment and interacts with the F-site of substrates such as Elk1, c-Fos, Lin1, Sap1, KSR, CRAF, DUSP1, and DUSP4 [5].

## 9. ERK scaffolds and anchors

Scaffolds play a central role in the spatial and temporal regulation of ERK signaling. Scaffolds bind different components of one pathway to bring them into proximity, thus facilitating signal transmission, while anchors can only bind to one element. Scaffolds can separate the components from related pathways or mediate crosstalk with other pathways. ERK has many scaffolds such as KSR1/2, IQGAP1, MP1, MORG1,  $\beta$ -arrestin1/2, Sef, MEKK1 and paxillin. ERK also has many anchors, including MEK1/2, PTP-SL, tubulin, actin, calponin, vimentin, and PEA-15. Scaffolds and anchors, which are fully described in Roskoski's paper [5], will be briefly discussed in this part.

KSR1/2 can interact with CRAF, MEK1/2, and ERK. While its interaction with MEK1/2 is constitutive, KSR1/2 only binds to ERK after stimulation. KSR2 can be phosphorylated by BRAF, increasing its catalytic activity. KSR2 then assembles the MEK1/KSR2/BRAF complex leading to an increase in MEK1 phosphorylation and activation by BRAF. The KSRs preferably act from plasma-membrane cholesterol-rich domains.

IQGAP1 is a large (189 kDa) ubiquitously expressed protein that regulates many signaling pathways and cellular functions. IQGAP1 binds directly to BRAF, MEK1/2 (MEK1 preferentially), and ERK-2, thus regulating their activity. An optimal IQGAP1 to MAPK ratio is required for efficient signaling propagation through complex formation.

MP1 (MEK partner 1) is a small (13,5 kDa) protein that binds to MEK1 and ERK-1 through an MP1/p14/p18 complex, regulating their activity. MP1 enhances Elk1 activation by ERK and MEK1 signaling by regulating its localization.

MORG1, an MP1 binding partner, interacts with MP1, BRAF, CRAF, MEK1/2, and ERK1/2 and stabilizes the assembly of these components into an oligomeric complex.

$\beta$ -arrestin2 can form a complex with CRAF and ERK1/2 and indirectly MEK1, stopping ERK translocation into the nucleus, thus restricting ERK activity to non-nuclear targets.

Sef can bind to activated MEK1/2, inhibiting their dissociation from ERK and consequently inhibiting ERK nuclear translocation.

MEKK1 (MAPK/ERK kinase kinase 1) is a MAP3K in the ERK and JNK MAPK pathways that can bind to CRAF, MEK1, and ERK-2, catalyzing MEK's activation by CRAF, among other activities.

Paxillin is found in focal adhesion sites that bind to protein kinases such as Src and the focal adhesion kinase (FAK). Paxillin, a target of ERK, can bind activated RAF, MEK, and ERK,

catalyzing MEK activation by RAF and ERK activation by MEK. This process plays a role in the regulation of FAK and cell spreading [5].

## **10. ERK nuclear translocation**

Dynamic changes in its cellular localization regulate ERK signal specificity. ERK targets are localized in the cytoplasm, various organelles, or the nucleus. ERK is localized in the cytoplasm of resting cells, maintained by anchoring proteins. Once an activating signal is transmitted, ERK translocates to the nucleus to activate its nuclear targets. ERK does not contain a classical nuclear localization signal (NLS), so ERK translocations do not occur through the canonical NLS and Importin nuclear-shuttling machinery. ERK conformational change releases it from anchoring proteins upon stimulation, revealing an SPS motif (Ser residues) within a unique nuclear translocation signal (NTS) within the kinase insert domain. These Ser residues are phosphorylated, mainly by CKII, facilitating ERK binding to importin 7 (Imp7) and, therefore, ERK translocation to the nucleus via the nuclear pores. Once inside the nucleus, the small GTPase Ran dissociates the ERK/Imp7 complex, leading to ERK accumulation in the nucleus, and Imp7 export back to the cytoplasm. This mechanism accounts for the translocation of most stimulated ERK molecules [21]. Other studies report that ERK dimerization enhances, but is not a prerequisite for, nuclear uptake [5].

ERK dimerization has been described to orchestrate the extranuclear signaling of ERK, while ERK monomers activate nuclear substrates [16], [34], [35]. Phosphorylated ERK dimerizes through interactions located outside the kinase domain and involving four leucines and the protruding PEHD or PDHD sequences [36] [37]. ERK dimers interact with scaffold proteins that connect them to cognate cytoplasmic substrates. However, ERK dimers and scaffold proteins are not involved in activating nuclear substrates since nuclear ERK acts mainly as monomers. ERK dimerization is essential in oncogenesis and tumor progression [34]. ERK dimerization and complex formation depends on the cellular context and the subsequent activity of scaffold proteins [37].

Active ERK is also found in the mitochondria, endosomes, plasma membrane, cytoskeleton, and the Golgi apparatus [38].

## 11. ERK dephosphorylation

As described in section I-8.2, removing one of the two phosphates within the activation lip of ERK inactivates the kinase. The MAPK phosphatases (MKPs) can dephosphorylate tyrosine, serine/threonine, or both tyrosine and threonine, in which case they are known as DUSPs (Dual-specificity phosphatases). Tyrosine-specific MKPs include PTP-SL, STEP, and HePTP. The serine/threonine-specific MKPs include phosphatase 2A and 2C. Ten identified DUSPs (1/2/4/5/6/7/8/9/10, and 16) are divided into three classes. The first class contains DUSP1/2/4/5, which are all localized in the nucleus. Except for DUSP5, specific to ERK, these DUSPs can inactivate ERK, p38, and JNK MAPK families. The class II enzymes (DUSP6/7/9) are three ERK-specific, closely related DUSPs in the cytoplasm. DUSP8/10/16 (Class III) are located in the cytoplasm and nucleus and preferentially inactivate p38 and JNK MAPK. DUSPs are critical phosphatases for the regulation of MAP kinases. They bind to their targets' DRS via their own interaction motif (KIM). Biphosphorylated ERK is a specific substrate of MKP3 (DUSP6), the latter only becoming active once bound to ERK. The tyrosine- and serine-threonine MKPs also play an important role in regulating MAPK pathways since many proteins in the cascades contain phosphorylated tyrosine, serine, or threonine residues.

### II. The ERK MAPK pathway in cancer

#### 1. ERK pathway and cancer

The RAS-ERK pathway is dysfunctional in most cancers [39]. Activation of this pathway occurs in most cancer types, with activating mutations in different components of this pathway. The most frequent mutation is that of *RAS*, occurring in ~ one-third of all cancer types and ~10% of all cancer patients. *Raf* (mainly *BRAF*) mutations are detected in ~ 8% of all cancer types. *MEK* and *ERK* mutations are rare, even though they have been reported in some cases [19]. Figure 5 shows the prevalence of MAPK component mutations in different cancers. All these alterations lead to ERK protein hyperactivation, which increases its proliferative activity. Given this pathway's vital roles (described in sections I – 4, 5, 6), most notably in regulating cellular proliferation, it is evident that its dysregulation could lead to uncontrolled proliferation and the absence of apoptosis, both characteristic of tumors. Dysregulation in the ERK pathway



plays a role in every step of the metastasis process: degradation of the tumor extracellular matrix, tumor migration, tumor invasion, and finally, metastasis [19].

Cancer type	Mutation type and rate (%)	Major mutation site
Prostate cancer	KRAS (90%)	G12D, G13D, G12V, G12S, G12C
NSCLC	NRAS (35%)	Q61K, Q61R, C186F, Q61L, Q61K,
CRC	KRAS (45%) BRAF (12%)	G12D, G12V, G13D, G12C, A146T, F566L V600E
Pancreatic cancer	KRAS (90%)	G12D, G12V, G12R, G12C,
Melanoma	NRAS (15%) BRAF (66%)	Q61R, Q61L, Q61K, Q61H V600E
Bladder cancer	KRAS (50%)	G12V, G12D, G12C,
AML	NRAS (30%)	G12D, G13D, G12V, Q61H, A59E, A164T
Ovarian Cancer	BRAF (30%)	V600E, A747V, G464E, V226M
Papillary thyroid cancer	RAS (60%) BRAF (35%–70%)	KRAS:G12R, NRAS:Q61R V600E

NSCLC, non-small cell lung cancer; CRC, colorectal cancer; AML, acute myeloid leukemia.

Figure 5: MAPK mutations in different cancers

Table from Feifei liu et al. (2018) [40]

## 2. ERK pathway inhibitors for cancer treatment

Protein kinases are involved in many vital cellular processes, and their dysregulation is implicated in various stages of carcinogenesis. The advent of protein kinase inhibitors in cancer therapy has led to a paradigm shift in how we treat cancer [41].

In light of the implication of the RAS-ERK pathway in cancers, extensive research has been carried out to target it. Inhibitors (whether in development or used in clinics) of this pathway include but are not limited to, Kinase Inhibitors (KIs) and other small-molecule inhibitors.

### 2.1. Kinase Inhibitors

The first KI used in clinics was Imatinib mesylate, an anti-BCR-ABL fusion protein in chronic myeloid leukemia, that demonstrated spectacular results [41]. Since then, hundreds of KIs have been developed and tested, with over 75 KIs approved for treating many cancer types. KI development and obstacles will be briefly summarized in this section. Please refer to Kannaiyan *et al.*, Cohen *et al.*, and Braicu *et al.* for details [37]–[39].

KIs can be divided into four classes: Types I, II and III and IV. Type I inhibitors bind reversibly to the ATP-binding site of the kinase but cannot bind when ATP is already bound to the enzyme. Type II inhibitors occupy the adenine (of ATP) binding site and an adjacent region called the back pocket. Once bound to the enzyme, these inhibitors induce the inactive DFG-aspartate out configuration. Both type I and type II inhibitors compete with ATP. Type III inhibitors bind to allosteric regions (sites other than the active ATP-binding region), so they are not in competition with ATP and cannot be displaced by it. Type IV are irreversible KIs that form covalent bonds with their targets; however, due to safety concerns, they are the least used KIs [5]. Efforts have been made to target RAS' kinase activity for over three decades. Mutant RAS binds GTP with a very high affinity, making the development of competitive inhibitors difficult. Other strategies include targeting proteins that regulate RAS activation, such as SoS, or targeting specific RAS mutants in development [40]. Recently, a breakthrough occurred with the approval of the first RAS KI, a KRAS p.G12C inhibitor in lung cancers [42]. Downstream of RAS, RAF kinases are important actors for transmitting RAS signals. Among the three RAF isoforms, CRAF was the first to be identified, and several anti-CRAF inhibitors, including sorafenib, were developed.

Considering the frequency of *BRAF* mutations in many cancers, most notably in melanoma (50%), several BRAF inhibitors were developed and approved for clinical use (Vemurafenib, Dabrafenib, and Encorafenib), significantly improving melanoma patients' outcomes. Unfortunately, the extent of the response to BRAF KIs is short, as in most cases, resistance emerges, leading to treatment failure. Resistance to KIs in melanoma will be detailed later on in this manuscript (section 15.2.1). Even though MEK is rarely mutated in cancers, MEK inhibitors (Trametinib, Binimetinib, Selumetinib, and Cobimetinib) have shown to be very interesting for treating different cancers as single agents or in combination with other KIs. In *BRAF*-mutated melanoma, the treatment standard would be combining a BRAF KI with a MEK KI to delay the emergence of resistance. As with other KIs, MEK inhibitors induce resistance within several months. Resistance to KIs means that, even though RAF and MEK are inhibited, ERK can still be activated by crosstalk with other pathways, hence the advantage of directly targeting ERK. Many ERK kinase inhibitors are in development, but only a few reached clinical trials (e.g., BVD-523/Ulixertinib and GDC0994/Ravoxertinib) [40], [43]. However, resistance to ERK1/2 KIs has also been described, where ERK-5 rescues the proliferation, thus weakening the effect of ERK1/2 KIs. Furthermore, inhibiting ERK kinase activity inhibits its negative

feedback, further activating upstream components that could activate different pro-proliferation pathways, such as the PI3K/AKT pathway [43].

## 2.2. Other small-molecule inhibitors

Targeting ERK, the final kinase of the MAPK pathway, inhibits it from relaying upstream signals to its many substrates. In the last years, identifying new inhibitors of ERK has been the focus of many researchers. In addition to the ATP-competitive KIs described in the previous section, covalent and allosteric inhibitors of ERK have been designed and developed. Covalent inhibitors can selectively and firmly bind to their target, inducing long-lasting inhibition. Cysteine residues near the ATP pocket (mainly Cys166 in ERK2) have the potential to form covalent bonds with inhibitors. Although promising, only one covalent ERK inhibitor (ERKi) has been in a clinical trial (CC-90003, phase I) that ended unsuccessfully due to poor efficacy. The safety risks associated with a covalent and irreversible binding should be considered while developing new covalent ERKi [43]. In addition to the ERK ATP pocket, targeting ERK DRS and FRS, the two substrate-binding pockets, is an exciting approach for allosterically inhibiting ERK. ERK DRS is a peptide-binding groove located on the back of the kinase, while the FRS is a shallow hydrophobic groove near the Ser/Thr-Pro binding site (section I- 8.3) [43].

The structural basis of the interaction between the DRS and its docking sequence has been determined by X-ray crystallography [44], allowing the development of several inhibitors, now in preclinical stages, targeting ERK DRS through *in silico* screening of large libraries. DRS exists in both active and inactive conformations of ERK, but FRS exists only in the activated form of ERK. Based on site identification by ligand competitive saturations (SILCs), Samadani et al. [45] developed FRS inhibitors that effectively inhibited FRS binding to AP-1 promoter. Allosteric inhibitors either inhibit ERK activation (by obstructing the ERK-MEK interaction) or block ERK phosphorylation of downstream targets such as RSKs. Another approach was developed by Herrero *et al.* [34], [35], where ERK dimerization is inhibited by a small molecule without affecting its kinase activity. ERK dimerization is essential for ERK extranuclear signaling, and its inhibition compromises cellular transformation and tumor development [16], [35]. DEL-22379 has proven effective in different cancers with dysregulated RAS-ERK signaling, such as melanoma and thyroid cancer [46], [47]. Since allosteric inhibitors and ATP-competitive KIs have two different action modes, combining both families of inhibitors could be an excellent

future approach to overcome the disadvantages of small-molecule inhibitors, such as low selectivity and off-target effects.

### **3. Crosstalk with other pathways**

The MAPK pathway is a central signaling pathway communicating with several other pathways, such as PI3K, WNT, TGF- $\beta$ , COX-2, and NOTCH. This communication is intensified during tumorigenesis to multiply cancer aggressiveness. Braicu *et al.* and Najafi *et al.* [48], [49] reviewed ERK crosstalk with these respective pathways in detail, which will be summarized in this section. MAPK and PI3K/AKT co-activation is commonly observed in cancers. PI3K reactivation is one of the most frequent underlying mechanisms of acquired resistance to MAPK inhibitors, and PI3K inhibitors could re-sensitize resistant cells to MAPK-targeted therapies. mTOR is a serine-threonine kinase downstream of PI3K and is considered to be the primary mediator of PI3K's tumorigenic activity. Suppression of both mTORC1 and mTORC2 sensitizes cells to MAPK inhibition and inhibits feedback reactivation of both MAPK and PI3K pathways (Figure 6a). MAPK exhibits bidirectional cross-talking with TGF- $\beta$  and COX-2 pathways, individually implicated in tumor initiation and progression. ERK is involved in the non-canonical pathway of TGF- $\beta$  that promotes epithelial-mesenchymal transition (EMT) and metastasis. COX-2 induces MAPK signaling to promote cell initiation and resistance to therapies. In turn, ERK acts on COX-2 via NF- $\kappa$ B signaling. NOTCH is another pro-oncogenic pathway activated in many tumors. Its interaction with ERK happens mainly in the infiltrative margin of cancer where cancer stem cells reside, and cancer cells undergo EMT (Figure 6b). ERK has also been shown to interact with the Toll-like and Interleukin-1 (TLRs/IL-1Rs) proinflammatory pathways by our team and others [50]–[56]. TLRs and IL-1Rs are required for innate immunity and defense against pathogens, but if dysregulated, they can cause inflammatory and autoimmune diseases and cancer [57]. A deeper look into these pathways will be taken in the next section.

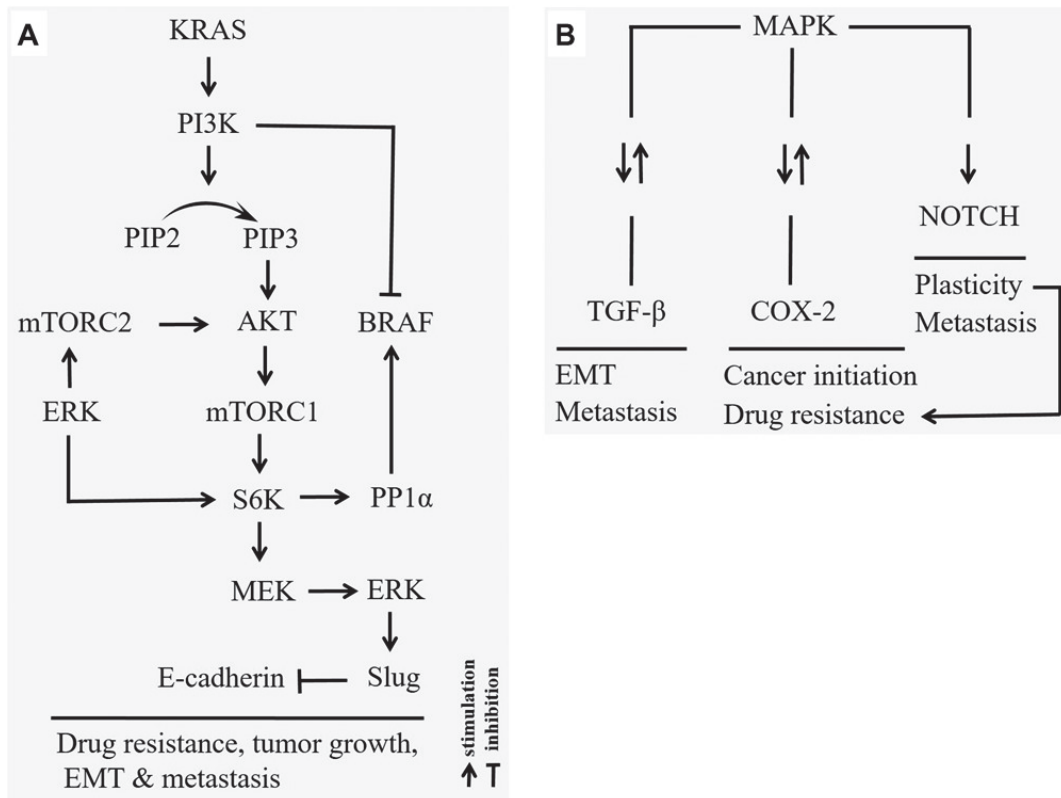


Figure 6: Cross-talking between MAPK and other tumor-promoting signaling pathways.

- A) PI3K and MAPK pathways cooperate to promote tumor growth, survival, and metastasis. RAS is upstream of both pathways. Once activated, PI3K induces the activation of AKT, which leads to mTOR activation. mTOR can activate MEK, which leads to a cycle of ERK and AKT/mTOR activation. PI3K mainly induces the direct inhibition of BRAF, but it can also indirectly induce its activation via the S6K/protein phosphatase 1 $\alpha$  (PP1 $\alpha$ ). The latter phenomenon is observed under the PI3K blockade.
- B) MAPK interacts with COX-2, TGF- $\beta$  and NOTCH signaling pathways to promote cancer initiation, plasticity, drug resistance, EMT, and metastasis. Adapted from [48]

#### 4. TLR and IL-1R signaling pathways and their adaptor protein MyD88

TLRs are crucial pattern recognition receptors (PRRs) activated by microbial products such as microbe-associated molecular patterns (MAMPs) and endogenous ligands like damage-associated molecular patterns (DAMPs) released during cell death or tissue damage. TLRs and IL-1Rs are required for innate immunity and defense against pathogens.

TLRs and IL1-Rs have an N-terminal leucine-rich repeat (LRR) domain, a transmembrane link, and a cytoplasmic domain known as the Toll-interleukin 1 receptor (TIR) domain. The TIR

domain is a conserved intracellular domain of approximately 200 amino acids in the cytoplasmic region that plays a crucial role in downstream protein recruitment. TLRs and IL-1Rs do not have intrinsic kinase activity, so their signal transduction requires different adaptor proteins, such as myeloid differentiation primary response protein 88 (MyD88), MyD88-adaptor-like (Mal), TIR-domain-containing adaptor protein inducing interferon- $\beta$  (TRIF), TRIF-related adaptor molecule (TRAM), and sterile- $\alpha$ - and armadillo motif-containing protein (SARM). These adaptor proteins associate with TLR/IL-1Rs through TIR-TIR homophilic interactions, and this association activates signaling kinases, transcription factors, and the production of inflammatory response factors and type-1 interferons. Due to the protein structural similarity of the IL-1R to the TLRs, functions of the IL1R/MyD88 signaling are similar to that of the TLR/myD88 signaling, i.e., activation of the TLRs/MyD88 or IL1R/MyD88 signaling will increase the level of inflammatory cytokines and chemokines [55], [57]–[59].

Of the various TLR/IL-1R adapter proteins, MyD88 is the canonical partner used by all IL-1Rs and TLRs except TLR3, which uses TRIF. TLR2 uses the adaptor protein MAL, also known as TIRAP, in conjunction with MyD88, while TLR4 initiates two distinct signaling pathways initiated by TIRAP with MyD88 for nuclear factor- $\kappa$ B (NF- $\kappa$ B)-mediated gene induction and TRIF-associated TRAM (TICAM2) for type-I IFN production. MyD88 contains three key domains: an N-terminal death domain (DD, residues 1–109), a short intermediate domain (ID), and a C-terminal TIR domain (residues 155–296) [58].

Upon pathogen-associated molecular patterns (PAMPs) binding to the TLRs, adaptor proteins, primarily MyD88, are recruited to the activated receptors via TIR-TIR domain interactions.

Interleukin receptor-associated kinase 4 (IRAK4) is then recruited to the DD domain of MyD88, followed by the interaction of IRAK1, IRAK2, and/or IRAK3 with IRAK4 to form a complex known as the Myddosome. During Myddosome formation, IRAK4 activates IRAK1, which is then autophosphorylated at several sites and released from MyD88. IRAK1 associates with the RING-domain E3 ubiquitin ligase TRAF6. TRAF6, along with ubiquitin-conjugating enzymes UBC13 and UEV1A, promotes K63-linked polyubiquitination of both TRAF6 itself and the TAK1 protein kinase complex, activating TAK1. TAK1 then activates two different pathways that lead to the activation of the IKK complex-NF- $\kappa$ B pathway and -MAPK pathway. The IKK complex is composed of the catalytic subunits IKK $\alpha$  and IKK $\beta$  and the regulatory subunit NEMO (also called IKK $\gamma$ ). TAK1 binds to the IKK complex through ubiquitin chains, which allows it to phosphorylate and activate IKK $\beta$ . The IKK complex phosphorylates the NF- $\kappa$ B inhibitory protein

I $\kappa$ B $\alpha$ , which undergoes proteasome degradation, allowing NF- $\kappa$ B to translocate into the nucleus to induce proinflammatory gene expression. TAK1 activation also results in activation of MAPK family members such as ERK1/2, p38, and JNK, which mediates activation of AP-1 family transcription factors or stabilization of mRNA to regulate inflammatory responses (Figure 7) [60], [61]. It has been shown that MyD88 has a central role in inflammatory pathways and that inflammation and cancer are closely related. In fact, MyD88 can play a pro-oncogenic role through the activation of NF- $\kappa$ B and the prolonged activation of ERK [50], [55], [56]. For instance, a somatic mutation in MyD88 that changes Leucine at position 265 to Proline activates this signaling network constitutively and underlies a third of diffuse large B-cell lymphoma (DLBCL) and 90% of Waldenstrom's lymphoma[57]. In addition, many reports have shown that MyD88, by carrying-out its regular functions downstream of the TLRs or IL-1 family receptors, contributes to carcinogenesis in cancer models including cancer of the skin, liver, pancreas, and colon, as well as in sarcoma[56]. These are part of the canonical activities of MyD88. MyD88 has a non-canonical function that will be discussed later on (section IV-1).

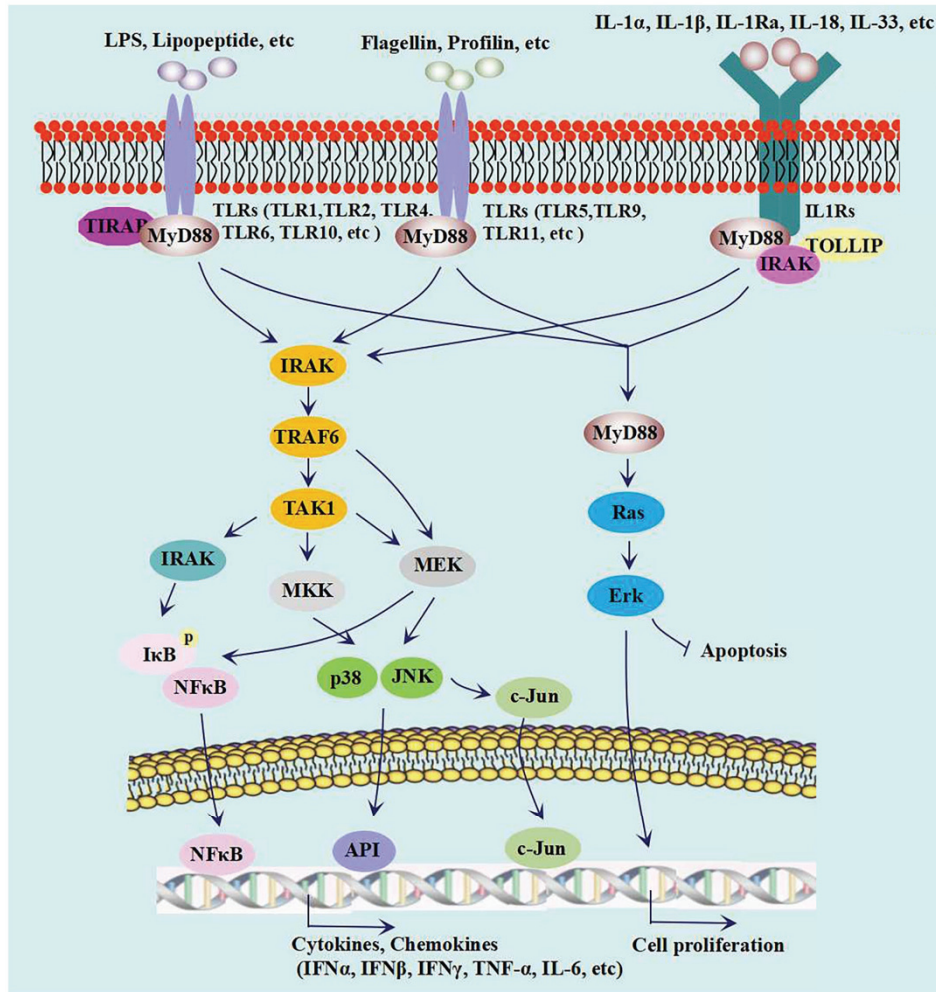


Figure 7: Toll-like receptors and Interleukin-1 receptors signaling pathways.

After TLR or IL-1R activation, MyD88 mediates the signal from the receptors to common downstream targets. The canonical activity of MyD88 leads to the production of pro-inflammatory cytokines and chemokines. MyD88 also acts as a bridge between TL/IL-1R-induced inflammation signaling and the RAS oncogenic signaling pathway. By activating ERK, MyD88 promotes cancer cell proliferation. Adapted from [55].

## 5. The ERK-MAPK pathway in cutaneous melanoma

As described in the sections above, the ERK-MAPK pathway is involved in many cancer types. In cutaneous melanoma, an aggressive subtype of skin cancer, ERK signaling is hyperactivated in virtually all cases, driving tumor development and resistance to therapies. There is a real need for novel therapeutic options in melanoma, due to innate or acquired resistance to current treatments. The following sections will focalize on the biology and epidemiology of melanoma, as well as the current treatments and obstacles encountered.



### III. Cutaneous Melanoma: an aggressive tumor on the rise

#### A. Normal Skin

##### 1. Skin biology

To better understand cutaneous melanoma, a skin cancer originating from pigment-producing melanocytes, a prior global understanding of skin biology is required.

Skin is part of the integumentary system and the human body's largest organ. It is also considered to be the first protective physical barrier against environmental factors, as it is responsible for temperature regulation and protection against ultraviolet (UV) light, trauma, pathogens, microorganisms, and toxins [62]–[64].

There are three main layers of skin: the epidermis, the dermis, and the hypodermis. The epidermis is the outermost layer of skin, followed by the dermis, which contains connective tissue, hair follicles, blood and lymphatic vessels, and sweat glands. The deeper subcutaneous tissue (hypodermis) comprises fat and connective tissue (Figure 8). This segment focuses on the epidermal layer of skin, where melanocytes reside and give rise to melanoma. The epidermis layers include, respectively, from the deepest to the most superficial part of the epidermis: the stratum basale, stratum spinosum, stratum granulosum, stratum lucidum, and stratum corneum (Figure 9). The stratum basale, separated from the dermis by the basal lamina, is mitotically active and contains melanocytes, a single row of keratinocytes, and stem cells. Melanocytes produce melanin, a pigment that gives our skin its color. Keratinocytes, the predominant cell type of the epidermis, evolve and mature as they travel upward to create the remaining layers. This layer also contains the oval-shaped Merkel cells located directly above the basement membrane and serve as mechanoreceptors connected to nerve endings from the dermis. Stratum spinosum includes 8 to 10 cell layers that contain irregular, polyhedral keratinocytes with cytoplasmic processes or “spines” that extend outward and contact neighboring cells by desmosomes. Dendritic and Langerhans cells can be found in this layer and are considered the skin’s first-line defenders that play an important role in antigen presentation. Stratum granulosum comprises 3 to 5 cell layers of diamond-shaped keratinocytes with keratohyalin and lamellar granules. Keratohyalin granules contain keratin precursors that eventually aggregate, crosslink, and form bundles. Lamellar granules contain

the glycolipids that get secreted to the surface of the cells and function as a glue, keeping the cells stuck together. Stratum lucidum is composed of 2 to 3 cell layers, present in thicker skin found in the palms and soles, and is a thin clear layer consisting of eleidin which is a transformation product of keratohyalin. The stratum corneum is the uppermost layer of 20 to 30 cell layers comprising keratin and dead keratinocytes known as anucleate squamous cells. Within this layer, the dead keratinocytes secrete defensins which are part of our first immune defense [62]–[64].

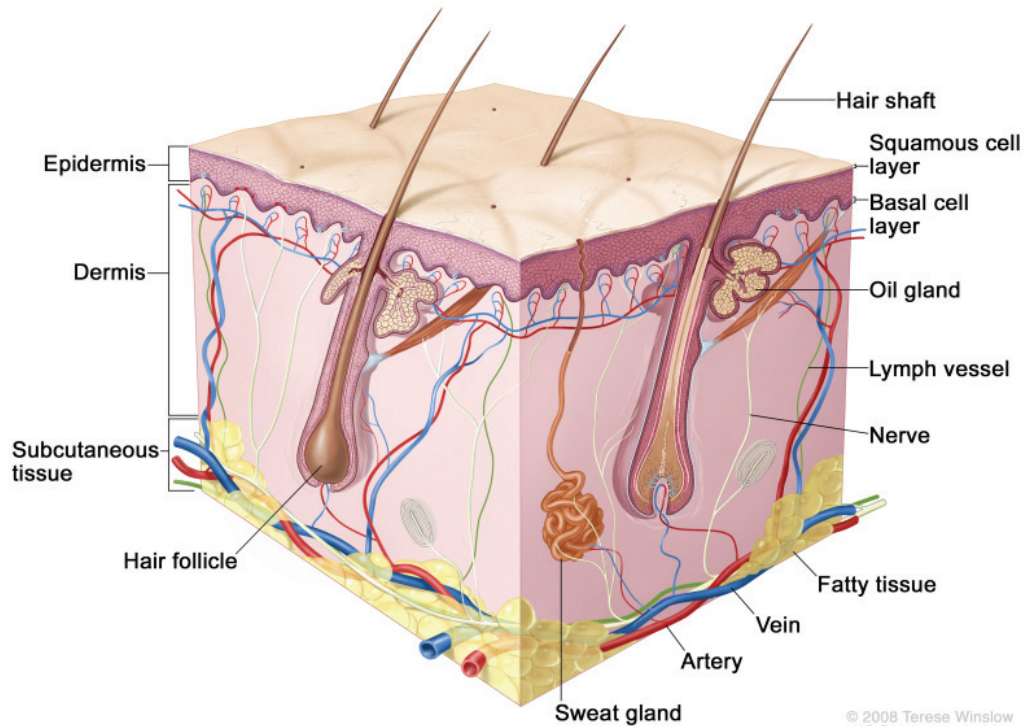


*Figure 8: Anatomy of the skin.*

*Adapted from [65].*

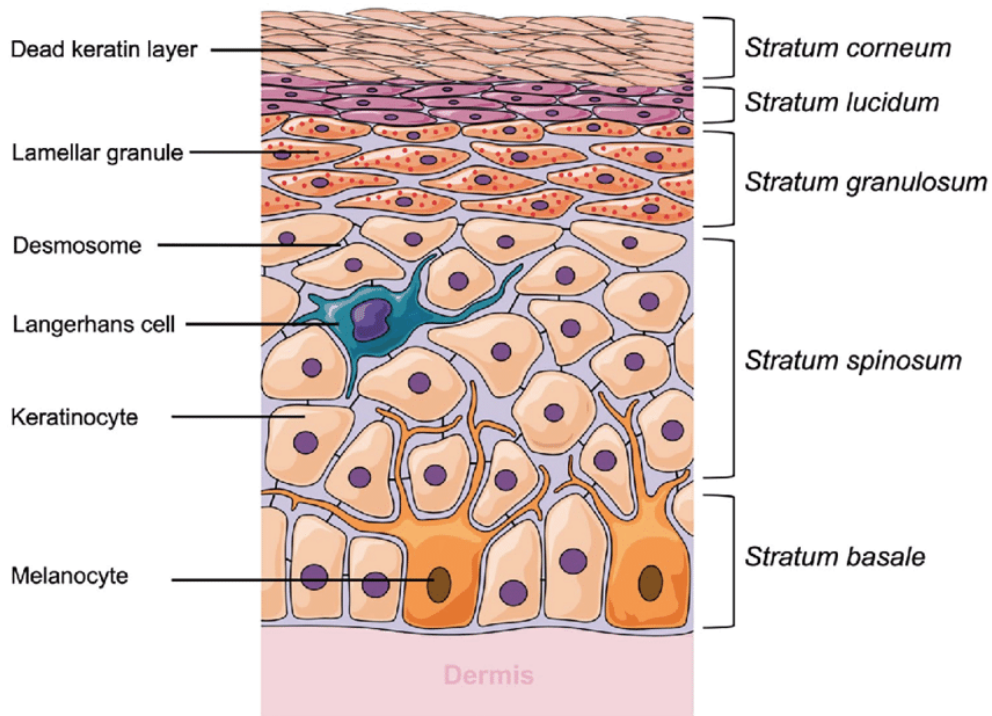


Figure 9: Anatomy of the epidermis.

Adapted from [66]

## 2. Melanocyte biology

Melanocytes are melanin-producing cells that are derived from neural crest cells. They are found in the epidermis, hair, and iris, where they give color to these structures, but they are also located in the inner ear, nervous system, and heart, where they have different functions [67]. The roles of non-cutaneous melanocytes will not be described in this manuscript. Melanocytes can absorb ultraviolet radiation and survive considerable genotoxic stress, mainly by melanin photoprotection [68]. Besides this photoprotective role, melanin is also a potent antioxidant [69]. In the epidermal basal layer, each melanocyte is associated with 30-40 keratinocytes via cell-cell contact structures (Figure 9). The contact between the dendritic processes of differentiated melanocytes and keratinocytes is necessary for melanin transfer into keratinocytes through melanosomes [67]. Melanosomes are structurally similar to lysosomes and encapsulate the proteins required to protect melanocytes from toxic intermediate products [70], [71]. Melanogenesis produces mixtures of eumelanin (black/brown pigment) and pheomelanin (red/yellow pigment) at different ratios. The ratio is mainly determined by tyrosinase activity and the substrate concentrations of tyrosine and

cysteine. The density of melanocytes in all types of skin is similar and constant; the distribution and amount of melanin determine the color of the skin [69]. Pigment production will be described in the next section.

### **3. Melanin synthesis**

Skin pigmentation is due to an accumulation of eumelanin and pheomelanin in keratinocytes. While eumelanin is UV absorbent, pheomelanin is photo-unstable and can even promote carcinogenesis [69], [72], [73]. After exposure to sunlight, damaged keratinocytes release the  $\alpha$ -melanocyte stimulating hormone ( $\alpha$ -MSH) and the adrenocorticotrophic hormone (ACTH), which bind to the Melanocortin 1 receptor (MC1R, a GPCR) on melanocytes, inducing eumelanin synthesis. Both hormones are synthesized from a common precursor: proopiomelanocortin (POMC). UV exposition damages the DNA of keratinocytes leading to the activation and stabilization of p53, which then binds the promoter of POMC to induce it. UVB exposition induces the activation of the stress-induced p38 MAPK signaling pathway in exposed keratinocytes, leading to the activation of the TF USF1 (upstream transcription factor 1), that can bind to the promoters of both POMC and MC1R, thus promoting melanin synthesis [74]. The binding of  $\alpha$ -MSH or ACTH to MC1R activates adenylate cyclase. It leads to the activation of the cAMP signaling cascade, ultimately leading to the activation of the protein kinase A (PKA), which then induces the TF CREB. CREB binds to the promoter of the microphthalmia-associated transcription factor MITF, the “master regulator” of melanocytic lineage, resulting in the transcription of enzymes necessary for eumelanin production such as Tyrosinase (Tyr) and the two Tyrosinase-related proteins TRP1 and TRP2/Dct [75]. While  $\alpha$ -MSH and ACTH are MC1R agonists, agouti signaling protein (ASP in mice, ASIP in humans) is an antagonist. ASP inhibits eumelanin synthesis by directly affecting the binding of  $\alpha$ -MSH, the activation of cAMP, and the downstream expression of MITF, thus inducing Tyr, TRP1, and TRP2/Dcr transcription and pheomelanin synthesis (Figure 10) [69].

Melanin synthesis occurs in melanosomes following the transfer of tyrosinase, which oxidizes tyrosine to dihydroxyphenylalanine (DOPA) and dopaquinone (DQ). Melanin is eventually deposited onto a fibrillar scaffold composed of modified PMEL17 (also known as gp100) molecules (an important marker of melanocytes) [69].

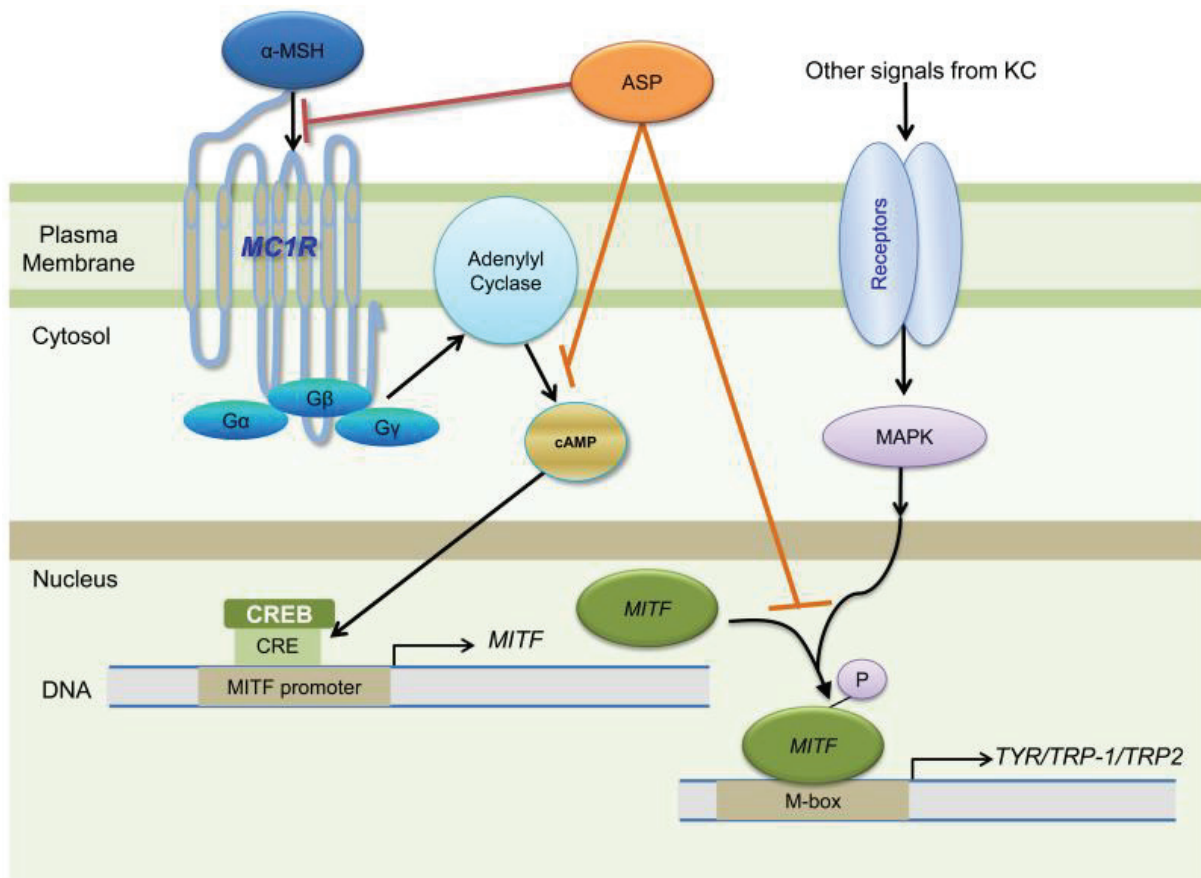


Figure 10: Melanogenesis through MC1R signaling and its downstream effectors.

Keratinocyte (KC) mediators activate MC1R and p38 MAPK signaling pathways leading to the activation of MITF, which induces the expression of enzymes necessary for eumelanin production. ASP can reduce eumelanin synthesis by inhibiting  $\alpha$ -MSH binding, cAMP synthesis, or MITF phosphorylation. From [69].

#### 4. Melanocyte regulation

Epidermal melanocytes are highly differentiated cells that have a low proliferation rate. Melanocytic homeostasis is tightly regulated by its micro-environment, mainly keratinocytes, through various mechanisms [76], [77]. Briefly, cell-cell contact between a melanocyte and its neighboring keratinocytes ensures the diffusion of paracrine signals produced in keratinocytes, such as  $\alpha$ -MSH, ACTH, vFGF, HGF, SCF, and endothelin 1/2/3. These signals induce several signaling pathways that either cause MITF and melanin production or regulate

cell proliferation [78]. Another example of melanocyte regulation by cell-cell contact is its anchoring by keratinocytes via E-cadherin junctions, thus inhibiting its proliferation [79].

## B. Cutaneous Melanoma

### 1. Melanocyte transformation to melanoma

As we discussed in the previous section, keratinocytes tightly regulate melanocytes. Several factors detailed in the following sections could lead to the escape of melanocytes from this regulation, giving rise to cutaneous melanoma, a form of skin cancer that originates from melanocytes, and to other forms of melanoma (e.g., mucosal and uveal melanomas) that this manuscript will not address. In the upcoming sections, “melanoma” will be about “cutaneous melanoma” unless otherwise specified. Melanomas are aggressive cancers that could disseminate through metastasis to sites where surgical removal is impossible. Malignant melanoma is considered one of the most metastatic cancers [80]. The treatment of melanoma has seen a significant improvement in the last decade, but unfortunately, due to innate or acquired resistance, a lot of research is still needed. The upcoming sections will review melanoma epidemiology, risk factors, classification, treatments, and obstacles.

### 2. Melanoma epidemiology: alarming numbers

Melanoma is the third most common cutaneous malignancy behind basal and squamous cell carcinomas, making up less than 5% of cases. Despite this, it remains the most aggressive skin carcinoma associated with most skin cancer-related mortality [81]. Melanoma is generally considered a modern disease exacerbated by sun-seeking behavior and global atmospheric changes. UV exposure to the skin has increased gradually, resulting in a paralleled increase in the incidence of melanoma. Melanoma is among the top ten most frequent malignancies in most European countries, and it’s even more prevalent in Australia, New Zealand, and the United States [80]–[82]. The incidence of cutaneous melanoma is rising worldwide, and this increase is occurring faster than other malignancies [83]. While melanoma incidence is lower among people <40 years of age, it is one of the most common cancers diagnosed among adolescents and young adults worldwide. In the United States, melanoma is the second most common cancer among women aged between 20 and 29 [84].

### 3. Melanoma epidemiology: risk factors

Many risk factors have been implicated in melanoma oncogenesis, including hereditary/personal or environmental factors.

Hereditary and personal factors include ethnicity, sex, age, and genetic background. Risk factors include skin color, with the highest melanoma prevalence occurring in people with lighter skin pigmentation and, thus, lower melanin photoprotection. Melanoma incidence increases with age, peaking among people >75 years of age after accumulating damage to melanocytes. Adolescent and young adult women are more susceptible to melanoma than men, likely due to the widespread use of indoor tanning among females, which is associated with increased melanoma risk. However, after age 40 and overall, melanoma occurs more frequently among men [84]. This could be due to the implication of androgens [84] or to the fact that men are less likely to self-examine for suspicious lesions and more likely to delay presentation until more advanced stages of the disease [85]. Melanoma can develop de novo (predominantly) or from benign nevi (rarely). The presence of nevi, their number, and their size are considered melanoma risk factors [80]. While most genetic alterations associated with melanoma are acquired, it is estimated that between 8% and 12% of patients with malignant melanoma have a family history of the disease. Genetic hereditary factors for melanoma include but are not limited to, the loss of CDKN2A (cyclin-dependent kinase inhibitor 2A), germline mutations of CDK4 (cyclin-dependent kinase 4), MITF and BAP1 (BRCA1-associated protein 1), as well as the alteration of MC1R, TYR, TRP1, and defects in DNA repair genes such as TERT (Telomerase reverse transcriptase) [80].

UV exposure and severe sunburn are the most critical risk factors for melanoma. Intermittent sunburn during childhood and youth was considered a significant risk factor, but severe sunburn during adulthood is now considered equally contributory [81], [84]. Melanoma progression is a multifactorial process involving genetic, epigenetic, and environmental factors. UV exposure is the only major modifiable factor for disease prevention, hence the importance of sun protective measures. Although environmental and hereditary mutations are responsible for melanoma development, newly acquired somatic mutations are the most crucial factor.

#### 4. Melanoma: oncogenic mutations

Cutaneous melanoma carries one of the greatest tumor mutational burdens (TMB) of all cancers (median of 14,4 mutations/Mb), mainly due to exposure to ultraviolet (UV) radiation, aging, and its associated deterioration in DNA repair mechanisms [81], [86]. Since the development of functional genetics and sequencing in the last decades, critical pathways involved in the initiation and progression of melanoma have been identified. These pathways are often responsible for controlling and maintaining central cellular activities such as growth and metabolism, replication, resisting apoptosis, cell cycle control, and proliferation, such as the MAPK-ERK and PI3K pathways. The most frequent gene defect in cutaneous melanoma is the activating mutation of the oncogene *BRAF*, found in almost half of the tumors. *NRAS* mutation is the second most common alteration in around 20% of melanoma cases. *BRAF* and *NRAS* mutations are mutually exclusive. Other mutations include *KIT* (proto-oncogene, receptor tyrosine kinase), *TP53* (tumor protein p53), *NF1* (neurofibromin 1), *CDKN2A*, *PTEN* (phosphatase and tensin homolog), and *CCND1* (Cyclin D1) (Figure 11) [80]. Loss or inactivation of *PTEN* has been found in more than 35% of melanomas, often at advanced stages and exclusively in *BRAF* melanomas. *PTEN* inhibits the pro-proliferation pathway PI3K/AKT, so its loss leads to the activation of this pathway. The cooperation of *BRAF* and *PTEN* mutations activates both the MAPK and PI3K pathways, promoting the progression of melanoma and metastasis [87], [88]. *PTEN* and *BRAF* co-mutations have also been described in mice models, where both mutations were necessary for melanoma progression [89], [90]. *PTEN* loss has also been associated with resistance to both current options for the treatment of melanoma, Kinase inhibitors and immunotherapies (reviewed in sections III – B. 6.2 and 6.3) [91], [92]. Melanoma is molecularly classified into four major categories, three involving mutations affecting the MAPK pathway: *BRAF*-mutant, *NRAS*-mutant, *NF1*-mutant, and triple wild-type melanoma. This manuscript will mainly focus on the two major mutations in melanoma: *BRAF* and *NRAS*, both part of the MAPK-ERK pathway. For more details concerning the other mutations in melanoma, please refer to the detailed review by Paluncic *et al.* [87].



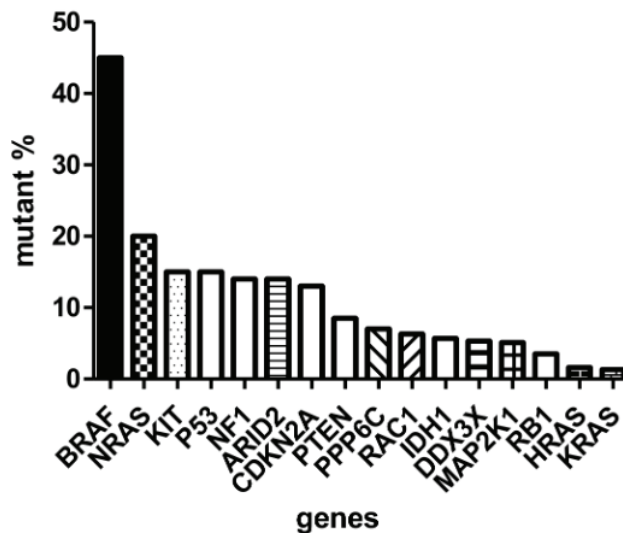


Figure 11: Mutation frequency of driver genes of skin melanoma based on TCGA data.

Adapted from [80]

#### 4.1. BRAF-mutated melanoma

*BRAF* V600 mutations have been detected in nearly 50% of all cutaneous melanoma patients. Non-V600 mutations, which are less frequent than V600 ones, have been found in 11% of all cutaneous melanoma patients. Melanoma with *BRAF* mutations is most commonly found on the skin of younger patients without marked solar elastosis, suggesting intermittent UV exposure in early life rather than chronic sun damage [93].

##### 4.1.1. BRAF V600 mutations

The most frequent mutation in melanoma is *BRAF* V600E, observed in around 70%-90% of all *BRAF*-mutated melanoma. It consists of an amino acid change from valine (V) to glutamic acid (E), resulting in a 480-fold increase in kinase activity (catalytically active conformation) compared with native protein. *BRAF* V600K is the second most common mutation (10–20% of all V600 *BRAF* mutations) in cutaneous melanoma and, as a V600E mutation, it consists of an amino acid change, with a valine (V) replaced by a lysine (K). Approximately 10% of all V600 mutations are V600R (<5%), V600D (<5%), V600E2 (<1%), V600M (<1%), and V600G (<1%). Among the two most common subtypes, *BRAF* V600K-mutant melanomas are considered more aggressive than the V600E ones, as they have shown a lesser response to kinase

inhibitors and, subsequently, a shorter progression-free survival. On the other hand, V600K melanomas are often diagnosed at an older age, with a higher degree of TMB due to cumulative sun damage, making them better responders to immune checkpoint inhibitors (ICI) than V600E melanomas. The other less frequent V600 mutations have shown a good response to BRAF inhibitors and a better OS than V600E/K-mutant melanoma patients [93].

#### 4.1.2. BRAF Non-V600 mutations

As previously stated, *BRAF* non-V600 mutations are less frequent than V600 ones. Without going into much detail, it should be noted that, to date, their prognostic and predictive role is still challenging to elucidate. The most frequent mutations, class II *BRAF* mutations, are at L597, K601, and G469. In contrast to *BRAF* V600 mutations, these mutations do not confer a catalytic activity to monomeric BRAF but rather induce its constitutive dimerization.

Melanomas with *BRAF* non-V600 mutations do not respond to V600 kinase inhibitors but could benefit from MEK kinase inhibition. Other less frequent modifications known as class III *BRAF* mutations include codon D594 and G596 mutations, and the rare N581 mutation, leading to an impairment of the catalytic activity of BRAF. These mutations have been associated with a good prognosis [93].

#### 4.1.3. BRAF fusions

Genomic rearrangement induces oncogenic *BRAF* fusions in 3-6% of all melanoma patients. These patients often show a moderate TMB, suggesting it is independent of UV exposure. These rearrangements induce the loss of the autoinhibitory domain of BRAF, leading to the constitutive activation of BRAF catalytic activity. To date, not enough data on the prognosis of this specific subtype has been collected [93].

### 4.2. *NRAS*-mutated melanoma

*NRAS*-mutant melanomas are more aggressive than the other melanoma categories, resulting in a lower median OS [86], [94]. This poor response is also due to a lack of effective targeted therapies compared to *BRAF*-mutant melanomas, where BRAF and MEK KIs are successful

treatment options. *NRAS*-mutant melanoma differs from *BRAF*-mutant melanoma from a clinical point of view. Patients are usually older (>55 years) with previous UV exposure. Aberrant RAS signaling is mainly caused by oncogenic missense mutations at codons 12, 13, and 61. *NRAS*<sup>Q61</sup> is the most predominant (>90%) *NRAS*-mutant melanoma. It induces conformational changes toward the GTP-bound active state, whereas oncogenic alterations at codons 12 and 13 impair GTP hydrolysis. Interestingly, the Q61R (glutamine to arginine) substitution has been shown to have a higher efficiency of tumor initiation in melanocytes than G12D (glycine to aspartic acid). Active *NRAS* then activates predominantly MAPK signaling but also the PI3K pathway. In contrast to normal melanocytes, *NRAS* activates CRAF rather than *BRAF* in melanoma. MAPK and PI3K pathways converge at the ribosomal protein S6 through RSK- and p70 ribosomal S6 Kinase (S6K1)-mediated activation of S6. S6 is phosphorylated by S6K1 under normal conditions and by RSK in the case of MAPK hyperactivation. The ribosomal protein S6 is a critical cell cycle regulator, as it can control the CDK4/6 – Cyclin D1 complex involved in the G1/S transition. *NRAS*-mutant melanomas display a dysregulated cell cycle with cyclin D1 upregulation and loss of p16INK4A, resulting in enhanced CDK4/6 activity and early G1-S transition. In addition, *TP53* is mutated in 17% of *NRAS*-mutant melanomas, amplifying RAS activity through hnRNP-mediated splicing that leads to inactive GAPs and, subsequently, a sustained GTP-bound RAS [86].

## **5. Melanoma: Non-genetic heterogeneity**

Melanoma is a heterogeneous tumor with neuroectodermal origins in which functionally diverse cell subpopulations co-exist, including stromal cells in the tumor microenvironment (TME). Within the TME, in addition to the extracellular matrix (ECM), a mixture of non-melanoma cells comprises cells such as fibroblasts, endothelial cells, and various immune cells, including tumor-infiltrating lymphocytes (TILs) that determine the success of immunotherapies.

Melanoma cell plasticity is a hallmark of non-genetic heterogeneity, where melanoma cells exhibit different phenotypic states within a tumor to cope with changing pressure and conditions in the TME. This plasticity allows melanoma cells to switch between distinct transcriptional programs unique to various phenotypic states. It has been shown that within the same tumor, some melanoma cells are highly differentiated, melanocytic, and more

proliferative, while others are slow-cycling, dedifferentiated, and more invasive, described as mesenchymal-like cells [95]. This degree of heterogeneity dictates the overall biological behavior of a tumor, disease progression, and treatment resistance [96]–[98].

Melanoma has been shown to dynamically shift between different transcriptional states or phenotypes. This is referred to as phenotype switching in melanoma, and it involves switching between quiescent and proliferative cell cycle states. This results in changes in invasiveness, signaling pathways and immune cell composition in the TME [22]. Indeed, the aggressiveness of melanoma is at least in part due to its phenotypic plasticity, whereupon early in the tumor evolution, melanoma metastasizes to lymph nodes, distant tissues, and organs [96]. Among the most well-characterized molecular changes that signify a phenotypic shift in melanoma is the expression level of the master regulator microphthalmia-associated transcription factor *MITF*. *MITF* is a key transcription factor that regulates melanocyte development, pigmentation and melanoma progression. *MITF* expression has been described as a rheostat model since its high activity promotes differentiation, its normal activity leads cells to proliferation and its low levels confer invasiveness and stemness properties. Accordingly, very low or absent expression of *MITF* is characteristic of invasive melanoma cells, while high expression of *MITF* characterizes non-invasive proliferative melanoma cells [95]. Another factor linked to the phenotype switch in melanoma is the receptor tyrosine kinase (RTK) *AXL*. The expression of *AXL* is inversely associated with *MITF* expression. *AXL* is expressed by melanoma and immune cells and plays a role in cancer progression, metastasis, and drug resistance when it binds with its ligand, growth arrest-specific protein 6 (*GAS6*). In melanoma, the  $MITF^{low}AXL^{high}$  signature is linked to an invasive, mesenchymal-like phenotype, whereas the  $MITF^{high}AXL^{low}$  signature promotes a more proliferative and drug-sensitive phenotype. Importantly, the expression of  $MITF^{low}AXL^{high}$  is common in *BRAF*-mutated melanoma and has been observed in patients who relapsed after treatment with *BRAF* and *MEK* inhibitors, indicating that this signature leads to drug resistance [95]. *MITF/AXL* expression correlates with *SOX10* and *SOX9* transcriptional signatures, which are molecular markers of epithelial-like and mesenchymal-like phenotypes, respectively [95]. Other factors that are involved in this phenotype switch include the EMT-transcription factors (EMT-TFs) *TWIST1*, *SNAIL2*, *ZEB1* and *ZEB2*. EMT-TFs cooperate the oncogenic pathways in order to regulate this switch. While in normal melanocytes, *SNAIL2* and *ZEB2* are expressed and drive an *MITF*-dependent melanocyte differentiation program, melanoma cells with an upregulated *ERK* activity show a decrease of both factors and an

upregulation of TWIST1 and ZEB1, both drivers of dedifferentiation. This reprogramming into a dedifferentiated state is dependent on MEK-ERK signaling, which is activated in virtually all cases of melanoma [99].

In dedifferentiated melanoma cells, E-cadherin is repressed in favor of N-cadherin expression, resembling the well-described epithelial–mesenchymal transition (EMT) [99]. Albeit the similarities between EMT and phenotype switching, EMT would not be the appropriate term to describe this process in melanoma, as melanocytes are not epithelial cells [96]. The EMT-like state in melanoma is induced by transcriptional and epigenetic changes as an adaptive response to cues in the TME such as hypoxia, glucose or amino acid deprivation, secreted and inflammatory factors like transforming growth factor  $\beta$  (TGF $\beta$ ) and tumor necrosis factor  $\alpha$  (TNF $\alpha$ ), ECM mechano-signaling and in response to immuno- and targeted therapies [95], [100].

While previously, melanoma was considered to switch between two states, a differentiated or undifferentiated state, the range of transcriptional programs is nowadays increasing, following a progressive model of plasticity. So far, six transcriptional programs have been described: hyperdifferentiated cells, melanocytic proliferation cells, transitory-intermediate migrating cells, therapy-induced starved-like melanoma cells, NCSC (Neural crest stem cells)-like cells, and MITF-negative undifferentiated cells. In the figure 12, all different transcriptional states are reported with their respective markers [98]. The six transcriptional stages reviewed in Pagliuca *et al.* [98] have been associated with different responses to KIs. A short exposure to BRAFi drives melanoma cells to a hyperdifferentiated state characterized by strong melanocytic features such as an upregulation of MART-1 (also known as MLANA) and gp100 (also known as PMEL) and increase in MITF expression [98]. The transitory state includes a subset of cells with both differentiation and neural crest phenotype. This state displays MITF<sup>High</sup>/AXL<sup>Low</sup>/SOX10<sup>High</sup> as the proliferative state and NGFR<sup>High</sup> (neural growth factor receptor) levels as the NCSC-like state. This subset of cells is moderately sensitive to KIs. Nutrient deprivation drives melanoma cells towards a starved-like state characterized by metabolic alteration and a slow-cycling dedifferentiated state. These cells are usually not able to synthesize monounsaturated fatty acids, thus requiring fatty acids uptake from the TME, sustained by increased expression of CD36, a fatty acid transporter. Longer exposure to BRAFi tends to stabilize the NCSC-like state. Such phenotype is described as MITF<sup>Low</sup> and is also known for its high expression of NGFR, SOX10, AXL, aquaporin 1 (AQP1), GDNF family receptor

alpha 2 (GFRA2), and retinoid X receptor gamma (RXR $\gamma$ ) [98]. The MITF-negative undifferentiated cells are prone to lose the expression of SOX10, hence acquiring a preneural crest phenotype upregulating SOX9, making them less responsive to KIs [98].

In addition, melanoma cell plasticity is associated with altered gene expression in immune cells and cancer-associated fibroblasts, as well as changes in extracellular matrix, which drive the metastatic cascade and therapeutic resistance [96]. Therefore, resistance to therapy in melanoma is not only dependent on genetic evolution, but it is also driven by gene expression changes and adaptive phenotypic cell plasticity. This will be discussed later on, in section III-B- 7.4.

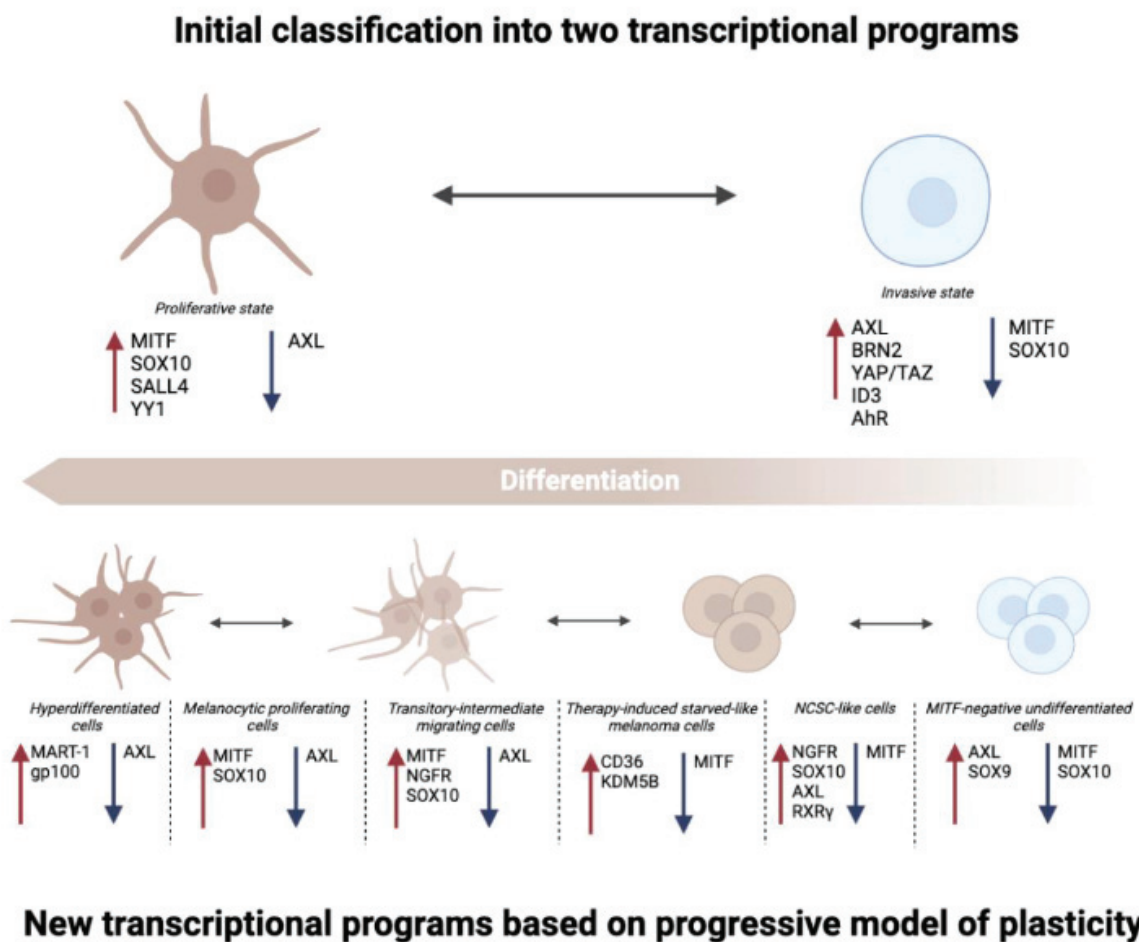


Figure 12: Transcriptional programs and plasticity in melanoma

Starting from an initial dual classification recognizing only a more differentiated “proliferative” state and a less differentiated “invasive” state, the range of transcriptional programs is nowadays increasing. Six transcriptional programs have been described so far: hyperdifferentiated cells, melanocytic proliferation cells, transitory-intermediate migrating cells, therapy-induced starved-like melanoma cells, NCSC (Neural crest stem cells)-like cells, and MITF-negative undifferentiated cells. From Pagliuca et al. [98]

## 6. Melanoma: Histological subtypes, stage classification, and diagnosis.

According to the World Health Organization's classification of skin tumors in 2018, melanomas are classified into nine sub-groups, according to their evolutionary pathways. These pathways are superficial spreading melanoma (or low cumulative sun damage melanoma, mainly *BRAF<sup>V600E</sup>*), lentigo magna melanoma (or high cumulative sun damage melanoma, mainly *BRAF<sup>V600K</sup>*, *NRAS*, *NF1* or *KIT* mutations), desmoplastic melanoma (mainly *NF1* mutation, extremely high TMB), spitz melanoma (*HRAS* mutation), acral melanoma (similar to superficial spreading melanoma but on the skin of the hands and feet), mucosal melanoma (*KIT* mutation), melanoma arising in congenital naevus (*NRAS* or *BRAF<sup>V600E</sup>* mutations), melanoma arising in blue naevus, and uveal melanoma (different non-*NRAS* nor -*BRAF<sup>V600E</sup>* mutations) [101]. Each melanoma subtype has specific etiology, markers, and prognosis, which this manuscript will not detail.

The depth of melanoma is the most important prognostic factor. Two staging systems are available to assess depth: Breslow and Clark levels. In the past, physicians used the Clark level. However, Breslow level is now the standard of care because it is more specific [102]. The American Joint Committee on Cancer (AJCC) report references melanoma staging. Like other cancers, melanoma staging is divided into stages: stages I and II for clinically localized primary melanoma, stage III for patients with locoregional metastases, and stage IV for patients with distant metastases (Figure 13). Tumor-Node-Metastasis (TNM) classification is used for melanoma staging. The T category, which describes the tumor's size and invasion of adjacent tissue, is divided into T1–T4 based on the tumor thickness, measured with the Breslow level. Each category is subdivided into a and b based on the absence or presence of ulceration [103]. N describes the spread of cancer to nearby lymph nodes and the presence of in-transit, satellite, and/or microsatellite metastases; and M represents metastasis to other organs (if present, stage IV independently of T and N staging) (Figure 14) [103]–[105].

Melanoma diagnosis at early stages is vital for effective treatment. Self-surveillance and non-invasive lesion checks by a doctor are key steps. Lesions are evaluated according to the ABCDE criteria: asymmetry, border irregularity, color (variation), diameter (more than 5 mm), and/or erythema. Any positivity in the exam should raise suspicion of malignant melanoma, and the practitioner should obtain a lesion biopsy [102]. Molecular diagnostics in melanoma are used for both diagnosis and treatment selection. Immunohistochemistry remains the standard

technique for identifying melanoma and its subtypes. DNA- and RNA-based mutation detection via Sanger sequencing, NGS, or PCR are also used to identify and classify melanomas correctly [87] .

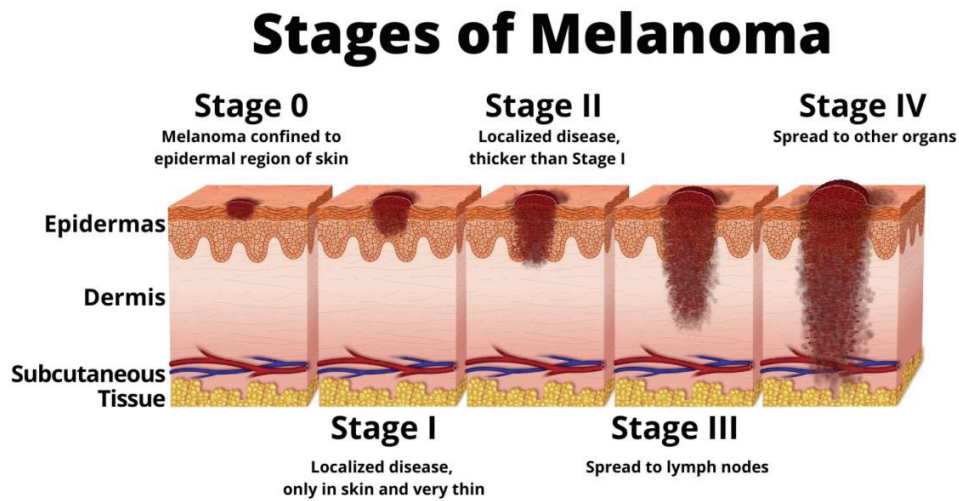


Figure 13: The four stages of melanoma.

Representation from the AIM at melanoma foundation website (<https://www.aimatmelanoma.org/stages-of-melanoma/>).



Stage and Category	Stage Definition
<b>T stage</b>	
T1	Breslow $\leq$ 1 mm; ulceration not known
T1a	Breslow $<$ 0.8 mm; ulceration absent
T1b	Breslow $\geq$ 0.8 mm
T2	Breslow 1.1-2.0 mm; ulceration not known
T2a	Breslow 1.1-2.0 mm; ulceration absent
T2b	Breslow 1.1-2.0 mm; ulceration present
T3	Breslow 2.1-4.0 mm; ulceration not known
T3a	Breslow 2.1-4.0 mm; ulceration absent
T3b	Breslow 2.1-4.0 mm; ulceration present
T4	Breslow $>$ 4.0 mm; ulceration not known
T4a	Breslow $>$ 4.0 mm; ulceration absent
T4b	Breslow $>$ 4.0 mm; ulceration present
T0	Melanoma of unknown primary
TX	Breslow thickness not known
<b>N stage</b>	
N1a	1 node, clinically occult, no MSI
N1b	1 node, clinically detected, no MSI
N1c	0 nodes, MSI present
N2a	2-3 nodes, clinically occult, no MSI
N2b	2-3 nodes, clinically detected, no MSI
N2c	1 node, clinically occult or detected, MSI present
N3a	$>$ 3 nodes, clinically occult, no MSI
N3b	$>$ 3 nodes, clinically detected, no MSI
N3c	$>$ 1 nodes, clinically occult or detected, MSI present
<b>Overall stage</b>	
III	T1, T2, T3, T4, TX, and any N stage
IIIA	T1a-b, T2a and N1a, N2a
IIIB	T0 and N1b, N1c
IIIC	T1a-b, T2a and N1b, N1c, N2b
	T2b, T3a and N1a-c, N2a, N2b
IIID	T0 and N2b, N2c, N3b, N3c
	T1a-b, T2a-b, T3a and N2c, N3a-c
	T3b, T4a, and any N stage
	T4b and N1a-c, N2a-c
	T4b and N3a-c

Figure 14: TNM staging of melanoma based on the recommendations of the 8th AJCC.

Adapted from [104].

## 7. Melanoma: Current treatment options and their obstacles

More than 90% of patients with melanoma have localized or regional disease at the time of initial clinical presentation and are successfully treated with surgical excision with adequate margins [106]–[109]. The treatment of metastatic melanoma has shown spectacular improvement over the past decade, with the introduction of targeted therapies (TT) and immunotherapy, mainly immune checkpoint inhibitors (ICI). Ten years ago, metastatic melanoma was considered fatal, with overall survival of  $<$ 5%. Today, one in two patients are alive five years after diagnosis when treated with combination immunotherapy, and over one in three patients with combination BRAF /MEK targeted therapy or single-agent PD-1 blockade [109]. Since 2010, the FDA has approved nearly a dozen new treatments, summarized in Figure 15. TNM stage and presence or absence of a *BRAF V600E/K* mutation are the most crucial features in determining eligibility for Food and Drug Administration (FDA) approved immunotherapy or targeted therapy options [109]. Unfortunately, most patients are either

resistant or become resistant to the available treatments, leading to disease progression [110], [111]. This section will review the currently approved therapies and their respective obstacles, focusing on the two major molecular subtypes of melanoma: *BRAF* and *NRAS*-mutated melanoma.

### 7.1. Previous treatments (pre-TT and -ICI)

Chemotherapy (Dacarbazine, Temozolomide, and Fotemustine) and cytokine therapy (high dose IL-2; Interferon  $\alpha$ -2b and Pegylated IFN  $\alpha$ -2b) were the standards of care for metastatic melanoma patients before the introduction of TT and ICI (pre-2010). Both treatment families showed low response rates in clinical trials and real-world clinical use [107].

### 7.2. Targeted Therapies

The era of molecular targeted therapy in cutaneous melanoma was ushered in following the discovery of *BRAF* mutations in several cancers, including melanoma (Davies et al., 2002, [112]). This discovery led to the initial evaluation of BRAF kinase inhibitors (BRAFi), with initial trials showing 50% response rates as a single agent in patients with metastatic melanoma [109]. Kinase inhibitors targeting MEK followed suit. Given the clinical activity of single-agent MEK kinase inhibition (MEKi) and appreciation of the importance of downstream MAPK pathway signaling, BRAFi/MEKi combinations were subsequently evaluated. They showed significantly better results than monotherapy [108]. To date, three BRAFis: Vemurafenib, Dabrafenib, and Encorafenib, and two MEKis (Trametinib and Binimetinib) have been approved by the FDA for the treatment of metastatic melanoma [108]. The FDA-approved combinations are Dabrafenib + Trametinib, Vemurafenib + Cobimetinib, and Encorafenib + Binimetinib. All single-agent therapies led to an average of 40% 2-year overall survival, while the different KI combinations led to 50-60% 2-year OS. Both cases are a significant improvement from previous treatments mentioned in section III-B-7.1 (Figure 16) [106] For patients unable to tolerate the recommended first-line systemic immuno-therapy, BRAFi/MEKi is the treatment of the choice. Patients with *BRAF*-mutated melanoma are treated with the combination of BRAFi+MEKi, while *NRAS*-mutant patients are treated with MEK KIs [113]. MEKi in *NRAS*-mutant melanoma have shown limited efficacy compared to

chemotherapy but are still used given the lack of other effective targeted therapy options [114]. BRAFi/MEKi therapy is usually brisk and may provide a more rapid disease control for patients requiring urgent treatment [109]. However, in most cases, patients who initially responded to KIs, acquire resistance to these inhibitors after several months of treatment, leading to further disease progression [108]–[110], [115]–[118]. We will discuss resistance to KIs later on, in section 7.4.

Agent	Mechanism	FDA-approved indications
<b>Targeted Therapies</b>		
Vemurafenib	BRAF inhibitor	- Unresectable/metastatic melanoma harboring BRAF V600E/K mutation
Cobimetinib	MEK inhibitor	- Unresectable/metastatic melanoma harboring BRAF V600E/K mutation
Dabrafenib + trametinib	BRAF inhibitor + MEK inhibitor	- Unresectable/metastatic melanoma harboring BRAF V600E/K mutation - Adjuvant treatment of resected stage III BRAF V600E/K mutant melanoma
Vemurafenib + cobimetinib	BRAF inhibitor + MEK inhibitor	- Unresectable/metastatic melanoma harboring BRAF V600E/K mutation
Encorafenib + binimetinib	BRAF inhibitor + MEK inhibitor	- Unresectable/metastatic melanoma harboring BRAF V600E/K mutation
<b>Immunotherapies</b>		
Ipilimumab	Anti-CTLA-4 monoclonal antibody	- Unresectable/metastatic melanoma (regardless of BRAF status) - Adjuvant treatment of resected stage III melanoma (regardless of BRAF status)
Nivolumab	Anti-PD-1 monoclonal antibody	- Unresectable/metastatic melanoma (regardless of BRAF status) - Adjuvant treatment of resected stage III melanoma (regardless of BRAF status)
Pembrolizumab	Anti-PD-1 monoclonal antibody	- Unresectable/metastatic melanoma (regardless of BRAF status) - Adjuvant treatment of resected stage III melanoma (regardless of BRAF status)
Ipilimumab-nivolumab	Anti-CTLA-4 antibody + anti-PD-1 antibody	- Unresectable/metastatic melanoma (regardless of BRAF status)
T-VEC	Modified, injectable oncolytic herpes virus	Local treatment of unresectable cutaneous, subcutaneous, and nodal lesions in patients with recurrent melanoma after surgery

Abbreviations: FDA, Food and Drug Administration; MEK, MAPK kinase; T-VEC, talimogene laherpraepvec.

Figure 15: FDA-approved targeted therapies and immunotherapies for the treatment of melanoma in 2020.

Adapted from [109].

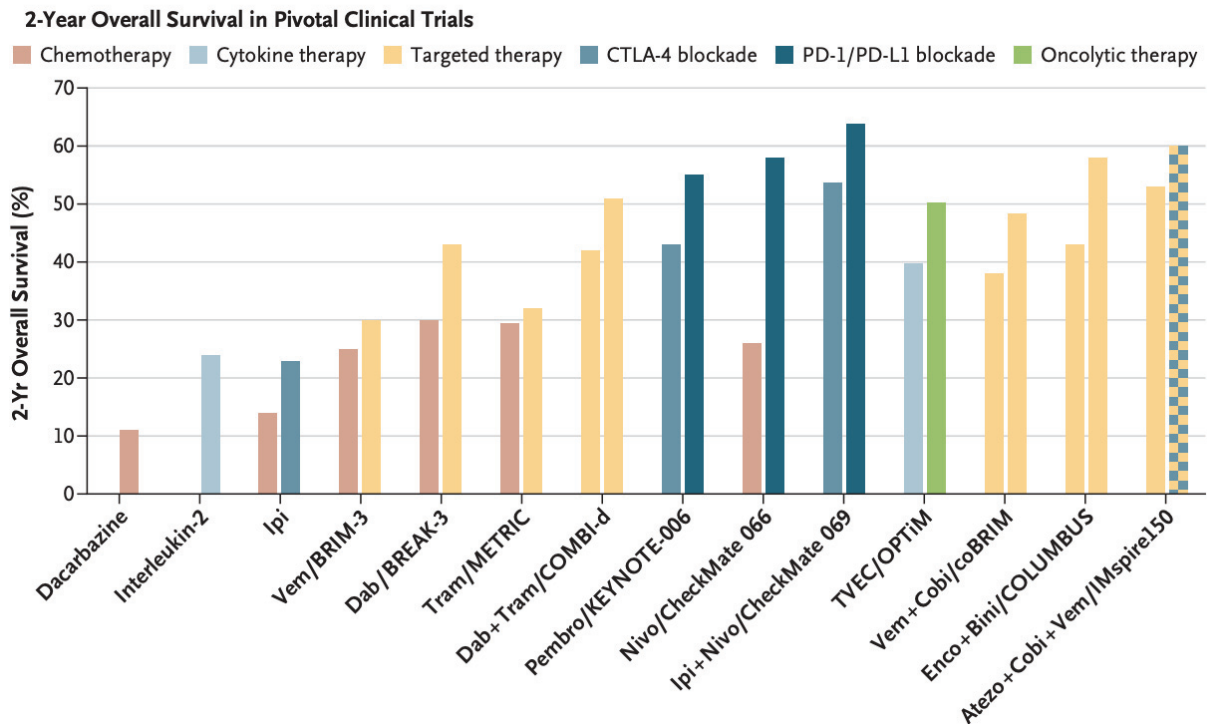


Figure 16: Overall two-year survival for advanced melanoma patients in pivotal clinical trials of current FDA-approved treatments.

Atezo denotes atezolizumab, Bini binimetinib, Cobi cobimetinib, CTLA-4 cytotoxic T-lymphocyte antigen 4, Dab dabrafenib, Enco encorafenib, Ipi ipilimumab, Nivo nivolumab, PD-1 programmed death 1, PD-L1 PD-1 ligand, Pembro pembrolizumab, Tram trametinib, TVEC talimogene laherparepvec, and Vem vemurafenib. Adapted from [106].

### 7.3. Immunotherapy: Immune Checkpoint Inhibitors

Immune checkpoint proteins PD-1 (programmed death-1) and CTLA-4 (cytotoxic T lymphocyte antigen) are coinhibitory protein receptors expressed on the cell surface of lymphocytes, whose primary physiologic role is maintaining self-tolerance and limiting inflammatory responses in normal tissues. The cognate ligands for PD-1 and CTLA-4 (PD-L1/PD-L2 and B7, respectively) are expressed on tumor cells or other immune cells (mainly antigen-presenting cells or APCs) and serve to restrain T-cell function (Figure 17) [109]. Immune checkpoint inhibitors (ICIs) are monoclonal antibodies that target these restraining mechanisms to reinstate T-cell position. To date, three ICIs have been approved for the treatment of melanoma: Pembrolizumab (anti-PD-1), Nivolumab (anti-PD-L1), and ipilimumab (anti-CTLA-4) [106]–[109], [119], [120], and other are in clinical trials (e.g., LAG-3 and TIM3) [121]. As

single agents, Pembrolizumab and Nivolumab are more effective than Ipilimumab, but the ipilimumab + Nivolumab combination had the most remarkable effect on patient 2-year OS (Figure 16) [106], [109].

However, dual immune checkpoint blockade induces high-grade toxicity (grade 3/4) in >50% of patients, leading to treatment interruption or discontinuation [109]. Common side-effects of ICIs manifest as immune-mediated reactions against healthy tissues, known as immune-related adverse events (irAEs). Fortunately, recent data shows that progression-free survival and overall survival are similar for patients who had to discontinue treatment because of irAEs compared with the general population [122]. ICIs increased patient outcomes significantly and durably, as over half of the melanoma patients (52%) treated with ipilimumab + nivolumab were still alive after five years [122]. Atezolizumab (anti-PD-L1) is another ICI approved in melanoma in combination with Cobimetinib and Vemurafenib for patients with *BRAFV600* mutation-positive unresectable or metastatic melanoma [106]. Overall, the current standard of care remains either ipilimumab + nivolumab or anti-PD-1 in *NRAS* or *BRAF* melanomas.

Despite the impressive data, which patients require dual ICB versus single-agent PD-1 blockade remains unclear. Given the lack of robust predictive biomarkers with a negative predictive value, the decision to treat with anti-PD-1 and/or anti-CTLA-4 mAbs may be driven by patient characteristics, including age, comorbid medical conditions (including autoimmune disorders), and the burden of metastatic disease. However, data supporting these practices are limited [92]. In addition, for still unclear reasons, response rates range from 45–60% in melanoma [123]. There are several explanations for the lack of response. These include oncogenes and oncoproteins, genetic and epigenetic dysfunction, loss of sufficient antigens, dysfunctional T cell compartment, lack of inflammation in the tumor microenvironment, dysregulated tumor immuno-metabolism, the influence of microbiome, and inept host immunity [111].

In conclusion, around half of the patients do not respond to ICIs (innate resistance), but those who do have a durable response that turns melanoma into a “chronic disease.” Much research is still needed to identify predictive markers of ICI response, but we can undoubtedly admit that ICIs have revolutionized melanoma treatment.

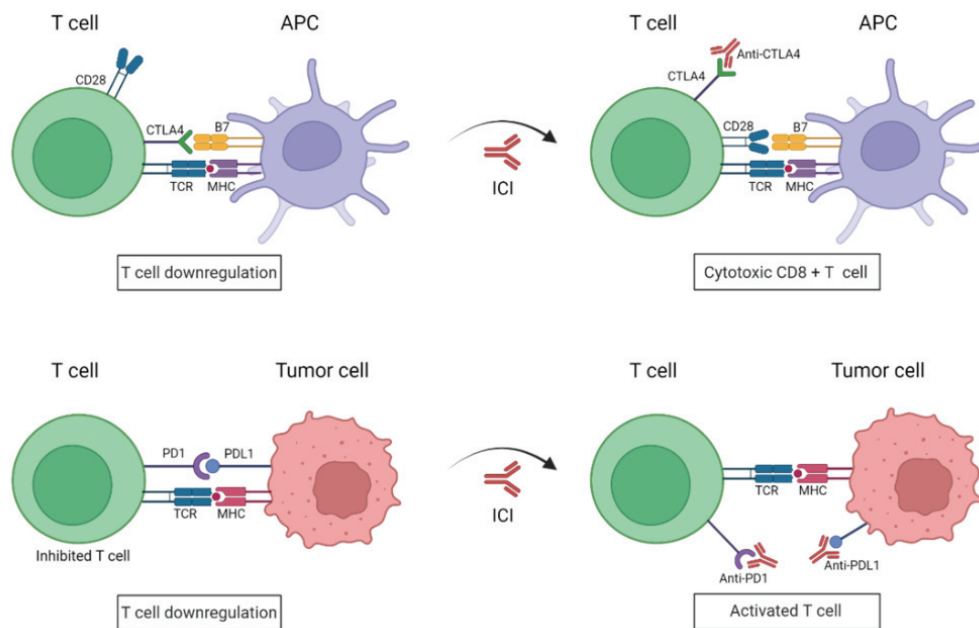


Figure 17: Representation of immune checkpoint blockade.

The two ligands CTLA-4 and CD28 present in T cells have the same receptor (B7) on antigen-presenting cells (APC). CTLA-4 inhibits the T-cell, whereas CD28 activates it. CTLA-4 has a higher affinity to B7 than CD28, leading to a predominance of inhibitory T-cell signals. PDL1 on tumor cells binds PD1 on the activated T cells, inducing T-cell exhaustion. Immune checkpoint inhibitors (ICI) are antibodies (anti-PD1, anti-PDL1, and anti-CTLA-4) that allow T cells to regain their functions. Adapted from Morante et al. [120].

#### 7.4. Resistance to KIs and ICIs

Even though *NRAS*-mutant melanoma constitutes around 20% of melanoma cases, not many studies were performed to understand the limited efficacy of MEKis in this context [114]. For this reason, this part will focus on *BRAF*-mutant melanoma and the well-described resistance encountered in patients treated with BRAFi/MEKi. Similar mechanisms could be expected in *NRAS* melanoma.

The leading cause of resistance to kinase inhibitors is the reactivation of the MAPK pathway, occurring in 80% of BRAFi-resistant tumors. This may be due to changes in the BRAF protein due to alternative splicing or overexpression of *BRAFV600E*. Moreover, as tumor heterogeneity for *BRAF V600*/wild-type *BRAF* is well documented, the resistance can be due to interactions of BRAF inhibitors with wild-type BRAF proteins. Overexpression of CRAF or COT1 kinases (Mitogen-activated protein kinase kinase kinase 8), activating mutations in *NRAS*, *MEK*, amplification of *MITF*, mutations in *RAC1* (Rac Family Small GTPase 1), and the

loss of *NF1* can also reactivate this or alternative pathways [110], [117]. The PI3K/AKT/mTOR pathway has also been implicated in resistance through mutations in *AKT1*, *AKT3*, *PIK3CA*, *PIK3CG*, *PIK3R2*, and *PTEN* loss. The overexpression of multiple receptor tyrosine kinases (RTKs), including epidermal growth factor receptors (EGFRs), insulin-like growth factor 1 receptors, platelet-derived growth factor receptors  $\alpha$  and  $\beta$  or fibroblast growth factor receptor 3, have been reported in resistant melanoma tumor [117]. These mechanisms are detailed in many papers, such as references [108]–[110], [115]–[118]. These events occur after months of treatment, leading to irreversible acquired resistance. Another mechanism occurs in the first hours after treatment with KIs, leading to a reversible KI tolerance: relief of MAPK negative feedback (please refer to section I-7 for more details). Within hours of MAPK inhibition, pathway rewiring will disturb feedback signals, allowing ERK activity to recover. Following this, intracellular signaling pathways rewire, partly due to extracellular signals leading to the adaption of cancer cells to the drug insult. Continuous treatment with KIs leads to resistant clones that will ultimately and irreversibly re-establish tumor growth (Figure 18) [118]. It is important to note that combining BRAFi with MEKi slows the development of resistance compared to BRAFi monotherapy [116]. Resistance occurs in most KI-treated patients in less than a year, highlighting the need for alternative treatments [101].

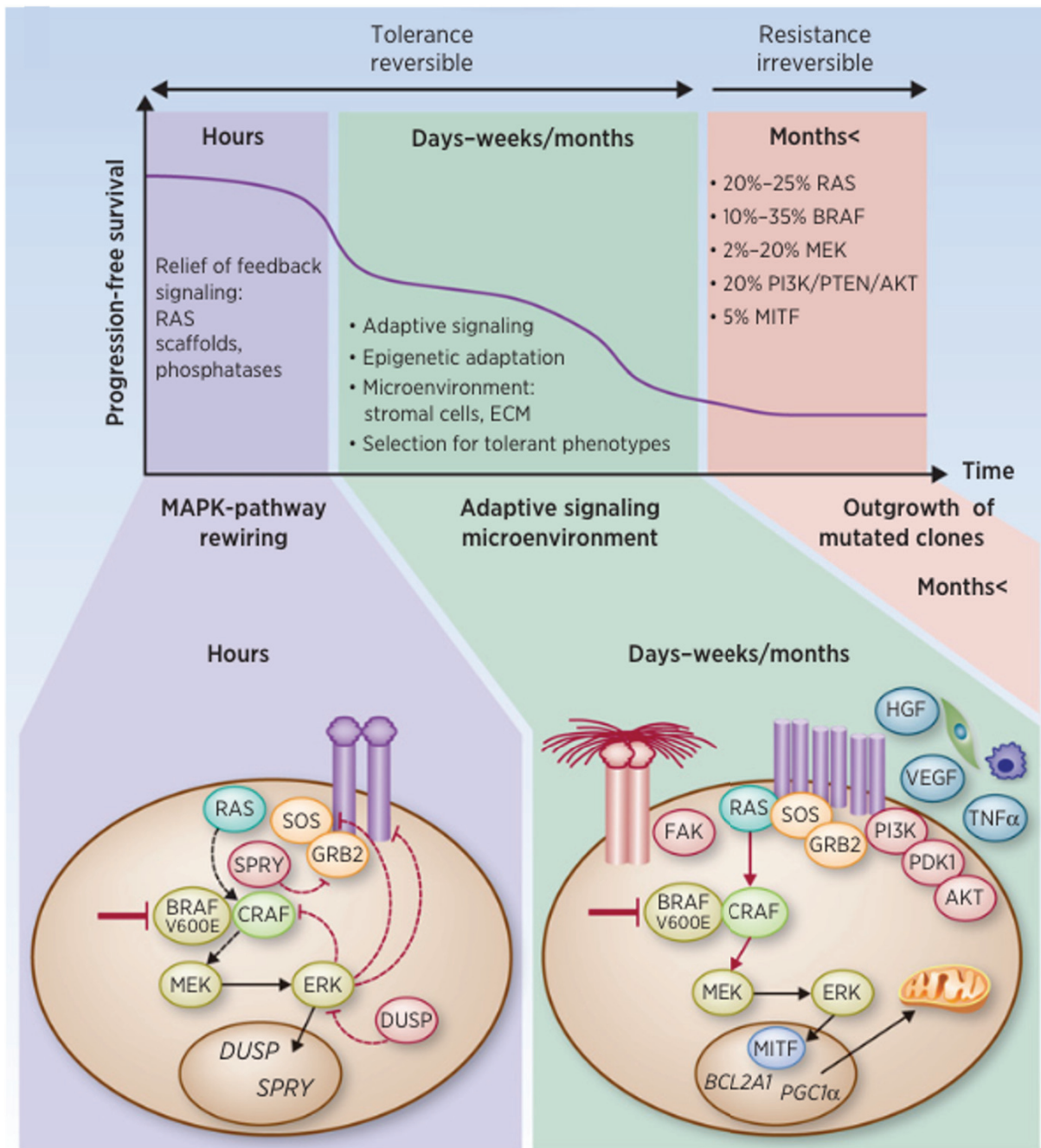


Figure 18: Dynamic responses to MAPK inhibition.

Following immediate responses to MAPK inhibitor therapy is a phase of reversible non-mutational tolerance before mutated resistant clones irreversibly re-establish tumor growth. Progression-free survival is proportionally reduced to follow the trend of resistance emergence. Within hours of MAPK inhibition, the pathway's feedback signals are modified to reinstate ERK activity. Following this, intracellular signaling pathways rewire through the alteration of many central proteins (described in the section above), leading to the adaption of cancer cells to the inhibitors. Adapted from [118].



As discussed previously, resistance to treatments in melanoma can occur through genetic alterations. Different studies have now shown that melanoma develops resistance to therapy through phenotype switching and TME remodeling as well [96]. For instance, Hossain et al. (2022) [124] showed that non-responding melanomas to anti-PD1 therapy are enriched for genes characteristic of undifferentiated and neural crest-like differentiation states, while in contrast, responding melanomas exhibit expression signatures mainly characterized by transitory and melanocytic state gene signatures, supporting the notion that phenotype switching behavior characterizes responding versus non-responding melanomas.

In addition to the epigenetic and translational alterations associated with melanoma phenotype switching (section III-B-5), recent studies revealed a novel mechanism of adaptation to KIs whereby melanoma cells establish a positive mechano-signaling loop powered by autocrine remodeling of a drug protective ECM [95], [125], [126]. BRAFi-resistant melanoma cells characterized by dedifferentiated mesenchymal-like or NCSC-like phenotypes display a pronounced mechano-sensitivity and elevated mechano-signaling when plated on rigid collagen substrate. This substrate reproduces what is seen *in vivo* with the accumulation of collagen fibers and tumor stiffening in KI-treated mice. The increase in mechano-signaling is caused by an increased nuclear translocation and transcriptional activity of YAP and MRTF, two major mechano-sensitive transcriptional co-activators [126]. Elevated YAP expression is a biomarker of poor response to KIs in patients with BRAF-mutant tumors, and combined YAP and MAPK inhibition is synthetically lethal in BRAF- and RAS-mutant melanoma through synergistic induction of apoptosis [126].

Diazzi *et al.* [126] also reviewed in their paper the known phenomena implicated in resistance to KIs through modulation of the ECM. BRAF kinase inhibitors have been described to alter the TME by acting on both melanoma-associated fibroblasts (MAF) and melanoma cells to promote resistance.

After treatment with KIs, activation of MAF in the TME induces the secretion of pro-survival factors such as hepatocyte growth factor (HGF) from fibroblasts, which underlies an innate mechanism of drug resistance. In addition, aged MAF release the secreted frizzled related protein 2 (sFRP2), a Wnt-antagonist, impairing the response to MAPK KIs by decreasing  $\beta$ -catenin and MITF signaling [126]. Moreover, exposure to KIs induces the autocrine production of TGF $\beta$  by melanoma cells, which activates local fibroblasts into myofibroblasts that deposit fibronectin in the TME, generating a “resistance tumor niche”, in which melanoma cell

adhesion to the fibronectin-enriched ECM amplifies the pro-survival signals released by MAF such as HGF [126]. The fibronectin-enriched ECM also promotes adhesion-dependent signaling through the integrin $\beta$ 1/FAK/SRC axis, allowing melanoma cells to tolerate BRAFi. Melanoma cells exposed to KIs have been described to induce a pro-fibrotic rewiring of the tumor niche, inducing fibrosis. Fibrosis is associated to inflammation, caused by the production of IL1 $\beta$  by tumor-associated macrophages which mediates the production of a CXC chemokine receptor 2 (CXCR2)-driven secretome by fibroblasts, further promoting tumor progression. In fact, the autonomous ability of melanoma cells to produce and shape their own ECM is now recognized as a major adaptation strategy in response to KIs [126].

BRAF inhibition increases the production of fibronectin by PTEN-null melanoma cells, as well as the cells' adhesion to  $\beta$ 1 integrin, which in turn promotes drug resistance through AKT signaling and MCL-1 (Myeloid cell leukemia 1) expression. BRAF inhibition also increases type I collagen production and deposition by melanoma cells, independently of TGF $\beta$  signaling.

The remodeling of the ECM and the TME by KIs in melanoma generates a host-tumor niche that protects melanoma cells from therapeutic insults. This highlights the importance of future combinational treatments targeting the TME in addition to the KIs [126]. Future approaches could involve targeting the collagen cross-linkers LOX and LOXL2, using anti-fibrotic drugs such as Nintedanib, blocking ECM signaling by targeting integrins, FAK kinase or collagen receptors DDR1/2 and blocking the aberrant intracellular mechano-transduction pathways by targeting the RHO GTPase and its mediated actomyosin cell contractility, or by targeting YAP or MRTF [126].

## 7.5. Adjuvant systemic therapy

For high-risk patients (high-risk stage II melanoma or node-positive disease) with resected melanoma, adjuvant systemic therapy is offered to reduce the risk of melanoma recurrence after surgery. Before 2015, high-dose IFN $\alpha$ -2b was the only approved therapy for adjuvant treatment, with a consistent albeit modest benefit in recurrence-free survival (RFS) and, to a lesser extent, an OS benefit [109]. Since 2015, all three ICIs (Ipilimumab, Nivolumab, and pembrolizumab) have been approved for use in the adjuvant setting. Similar to what has been described in treatment, Nivolumab and Pembrolizumab demonstrate better responses than

Ipilimumab. The combination of dabrafenib + trametinib has also been approved for adjuvant use in *BRAFV600-mutant* melanoma. Completion lymph node dissection is no longer the standard of care for patients with positive sentinel lymph node biopsy, and anti-PD-1 or BRAFi/MEKi therapies are the new frontline options for adjuvant therapy [109]. It is still unclear whether ICI or dual KI therapy is preferable, as both show a similar recurrence-free survival of around 67% of patients 18 months after treatment. Even though PD-1 ICI seems more tolerable than BRAFi/MEKi (15% vs. 25% patients stopping treatment because of adverse events), PD1 ICI, as all ICIs, harbor the risk of severe or irreversible irAEs. Similarly to what occurs in therapy for patients eligible for both ICIs and dual KI (i.e., *BRAFV600-mutant* melanoma), the adjuvant choice between PD-1 blockade or BRAFi/MEKi therapy is driven by patient characteristics. Management of patients who recur after adjuvant therapy includes surgical resection of locoregional disease, alternative active agents, and clinical trials [109].

## 7.6. Emerging therapies

This section will briefly review emerging therapies from ongoing clinical trials [94].

The high effectiveness of TTs and ITs led to the evaluation of sequential combinations of these drugs in *BRAFV600-mutated* melanomas [119].

Another interesting approach in clinical trials is using intralesional vaccines to stimulate the immune system. Talimogene laherparepvec (T-VEC) is an oncolytic vaccine derived from herpes simplex type 1. It selectively replicates within tumors, leading to a systemic antitumor immune response by producing granulocyte-macrophage colony-stimulating factor (GM-CSF).

mRNA vaccines are emerging as new therapeutic tools to increase the anti-tumoral immune response. In the recent years, many mRNA vaccines have been developed and tested in melanoma. Vaccines could be based on melanoma-associated antigens or tumor-specific antigens [127]. The first category of vaccines targets one of several markers including, but not restricted to, glycoprotein 100 (gp100), melanocyte antigen (MELAN-A/MART1), melanoma chondroitin sulfate proteoglycan (MCSP) and NY-ESO. Unfortunately, these vaccines have been shown to induce an autoimmune reaction that targets healthy melanocytes. mRNA vaccines based on tumor-specific antigens, known as neoantigens, elicit stronger immune responses than those based on tumor-associated antigens. Neoantigens or neoepitopes are new proteins caused by mutations that occur in tumor DNA, making them a specific target in

cancer cells. Neoepitopes can be divided into two classes: neoantigens that are only found in a particular type of cancer are called shared, and those that are specific to a patient are called personalized. *BRAF* and *NRAS* mutations, for example, are shared neoepitopes that are observed in approximately 50% and 15–25% of melanomas, respectively. For vaccination involving neoantigens, the whole genome is sequenced after tumor biopsy and compared with healthy tissues to identify existing mutations. Each mutation is then evaluated using bioinformatics algorithms to determine its affinity to bind to the MHC molecule and elicit an immune response. Bidram *et al.* [127] reviewed the mRNA vaccines currently being investigated in melanoma, and they described the several ongoing phase II studies that are evaluating personalized mRNA vaccines in advanced melanoma. One ongoing study that stand out is mRNA-4157 (NCT 03897881), a candidate mRNA vaccine developed by Moderna and Merck. mRNA-4157 is a novel mRNA-based personalized cancer vaccine that encodes up to 34 patient-specific tumor neoantigens. The randomized KEYNOTE-942 trial assessed the efficacy of this vaccine in prolonging the recurrence free survival (RFS) in patients advanced melanoma, when given in combination with pembrolizumab, the standard-of-care adjuvant therapy in this patient population. According to the results of the primary trial analysis, after 18 months, there was a 44% reduction in the risk of recurrence or death in patients who received both the vaccine and pembrolizumab compared to those who only received pembrolizumab (Date from clinicaltrials.gov, NCT 03897881). Final results of the trial are expected for 2024 but are nonetheless very promising.

Other arising therapies in melanoma clinical trials include immunostimulatory cytokines (Darleukin and Bempegaldesleukin), oncolytic viruses, anti-vascular endothelial growth factor (e.g., Bevacizumab), the targeting of inhibitory molecules involved in monocyte/macrophage differentiation (CSF1Ri) or immune tolerance (IDO1), T cell agonists (of TLR9, OX40, GITR, 4-1BB, CD27), and adoptive T cell therapy [108].

## **8. Melanoma: conclusion and unanswered questions**

Despite the extraordinary improvement in clinical outcomes of melanoma patients in the past decade, mainly due to targeted therapies (KIs) and immunotherapy (ICIs), not all patients respond to the approved systemic treatments. Single-agent PD-1 blockade and combination BRAFi/MEKi therapy demonstrated a long-term, 5-year OS benefit of 30-40%. Superior

response rates have been shown with combined PD-1/CTLA-4 blockade, with a numerically higher, although not statistically significant, OS benefit compared with single-agent PD-1 blockade [109]. In addition, most clinical trial focus on the most frequent (>50%) molecular subtype of melanoma: *BRAF*-mutated melanoma, while *NRAS*-mutated melanoma (in >20% of patients) and other less frequent subtypes still lack effective treatments. Although progress has been made in identifying features associated with response and resistance to cancer immunotherapy, more work is needed to establish reliable predictors of long-term response to ICIs. Another critical feature of melanomas is the adaptation and resistance to KIs, mainly through the reactivation of the MAPK pathway. Patients could benefit from inhibiting alternative pathways along with the MAPK pathway to counteract this resistance. Another critical question focuses on the identity of the tumor-targeted antigens. There is broad consensus that UV-induced tumor-specific neoantigens may be recognized by CD8 T cells, but the overall mutational burden is an imperfect predictor of clinical response [109]. In short, much research is still needed for more effective and durable melanoma treatment.

## IV. Context and objectives of my Ph.D. research

### 1. ERK-MyD88 interaction as a novel target for cancer treatment

Previous reports showed that the TLRs/IL-1Rs adaptor protein MyD88 plays a part in the pro-tumorigenic inflammatory response [128], [129]. Our team showed that MyD88 has a non-canonical function, in which MyD88 could be pro-tumorigenic, independently of inflammation. MyD88 interacts via its D-domain with the DRS (more specifically, CD region of the DRS) of ERK and that this protein-protein interaction (PPI) is required for *RAS*-dependent cell transformation and cancer cell survival *in vitro* and *in vivo* [50], [51]. This interaction occurs selectively in cancer cells [51], making it an ideal target for cancer treatment. Accordingly, we screened for small chemical molecules that inhibit the ERK-MyD88 interaction (Virard *et al.*, in review, found at the end of this manuscript, Annex 2, Article 1). Two families of inhibitors were identified, including our proof-of-concept molecule EI-52. EI-52 induces rapid immunogenic apoptotic cancer cell death *in vitro* and an anti-tumoral activity *in vivo* by direct cancer cell death induction and activation of an anti-tumoral T-cell response (Virard *et al.*, Annex 2).

### 2. ERK-MyD88 interaction inhibitor: EI-52

EI-52's structure and biological activities are explained in our recent paper (Virard *et al.*, Annex 2). In this section, the outlines of these findings will be discussed. Please refer to the article at the end of the manuscript for further information.

A small-molecule library was screened for ERK-MyD88 interaction disruptors using a homogeneous time-resolved fluorescence (HTRF) assay containing a MyD88 D-domain peptide and a recombinant ERK protein. Two distinct chemical families were found with similar *in vitro* and cellular activities. EI-52 is a benzimidazole compound (Figure 19) that binds directly to ERK-1 and ERK-2 (predicted interactions with D316, D319, and E79 in ERK-2).

In *KRAS* mutant HCT116 colon cancer cells, ERK KIs (VX11e, GDC0994, SCH772984, and LY3214996) only slowed cell recovery, while EI-52 induced rapid cell death. Untransformed human cells (HCEC and HBEC) did not show cell death after treatment with EI-52, indicating that EI-52 induces cell death, specifically in cancer cells. An extended analysis of 301 cell lines

from the Oncopanel™ collection (Eurofins) showed that most were sensitive to EI-52 at the micromolar range and that EI-52 shows a distinctive sensitivity pattern, different from that of KIs and other classes of drugs. EI-52 does not impact ERK kinase activity, and neither its activation by MEK consistent with the ability of MEK to interact with ERK independently of the DRS [130]. Interestingly, in contrast to KIs, EI-52 treatment resulted in the activation of RSK, but not c-Myc, and the increased expression of DUSP5 and DUSP6, indicating that EI-52 considerably perturbs the activation and regulation of ERK partners. EI-52 induces phospho-ERK accumulation in the cytoplasm. This delocalization is accompanied by an increased eIF2 $\alpha$  phosphorylation and expression of ATF4 and CHOP, all of which point to an ongoing integrated stress response (ISR), which leads to apoptosis.

In two different mouse models (a syngeneic Lewis Lung Carcinoma and a spontaneous lung tumor model), EI-52 showed a dose-dependent inhibition of/protection from (respectively) tumor growth. No signs of toxicity were detected in the treated mice's liver, kidney, and spleen, and none died while in treatment (n=107). EI-52 toxicity was also assessed in the highly sensitive chicken embryonic chorioallantoic membranes (CAM). It resulted in no embryo death or malformations, indicating that inhibiting ERK-MyD88 interaction might be safe *in vivo*.

Cell death was assessed 48 hours after EI-52 treatment of patient-derived tumor organoids from colorectal and lung tumor surgical samples. ERK-MyD88 interaction inhibition induces apoptosis in both models. We also evaluated EI-52's activity using a different *ex vivo* approach in undissociated thick sections of head and neck cancer surgical pieces. EI-52 treatment for 24 hours induced strong c-PARP staining almost exclusively restricted to tumor cells. These results suggest ERK-MyD88 PPI with EI-52 can kill human cancer cells *ex vivo* without apparent toxicity.

Transcriptomic analysis of HCT116 cells treated with EI-52 showed an upregulated transcription of NF- $\kappa$ B-dependent inflammatory genes, including chemokines. Production of chemokines by dying cancer cells indicates immunogenic cell death (ICD). Other markers of ICD detected after treatment with EI-52 include the release of damage-associated molecular patterns such as ATP, which has chemotactic activity, and HMGB1, an endogenous TLR4 ligand. U0126, a MEK kinase inhibitor that inhibits ERK activation, did not induce any mediator of ICD, further highlighting the difference between inhibition of ERK kinase activity and ERK-MyD88 PPI. Mice models of CT26 colon cancer treated for 24 hours with EI-52 show a rapid

apoptotic cancer cell death *in vivo*, assessed by cleaved-PARP staining. Using the same CT26 colon cancer cells, syngeneic models with wild-type (WT) or BALB/c mice were generated. EI-52 showed a much more significant anti-tumoral effect in WT T-cell competent mice, suggesting that EI-52 induces an immunogenic cancer cell death and activates an anti-tumoral T-cell response *in vivo*.

In conclusion, these results suggest that disrupting ERK activity by targeting its interaction with MyD88 could be an interesting novel approach for cancer treatment.

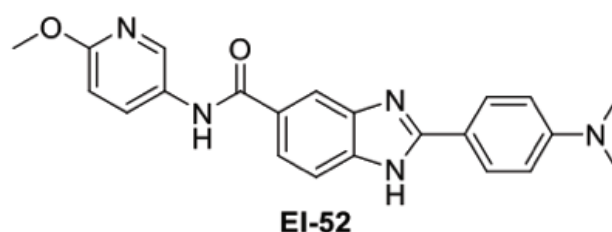


Figure 19: EI-52 chemical structure.

### 3. Objectives of my Ph.D. research

The dramatic advances in the past decade with KIs and ICIs represent a qualitative jump from the previous standard of care for melanoma. Progress in the coming decade will focus on new strategies to avoid the obstacles to treatment described in the earlier sections, such as innate and acquired resistance.

In this context, given the constitutional activation of ERK in melanoma, as well as the need for new treatment options due to resistance to current treatment, my Ph.D. work focused on evaluating EI-52 in a melanoma model. EI-52 was evaluated as a novel inhibitor for treating melanoma, including KI-resistant melanoma and the often-neglected *NRAS*-mutant melanoma subtype. Using EI-52, we studied a novel approach to MAPK inhibition in melanoma through protein-protein interaction inhibition.

First, we evaluated the impact of ERK-MyD88 interaction inhibition in *BRAF* and *NRAS* melanoma *in vitro*. We then generated KI-resistant cell lines and compared their response to that of KI-sensitive cell lines. Proliferation and cell death were measured, and the type of cell death was characterized. EI-52 was also tested in 3D melanoma spheroid models that are sensitive or resistant to KIs, and in two KI-resistant patient-derived cell lines. In addition, we



tested the capacity of EI-52 to induce resistance using two different resistance-induction protocols and analyzed the molecular and functional response to EI-52 in this context. Given the urgent need for novel targeted therapies in *NRAS*-melanoma, we tested EI-52 efficacy in syngeneic *NRAS*-melanoma models *in vivo* as a single agent or in combination with an anti-PD1.

Another part of my Ph.D. research aimed to understand the impact of ERK-MyD88 inhibition on the ERK interactome. This question was addressed by ERK co-immunoprecipitation in the presence or absence of EI-52, followed by mass spectrometry. Although this part is still preliminary, it will be reported and discussed in this thesis.



## Results

Article in preparation:

**ERK-MyD88 interaction inhibition, a novel therapeutic approach in resistant melanoma.**

Rita Frem<sup>1</sup> ; Melissa Masmoudi<sup>1</sup> ; Nader Hussein<sup>1</sup> ; Valentin Benboubker<sup>1</sup> ; Julie Caramel<sup>1</sup> ; Stéphane Dalle<sup>1 2</sup> ; Toufic Renno<sup>1</sup> ; Isabelle Coste<sup>1</sup>.

<sup>1</sup> Université de Lyon, Université Claude Bernard Lyon 1, INSERM 1052, CNRS 5286, Centre Léon Bérard, Centre de Recherche en Cancérologie de Lyon, Lyon, France.

<sup>2</sup> Dermatology Unit, Hospices Civils de Lyon, CH Lyon Sud, Pierre Bénite Cedex, France.

**Keywords:** ERK, Melanoma, Resistance, Protein-Protein Interactions, Therapy

**Financial support:** La Ligue contre le cancer – comité de l'Ain.

**Corresponding author:** Coste Isabelle

Lyon Cancer Research Center, 28 rue Laennec 69373 Lyon, France.

Tel: +33 469 166 630, Email: isabelle.coste@lyon.unicancer.fr

**Conflicts of interest:** The authors declare no conflicts of interest.

## Abstract

Melanoma is the deadliest form of skin cancer, with most patients harboring activating mutations in the Ras-MAPK pathway. Targeted therapies have greatly improved the outcome for melanoma patients. However, resistance emerges in most patients. The only other option for these patients is immunotherapy with immune checkpoint inhibitors, which have proven to be effective. Unfortunately, they are only effective in less than one third of the patients, for yet-to-be defined reasons.

We developed a new targeted therapy that perturbs ERK protein-protein interactions (PPI) rather than its kinase activity. This novel molecule, EI-52, induces an immunogenic and apoptotic cell death in both kinase inhibitor (KI)-sensitive and KI-resistant melanoma cell lines. In addition, melanoma cells chronically exposed to EI-52 (>1 year), retain the same sensitivity as EI-52-naïve cells, indicating a lack of acquired resistance.

*In vivo*, we showed that EI-52 treatment reduces tumor progression of *NRAS*-mutated melanoma, and that EI-52 synergizes with anti-PD1.

Together, these results show that our novel ERK PPI inhibitor, EI-52, induces apoptosis in melanoma *in vitro* and *in vivo*, with no emergence of resistance *in vitro*.

## Introduction

Melanoma is a malignant and aggressive form of skin cancer that is responsible for the most deaths out of all cutaneous cancers [131] [132]. It is relatively rare compared to other types of skin cancers, but its incidence has been increasing in the recent years [133]. If diagnosed at an early stage, most melanoma lesions are excisable and thus curable. However, at later stages, the treatment of metastatic melanoma is a great challenge [134]. Melanoma occurs when a melanocyte, the melanin-producing cell, undergoes a malignant transformation due to external or genetic factors. External factors include exposure to ultraviolet (UV) radiation, ageing and its associated deterioration in DNA repair mechanisms. All these factors lead to an increase in the somatic tumor mutational burden (TMB), making melanoma one of the cancers with the highest TMB (median of 14,4 mutations/Mb) of all cancer types [86].

Several signaling pathways are altered in melanoma, but the most frequent mutations are found in the MAPK-ERK pathway (mitogen-activated protein kinase – extracellular signal-regulated kinase), also known as the RAS-RAF-MEK-ERK pathway, a central pathway that regulates cell growth, proliferation, and apoptosis. Recent studies show that in over 50% of cutaneous melanomas, BRAF is constitutively active due to mutations, which are a substitution of a valine by a glutamic acid at the position 600 (*BRAFV600E*) in >80% of the cases. Another common mutation is the *NRAS* mutation, found in approximately 25% of melanoma patients, in most of the cases due to substitution of a glutamine at position 61 by an arginine, lysine, or histidine (respectively Q61R, Q61K and Q61H). *NRAS*-mutated melanomas are generally more aggressive and have a poorer response to treatments than *BRAF*-mutated melanomas [135]–[137]. Melanomas that possess a wild-type *BRAF* and *NRAS* often have other mutations in genes encoding proteins upstream of the MAPK pathway, such as NF1 and KIT, highlighting the importance of this pathway for melanoma carcinogenesis [87]. For this reason, this pathway has been the subject of intensive research for the development of novel treatments. In the last decade, a new era of targeted therapies changed the outcome for melanoma patients, with the discovery and the use of kinase inhibitors (KIs). Vemurafenib was the first KI approved for the treatment of patients with a *BRAFV600E* mutation, followed by dabrafenib and encorafenib. MEK inhibitors, such as trametinib and cobimetinib, were also introduced and used alone in *NRAS* melanoma, or in combination with *BRAFV600E* inhibitors in *BRAF*-mutated melanoma. These KIs have proven to be effective, continuously lowering the melanoma mortality rate [138]. However, in most cases, patients who initially responded to

KIs acquire resistance to these inhibitors, leading to further disease progression [115]. More recently, immunotherapies, more specifically immune checkpoint inhibitors (ICIs), have shown great and sustained responses in melanoma patients [122]. However, only around 40% of patients respond, for yet-to-be identified reasons [139]. Given the innate and acquired resistance to KIs and ICIs, there is an urgent need for novel treatments.

Previous work done in our lab shows that MyD88, an adaptor molecule in TLR and IL-1R (Toll Like Receptors and Interleukin-1 receptors) pathways, interacts with ERK, preventing its inactivation by its phosphatase MKP3 and therefore amplifying the activation of the MAPK pathway. This interaction was also required in a cell-autonomous fashion for MAPK activation and transformation *in vitro*, and RAS-mediated carcinogenesis in mice *in vivo* [50], [51].

Based on these results, we developed a novel protein–protein interaction (PPI) inhibitor, EI-52, that inhibits the ERK-MyD88 interaction, thus modifying the interactome of ERK without affecting its kinase activity. In many different cancer types, we have shown that EI-52 induces immunogenic, apoptotic cell death *in vitro* and an anti-tumoral T cell response *in vivo* (Virard *et al.*, Annex 2).

Considering that the majority of melanoma patients have an overly active RAS-MAPK pathway, as well as the urgent need for new treatments, we investigated the effects of EI-52 in melanoma models. In this study, we show that EI-52 induces an immunogenic and apoptotic cell death in KI-sensitive and KI-resistant *BRAF* and *NRAS* melanoma cells, without inducing resistance after up to one year of continuous treatment *in vitro*. In addition, EI-52 significantly improves survival in *NRAS* melanoma mouse models as a single agent and in combination with ICIs *in vivo*.

## Results

### **ERK-MyD88 interaction inhibition via EI-52 induces rapid apoptotic and immunogenic cell death in *BRAF* and *NRAS* melanoma.**

We have previously shown that ERK-MyD88 interaction inhibition by EI-52 induces apoptotic and immunogenic cell death. In fact, the effect of EI-52 was evaluated in multiple cancer types from a panel of 301 human cancer cell lines (Oncopanel™, Eurofins) (Virard *et al.*, Annex 2), and we showed that the majority of the cancer cell lines tested were sensitive to the ERK-MyD88 PPI inhibitor EI-52 at the micromolar range. Given the frequency of mutations affecting the RAS-ERK pathway in melanoma, as well as the need for novel therapeutic options due to innate or acquired resistance to current treatments, we thoroughly investigated EI-52's efficacy in this cancer type. We used two *BRAF*-mutated (A375, 501mel) and two *NRAS*-mutated (SKMEL2 and ALL-RAY) human melanoma cell lines. We treated A375 and SKMEL2 cells with different doses of EI-52 in comparison with the standards of treatment kinase inhibitors (KI), Vemurafenib and Trametinib, respectively. We measured cell proliferation and cell death for 48h using the Incucyte® live imaging system (Sartorius). We found that while, as expected, kinase inhibitors only block cell proliferation (Figure 1a), EI-52 induces a rapid dose-dependent cell death in all the melanoma cell lines tested, independently of the harbored mutation (Figure 1b). We focused on A375 and SKMEL2 for the rest of the study. Next, we treated A375 and SKMEL2 cells with EI-52 (6µM) for 24h and evaluated the activation of Caspase 3/7 and quantified the secretion of IL-8 and extracellular ATP in cell supernatants. Consistent with what we described in our previous work (Virard *et al.*, Annex 2), EI-52 induces an apoptotic cell death in both melanoma cell lines. This cell death is accompanied with an increased production of IL-8 and a significant release of extracellular-ATP, both markers of an immunogenic cell death (Figure 1c).

### **Inhibition of ERK-MyD88 interaction with EI-52 induces cell death in KI-resistant melanoma.**

Most melanoma patients who initially respond well to KIs acquire resistance to these inhibitors in a relatively short period of time. Apart from ICIs, that are only effective in around 40% of all melanoma cases, patients with acquired or innate resistance to KIs have no available effective targeted therapeutic option. In order to create a similar context *in vitro*, we treated A375, 501mel and SKMEL2 cells with increasing doses of Vemurafenib and/or Trametinib

starting at the IC50, until cells were able to grow in ten times the IC50 after approximately 12 weeks of treatment (Supplemental Figure1).

We then tested whether these KI-resistant and WT melanoma cell lines responded in a similar way to EI-52. We observed the same dose-dependent cell death induction after treatment with EI-52 in the Vemurafenib-resistant (VR) or Vemurafenib/Trametinib-resistant (VTR) A375 cell lines as compared to the parental cell line (Figure 2a). A similar result was obtained in the Trametinib-resistant (TR) SKMEL2 cell line as compared to the WT cell line.

In order to test EI-52 in more relevant cellular models, we generated WT or Vemurafenib-resistant 501mel cell spheroids using the hanging-drop technique. Both WT and resistant A375 and SKMEL2 cells failed to generate spheroids. 501mel spheroids were treated with Vemurafenib at IC50 (0,4  $\mu$ M) or EI-52 8  $\mu$ M, respectively and imaged for 7 days (Figure 2b). Vemurafenib slowed the growth of the sensitive spheroids, but not the resistant spheroids, confirming the acquired resistance of these cells. Propidium iodide staining, performed 48h after treatment, shows that spheroids were dying exclusively in the EI-52 condition, until almost no 3D structures could be seen, in both sensitive and resistant models. This shows that EI-52 efficiently induces cell death in resistant melanoma spheroids.

We then tested efficacy of EI-52 in a *BRAF*-mutated cell line (Goka) derived from a patient who acquired resistance to BRAFi. Cells were treated with different doses of single-agent or combination Vemurafenib/Trametinib, or EI-52. Cell proliferation and cell death were then measured for 72 hours using the Incucyte® live imaging system. As expected, Vemurafenib alone did not have any effect on the Goka cell line, while Trametinib as single agent or in combination with Vemurafenib, slightly slowed cell proliferation. However, neither of these kinase inhibitors as single agents, nor their combination, induced cell death, even when used at very high doses (up to 25x average *in vitro* standard IC50 for Vemurafenib, 10x for Trametinib). In contrast, EI-52 induces strong and rapid cell death (Figure 2c). Similar results were obtained with another *BRAF*-mutated cell line (ESP) derived from a patient who acquired resistance to BRAFi (Supplemental figure 2). Taken together, these data suggest that ERK-MyD88 PPI inhibition could potentially be an interesting option for second-line treatment of relapsed patients with acquired resistance to KI.



### **EI-52 does not induce resistance in melanoma cell lines after up to 1 year of continuous treatment.**

Having shown that EI-52 is effective on KI-resistant cells lines, we asked whether EI-52 itself induces resistance. Two protocols are described for generating resistance. The most commonly used is to increase the treatment dose to obtain a line proliferating at 10 times the IC50. While cells treated according to this protocol readily developed resistance to Vemurafenib and Trametinib, no resistance was observed with EI-52, which killed virtually all cells at 2xIC50 (Figure 3a) (n=2).

KI inhibitors induce resistance partly by rapidly altering the MAPK pathway negative feedback loop [118]. Since EI-52 does not induce resistance, we asked whether this was due to an absence of effect of EI-52 on this feedback loop. Given the continuously activated status of the MAPK pathway in melanoma cell lines, these would not be an ideal model to study feedback loops regulation. We instead used an inducible NIH3T3 ER:RAS system, which allows the analysis of the MAPK as early as minutes following RAS activation. Western Blot analysis of the inhibitory phosphorylation of CRAF on residues S289/296/301 and MEK on Thr292 - both part of the negative feedback regulation of the MAPK pathway by ERK- was performed. We show that whereas the MEK KI U0126 strongly reduced these inhibitory phosphorylations, EI-52 had no effect on these loops, as compared to the control condition (Figure 3b). This indicates that EI-52 does not impact the early drug-resistance mechanisms that are described in KI-resistance.

Another protocol is to maintain the treatment at a low dose over a long period of time to induce a chronic adaptation. SKMEL2 and A375 cells were continuously treated with 4 $\mu$ M of EI-52 for 8 months and 1 year, respectively. The IC50 response to EI-52 in parental and chronically treated cells was measured using the CellTiter-Glo ATP assay (Figure 4a). We found at the end of the treatment periods that both parental and chronically exposed cells had a comparable IC50 in response to EI-52. As in WT cells, death of both KI-resistant and chronically-exposed cell lines in response to EI-52 was apoptotic (figure 4b) and showed immunogenic cell death markers such as IL-8 (figure 4c), and ATP secretion (Supplemental figure 3).

We had shown that EI-52 deregulates the expression of the ERK phosphatase DUSP5 (Virard et al., Annex 2). Similarly, we found that EI-52 induces an up-regulation of DUSP5 both in WT and resistant melanoma cell lines (Figure 5), suggesting that EI-52 has the same mode of action

in melanoma as in other tumor types. In addition, different proteins associated with resistance mechanisms in melanoma were assessed in WT, KI-resistant, and EI-52-chronically treated cells. While the KI-resistant cell lines showed a distinctive molecular signature of resistance such as the loss of the inhibitory CRAF phosphorylation by ERK negative feedback and the activation of pAKT as a parallel pathway, the EI-52-chronically treated cells did not show a resistance signature (Figure 6a). Slight variations in MITF levels were detected in the EI-52 chronically treated cells: decrease in A375 and increase in SKMEL2 (Figure 6a). MITF dysregulation is linked to melanoma's "phenotype-switching" and cellular plasticity (differentiation and invasive capacities) [140]. To evaluate the impact of the alteration of MITF levels in these cells, we evaluated their migration potential in a scratch wound system. After treating the cells with mitomycin to block cell proliferation, cell migration was evaluated for 72 hours as the percentage of cell density migrating to close the wound (n=2) (figure 6b). In both *BRAF*- and *NRAS*-mutated cell lines, the WT cells migrated faster than the others, and with exception of the Vemurafenib-Trametinib-resistant variant of the *BRAF*-mutated A375 cells, there was no significant difference between KI-resistant and chronically-treated non-resistant cell lines. This is an important finding, since it suggests that neither resistance to KI nor chronic treatment with EI-52 is likely to bestow on melanoma cells an increased migration ability.

### **EI-52 treatment improves survival in a syngeneic *NRAS* melanoma mouse model**

The *NRAS*-mutated mouse melanoma cell line, TyrNRas 6.1, was first tested *in vitro* in order to determine the experimental conditions for *in vivo* studies. Cells were treated with different doses of EI-52 or Trametinib. Cell proliferation and cell death were measured for 48 hours using the Incucyte® live imaging system. We found that EI-52 induces cell death whereas Trametinib only marginally reduced cell proliferation and did not induce any cell death even at the higher concentrations (Figure 7a). Accordingly, we decided to investigate the anti-tumoral activity of EI-52 *in vivo*. We tested EI-52 in a syngeneic model where C57BL/6 mice (n ≥ 6/group) were injected subcutaneously with TyrNRas 6.1 cells. When tumors reached 100 mm<sup>3</sup>, mice were treated daily by intraperitoneal injection of EI-52, until any endpoint was reached (tumor volume ≥ 2500 mm<sup>3</sup> or necrosis). The treatment resulted in a dose-dependent reduction in tumor growth and an increase of survival probability (Figure 7b). In view of these data and other data from our lab showing that EI-52 induces immunogenic cell death *in vitro*

and an anti-tumoral T cell response *in vivo*, we hypothesized a potential synergy between EI-52 and immune checkpoint inhibitors *in vivo*. Using the same syngeneic mice model, we treated mice intraperitoneally with EI-52, anti-PD1, or a combination of both. We found that EI-52 as single agent increased the survival probability compared to control and anti-PD1 (Figure 7c). The combination of EI-52 with anti-PD1 had the most remarkable effect, with the survival probability significantly increased, compared to either molecule as a single agent (n=2). This shows that EI-52 synergizes with immune checkpoint inhibitors such as anti-PD1.

## Discussion and conclusion

Protein kinases regulate nearly all aspects of cell life, and alterations in their expression, or mutations in their genes, cause cancer and other diseases. The emergence of protein kinase inhibitors in cancer therapy has led to a paradigm shift in cancer therapy, greatly improving the outcome of cancer patients. To date, more than 70 KIs are approved by the FDA for clinical use [141]. Melanoma patients, especially those harboring a *BRAF V600E* mutation, have seen a remarkable improvement in overall survival after the discovery of BRAF kinase inhibitors [142]. *BRAF* mutation remains the main driver event in melanoma, detected in about 50% of tumors, while *NRAS* is the predominant *RAS* isoform mutated in 25% of all cutaneous melanomas [143]. *NRAS* melanomas are more aggressive and respond less to current treatment options than *BRAF* melanomas [114], [135]. KIs and immune checkpoint inhibitors (ICIs), mainly anti-CTLA4 and anti-PD1, are recommended for the treatment of melanoma patients. Unfortunately, due to innate or acquired resistance, patients either do not or stop responding to both treatments [40] [139] [144]–[150]. All these factors highlight the urgent need for new effective melanoma treatments.

In this report, we describe the effects of our novel ERK-MyD88 PPI inhibitor, EI-52 (Virard *et al.*, Annex 2) in KI-sensitive and KI-resistant melanoma models *in vitro*, as well as in a *NRAS* syngeneic mouse model *in vivo*.

Kinase inhibitors are described to induce a late cell death after a prolonged cell cycle arrest *in vitro* [151], [152], [153]. This delay could be responsible for the emergence of resistance to KIs, through different adaptative processes that lead to the reactivation of the MAPK pathway in the majority of the cases [110], [117]. In this study, we show that EI-52 induces a rapid apoptotic cell death that begins 8h post-treatment in both KI-sensitive and KI-resistant *BRAF* and *NRAS* melanoma cell lines *in vitro*, as well as in KI-sensitive and KI-resistant *BRAF*

melanoma 3D spheroid models. This fast-occurring death prevents the onset of the long adaptative processes involved in resistance to KIs. While the long mutational processes may take months or years to happen [147], they begin with the rapid inhibition of the negative feedback loops of the MAPK pathway, a few hours after the treatment with KIs [118]. Treatment with EI-52 did not inhibit these loops, while U0126, a MEK KI, effectively inhibited them (Figure 3b). This is due to the fact that EI-52 does not impact the kinase activity of ERK, leading to undisturbed negative feedback loops. The dose-escalating protocol we used to generate our KI-resistant cell lines is the most commonly used technique for generating KI-resistant models *in vitro* [154]. Using this protocol, EI-52 did not induce resistance (Figure 3a). Another common protocol is through continuous treatment at low doses [154]. The chronic exposition of melanoma cells to EI-52 (up to one year) did not have an impact on the cells' sensitivity to EI-52 (Figure 4), or on the negative feedback loops of the pathway (Figure 6a), or on their migratory capacities (Figure 6b), suggesting that EI-52 does not induce the later-occurring resistance mechanisms we mentioned above. Of course, an in-depth look should be taken on the genomic level, to verify if new mutations are acquired.

In accordance with what we described in our previous work (Virard *et al.*, Annex 2), the EI-52-induced cell death is accompanied with the release of ATP, and the production of IL-8, pointing to an immunogenic cell death (ICD), a form of regulated cell death known to activate an adaptive immune response in immunocompetent syngeneic hosts [155]. ICD improves the tumors' response to immunotherapy, by actively recruiting effector T cells in the tumor microenvironment (TME) [111]. The presence of T cells in the TME defines two subtypes of tumors, the "hot inflammatory tumors" and the "cold noninflamed tumors". Cold tumors represent the majority of human tumors and are less responsive to immunotherapy than "hot tumors" [111]. Kinase inhibitors have been linked to a negative regulation of the TME in melanoma [156]. We had previously shown the implication of an anti-tumoral T cell response to EI-52 treatment *in vivo* in a CT26 colon cancer model, most certainly induced by the ICD. This could explain the synergistic effect we obtained when combining EI-52 with the ICI anti-PD1 in our syngeneic *NRAS*-melanoma *in vivo* studies (Figure 7). This suggests that EI-52 could sensitize "cold tumors" to immune checkpoint inhibitors, potentiating both molecules' effects. Nonetheless, the mechanisms behind this synergy warrant an exhaustive investigation through a comprehensive immune infiltrate analysis.

Together, these data show that our novel molecule EI-52, an ERK-MyD88 PPI inhibitor, could potentially be an interesting treatment option for melanoma, and highlight the possible use of EI-52 as a treatment for KI- or ICI- resistant patients, who to this day have no alternative and effective targeted therapy option.

## **Material and Methods**

### **Cell lines and reagents**

The *BRAFV600E*-mutated melanoma cell lines A375 and 501mel, *NRASQ61R*-mutated melanoma cell line SKMEL2, and mouse fibroblastic cell line NIH/3T3 were purchased from ATCC. The patient-derived BRAFi-resistant cell lines GOKA and ESP, and the mouse *NRAS*-mutated melanoma cell line TyrNRas6.1 were obtained from team J. Caramel and S. Dalle at the Cancer Research Center of Lyon. A375, 501mel, SKMEL2, and NIH/3T3 cells were cultured in DMEM (Gibco, Ref: 41965). GOKA, ESP, and TyrNRas6.1 were cultured in RPMI 1640 medium (Gibco, Ref: 21875), both supplemented with 10% fetal bovine serum and 1% penicillin/streptomycin. Cells were maintained at 37°C and 5% CO<sub>2</sub>.

Kinase inhibitors vemurafenib (PLX4032) and trametinib (GSK1120212) were purchased from Selleckchem, and U0126 was purchased from Promega. All drugs, including EI-52, were dissolved in DMSO.

### **Real-time proliferation, cell death, and apoptosis assay**

10<sup>5</sup> cells were seeded onto 96-well plates. After 24 hours, cells were treated with the different inhibitors or EI-52 in medium containing 0,33 µg/mL propidium iodide (Sigma-Aldrich). Cell confluence and the number of dead cells were determined using the Incucyte™ S3 Live-Cell Analysis Instrument (Essen BioScience) at 2-hour intervals and up to 72 h. Data was plotted as mean ± SD using GraphPad Prism 9. Ratios of death/proliferation were used when comparing different cell lines in order to reduce the bias due to the proliferation speed of each cell line.

### **Caspase 3/7 activity**

3.10<sup>4</sup> cells were seeded onto 24-well plates. After 24h, the cells were incubated with vehicle (DMSO) or 6µM of EI-52 for 24h. Caspase 3/7 activity was evaluated using the Caspase-Glo®

3/7 assay according to the manufacturer's protocol and using a Tecan Infinite M200 Pro. Data was plotted as mean  $\pm$  SEM using GraphPad Prism 9.

### **IL-8, HMGB1 and ATP quantification**

$3 \times 10^4$  cells were seeded onto 24-well plates. The next day, cells were treated with vehicle (DMSO) or EI-52 at  $6 \mu\text{M}$  for 24 h. Extracellular-ATP was quantified in supernatants, and total ATP for IC50 measurements was quantified after cell lysis, both using the CellTiter-Glo<sup>®</sup> assay (Promega) according to the manufacturer's instructions. Luminescence was then quantified using a Tecan Infinite M200 Pro. Secreted CXCL8 or HMGB1 were measured using ELISA from Biolegend or Tecan, respectively. Data was plotted as mean  $\pm$  SEM using GraphPad Prism 9.

### **Spheroids**

Parental or vemurafenib-resistant 501-mel spheroids were generated using the hanging-drop technique, with 1000 cells per drop. After 5 days, spheroids were gently collected and distributed evenly into 3 experimental groups: vehicle,  $0,4 \mu\text{M}$  vemurafenib, and  $8 \mu\text{M}$  EI-52. Spheroids were then imaged every day for 7 days. Propidium iodide staining was performed 48h after treatment. It should be noted that both parental and KI-resistant A375 cells failed to generate spheroids, while only the parental SKMEL2 (but not the KI-resistant) cells were able to generate spheroids.

### **Dose escalation resistance assay**

$5 \times 10^5$  cells were plated in 6-well plates and treatments began 24 hours after plating. Cells were split at 80-90% confluency and treated 24 hours later with a higher dose. Media was changed and the treatment was renewed 2x per week for cells that were not split.

Cells were exposed to increasing doses of Vemurafenib, Trametinib, or EI-52, starting at the IC50. Double-resistant A375 cells were generated by sequential exposure to Vemurafenib, then Trametinib. Cells were considered resistant when they continued to proliferate at  $10 \times \text{IC}_{50}$ .

### **Chronic treatment resistance assay**

$5 \times 10^5$  cells were plated in 6-well plates and treatments began 24 hours after plating. Cells were split at 80-90% confluency and treated 24 hours later with the same dose. Media was changed and the treatment was renewed 2x per week for cells that were not split.

Cells were treated with EI-52 at  $4 \mu\text{M}$  ( $< \text{IC}_{50}$ ) for up to 1 year, then EI-52  $\text{IC}_{50}$  and effects were measured and compared to parental cell lines.

### **Western Blot**

Cells were lysed in Laemmli buffer (0,5M Tris-HCL pH6,8, SDS 10%, 0,1M DTT) complemented with protease and phosphatase inhibitors. Proteins were separated on SDS-PAGE gels then transferred onto nitrocellulose membranes by electroblotting using the Trans-Blot Turbo (Bio-Rad). After transfer, membranes were blocked with 5% BSA/milk in Tris-buffered-saline-0,1%Tween (TBST) buffer for 1 hour at room temperature. Primary antibodies (see table at the end of this section) were incubated overnight at  $4^\circ\text{C}$ . Membranes were then washed with TBST, incubated with secondary HRP-linked antibodies, and revealed by chemiluminescence using Bio-Rad Clarity Western ECL and BIO-Rad Chemidoc.

### ***Syngeneic in vivo models***

Mice were housed in a specific pathogen-free animal facility (P-PAC, Lyon, France) and stored in sterilized filter-topped cages. Mice were handled in agreement with the institutional recommendations and procedures approved by the animal care committee.

The *NRASQ61R*-mutated mouse melanoma cell model TyrNRas6.1 was obtained from J. Caramel and S. Dalle at the Cancer Research Centre of Lyon. NR6.1 cells ( $1,5 \times 10^6$  cells) in phosphate buffered saline (PBS)/Matrigel (BD Biosciences, Oxford, UK) (1/1) were injected subcutaneously into the flank of 6-week-old male C57BL/6 J mice (Charles River laboratories) (groups of 10 mice per condition). When tumors reached  $100 \text{ mm}^3$ , mice were treated by daily intraperitoneal injections of vehicle or EI-52 at the indicated dose. In immune checkpoint inhibitor (ICI) combination experiments, 200  $\mu\text{g}$  of anti-PD-1 rat anti-mouse PD-1 clone RMP1-14 (BP0146, Bio X Cell) or control isotype were administered simultaneously with the daily doses of EI-52 or vehicle on days 3, 5, and 7. Tumor volume was measured twice a week with an electronic caliper. Toxicity was evaluated by visual examination and body weight assessment. Mice survival was analyzed by the Kaplan-Meier method, using as endpoint the

day when the tumors reached a volume  $\geq 2500 \text{ mm}^3$  or the day of euthanasia for mice showing any sign of distress, tumor necrosis, or weight loss  $\geq 20\%$ .

### **Migration tracking by scratch assay**

Fifty thousand cells were seeded onto 96-well plates. After 24 hours, cells were treated with  $10\mu\text{g/mL}$  Mitomycin C (from Sigma-Aldrich, #M4287) for 2 hours in order to inhibit the potential bias due to cell proliferation, medium was then removed, cells were washed with PBS, and complete medium was added. Scratch assay (Incucyte<sup>®</sup>) was then performed according to the manufacturer's instructions. Cell migration was evaluated by imaging every 2 hours for 72 hours using the IncuCyte™ S3 Live-Cell Analysis Instrument (Essen BioScience). Data was plotted as mean  $\pm$  SD using GraphPad Prism 9.

### **Statistical analysis**

Statistical tests were performed with an unpaired Student *t* test. Log-rank Mantel-Cox test was used for comparison of animal groups. For all tests,  $P < 0.05$  was considered significant. Data were graphed and analyzed using GraphPad Prism v.9.

### ***In vivo* study approval**

Mouse experiments were conducted in agreement with the local ethics committee, (Comité d'Evaluation Commun au Centre Léon Bérard, à l'Animalerie de transit de l'ENS, au PBES et au laboratoire P4; CECCAP), authorization number #23715.



Table 1: List of primary antibodies.

<b>Antibody</b>	<b>Reference</b>
p-CRAF S289/296/301	CST 9431
CRAF	CST 9422
p-MEK Thr292	CST 26975
MEK1/2	SC 81504
p-p44/42 ERK1/2 Thr202 Tyr204	CST 9101
p44/42 ERK1/2	CST 4696
DUSP5	Abcam 200708
DUSP6	Abcam 76310
MITF	MAB3747-I
pAKT	CST 9271
GAPDH	CST 2118
Tubulin	Sigma T6199
Actin	MP 691001

# Figures

## Figure 1

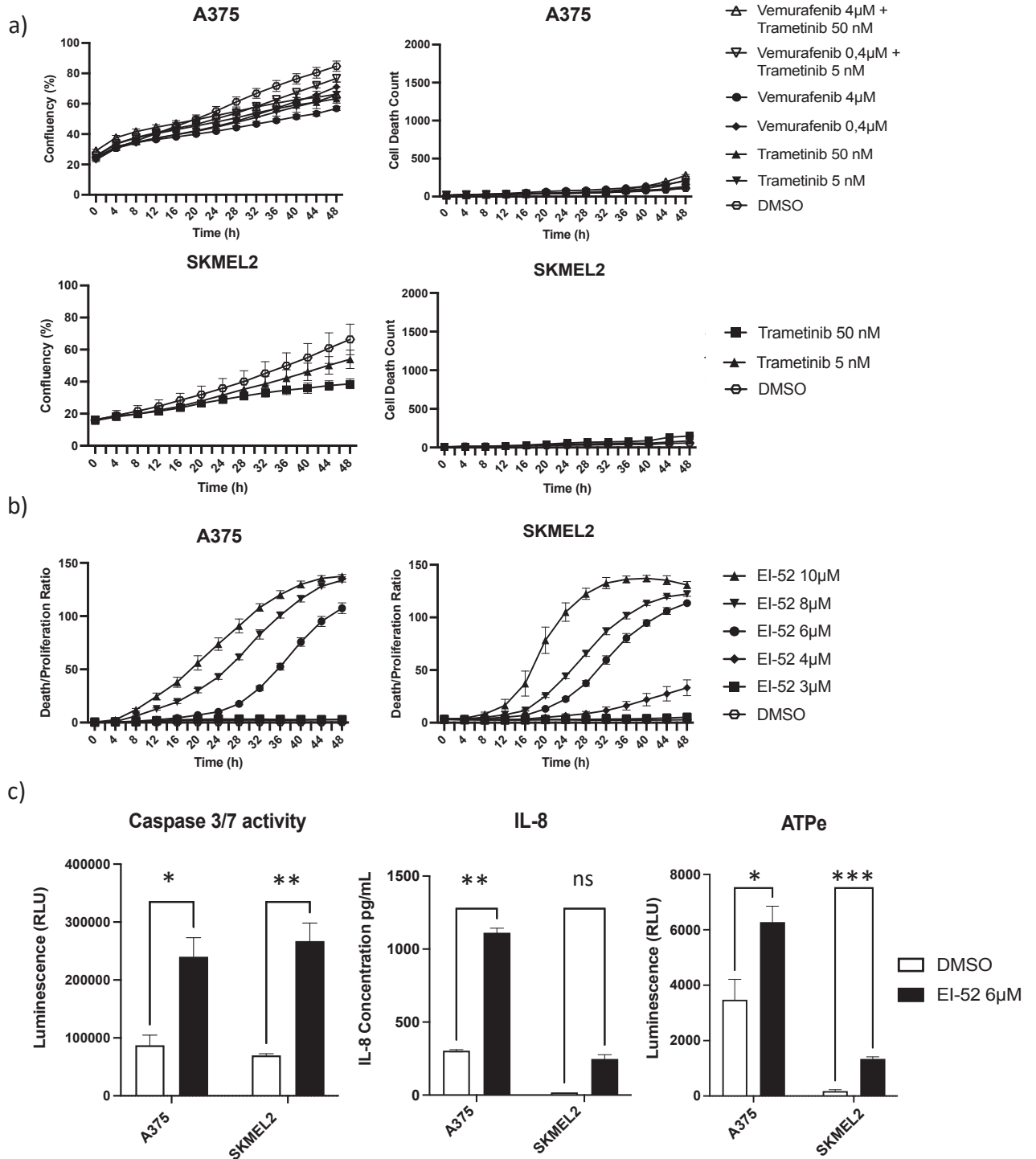
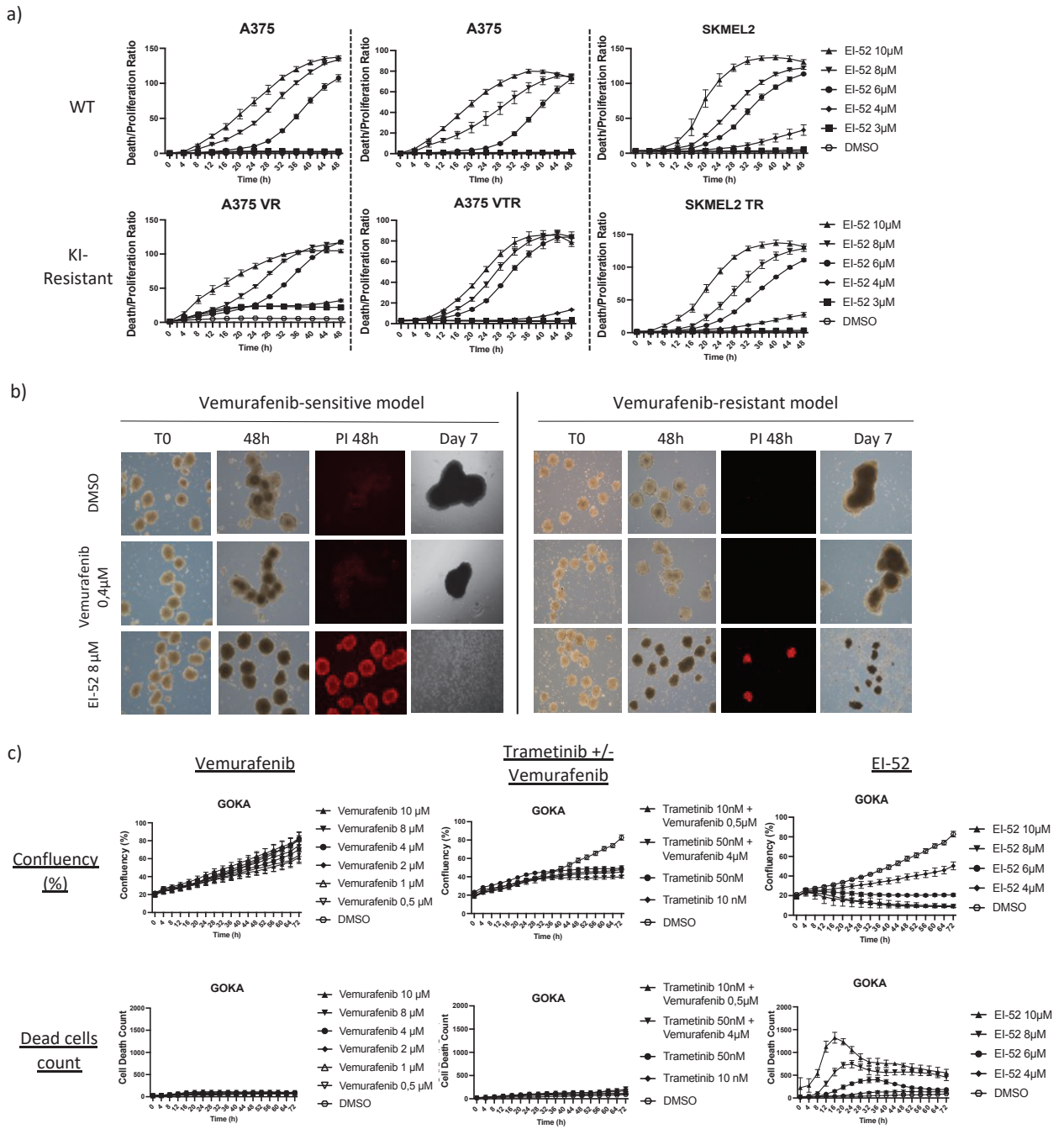
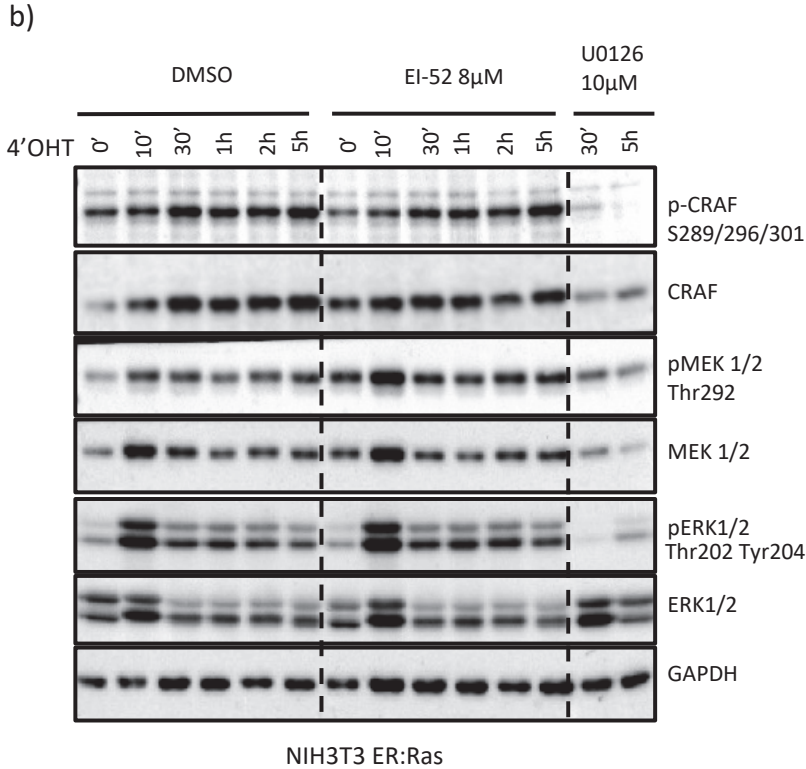
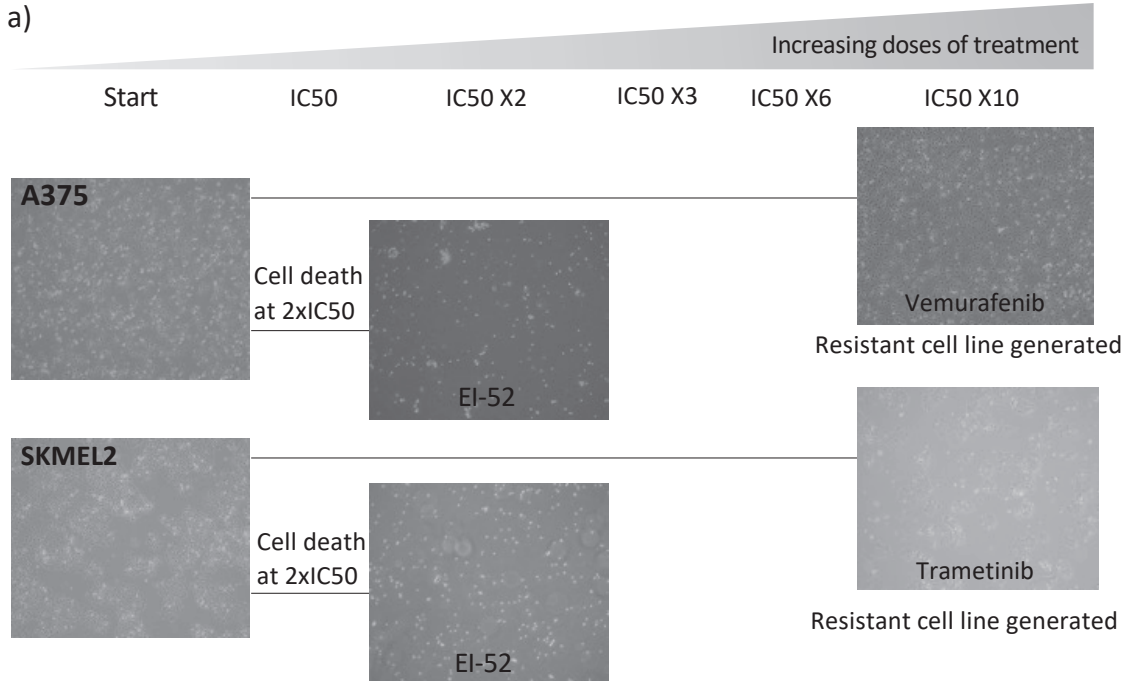


Figure 2



**Figure 3**



**Figure 4**

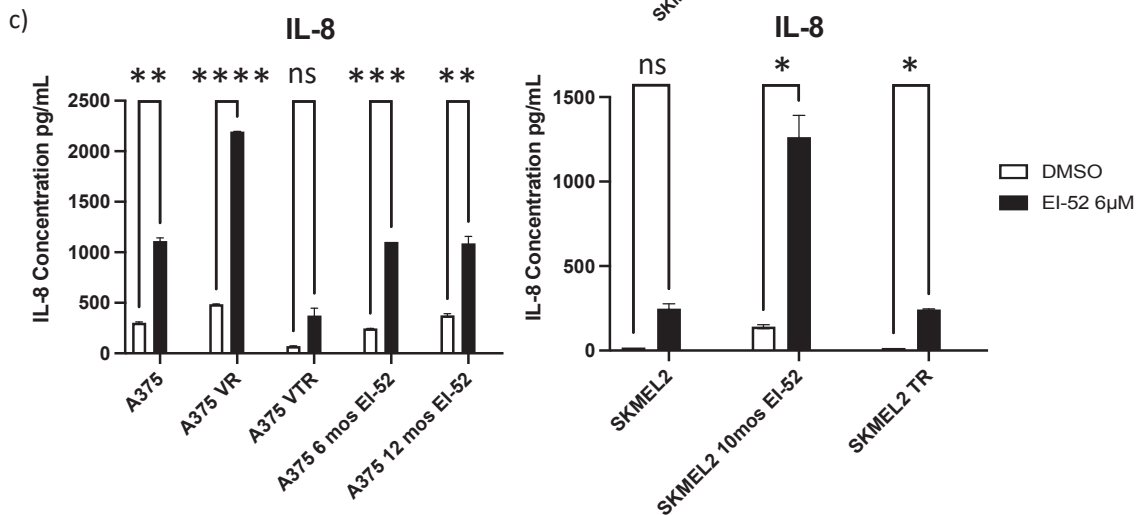
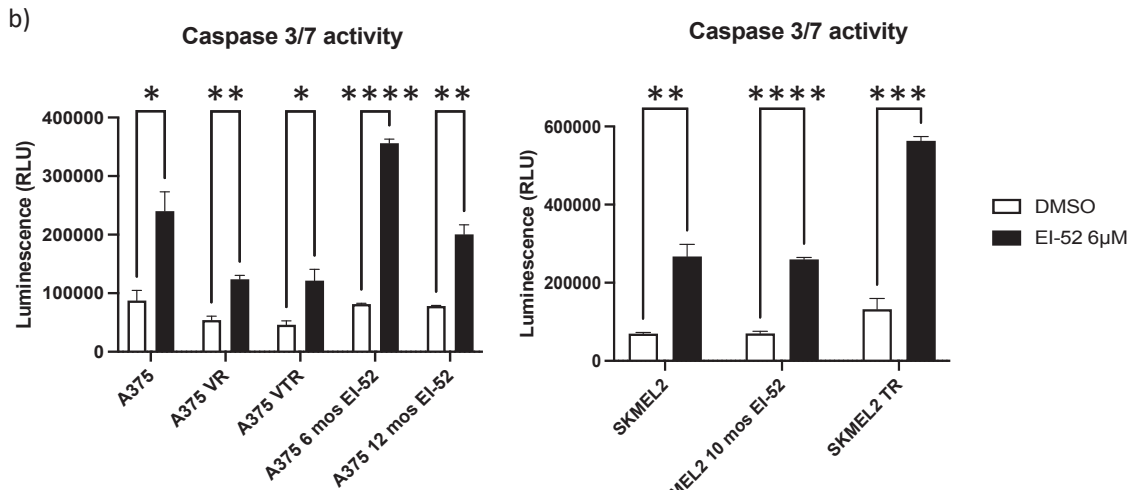
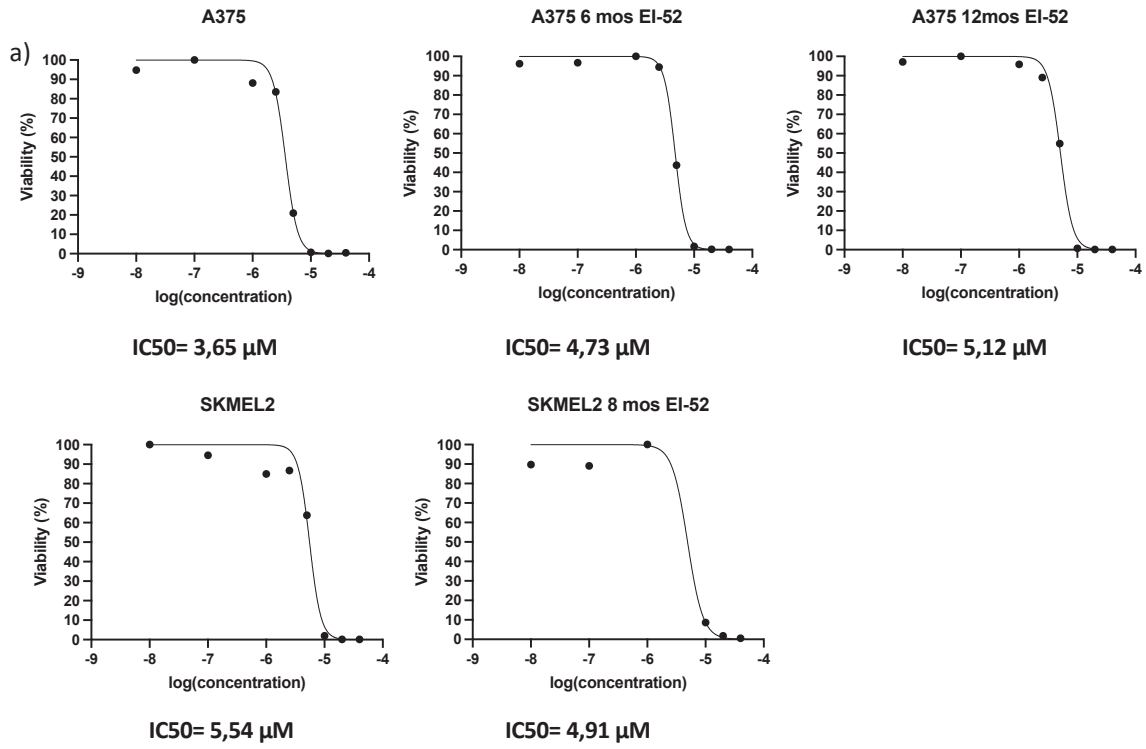


**Figure 5**

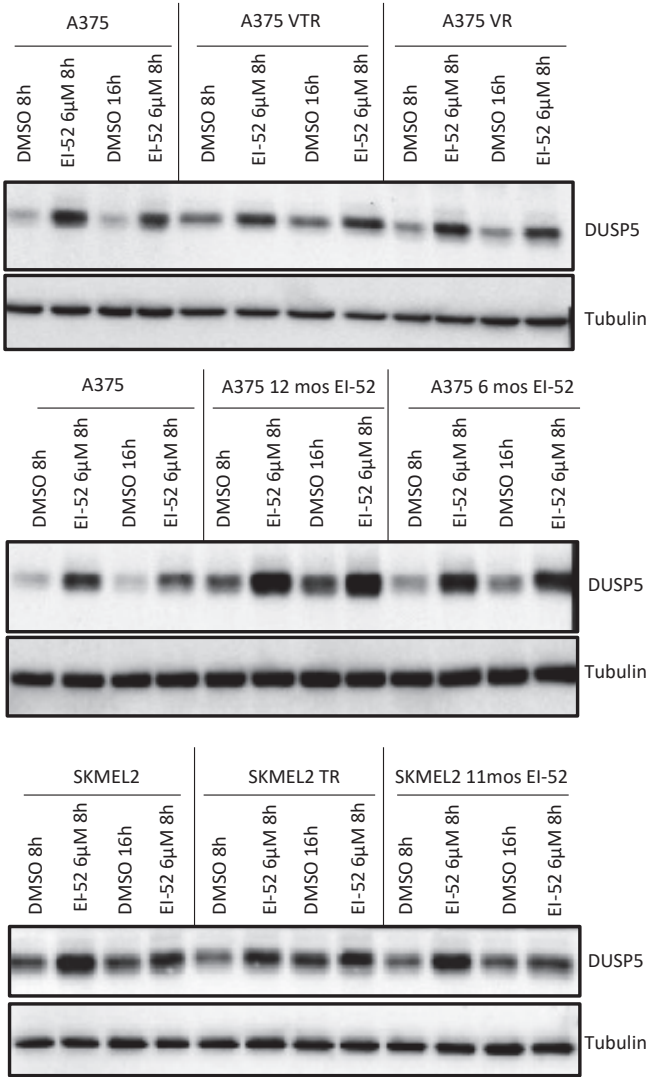
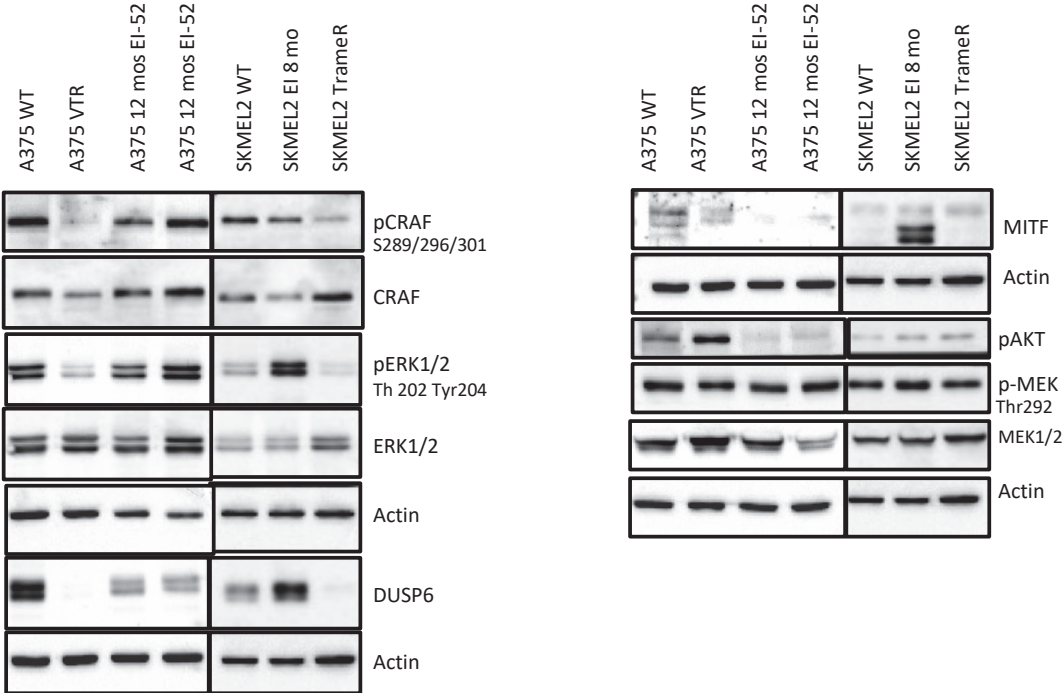
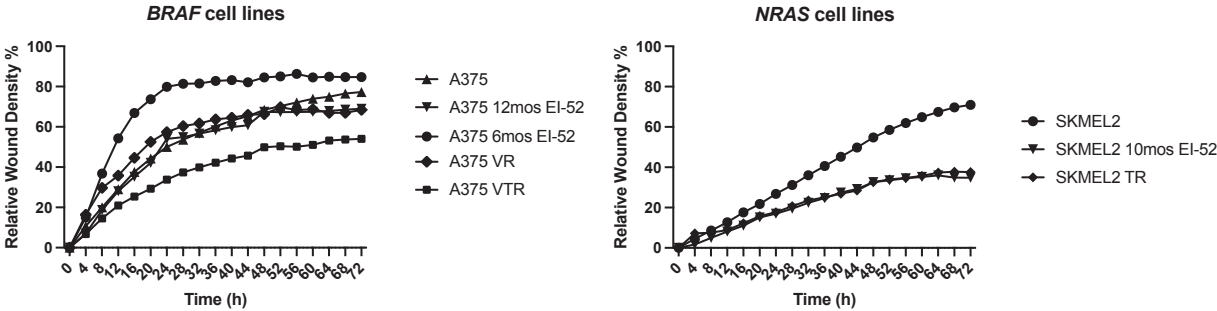


**Figure 6**

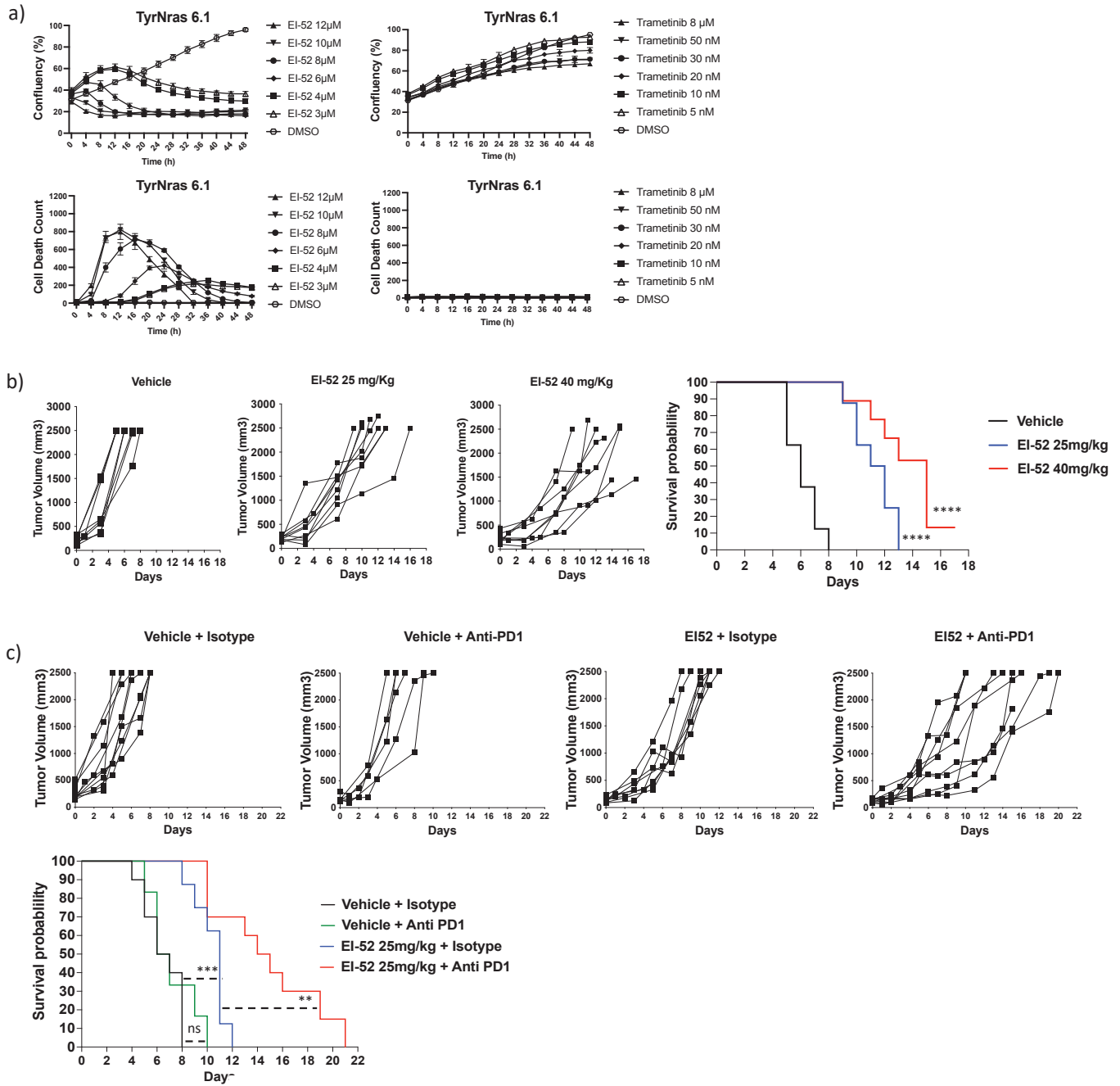
a)



b)



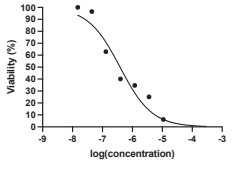
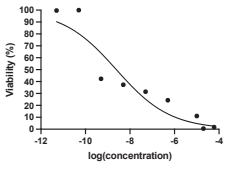
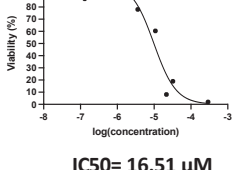
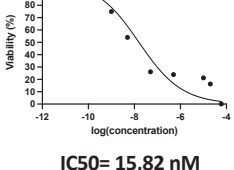
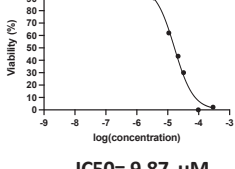
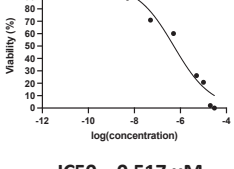
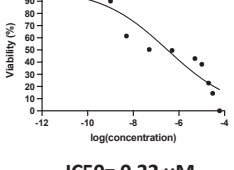
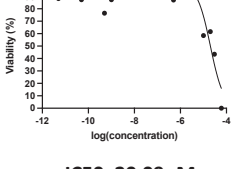
**Figure 7**



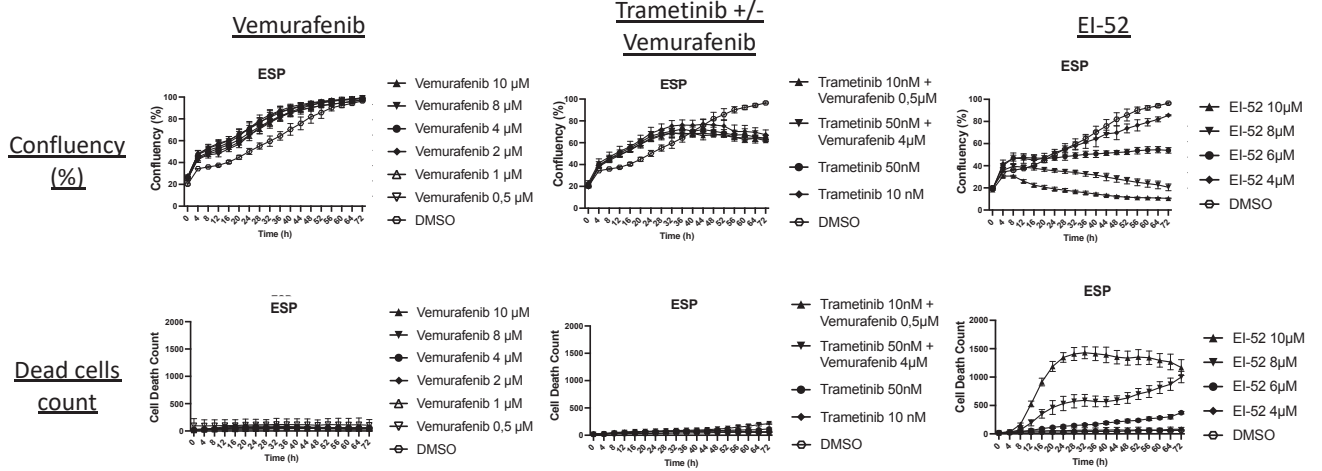


Supplemental

Supplemental Figure 1

<div style="text-align: center;">KI</div> <div style="text-align: left;">Cell line</div>	Vemurafenib	Trametinib
A375	 <p style="text-align: center;"><b>IC50= 0,387 μM</b></p>	 <p style="text-align: center;"><b>IC50= 2,45 nM</b></p>
A375 VR	 <p style="text-align: center;"><b>IC50= 16,51 μM</b></p>	 <p style="text-align: center;"><b>IC50= 15,82 nM</b></p>
A375 VTR	 <p style="text-align: center;"><b>IC50= 9,87 μM</b></p>	 <p style="text-align: center;"><b>IC50= 0,517 μM</b></p>
SKMEL2		 <p style="text-align: center;"><b>IC50= 0,32 μM</b></p>
SKMEL2 TR		 <p style="text-align: center;"><b>IC50=20,09μM</b></p>

## Supplemental Figure 2



## Supplemental Figure 3

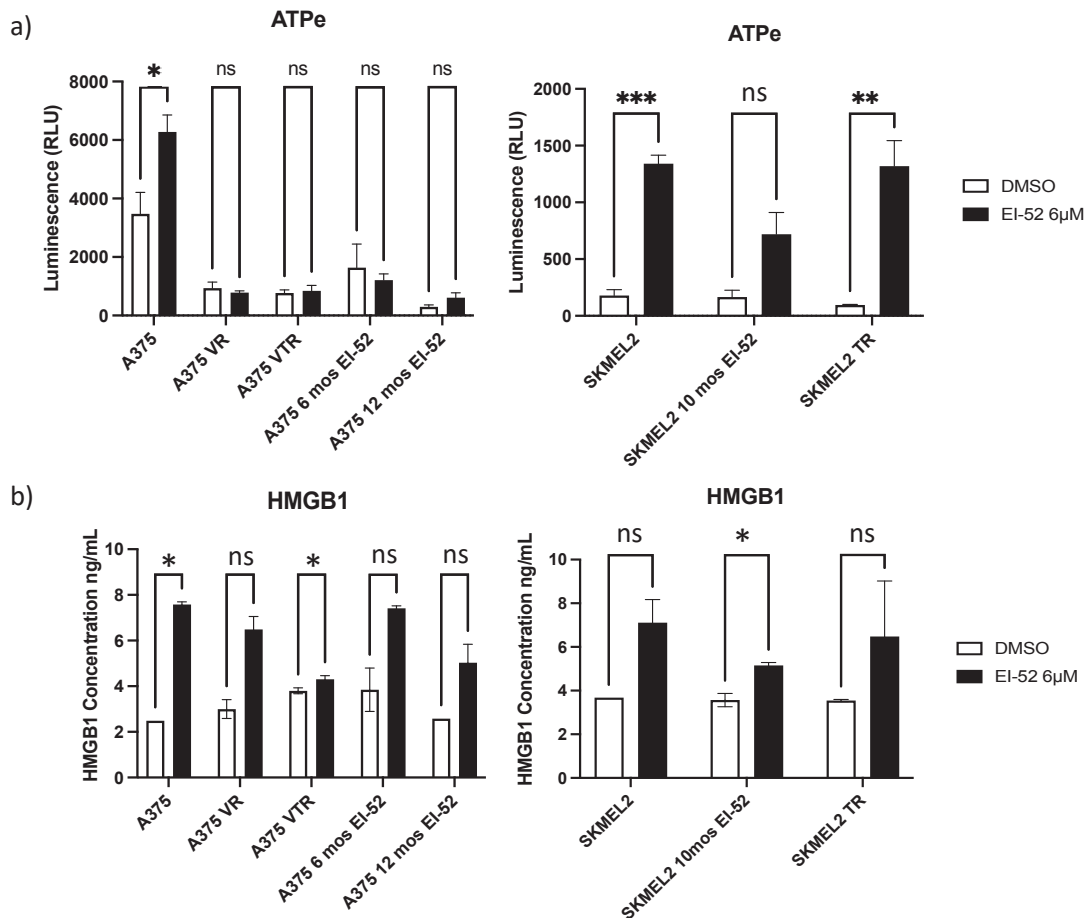


## Figure legends

**Figure 1: EI-52 induces rapid immunogenic cell death in *BRAF* and *NRAS* melanoma.** **a)** A375 and SKMEL2 cells were treated with different doses of Vemurafenib and/or Trametinib. Cell proliferation and cell death were measured for 48 hours using the Incucyte® live imaging system. Data shown as percentage of confluency and number of PI+ dead cells (representative data, n=3). **b)** A375 and SKMEL2 cells were treated with different doses of EI-52. Cell proliferation and cell death were measured for 48 hours using the Incucyte® live imaging system. Data shown as ratio of number of dead cells / percentages of confluency, referred to as death/proliferation ratio (representative data, n>3). **c)** Caspase 3/7 activation, IL-8 and extracellular ATP production after a 24h treatment of A375 and SKMEL2 cells with EI-52 (6µM) (representative data, n=3), p<0.05 unpaired t test.

**Figure 2: EI-52 treatment induces cell death in KI-sensitive or -resistant melanoma 2D and 3D models, as well as in a resistant patient-derived melanoma cell line.** **a)** WT and KI-resistant A375 and SKMEL2 cells were treated with different doses of EI-52. Cell proliferation and cell death were measured for 48 hours using the Incucyte® live imaging system. Data shown as death/proliferation ratio (representative data, n=3). **b)** Vemurafenib-sensitive or Vemurafenib-resistant 501mel spheroids were treated with Vemurafenib at IC50 or EI-52 at 8µM and imaged for 7 days. Propidium Iodide staining was performed 48h after treatment. **c)** A *BRAF*-mutated melanoma cell line, derived from a patient who acquired resistance while in treatment, was treated with single agent or combination Vemurafenib – Trametinib in comparison to EI-52. Cell proliferation and cell death were measured for 72 hours using the Incucyte® live imaging system. Representative data (from n=3) shown as percentage of confluency and number of PI+ dead cells.

**Figure 3: EI-52 does not induce resistance in melanoma cell lines in a dose-escalation protocol and does not impact the early negative feedback loops of the MAPK pathway.** **a)** A375 and SKMEL2 cells exposed to increasing doses of EI-52, Vemurafenib or Trametinib. **b)** Representative Western Blots (from n=3) of NIH3T3 ER:RAS cells that were starved for 24h, then pre-treated with 8µM EI-52 or 10µM of the MEK kinase inhibitor U0126 for 1h before

activating RAS with 4'OHT. We assessed the status of ERK's negative feedback regulation by phosphorylation of CRAF on residues S289/296/301 and MEK on Thr292.

**Figure 4: EI-52 does not induce resistance in melanoma cell lines after up to 1 year of chronic treatment. a)** IC50 of EI-52 in A375 and SKMEL2 cells that were chronically treated with EI-52 for 6, 8 or 12 months, determined by Cell-Titer Glo assay after treatment with EI-52 for 24h. **b)** Caspase 3/7 activity and IL-8 production in WT, KI-resistant and EI-52-chronically-exposed cells after a 24h treatment with EI-52 at 6 $\mu$ M (representative data, n=3), p<0.05 unpaired t test.

**Figure 5: EI-52 induces an increase in DUSP5 levels in WT, KI-resistant and EI-52-chronically-exposed cells.** Representative Western Blots of lysates from WT, KI-resistant and EI-52-chronically-exposed cells after treatment with DMSO or EI-52 at 6 $\mu$ M for 8h or 16h (representative data, n=3).

**Figure 6: Molecular and functional comparison of WT, KI-resistant and EI-52-chronically-exposed cells. a)** Representative Western Blots of lysates from WT, KI-resistant and EI-52-chronically-exposed cells, untreated for 7 days prior to lysis (n=3). **b)** Representative data showing the migration potential of WT, KI-resistant and EI-52-chronically-exposed cells in a scratch wound system after treatment with mitomycin. Data shown as the percentage of cell density migrating to close the wound over 72h (n=2).

**Figure 7: EI-52 treatment improves survival in a syngeneic NRAS-melanoma mouse model: a)** Mice TyrNRas 6.1 cells were treated *in vitro* with different doses of EI-52 or Trametinib. Cell proliferation and cell death were measured for 48 hours using the Incucyte<sup>®</sup> live imaging system. Data shown as percentage of confluency and number of PI+ dead cells (representative data, n=4). **b)** C57BL/6 mice (n  $\geq$  6/group) injected subcutaneously with TyrNRas 6.1 cells were treated daily with vehicle or with 25 or 40 mg/kg EI-52 intraperitoneally. Tumor volume was measured twice a week with an electronic caliper. Experiment endpoints: tumor volume  $\geq$  2500 mm<sup>3</sup> or after showing high distress signs, whichever came first. Graphs showing tumor volumes and the survival probabilities (the Kaplan-Meier method) of each experimental group. P< 0.05, Log-rank Mantel-Cox test. **c)** C57BL/6 mice (n  $\geq$  6/group) injected

subcutaneously with TyrNRas 6.1 cells were treated intraperitoneally with 25 mg/kg EI-52 (daily) or anti-PD-1(total of three doses), as single agents or in combination. Tumor volume was measured twice a week with an electronic caliper. Experiment endpoints: tumor volume  $\geq 2500 \text{ mm}^3$  or after showing high distress signs, whichever came first. Graph showing tumor volumes and the survival probabilities (the Kaplan-Meier method) of each experimental group.  $P < 0.05$ , Log-rank Mantel-Cox test. (representative data, n=2)

**Supplemental Figure 1: Vemurafenib and Trametinib IC50 measurements in WT and KI-resistant melanoma cell lines.** IC50 values were determined by Cell-Titer Glo assay after treatment with either KI for 72 hours (representative data, n=3).

**Supplemental Figure 2: EI-52 treatment induces cell death in another KI-resistant patient-derived melanoma cell line.** ESP cells, a *BRAF*-mutated melanoma cell line derived from a patient who acquired resistance while in treatment, were treated with single agent or combination Vemurafenib – Trametinib in comparison to EI-52. Cell proliferation and cell death were measured for 72 hours using the Incucyte® live imaging system. Representative data (from n=3) shown as percentage of confluency and number of PI+ dead cells.

**Supplemental Figure 3: Comparison of extracellular-ATP and HMGB1 levels in WT, KI-resistant and EI-52-chronically-exposed cells after treatment with EI-52.** Cells were treated with EI-52 at  $6 \mu\text{M}$  for 24h before the supernatants were collected and e-ATP and HMGB1 were measured (representative data, respectively n=3 and n=2).  $p < 0.05$  unpaired t test.



## Discussion

The discovery of kinase inhibitors has improved the outcome of many cancer types poorly responsive to conventional treatments such as cytotoxic chemotherapy and radiotherapy. Melanoma patients, especially those harboring a *BRAF V600E* mutation, have seen a remarkable improvement in overall survival after the discovery of BRAF kinase inhibitors (KIs) [142]. *BRAF* mutation remains the main driver event in melanoma, detected in about 50% of tumors. The V600E mutation is found in 80% of the cases. *NRAS* is mutated in 25% of all cutaneous melanomas [143]. *NRAS* melanomas are more aggressive and respond less to KIs than *BRAF* melanomas [114], [135]. In both subtypes, almost all patients treated with KIs develop resistance within a year [40]. Immune checkpoint inhibitors (ICIs), mainly anti-CTLA4 and anti-PD1, are another melanoma treatment option that proved effective with a long-lasting response independently of the harbored mutation. However, for unclear reasons, only around 40% of melanoma patients benefit from ICIs [139]. All these factors highlight the urgent need for new effective melanoma treatments.

Previous work in our lab shows that MyD88, an adaptor molecule in Toll-Like receptors and Interleukin-1 receptors pathways, interacts with ERK, preventing its inactivation by its phosphatase MKP3. This interaction is required in a cell-autonomous fashion for MAPK activation and transformation *in vitro* and RAS-mediated carcinogenesis in mice *in vivo* [50], [51]. Based on these results, we developed a new small molecule, EI-52, that targets ERK1/2 through their DRS, leading to the loss of ERK-MyD88 interaction and perturbation of the ERK complex rather than its kinase activity. EI-52 is part of the protein-protein interaction (PPI) inhibitors family, a class of pharmacological inhibitors that has attracted the attention of researchers in the last decade [157]. In many types of cancer, we have shown that inhibition of ERK-MyD88 interaction results in early immunogenic cell death *in vitro* and an anti-tumoral T cell response *in vivo* (Virard *et al.*, Annex 2).

Throughout my Ph.D., I evaluated the option of targeting ERK's PPIs as a novel approach for melanoma treatment. We showed that EI-52 induces immunogenic and apoptotic cell death in KI-sensitive and KI-resistant *BRAF* and *NRAS* melanoma cells without causing resistance after up to one year of continuous treatment *in vitro*. In addition, EI-52 significantly reduces tumor progression of *NRAS*-mutated melanoma and synergizes with anti-PD1 *in vivo*.

All these findings will be discussed below, along with the questions they raise for future investigation.

### **I. ERK PPI inhibition in melanoma: the *in vitro* approach**

To evaluate the impact of ERK-MyD88 inhibition in melanoma models *in vitro*, we used *BRAF* and *NRAS* melanoma cell lines. *BRAF* and *NRAS* driver mutations, the two most common molecular subtypes in melanoma, are mutually exclusive [143]. *NRAS* melanoma is often described as more aggressive and less responsive to current treatments (KIs and ICIs) than *BRAF* melanoma [157]–[160]. Throughout my melanoma literature review, one thing that stood out was the gap between *BRAF*-melanoma research and the other less frequent subtypes, including *NRAS*-melanoma [135]. For these reasons, including both models in our *in vitro* approach was very important to our study. In both models, we compared EI-52 to Vemurafenib (BRAFi) and Trametinib (MEKi), two KIs used in the clinic. As expected, at standard *in vitro* doses, both KIs blocked cell proliferation without inducing significant cell death. This observation is consistent with the literature [161]–[167]. Kinase inhibitors are described to cause late cell death after a prolonged cell cycle arrest [151], [152]. In the same experimental settings, EI-52 induced rapid apoptotic cell death that begins around 8 hours after treatment and leads to the death of all the treated cells. This fast-occurring cell death could be one of the reasons why we failed to generate EI-52-resistant melanoma cell lines using the standard dose-escalation protocol.

#### **1. Resistance**

Resistance to KIs in melanoma occurs through various mechanisms (described in section III-B-7.4) that involve MAPK reactivation in more than 80% of the cases [110], [117]. M. P. Smith *et al.* [118] emphasized the notion of an adaptation timeline after MAPK pathway kinase inhibition. They described three stages of resistance, all leading to the reactivation of the pathway. The first stage occurs merely hours after KI treatment and involves dysfunctions in the auto-inhibitory feedback loops of the MAPK pathway. The second stage occurs days to a few months after a sustained MAPK inhibition, leading to an adaptive signaling microenvironment, producing resistant clones. These stages represent non-mutational



tolerance. The last step appears after several months of treatment. It is irreversible since it is characterized by the appearance of activating mutations (80% *RAS/BRAF/MEK*, 20% *PI3K/PTEN/AKT*) in the resistant clones. Indeed, when we treated melanoma cells with a MEK KI (U0126), we observed the same rapid inhibition of negative feedback loops of the MAPK pathway described by Smith *et al.* [118]. In contrast, EI-52 did not impact the negative feedback loops, consistent with the fact that EI-52 does not inhibit ERK kinase activity or its ability to phosphorylate negative feedback residues feedback. Logically, EI-52 failed to induce resistance in a short-term dose escalation test. Likewise, cell exposure to low doses of EI-52 for over a year did not induce resistance. This test reflects the mutational and irreversible phase of resistance, characterized by the outgrowth of mutated clones [27]. Additional functional tests show that compared to their respective parental cells, the EI-52-chronically-exposed melanoma cells do not indicate an increased migratory capacity (Results, Figure 6b) or a variation in their cytokine-production response to EI-52 (Figure 4c). Molecular comparison of these cells to their respective parental cell lines shows the same DUSP5 increase after EI-52 treatment (results, figure 5), a signature of EI-52 activity (Virard *et al.*, Annex 2). The long treatment did not impact the pathway's negative feedback loops (Results, Figure 6a). These results imply that EI-52-treated cells never reached the third stage of resistance, even after up to one year of chronic exposure. A genomic approach may help examine whether new mutations are acquired or if genes are differentially expressed in these cells.

Based on the above, one may be tempted to conclude that inhibiting protein-protein interactions instead of blocking its kinase activity could circumvent acquired resistance. However, other PPI inhibitors, like those against BCL-2 and p53-MDM2, are subject to resistance development [168]. This finding suggests that factors other than the treatment modality – PPI vs. KI – influence the treatment's ability to elude resistance, such as the efficiency of the inhibitors in inducing cell death. EI-52 induces a rapid and total cell death at 2xIC50, consistent with what we described above in the dose-escalation protocol, while cells treated with either BCL-2 or p53-MDM2 PPI inhibitors do not entirely die, since some tolerate the escalation of doses. Ultimately, this leads to the outgrowth of resistant clones with acquired mutations [168], This highlights the advantage of the novel action mode of EI-52.

Virtually all melanoma patients treated with KI inhibitors become resistant within a year [5], [23], [26]. We tested EI-52 efficacy in KI-resistant melanoma cells. Indeed, we found that EI-

52 treatment induces the same response in both KI-resistant and KI-sensitive cell lines in 2D and 3D spheroids. This result reinforces the interest in targeting ERK, the distal kinase of the pathway, allowing it to bypass the resistance mechanisms developed upstream [110], [117], [147], [154], [169] and the different modes of action of EI-52.

Our experiments compared KI-resistant cells generated through dose-escalation to chronically-exposed cells. Both approaches have been extensively used [135] and resistance mechanisms were suggested to be similar (reviewed in Luebker *et al.* [154]). Nevertheless, a more suitable approach in the future would be to compare cells generated through the same protocol. In addition, analysis of the molecular signature of KI-resistant cells revealed that the pathway's negative feedback loops (mainly through p-CRAF and DUSP6) were inhibited. It should be noted that even though resistant cells are maintained under continuous treatment, the Western Blot analysis was performed after one week of treatment deprivation, indicating that the inhibition we observe is due to an underlying molecular mechanism rather than a direct effect of the treatment (Results, Figure 6a). We also found that pAKT is activated in the double KI-resistant *BRAF* melanoma model (A375 VTR) (Results, Figure 6a). This is consistent with what is widely described in melanoma KI-resistance [110], [117], [147], [154], [169].

In a more physiological model, we obtained two cell lines from *BRAF*-mutant melanoma patients who developed resistance to BRAF KIs during treatment. Although we did not investigate the underlying resistance mechanisms, we checked their response to BRAF and MEK KIs. The BRAF inhibitor, as expected, did not have any effect on either cell line, while the MEK inhibitor slowed cell proliferation. These KIs did not induce cell death alone or their combination, even at very high doses (over 10X the IC50), whereas EI-52 caused rapid cell death at the usual concentrations.

These data suggest that ERK-MyD88 PPI inhibition could be an option for second-line treatment of relapsed patients with acquired resistance to KI.

## **2. Immunogenic cell death**

We have shown that EI-52 induces an immunogenic cell death (ICD) characterized by the release of damage-associated molecular patterns (DAMPs) such as extracellular ATP (eATP), HMGB1, and CXCL8 *in vitro* and an anti-tumoral T cell response *in vivo* (Virard *et al.*, Annex 2). Hernandez *et al.* [155] describe ICD as "a form of regulated cell death sufficient to activate an

adaptive immune response in immunocompetent syngeneic hosts." Briefly, they report three ICDs: pathogen-induced, necroptotic, and oncotherapy-induced. The latter occurs after exposure to anti-tumor agents such as paclitaxel, oxaliplatin, anthracyclines, and cardiac glycosides. This leads to the activation of eukaryotic translation initiation factor 2A (eIF2A), phosphorylation of endoplasmic reticulum (ER) chaperones, and subsequent membrane translocation. Dendritic cells exposed to dying cells regulate co-stimulatory molecules, release pro-inflammatory cytokines, and recruit tumor-specific CD8+ T cells. Classic DAMPs include calreticulin exposure on the cell membrane and the release of HMGB1, extracellular ATP, Type 1 Interferon, and heat shock proteins (HSPs) [155]. IL-8 is a pro-inflammatory cytokine often described as pro-tumorigenic through the promotion of immune-evasiveness [170], [171]. However, IL-8 production has also been linked to anti-tumoral ICD (reviewed in Showalter et al. [172]). Sukkurwala *et al.* [173] showed that calreticulin exposure, a major event in ICD, occurs through a stress pathway involving IL-8, highlighting the role of this chemokine in ICD. BRAF kinase inhibitors have been shown to inhibit IL-8 production [30], [31], [34], a process that most probably impacts the ICD but has not been linked to a decreased overall immune response [174].

In the melanoma context, WT, KI-resistant, and EI-52-chronically-exposed cells showed the same increase in eATP and IL-8 production levels in response to EI-52. While IL-8 is stable enough for accurate dosage by ELISA, eATP is highly unstable, so even though measures were taken to ensure rapid dosage, results should be interpreted cautiously. In our experiments, we measured eATP in our supernatants 24h after treatment, based on previous results we had in different non-melanoma models. A time course could be of benefit, in order to determine the peak timing of eATP production post EI-52 treatment in our model. We still need to perform HMGB1 dosage, as this mediator strongly activates dendritic cells.

In the recent years, ICD has been closely investigated as a way to improve response to KIs in different cancers, including melanoma [175]–[180]. In one paper, Bommareddy *et al.* [180] describe a Trametinib (MEK KI)- induced ICD that increases the response to oncolytic vaccine immunotherapy in melanoma patients. This was one of the very few studies that link KIs to ICD in melanoma. In another recent study by Erkes *et al.* [181], BRAF and MEK KIs were linked to a negative regulation of the melanoma immune microenvironment via pyroptosis, an inflammatory cell death that plays a crucial role in the proliferation and migration of cancer cells [156]. Until we decipher the exact impact of KIs on ICD in melanoma, it is safe to say that

a new approach is needed to sensitize resistant patients and improve their treatment efficacy. In our work, we suggest EI-52 as a potential novel strategy to tackle innate or acquired resistance to ICIs in melanoma patients, through the activation of an ICD leading to a potentiated anti-tumoral immune response. Additional investigation is required to strengthen the link between EI-52 and ICD in melanoma. This link can be demonstrated *in vivo*, as discussed in the next section.

## II. ERK PPI inhibition in melanoma: the *in vivo* approach

*NRAS*-mutant melanoma is aggressive, has fewer treatment options, and responds less to available treatments [114], [135]. For this reason, we investigated the efficacy of EI-52 in a syngeneic *NRAS* melanoma model. We showed that EI-52 effectively reduces tumor growth as a single agent and synergizes with anti-PD1 when combined for an even more remarkable effect. ICI and KI combinations are currently being tested in several preclinical and clinical trials [182]–[184] and are showing some promise. However, as mentioned above, most melanoma patients experience an innate or acquired resistance to both KIs and ICIs [40]. EI-52 as a single agent or in combination with an ICI could be an exciting treatment option for KI- and ICI-sensitive or resistant patients, as EI-52 can be effective alone, but its combination with anti-PD1 potentiates the effects of both molecules, potentially sensitizing ICI-resistant patients to ICIs .

First, we established that Trametinib, a MEK KI used in the clinic, did not impact melanoma cell proliferation and survival. Consequently, we decided to omit the Trametinib group from our *in vivo* studies. However, we plan to include it in future experiments for a more direct head-to-head comparison.

The synergy between EI-52 and anti-PD1 was not unexpected since we had already observed and described in our previous work (Virard *et al.*, Annex 2) that an anti-tumoral T cell response is implicated in the efficacy of EI-52 *in vivo*. Karasarides *et al.* [111] reviewed the hallmark mechanisms of resistance to ICIs, that could be genetic or caused by a dysregulation of the immune system. The lack of inflammation in the tumor microenvironment (TME) is one of the main resistance mechanisms, giving rise to three separate phenotypes: hot inflamed tumors and cold noninflamed immune-excluded or immune-desert tumors. Cold tumors characterize most human tumors, making them a central investigation target given the clinical significance.

Hot tumors are inflamed, ultimately leading to the recruitment of functional effector T cells in the TME. The absence of these cells is a central characteristic of cold tumors. Many ongoing studies aim to create a controlled inflammatory climate in the TME in order to improve the tumors' response to ICIs, a delicate approach that could lead to immune-evasiveness or tumor aggressiveness if pro-tumoral inflammation factors were to be produced[111]. In this context, the ICD induced by EI-52 that we described above, could create a prolific environment for immune cells in the TME, probably explaining the synergy we observe between EI-52 and the ICI anti-PD1 *in vivo*.

Nonetheless, the mechanisms behind this synergy should be investigated with a comprehensive immune infiltrate analysis. We performed a preliminary immune infiltrate analysis in the *NRAS*-mutated melanoma model treated with EI-52. The results were inconclusive, most likely due to wrong timing. We analyzed tumors on day seven post-treatment, which is probably late. We plan to determine the appropriate time to explore the immune infiltrate after treatment with EI-52 by quantifying CD45+ cells at different times post-treatment. Secondly, since in the current model (TyrNRas6.1), tumors grow very fast (2500 mm<sup>3</sup> in 7 days), we will use another clone of this cell line (TyrNRas6.1 CT), which grows much more slowly. The goal is to give more time for the immune response to form and function in the tumor.

We will also investigate the effect of EI-52 in KI-sensitive or KI-resistant *BRAF*-mutant melanoma mice models. We have already shown the efficiency of EI-52 in various KI-resistant models *in vitro*, this will allow us to test it *in vivo*. Previous *in vitro* tests we did using mice *BRAF* melanoma cell lines that are sensitive (Br16M3) or resistant (Br16M3-R) to the BRAF KI Vemurafenib were promising, with the onset of the same rapid cell death after EI-52 treatment in both models (not shown). However, *in vivo* tests using the same two models were inconclusive due to several reasons. The sensitive model had an exaggerated aggressiveness and tumor growth speed, with 100 mm<sup>3</sup> tumors reaching 2500 mm<sup>3</sup> in less than 5 days, while the resistant cells did not grow in mice (only 3 of the 30 mice we implanted mice showed a detectable tumor 3 weeks post-implantation).

Still, we plan on looking deeper into this part, given the lack of alternative therapeutic options for KI-resistant patients, whose treatment remains challenging [185].

In addition, the question of whether EI-52 induces resistance *in vivo* will also be addressed. No protocols for generating models with acquired resistance to KIs exclusively *in vivo* have

been described to date, but a two-step *in vivo* and *in vitro* selection approach is often used [186]. Denis *et al.* [187] recently described an approach to generate *in vivo* syngeneic tumor models with acquired resistance to anti-PD-1/PD-L1 therapies in different models, including a TyrNRas melanoma model. Tumors obtained from mice with initial responses to ICI were serially reimplanted subcutaneously into new groups of naive mice and treated to maintain selection pressure. At each passage, three naive mice were implanted with tumor fragments, and the most aggressive tumor was selected for reimplantation. At least five passages were necessary to induce acquired resistance (see figure below). A similar protocol could be considered to evaluate the resistance potential of EI-52 *in vivo*.

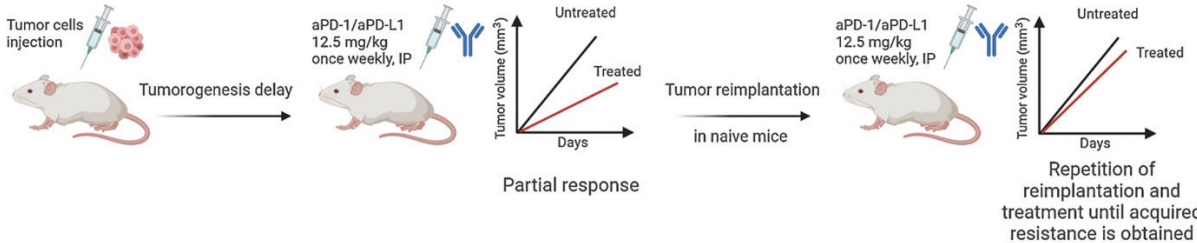


Figure 20: Protocol for generating *in vivo* tumor models with acquired resistance to ICIs.

From Denis *et al.* [187]

## Conclusion

In this work, we showed that our ERK-MyD88 PPI inhibitor induces an immunogenic apoptosis in KI-sensitive or -resistant melanoma cells, without acquired resistance *in vitro*. In addition, EI-52 significantly improves survival in *NRAS* melanoma mouse models as a single agent and in combination with ICIs *in vivo*. Together, these data show that EI-52 could potentially be an interesting treatment option for melanoma and highlight the possible use of EI-52 as a treatment for KI- or ICI- resistant patients, who to this day have no alternative and effective targeted therapy option.

Of course, more investigation is needed to understand the molecular basis of the biological effects of EI-52. A proteomic approach will help us pinpoint the underlying modifications in ERK complexes, and how they can be linked to the apoptotic and immunogenic cell death induced by EI-52 in cancer cells.





# Annexes

## 1. Additional preliminary results

### EI-52 modifies the ERK interactome

#### Context

As described in our previous work (Virard *et al.*, Annex 2), EI-52 is predicted to bind to the DRS of ERK, a conserved site that interacts with a consensus motif named D-domain, harbored by the interacting proteins. By inhibiting ERK protein-protein interactions, EI-52 induces rapid immunogenic cell death in different cancer types but not in untransformed cells. Treatment with EI-52 leads to the delocalization and accumulation of phospho-ERK in the cytoplasm, which leads to an increased eIF2a phosphorylation and expression of ATF4 and CHOP, all of which characterize an ongoing integrated stress response, a cellular process reported to lead to apoptosis [188].

The perturbations in ERK complexes after EI-52 treatment are still not fully characterized. We sought to identify which interactions of ERK are affected, whether gained, lost, increased, or decreased, by EI-52 treatment to determine the functional consequences of these changes. We co-immunoprecipitated (co-IP) ERK complexes in the presence or absence of EI-52 and analyzed ERK partners by mass spectrometry (MS).

#### Material and Methods

The co-IP was performed in HeLa cells, given their ease of transfection.  $3 \cdot 10^6$  cells were plated in 10 cm petri dish. After 24 hours, cells were transfected with 10 $\mu$ g of an ERK2-HA vector (pcDNA3-HA-ERK2 WT, rat, addgene #8974) or an HA-tagged empty vector (pCMV-HA), using jetPRIME<sup>®</sup> transfection reagent according to the manufacturer's protocol. Both vectors are tagged in their N-terminal parts. We used the available rat EKR2-HA vector considering the homology between ERK-1 and ERK-2's protein sequence [189], as well as the similarity between human and rat ERK protein sequence (>99,5% similarity, UniProt). Cells were treated

for 4 hours with EI-52 at 8 $\mu$ M or DMSO before being harvested and lysed using a mild non-denaturing buffer (1% NP40, 20 mM Tris pH=7.5, 150 mM NaCl, 2 mM EDTA) complemented with protease inhibitors (Roche, 11836145001) and phosphatase inhibitors (Sigma-Aldrich, P2850+ P5726). To reduce the non-specific binding of proteins, lysates were precleared by incubation with 10  $\mu$ L slurry (beads – lysis buffer at V/V) of Protein G Plus/Protein A agarose suspension (Millipore, IP05) per 1 mg of protein for 1 hour on a rotator in a cold chamber. Precleared lysates were then incubated overnight with 10  $\mu$ L slurry (beads – lysis buffer at V/V) of mouse monoclonal anti-HA-agarose beads (Millipore, A2095) per 1 mg of protein on a rotator in a cold chamber. After 3 washes with the same buffer used for lysis minus the phosphatase inhibitors, elution was performed by incubation with HA-peptide (Sigma Aldrich, I2149) at a final concentration of 0,5 mg/mL in a volume corresponding to 1,5x beads' volume, for 2 hours on a rotator in a cold chamber. The eluates were transferred to new tubes and either sent for MS analysis or heated at 95°C for 5 min after adding Laemmli-6X to be analyzed by Western Blot.

Antibodies against MyD88 (Invitrogen PA5-19918), RSK1/RSK2/RSK3 (Cell Signaling Technologies 9355), HA (Covance PRB-101C), P62 (Genetex GT1478), and DUSP6 (Abcam 76310) were used according to the manufacturers' protocols. Mass spectrometry analysis was performed by the EDyP team at CEA-Grenoble.

## Results

Western Blot analysis shows that, as expected, EI-52 inhibits MyD88 and RSK interactions with ERK. However, it does not impact ERK binding to DUSP6 or p62 (Figure 21, Annex, a-b) (n=3). Mass spectrometry analysis was performed one time (n=1) using the same conditions as in Figure Annex b, and the preliminary results show that only a small number of ERK-interacting proteins could be identified using our experimental protocol. While more than 1290 interacting proteins were identified, we only analyzed the 9 that were decreased or lost in control conditions (empty vector: DMSO / EI-52) and with at least 5 peptides detected per condition (Table 2 Annex). We found that under EI-52 treatment, ERK complexes contained less RSK1, RSK2, and HSP90 co-chaperone CDC37 and more DHPS, an enzyme necessary for activating eIF-5A (Figure Annex c). STRING database analysis shows that while RSK1/2 and

CDC37 are known interactors of ERK, no connection was found between DHPS and ERK in this database (Figure Annex d). The decrease in the pro-proliferation proteins RSK1/2 and the ERK-stabilizing CDC37 could be expected since EI-52 treatment leads to cell death. Wang *et al.* [190] showed that ERK1/2 could activate DHPS by phosphorylation on Ser233, leading to eIF-5A hypusination, a post-translational modification necessary for eIF-5A activation, subsequently leading to translation elongation and termination, thus cell proliferation and survival. The slight increase of DHPS in the presence of EI-52 seems counter-intuitive. If confirmed, it would be of interest to explore the underlying mechanisms. Other proteins appear to be wholly gained or lost under EI-52 treatment (Figure Annex e). No connection among these proteins or between them and ERK could be found using the STRING database. YARS2, a mitochondrial Tyrosine--tRNA ligase, and CRISPLD1, a Cysteine Rich Secretory Protein, were found in ERK complexes after EI-52 treatment. Proteins lost after treatment with EI-52 include PDHB, the mitochondrial pyruvate dehydrogenase E1 component subunit; and GBE1, the 1,4-alpha-glucan-branching enzyme implicated in glycolytic pathways, as well as TRIM29, the tripartite motif-containing protein 29 involved in the DNA damage response. No clear link could be established between these proteins, but should these results be confirmed, a deeper look into the possible connections should be taken.

## **Discussion and Conclusion**

EI-52 is predicted to bind to the CD domain in the DRS of ERK, a conserved site that interacts with a consensus motif named D-domain, harbored by the interacting proteins (Virard *et al.*, Annex 2). Several groups are currently investigating ERK PPI inhibition, a promising alternative to direct kinase inhibition. Most of the described ERK PPI inhibitors that target the ERK DRS domain inhibit its interaction with RSK, leading to its inactivation. Some inhibit MEK interaction with ERK, leading to an enzymatically inactive ERK [34], [191]–[193]. In contrast, EI-52, selected based on inhibition of ERK-MyD88 PPI, does not impact ERK phosphorylation and activation by MEK (Virard *et al.*, Annex 2). Moreover, EI-52 treatment induces the activation of RSK but not that of c-Myc and increases the expression of both DUSP5 and DUSP6 (Virard *et al.*, Annex 2), suggesting a novel mechanism of ERK partner disruption after treatment with EI-52. To identify which partners of ERK are affected by EI-52, we opted to co-IP ERK complexes in the presence or absence of EI-52 and analyze the precipitates by MS. Co-

immunoprecipitation experiments confirmed at the biochemical level that EI-52 inhibits the ERK-MyD88 interaction (Figure Annex a).

Several problems were encountered in the co-immunoprecipitation experiments, mainly related to the intricate balance between the buffer being delicate enough not to lose many interactants but strong enough to reduce non-specific binding to the beads. We nevertheless found suitable conditions and performed an MS analysis. We found that under EI-52 treatment, ERK complexes contain less RSK1, RSK2, HSP90 co-chaperone CDC37, and more DHPS, an enzyme necessary for activating eIF-5A. The decrease in RSK1 and RSK2 and the increase in p-RSK levels under EI-52 are a result of the undisturbed capacity of ERK to activate RSK. In fact, RSK activation by ERK leads to the dissociation of RSK-ERK complexes and an increase in pRSK [194]. Whereas RSK1/2 and CDC37 are known interactors of ERK, there are no reports of an interaction between DHPS and ERK, other than one article from Wang et al. [190].

Not many common ERK substrates were found using our protocol in control and EI-52 conditions, even though it was similar to what is usually used for ERK IPs and co-IPs [195]–[197]. Several reasons could be behind this, including buffer salt concentrations, elution technique, elution efficacy, and the final protein quantity sent for MS analysis after elution.

We would expect a decrease in some, but not all, of the DRS-binding proteins interacting with ERK after EI-52 treatment. EI-52 binds to the CD domain of ERK, inhibiting the ERK-MyD88 interaction, as well as other interactions that we are currently investigating, including DUSP6 that interacts with ERK via this domain. EI-52 also induces new interactions such as p65-ERK (Virard *et al.*, Annex 2) indicating further modification in ERK complexes. In addition, it seems that RSK-ERK and MEK-ERK interactions are not impacted by EI-52. MEK1 interacts with ERK through the CD domain in the DRS, but also through the DEF domain, explaining the undisturbed activation of ERK by MEK after EI-52 treatment [198], [199]. RSK also interacts with the DRS of ERK, but new studies show that it can also interact with ERK via the Lys729 on the C-terminal tail, independently of the RSK D-domain [200]. These results and hypotheses indicate that interference with the ERK CD domain modifies the ERK protein complex by inhibiting some interactions, but also gaining others, leading to EI-52's biological outcomes.

Overall, the results described in this part are inconclusive because the MS experiment was performed only once. The preliminary MS results need to be repeated and confirmed by other techniques such as co-IPs or Proximity Ligation Assay, before further investigation into the

results we obtained. However, this proteomic approach deserves to be pursued, as it can help understand the mechanisms by which EI-52 induces its biological effects, the rapid apoptotic and immunogenic cell death.

*Table 2: Annex: List of differentially detected proteins by MS following treatment with EI-52. Listed from the most to the least abundant based on the number of peptides detected.*

<b>Protein Name</b>	<b>DMSO/EI-52 ratio</b>
RSK2	1,81
DHPS	0,82
RSK1	2,67
CDC37	1,57
YARS2	Only in EI-52 condition
CRISPLD1	Only in EI-52 condition
PDHB	Only in DMSO condition
GBE1	Only in DMSO condition
TRIM29	Only in DMSO condition

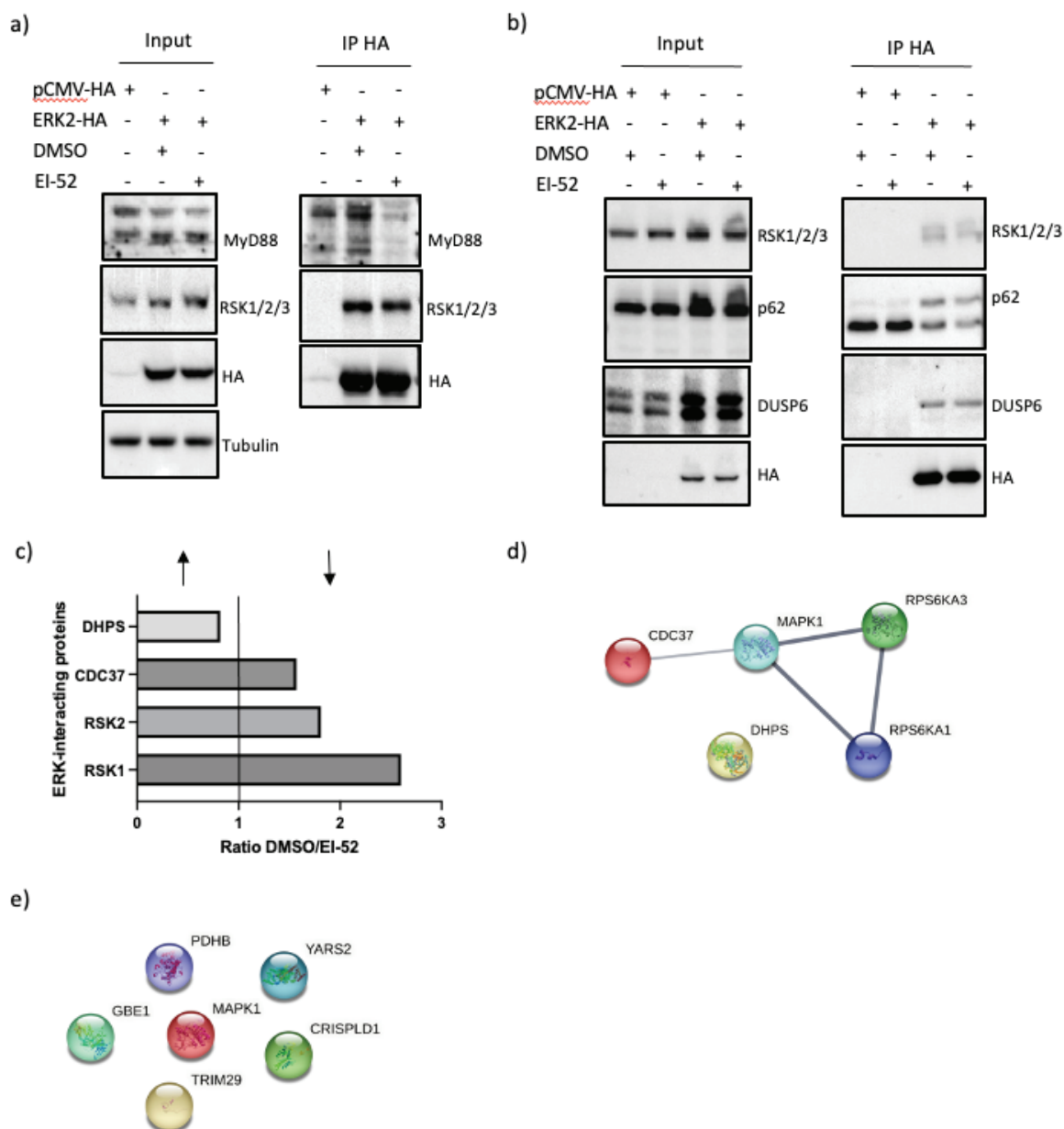


**Figure 21: Annex: EI-52's impact on ERK interactions.**

**a-b)** Western Blot analysis of total or immunoprecipitated lysates in HeLa cells transfected with empty vector or ERK-HA and treated with DMSO or EI-52 8 $\mu$ M for 4 hours. **c-d)** Upregulated and downregulated proteins in ERK complexes after treatment with EI-52. **e)** Proteins gained (YARS2 and CRISPLD1) or lost in ERK complexes after treatment with EI-52.



2. Article 1, submitted, in review in Nature Cancer.

**Targeting ERK-MyD88 interaction leads to ERK dysregulation and immunogenic cancer cell death**

François Virard<sup>1,7,#</sup>, Stéphane Giraud<sup>1,2,#</sup>, Mélanie Bonnet<sup>1</sup>, Léa Magadoux<sup>1</sup>, Laetitia Martin<sup>1,2</sup>, Sophie Deneuve<sup>1</sup>, **Rita Frem**<sup>1</sup>, Bruno O. Villoutreix<sup>3</sup>, Jonathan Reboulet<sup>4</sup>, Samir Merabet<sup>4</sup>, Vincent Chaptal<sup>5</sup>, Cédric Chaveroux<sup>1</sup>, Nader Hussein<sup>1</sup>, Nicolas Aznar<sup>1</sup>, Tanguy Fenouil<sup>1,8</sup>, Isabelle Treilleux<sup>6</sup>, Pierre Saintigny<sup>1</sup>, Stéphane Ansieau<sup>1</sup>, Serge Manié<sup>1</sup>, Serge Lebecque<sup>1,8</sup>, Toufic Renno<sup>1,§</sup>, Isabelle Coste<sup>1,§</sup>.



## **Targeting ERK-MyD88 interaction leads to ERK dysregulation and immunogenic cancer cell death**

François Virard<sup>1,7,#</sup>, Stéphane Giraud<sup>1,2,#</sup>, Mélanie Bonnet<sup>1</sup>, Léa Magadoux<sup>1</sup>, Laetitia Martin<sup>1,2</sup>, Sophie Deneuve<sup>1</sup>, Rita Frem<sup>1</sup>, Bruno O. Villoutreix<sup>3</sup>, Jonathan Reboulet<sup>4</sup>, Samir Merabet<sup>4</sup>, Vincent Chaptal<sup>5</sup>, Cédric Chaveroux<sup>1</sup>, Nader Hussein<sup>1</sup>, Nicolas Aznar<sup>1</sup>, Tanguy Fenouil<sup>1,8</sup>, Isabelle Treilleux<sup>6</sup>, Pierre Saintigny<sup>1</sup>, Stéphane Ansieau<sup>1</sup>, Serge Manié<sup>1</sup>, Serge Lebecque<sup>1,8</sup>, Toufic Renno<sup>1,§</sup>, Isabelle Coste<sup>1,§</sup>.

<sup>1</sup>University Claude Bernard Lyon 1, INSERM U1052–CNRS UMR5286, Lyon Cancer Research Center, Centre Léon Bérard, Lyon, France

<sup>2</sup>Center for Drug Discovery and Development, Synergie Lyon Cancer Foundation, Lyon Cancer Research Center, Centre Léon Bérard, Lyon, France

<sup>3</sup>Université de Paris, NeuroDiderot, Inserm, Hôpital Robert Debré, 75019 Paris, France

<sup>4</sup>Institut de Génomique Fonctionnelle de Lyon, UMR 5242-CNRS/ENSL, Université Claude Bernard Lyon 1, Lyon, France.

<sup>5</sup>Drug Resistance & Membrane Proteins group, Molecular Microbiology and Structural Biochemistry Laboratory (CNRS UMR 5086), University of Lyon, France.

<sup>6</sup>Pathology Department, Centre Léon Bérard, Lyon, France

<sup>7</sup>University of Lyon, Faculté d'Odontologie, Hospices Civils de Lyon, France.

<sup>8</sup>University of Lyon, Faculté de Médecine, Hospices Civils de Lyon, France.

#F. Virard and S. Giraud contributed equally to this work

§T. Renno and I. Coste contributed equally to this work.

Corresponding authors:

Isabelle Coste, Centre de Recherche en Cancérologie de Lyon, 28 rue Laennec, 69373

Lyon. Phone : +33469166630. Email: [isabelle.coste@lyon.unicancer.fr](mailto:isabelle.coste@lyon.unicancer.fr)

Toufic Renno, Centre de Recherche en Cancérologie de Lyon, 28 rue Laennec, 69373

Lyon. Phone: +33469166629. Email: [toufic.renno@lyon.unicancer.fr](mailto:toufic.renno@lyon.unicancer.fr)

[toufic.renno@lyon.unicancer.fr](mailto:toufic.renno@lyon.unicancer.fr)

### **Disclosure of Potential Conflicts of Interest**

The authors have declared that no conflict of interest exists.

1 **One-sentence summary**

2 Targeting ERK interaction with specific protein partners induces direct cancer cell death  
3 and activates an anti-tumoral T cell response.

4

5 **Abstract**

6 The quest for targeted therapies is critical in the battle against cancer. The RAS/MAP  
7 kinase pathway is frequently implicated in neoplasia, with ERK playing a crucial role as  
8 the most distal kinase in the RAS signaling cascade. Our previous research demonstrated  
9 that the interaction between ERK and MyD88, an adaptor protein in innate immunity, is  
10 crucial for RAS-dependent transformation and cancer cell survival. In this study, we  
11 examine the biological consequences of disrupting the ERK-MyD88 interaction through  
12 the ERK D-recruitment site (DRS), while preserving ERK's kinase activity. Our results  
13 show that treatment with EI-52, a benzimidazole-based small-molecule inhibitor of the  
14 ERK-MyD88 interaction, triggers immunogenic apoptotic cell death *in vitro* and elicits an  
15 anti-tumor T cell response *in vivo*. This evidence suggests that inhibiting the ERK-MyD88  
16 interaction may be a promising therapeutic approach in cancer treatment.

17

18

19

20

## 21 **Introduction**

22 The extracellular signal-regulated kinase proteins (ERK1 and ERK2, hereafter designated  
23 as ERK) represent a protein kinase hub, interfaced to different cellular sub-routings  
24 regulating cell division and survival, cellular biomass and metabolism, as well as  
25 differentiation and tissue fate <sup>1</sup>.

26 While the rules that drive ERK signal across this functional diversity are not fully  
27 understood, some key elements regarding ERK signal integration have been identified.  
28 First, although ERK targets a vast catalog of proteins with more than three hundred direct  
29 substrates <sup>2</sup>, specific substrate repertoires are selected by at least two distinct interaction  
30 modes. Indeed, the specificity and fidelity of ERK-induced pathways rely on docking sites  
31 distant from the catalytic site, known as the D- and F-recruitment sites (DRS and FRS,  
32 respectively), which interact with conserved motifs, the D or F domains, harbored by the  
33 interacting proteins <sup>3</sup>. These interaction sites are also used by scaffold proteins to regulate  
34 the spatial distribution of ERK, decoupling its nuclear from its cytosolic function. Finally,  
35 in addition to this spatial assignment, ERK-signaling outcome is influenced both in  
36 duration and frequency by a set of phosphatases. Together, these elements sustain the  
37 diversity and selectivity of ERK responses to extra- and intracellular cues.

38 In the course of carcinogenesis, cancer cells hijack and rewire cellular programs to  
39 acquire selective proliferation, survival, and adaptive advantages <sup>4</sup>. Indeed, the RAS/MAP  
40 kinase pathway is frequently over-activated in cancer and since the effector proteins of  
41 the RAS pathway (RAF, MEK, and ERK) are kinases, several small molecule kinase  
42 inhibitors have been developed and are used in the clinic. This approach has been  
43 demonstrated to be effective in shutting down the RAS signal to drive cells into an  
44 underactive state and restore control over tumor growth. However, clinical practice has

45 revealed that blocking RAS signal at the kinase level can be evaded by cell adaptation and  
46 leads to treatment resistance, suggesting the need for alternative strategies.

47 We previously demonstrated that MyD88, an adaptor protein involved in innate  
48 immunity, interacts *via* its D-domain with the DRS of ERK and that this protein-protein  
49 interaction (PPI) is required for RAS-dependent cell transformation and cancer cell  
50 survival *in vitro* and *in vivo* <sup>5,6</sup>. Our finding that the ERK-MyD88 interaction occurs  
51 selectively in cancer cells <sup>5</sup>, suggests that this PPI carries an essential function for tumor  
52 cells and that its disruption could be an effective strategy for cancer therapy.

53 Consequently, we screened for small chemical molecules that inhibit ERK-MyD88  
54 interaction. Two families of inhibitors were thus identified, including the proof-of-  
55 concept molecule, EI-52. Here, we show that EI-52 induces rapid, immunogenic apoptosis  
56 specific to cancer cells *in vitro* and that it exerts an anti-tumoral activity *in vivo* via both  
57 the direct killing of tumor cells and the activation of an anti-tumoral T-cell response.

58

59

## 60 **Results**

### 61 **Identification and characterization of EI-52, a novel inhibitor of ERK-MyD88** 62 **interaction**

63 To identify molecules that disrupt the interaction between MyD88 D-domain and ERK  
64 DRS, we screened a library of about 66,000 small molecules in a homogeneous time-  
65 resolved fluorescence (HTRF) assay using a short peptide containing the MyD88 D-  
66 domain and a recombinant ERK protein. Two distinct chemical families, with  
67 benzimidazole and spiro scaffolds, were identified with similar *in vitro* and cellular  
68 activities. The benzimidazole compound EI-52 was selected for proof-of-concept and  
69 mode of action studies (Fig. 1A). In the HTRF assay, EI-52 behaved similarly with ERK1  
70 and ERK2 to inhibit their interaction with MyD88 in a dose-dependent manner (Fig. 1B).  
71 And as shown by fluorescence quenching *in vitro*, EI-52 binds directly to both kinases (Fig.  
72 1C).

73 To determine the putative binding domain of EI-52 on ERK, we used P2Rank pocket  
74 prediction tools <sup>7</sup> and identified several binding pockets on the surface of ERK, including  
75 the catalytic site and a region that we will hereafter call Zone A, which contains the DRS  
76 (Fig. 1D). Zone A predicted strong interactions with co-crystallized peptide, as estimated  
77 with pyDockEneRes <sup>8</sup>. Another ERK region with relatively stable interactions peptide  
78 involves a small, partly hydrophobic cavity herein named Zone B, which includes the ED  
79 site. Note that the catalytic site is located far away from Zones A and B. EI-52 was  
80 predicted to bind in Zone A, and the two orientations with the highest binding scores are  
81 shown (Fig. 1D). For both orientations, the dimethylaminophenyl group of EI-52 is  
82 predicted to interact strongly with the aspartic and glutamic acid residues (D316, D319,

83 E79 in ERK2) of Zone A. This is consistent with the interactions described for ERK/D-  
84 domain peptide co-crystals<sup>9,10</sup>.

85 The ability of EI-52 to inhibit ERK-MyD88 PPI was next investigated in cells, using two  
86 different approaches. First, a bimolecular fluorescence complementation (BiFC) assay  
87 was performed in HEK293T cells transfected with ERK and MyD88 tagged with the N- and  
88 C-terminal fragments of Venus protein, respectively. It showed that EI-52 inhibits ERK-  
89 MyD88 interaction in a dose-dependent manner in the micromolar range (Fig. 1E). Then,  
90 using a proximity ligation assay (PLA), we showed that EI-52 also inhibits endogenous  
91 ERK-MyD88 interaction in HCT116 cells (Fig. 1F, Supplemental Fig. 1).

## 92 **Blocking ERK-MyD88 interaction with EI-52 induces cancer cell death**

93 Having previously shown that the ERK-MyD88 PPI is key for cancer persistence<sup>6</sup>, we  
94 investigated whether treatment with EI-52 affects cancer cell survival. We treated the  
95 human colon cancer K-Ras<sup>G13D</sup> mutant HCT116 cells with EI-52 (8  $\mu$ M) or ERK kinase  
96 inhibitors at same concentration and evaluated cell recovery and death over 48 hours. We  
97 observed that EI-52 induced a rapid and robust cancer cell death. In contrast, ERK kinase  
98 inhibitors reduce cell recovery without inducing cell death (Fig. 1G).

99 To determine whether the effect of ERK-MyD88 inhibition PPI is specific to cancer cells, we  
100 compared the activity of EI-52 in colorectal (HCT116) and lung (NCI-H292) cancer cell  
101 lines with untransformed human colonic epithelial cells (HCEC) and human bronchial  
102 epithelial cells (HBEC), respectively. As shown on Figure 1H, EI-52 (8  $\mu$ M) triggered with  
103 similar kinetics the death of both cancer cell lines but not of their untransformed  
104 counterparts. Furthermore, primary HUVEC isolated from 3 different donors were  
105 resistant to EI-52 (Fig. 1I). These data indicate that EI-52 induces cell death specifically in  
106 cancer cells and that this cell death is not the result of non-specific toxicity.

107 In light of these results, we extended the analysis to 301 cell lines from the Oncopanel™  
108 collection (Eurofins). Cell lines were tested with 10 concentrations of EI-52 in two-fold  
109 dilution series starting from 30μM. Cell viability was measured and IC50 was calculated  
110 for each cell line. Figure 2A shows that the majority of the cancer cell lines tested were  
111 sensitive to the ERK-MyD88 PPI inhibitor EI-52 at the micromolar range. The response  
112 was heterogeneous within tumor types (Figure 2B). Nevertheless, some tumor types such  
113 as liver cancer and lymphoma were more frequently sensitive whereas prostate and  
114 bladder cancer were more often resistant to EI-52-triggered cell death. Interestingly,  
115 comparing the response pattern of these 301 human cancer cell lines to EI-52 with that  
116 to 63 anti-tumor reference compounds showed a distinctive, new pattern of sensitivity,  
117 distinct from that of kinase inhibitors and other classes of drugs (Fig. 2C), suggesting that  
118 EI-52 represents a new class of antitumor agent with a unique mechanism of action.

### 119 **Blocking ERK-MyD88 interaction with EI-52 modifies ERK localization and leads to** 120 **stress and apoptotic cell death**

121 To elucidate the mechanism of action of EI-52 and the consequences of ERK-MyD88 PPI  
122 inhibition on ERK signaling, we first ascertained that EI-52 does not indirectly interfere  
123 with its kinase activity. Using an *in vitro* kinase assay, we found that the catalytic activity  
124 of ERK remained intact following treatment with EI-52 at concentrations ranging from 1  
125 to 100 μM, whereas it was lost upon treatment with increasing concentrations of the pan-  
126 kinase inhibitor K252a or the ERK kinase inhibitor FR180204<sup>11,12</sup> (Fig. 3A). As expected,  
127 since ERK kinase activity is not compromised, EI-52 treatment has no significant impact  
128 on HCT116 cell cycle compared to control (Fig. 3B). Moreover, EI-52 did not affect ERK  
129 phosphorylation (Fig. 3C), consistent with the ability of MEK to interact with ERK  
130 independently of the DRS<sup>13</sup>. Interestingly, in contrast to kinase inhibitors, treatment with



131 EI-52 resulted in the activation of RSK, but not c-Myc, and the increased expression of  
132 DUSP5 and DUSP6 (Fig. 3C), indicating substantial perturbations of activation and/or  
133 regulation of ERK partners.

134 As disruption of ERK interactions can alter subcellular protein distribution and function  
135 <sup>14,15</sup>, we monitored ERK localization after exposure to EI-52. We found that after 6 hours  
136 of treatment, ERK localization remained unperturbed, while almost all phospho-ERK had  
137 accumulated in the cytoplasm (Fig. 3D). This phospho-ERK delocalization was  
138 accompanied by increased eIF2 $\alpha$  phosphorylation and expression of ATF4 and CHOP (Fig.  
139 3E), all of which characterize an ongoing integrated stress response (ISR), a cellular  
140 process reported to lead to apoptosis <sup>16</sup>. Indeed, inhibition of ERK-MyD88 PPI with EI-52  
141 triggered the caspase 3/7-mediated apoptosis of HCT116 cells that was almost  
142 completely abolished by co-treatment with ISRIB, an inhibitor of the key mediator of ISR,  
143 phospho-eIF2 $\alpha$  (Fig. 3F).

144 Taken together, these results indicate that EI-52 is an inhibitor of ERK-MyD88 PPI which,  
145 without affecting ERK phosphorylation or kinase activity, results in phospho-ERK  
146 delocalization accompanied by an integrated stress response that leads to apoptosis of  
147 cancer cells.

148 **ERK-MyD88 PPI inhibitor EI-52 displays anti-tumor activity in mice and in patient-**  
149 **derived tumors.**

150 To investigate the anti-tumoral activity of EI-52 *in vivo*, we tested the compound in a  
151 syngeneic Lewis lung carcinoma (LLC) model. When tumors reached 100 mm<sup>3</sup>, mice were  
152 treated daily by intraperitoneal injection of EI-52, which resulted in a dose-dependent  
153 inhibition of tumor growth (Fig. 4A). More notably, EI-52 also displayed a protective effect

154 in the aggressive Kras-LA2 spontaneous lung tumor model <sup>17</sup>. In this model, sporadic  
155 activation of K-RAS leads to lung tumors first detectable as small pleural nodules at one  
156 week of age. As shown in Figure 4B, EI-52 treatment for ten weeks induced a significant  
157 reduction of the tumor load in the lungs of treated mice. Anatomopathological analysis of  
158 liver, kidney, and spleen from mice treated for ten weeks with EI-52 did not show signs  
159 of toxicity at the end of the protocol (Supplemental Figure 2). Moreover, none of the mice  
160 treated with EI-52 died during the course of the project (n=107). Finally, the toxicity of  
161 EI-52 was assessed in chicken embryonic chorioallantoic membranes (CAM), an  
162 alternative predictive model of acute toxicity for new drugs <sup>18</sup>. EI-52 treatment resulted  
163 in no embryo deaths or malformations (Table 1) in this highly sensitive model, further  
164 indicating that inhibition of ERK-MyD88 PPI may be safe *in vivo*.

165 We next investigated the effect of EI-52 in *ex vivo* human tumors using available surgical  
166 resection samples. Patient-derived tumor organoids (PDOs) were generated from fresh  
167 colorectal and lung tumor surgical samples and treated for 48 hours at different doses of  
168 EI-52. Using propidium iodide uptake and caspase 3/7 activation, we demonstrated that  
169 of ERK-MyD88 PPI inhibition with EI-52 leads to apoptosis in both human colon and lung  
170 tumoroids (Fig. 4C). We then evaluated EI-52 efficacy in undissociated primary human  
171 cancers. We generated thick sections from head and neck cancer surgical pieces. Then,  
172 tumor slices were cultured and treated with vehicle or EI-52 for twenty-four hours. In  
173 these *ex-vivo* models, EI-52 treatment resulted in strong c-PARP staining that was almost  
174 exclusively restricted to tumor cells (Figure 4D), consistent with the tumor specificity of  
175 EI-52-triggered apoptosis described above. Altogether, these results show that disrupting  
176 ERK-MyD88 PPI with EI-52 can kill human cancer cells *ex vivo* without apparent toxicity.

177 **Inhibition of ERK-MyD88 PPI with EI-52 triggers immunogenic cancer cell death.**

178 To gain insight into the effect of EI-52 on global transcriptional activity, gene expression  
179 was measured on Affymetrics arrays. Transcriptomic analysis of HCT116 cells treated for  
180 16h with EI-52 revealed upregulated transcription of NF- $\kappa$ B-dependent inflammatory  
181 genes (Fig. 5A) including chemokines (Fig. 5B), whose expression and secretion was  
182 confirmed at the RNA (Fig. 5C) and protein levels (Fig. 5D). In contrast, the MEK kinase  
183 inhibitor U0126 did not induce chemokine production.

184 We therefore investigated the status of p65/RelA, one of the components that form the  
185 NF- $\kappa$ B transcription factor. We treated HCT116 cells with EI-52 and found that EI-52  
186 treatment leads to nuclear translocation of p65 (Fig. 5E), as well as the activation of NF-  
187  $\kappa$ B, CXCL1, and CXCL8 transcription (Fig. 5F). Knocking down p65 strongly inhibited IL-  
188 8 production in response to EI-52, indicating that NF- $\kappa$ B is required to induce its secretion  
189 (Fig. 5G). Interestingly, transfected p65 and ERK co-immunoprecipitated in HEK293T  
190 cells treated with EI-52 (Fig. 5H), indicating that interference with the ERK CD domain  
191 not only modifies the ERK protein complex by losing interactions but also by gaining other  
192 partners such as p65, with new downstream biological outcomes.

193 Production of chemokines by dying cancer cells has been reported to be an indication of  
194 an immunogenic cell death (ICD) program<sup>19,20</sup>. Indeed, EI-52-induced cell death was also  
195 accompanied by the release of damage-associated molecular patterns such as ATP, which  
196 has chemotactic activity, and HMGB1, an endogenous TLR4 ligand (Fig. 5I). Consistent  
197 with the ability of EI-52 to induce CXCL8 and ATP release by dying cells, we showed that  
198 supernatant from EI-52-treated cells was able to attract THP1 macrophages (Fig. 5J). In  
199 contrast, U0126 did not induce either mediators of ICD or chemoattraction of  
200 macrophages by HCT-116 cells (Fig. 5I, J), further highlighting the functional differences  
201 between inhibition of ERK kinase activity and ERK-MyD88 PPI.

202 To investigate ICD *in vivo*, we first verified whether EI-52 induces the direct killing of  
203 murine CT26 colon tumor cells implanted subcutaneously in mice. We found that tumors  
204 from mice treated intraperitoneally with EI-52 for 24 hours exhibited strong PARP  
205 cleavage (Fig. 6A, B), demonstrating that EI-52 treatment leads to rapid apoptotic cancer  
206 cell death *in vivo*.

207 Because ICD activates adaptive immunity, we investigated a possible T-cell  
208 contribution to the antitumor activity of EI-52. Murine CT26 colon cancer cells were  
209 injected subcutaneously into syngeneic wild-type and nude BALB/c mice, which differ by  
210 the presence or absence of T cells, respectively. When tumors reached 100 mm<sup>3</sup>, mice  
211 were treated daily with the suboptimal dose of 25 mg/kg of EI-52 to reduce direct killing  
212 and thus facilitate the detection of a possible contribution from T-cell immunity. Indeed,  
213 EI-52 treatment only weakly slowed the tumor growth in nude mice, whereas it had a  
214 much greater antitumor effect in T-cell competent mice. These results demonstrate that  
215 treatment with EI-52 triggers immunogenic cancer cell death and activation of an anti-  
216 tumoral T cell response *in vivo* (Fig. 6C).

217

## 218 **Discussion**

219 For over two decades, researchers in the field of cancer have been striving to develop new  
220 inhibitors for the MAPK enzymatic activity of the RAS pathway. These inhibitors have  
221 been found to impact cell proliferation by affecting the quantitative signaling output of  
222 ERK. While interruption of RAS signaling eventually affects cell survival and death, this  
223 process is typically slow, resulting from prolonged cell cycle arrest.

224 In this report, we present the discovery of EI-52, a small benzimidazole-based chemical  
225 molecule that targets ERK1/2 through their DRS, leading to the loss of ERK-MyD88

226 interaction and perturbation of the ERK complex. This results in early immunogenic  
227 apoptosis and anti-tumoral T cell response *in vivo*. The molecular consequences of ERK-  
228 MyD88 PPI inhibition with EI-52 on cancer cells need further investigation. However, the  
229 atypical regulation of ERK partner proteins, cell death kinetics, and cell line sensitivity  
230 spectra support its novel mode of action. Our research shows that EI-52 induces the  
231 cytoplasmic relocalization of activated ERK, which triggers an integrated stress response  
232 and rapid apoptosis (Fig. 7). These findings align with previous research indicating that  
233 activation of ERK in inappropriate cellular locations leads to cell death <sup>21-22</sup>.

234 ERK PPI inhibition has recently emerged as a promising alternative to direct kinase  
235 inhibition strategies. For example, selective ERK docking inhibition has been explored by  
236 Shapiro *et al.* <sup>23</sup>, who described ERK PPI inhibitors that mainly inhibit the interaction  
237 between ERK and RSK, leading to RSK inactivation. More recently, Kaoud and colleagues  
238 identified a small molecule that binds to the ED pocket of ERK2 DRS <sup>24</sup>. Treatment with  
239 this molecule inhibited ERK and RSK phosphorylation, resulting in a marked G1 growth  
240 arrest followed by late apoptosis. Herrero *et al.* developed an inhibitor of ERK  
241 dimerization, which binds outside the DRS and targets the cytoplasmic function of ERK  
242 without altering its nuclear function. This dimer inhibition compromises RSK activation  
243 and results in proliferation blockade and apoptosis specifically in cancer cells carrying  
244 RAS or BRAF mutations <sup>25</sup>. In contrast, EI-52, which docks in the CD pocket (Zone A) of  
245 the DRS, was selected based on inhibition of ERK-MyD88 PPI, without subsequent  
246 reduction of ERK or RSK phosphorylation. This difference in ERK partner disruption could  
247 explain the novel biological consequences of EI-52 treatment.

248 The fast onset of apoptosis induced by EI-52 may limit the development of resistance that  
249 is commonly seen with kinase inhibitors. Additionally, ERK-MyD88 PPI inhibition with EI-

250 52 unexpectedly activates ICD, a phenomenon previously associated with chemotherapy,  
251 oncolytic viruses, antibiotics, cardiac glycosides, and nano pulse activation.

252 In conclusion, our findings suggest that disrupting ERK activity by targeting its interaction  
253 with MyD88 could be a novel and attractive approach in cancer treatment.

Table 1: Effect of EI-52 on chicken embryos

	Total	Alive	Dead	Malformations			
				Head	Body	Limbs	Skin
DMSO	19	17	2	0	0	0	0
EI-52 (6 $\mu$ M)	18	18	0	0	0	0	0
EI-52 (12 $\mu$ M)	18	17	1	0	0	0	0

## **Methods**

### **Cell lines and reagents**

HCT116 colorectal cancer cell line, NCI-H292 lung cancer cells, murine colon carcinoma CT26 and Lewis lung carcinoma LLC1 were purchased from ATCC.

ERK inhibitors (GDC-0994, LY3214996, VX-11e, SCH772984) were purchased from Selleckem.

### **Homogeneous time-resolved fluorescence (HTRF) assay**

The HTRF assay was performed in white low volume 384-well microplates (Greiner). First, 18.75 nM His-ERK1 protein (Origene) and 50  $\mu$ M of drugs were mixed and incubated in a total volume of 8  $\mu$ L of optimized buffer 20 mM Tris-HCl pH 8.0, 0.05% Tween20, 0.1% BSA, 2.5% DMSO for 30 min at room temperature. Then, 4  $\mu$ L/well of 125 nM biotinylated MyD88 peptide (Biotin-Ahx-PLAALNMRVRRRLSLFLNVR), 8  $\mu$ L/wells of 6.66 nM anti-6His-Eu cryptate (Cisbio) 3.125 nM SA-XL Streptavidine-XL665 (Cisbio) in 20 mM Tris-HCl pH 8.0, 0.05% Tween20, 0.1% BSA were added into each well and incubated for 2 h at room temperature. After incubation, HTRF signals were measured using an Infinite F500 microplate reader (TECAN) at 620 nm and 665 nm emission. Signals were analyzed with an integration time of 500  $\mu$ s, and the DeltaF and Z' values were calculated.

### **Fluorescence spectroscopy and titration**

For fluorescence spectroscopy, recombinant ERK was diluted into 20 mM Tris-HCl pH 8. Titration was performed by adding increasing concentrations of EI52 compound diluted in 70% PEG400/30% Propylene glycol in presence of 5 $\mu$ M of His-ERK. The excitation wavelength was 295nm and the emission was recorded between 310nm to 380 nm in a spectrofluorimeter (SAFAS). The fluorescence of free Tryptophane was also recorded



using a solution of 30 $\mu$ M of NATA with or without the same concentrations of compounds. Ratio of F/F<sub>0</sub> were calculated and the dissociation constant K<sub>D</sub> were determined using the equation  $Y = (B_{max} * X) / (K_D + X)$  where X is the concentration of the ligand and Y the specific interaction. The curves were drawn with GraphPad Prism software.

### ***In silico* docking**

Several experimental structures of ERK co-crystallized with different peptides were analyzed with the molecular graphic system PyMol (Schrödinger), and per-residue interaction energies between the peptides and the proteins were computed with pyDockEneRes<sup>8</sup> to evaluate hot residues in the peptides and proteins. The protonation states of protein titratable residues were predicted with the PCE server<sup>26</sup>. The ligand-binding pockets on ERK structures were further investigated using the machine learning-based pocket prediction tool P2Rank<sup>7</sup>. Docking of EI-52 was then performed with Surflex-Dock<sup>27</sup>, Vina<sup>28,29,30</sup> and Smina using the Vinardo scoring function<sup>31, 32</sup>.

### **Bimolecular fluorescence complementation (BiFC)**

The BiFC method was used as described<sup>33</sup>. Briefly, HEK293T cells were transfected with pCDNA3-hERK1 and pCDNA3-hMyD88 tagged with N-and C-fragments of the Venus protein, respectively. Four hours after transfection, cells were treated with DMSO or EI-52 at 8 or 12  $\mu$ M. Fluorescence intensity was measured by flow cytometry on a BD FACScalibur and analyzed using the FlowJo software.

### **Proximity ligation assay (PLA)**

The PLA method was used as described<sup>34</sup>. Briefly, cells were treated with DMSO or 4  $\mu$ M EI-52 for 3 h, washed with PBS1X and fixed with methanol for 2 min at -20°C. Cells were

then washed 3 times with PBS1X, then blocked with blocking solution for 30 min at 37°C. Cells were then incubated with primary antibodies against MyD88 (Invitrogen) and ERK (Cell Signaling technology), then with the appropriate DNA-linked secondary antibodies according to the manufacturer's instructions. Fluorescence was quantified using the PerkinElmer Columbus software. Quantification with ImageJ Software.

### **Cell recovery and cell death**

10<sup>5</sup> HCT116 cells were seeded onto 96-well plates. The cells were then incubated with or without 8 µM of ERK kinase inhibitors or EI-52 in medium containing propidium iodide at 3.5 µg/mL. Cell confluence and the number of dead cells were determined using the IncuCyte™ Kinetic Live Cell Imaging System (Essen BioScience) at 2 h-intervals and up to 48 h.

### **Eurofins Oncopanel Activity Data**

Cells were grown in standardized media, seeded into 384-well plates and incubated in a humidified atmosphere of 5% CO<sub>2</sub> at 37°C. Compounds were added 3 days following cell seeding. At the same time, a time zero untreated cell plate was generated. EI52 was serially diluted in 2-fold steps from the highest test concentration (30 µM), and assayed over 10 concentrations with a maximum assay concentration of 0.1% DMSO. After a 2-day incubation period, cells were lysed with cell viability detection reagent CellTiter-Glo® (Promega). Bioluminescence was read by a PerkinElmer Envision® microplate reader. Cell viability was measured by the bioluminescence signal generated by the production of ATP in viable cells. The output is referred to as the relative cell count, where measured bioluminescence intensity was transformed to percent of control. Cellular response parameters were calculated using nonlinear regression to a sigmoidal single-site dose

response model. IC50, defined as the test compound concentration at 50% of the maximum possible response.

### **Kinase assay**

ERK1 kinase activity assay was performed in white 384-well microplates (Greiner) using Myelin Basic Protein as substrate (MBP, Sigma), active ERK1 protein (Millipore), and ADP-Glo™ Kinase Assay (Promega). 15 ng of ERK1 were incubated at room temperature for 1h in the dark with 1µg of MBP in 40 mM Tris-HCl buffer pH 7.5, 20 mM MgCl<sub>2</sub>, 50µM DTT, 0.1 mg/mL of BSA with various concentrations of test compounds or known ERK1 inhibitors K252a and FR180204 (Sigma). 5µL of ADP-Glo® reagent was incubated for 40 min at room temperature, then with 10µL of Kinase Detection Reagent for 30 min at room temperature. Luminescence was measured using an Infinite M200 microplate reader (TECAN). Signals were converted to % of ATP/ADP production and response curves were drawn using GraphPad Prism.

### **Transcriptomic analysis**

Messenger RNA was extracted from HCT116, after 18h treatment in triplicate with 6µM of EI52 (CER) or DMSO using NucleoSpin RNA Kit (Macherey-Nagel) according to manufacturer instructions. Gene-expression profiling was first done using the Affymetrix GeneChip Human Genome U133 Plus 2.0 array (ThermoFischer Scientific). Data are available at:

<https://www.ncbi.nlm.nih.gov/geo/query/acc.cgi?acc=GSE%20GSE153759>".

Gene expression analysis was performed using Array Studio software (Omicsoft Corporation). Raw microarray data (CEL files) were processed using quantile normalization and robust multiarray average algorithm. Standard quality controls were

performed (median average deviation score, principal component analysis) to identify outlier samples. To review GEO accession GSE153759, enter token kfuxcggmhxyxvmx into the box.

### **GSEA Analysis**

Functional analyses were performed using Gene Set Enrichment Analysis (GSEA) software v2.0.4 (Subramanian A, et al. Proc Natl Acad Sci U S A. 2005;102:15545–50). GSEA is a robust computational method that determines whether an a priori defined set of genes shows statistically significant, concordant differences between two biologic states (e.g., high risk v low risk). GSEA aims to interpret large-scale expression data by identifying pathways and process. The main advantage of this method is its flexibility in creating molecular signature database of gene sets, including ones based on biologic pathways, chromosomal location, or expression profiles in previously generated microarray data sets. The input data for GSEA procedure were the following: (1) a complete table of genes ranked according to the log<sub>2</sub> fold change between HCT116 treated 16h with DMSO and EI-52, (2) a mapping file for identifying transcripts in U133 Plus 2.0 array platform, and (3) a catalog of 50 “hallmark” gene sets from the Molecular Signature Database (MSigDB) (Liberzon et al., 2015, Cell Systems1, 417–425) (MSigDB, version 5.1 release, [www.broad.mit.edu/gsea/msigdb/msigdb\\_index.html](http://www.broad.mit.edu/gsea/msigdb/msigdb_index.html)). Default parameters were used. Inclusion gene set size was set between 15 and 500 and the phenotype was permuted 1,000 times. Gene sets that met the FDR 0.25 criterion were considered (Supplementary Material).

### **Western Blot**

Cells were lysed in Laemmli buffer (0,5M Tris-HCL (pH6,8), SDS 10%, DTT) during several cycles of five minutes at 95°C. Proteins were resolved on SDS- PAGE, transferred onto PVDF membranes by electroblotting, and nonspecific binding sites were blocked using Tris-buffered saline containing 5% (w/v) milk. After incubation with primary antibody, anti-p-ERK, -Erk, -p-RSK, -RSK, -p-c-Myc, -c-Myc (Cell Signaling Technology), -DUSP5, -DUSP6 (Abcam), and actin (MP Biomedicals) overnight at 4° C, membranes were rinsed, incubated with horseradish peroxidase-conjugated secondary antibody and revealed by chemiluminescence using Bio-Rad Clarity Western ECL and BIO-Rad chemidoc.

### **Cell cycle**

Cells were plated and treated with DMSO, MEK inhibitor (U0126) at 10 µM, paclitaxel (Sigma) at 1 µM or EI-52 at 8 µM. Simultaneous staining for BrdU incorporation and DNA content was performed. Briefly, subconfluent adherent cells were pulsed with 1µg/ml BrdU (Sigma) for 60 minutes prior to harvesting. Cells were then fixed in 70% ethanol for at least 30 min and the DNA was partially denatured in 3 N HCl, then neutralized with 0.1 M Na<sub>2</sub>B<sub>4</sub>OH. The cells were subsequently stained with FITC-coupled anti-BrdU (BD Biosciences), resuspended PBS containing 2.5% FCS and Propidium Iodide 2,5 µg/ml. Cells were analyzed on a FACSCalibur equipped with a doublet discrimination module.

### **Immunofluorescence**

HeLa cells were serum starved for twenty-four hours and treated with control (DMSO) or EI-52 (8 µM) during 6 hours. Then cells were fixed with 4% paraformaldehyde, and permeabilized with ice-cold methanol 5 min. The immunofluorescence staining p-ERK and ERK was performed according to the protocol of the antibody supplier and fluorescence was observed by microscopy (Nikon)

### **Toxicity on Chicken embryos**

Toxicity evaluation was performed by INOVOTION (Grenoble). Briefly, fertilized White Leghorn eggs were incubated at 37,5°C, 50% relative humidity for 9 days. At day 10, embryos were treated every two days for 10 days by dropping 100 µl of medium with DMSO, or 8 or 12 µM EI-52. The number of dead embryos and organ abnormalities in surviving embryos reflect toxicity.

### **Caspase 3/7 activity**

10<sup>4</sup> cells were seeded onto 96-well plates. The cells were then incubated with or without 8 µM of EI-52 for 16 h. Caspase 3/7 activity was evaluated using Caspase-Glo 3/7 (Promega) according to the manufacturer's protocol and using a Tecan Infinite M200 Pro.

### **Chemokine mRNA quantification**

HCT116 cells were seeded onto 12-well plates. The next day, cells were treated with vehicle (DMSO) or EI-52 8 µM for 16 h. For qPCR, total cellular RNA was extracted using the NucleoSpin RNA Kit (Macherey-Nagel). Then 0.5 µg of RNA were reverse transcribed using the High-Capacity cDNA reverse transcription Applied Biosystems kit (ThermoFischer Scientific) and quantified by real time PCR using specific primers for CXCL1 5'-TCCTGCATCCCCATAGTTA-3', 5'-CXCL2 CCCATGGTTAAGAAAATCATCG-3', CXCL3 5'-TGAATGTAAGGTCCCCCGGA-3' and CXCL8 5'-AGACAGCAGAGCACACAAGC-3' and the SYBR Green Master Mix (Applied Biosystems). qPCR was performed using the CFX connect real-time PCR system (Biorad). Expression of target genes was normalized against endogenous HPRT mRNA levels, used as an internal control, and assessed using the comparative 2<sup>-ΔΔCt</sup> method.

### **Chemokine, ATP and HMGB1 quantification**

10<sup>5</sup> HCT116 cells were seeded onto 12-well plates. The next day, cells were treated with vehicle (DMSO), EI-52 8  $\mu$ M, or MEK inhibitor (U0126) 10  $\mu$ M for 24 h. ATP was quantified in the supernatant with Cell Titer-Glo (Promega) according to the manufacturer's instructions, using Tecan Infinite M200 Pro. Secreted CXCL8, CXCL1, CXCL2 and HMGB1 were quantified using ELISA from Biolegend, R&D Systems and IBL, respectively.

### **Patient-derived tumor organoids**

Patient-derived lung tumor organoids were maintained in advanced DMEM containing HEPES, GlutaMax, Penicilline/Streptomycin and primocine and B27, and supplemented with R-spondin-1, NOGGIN, A83-01 and Y-27632 from Miltenyi Biotec, SB202190 (Sigma), FGF7 and FGF10 (Thermo Fisher) and Nicotinamide (Sigma).

Patient-derived colon tumor organoids were maintained in advanced DMEM containing HEPES, GlutaMax, Penicilline/Streptomycin primocine and B27, and supplemented with NOGGIN, A83-01 and Y-27632 from Miltenyi Biotec, SB202190 (Sigma), EGF (Miltenyi), Gastrin and PGE2 (Sigma).

One hundred tumoroids per well are seeded in 96-well plates (Greiner) in 100 $\mu$ L of medium containing 5% Matrigel and incubated at 37°C for 24h. EI-52 or vehicle treatment was added using the HP D300 Digital Dispenser. After 48 hours of treatment, cell death was evaluated by imaging caspase 3/7 activity (CellEvent™ Caspase-3/7 Detection Reagents, Invitrogen) and propidium iodide (Sigma) incorporation with OPERA Phoenix (Perkin Elmer) using an objective magnification of 5 (non-confocal mode).

## **Organotypic culture**

Patients signed a written informed consent agreeing to the use of tumor samples for research, according to the French regulations on the protection of persons (French Ethics Committee). Tumor tissue from surgical resections was obtained. Excess necrotic tissue was discarded and a 200 mm<sup>3</sup> tumor fragment was included in an agarose gel. Automated slicing was performed using Microm HM650V Vibratome with slice thickness set at 250 µm. Adjacent slices were treated with DMSO or EI-52 8 µM for 24 hrs in Dulbecco's Modified Eagle Medium culture medium supplemented with 10% Fetal Bovine Serum, penicillin/streptomycin/neomycin, and 1 % glutamine at 37°C in 5 % CO<sub>2</sub>.

After 24 hours, the culture supernatant was harvested and the tissue was fixed in 4% formalin, then imbedded in paraffin. Histological sections were performed and stained for hematoxylin-phloxin-saffron or cleaved-PARP (Cell Signaling Technology) on an automated Ventana Discovery XC (Roche) according to the manufacturer's instructions. Cleaved-PARP was measured using a IHC score with 0= no staining, 1= 1-9%, 2= 10-19%, and 3= more than 30% of cells are stained.

## ***In vivo* models**

Animals were maintained in a specific pathogen-free animal facility (P-PAC, Lyon-France) and stored in sterilized filter-topped cages. Mice were handled in agreement with the institutional recommendations and procedures approved by the animal care committee (Comité d'Evaluation Commun au Centre Léon Bérard, à l'Animalerie de transit de l'ENS, au PBES et au laboratoire P4; CECCAP).

*Syngeneic graft models:* 5 x 10<sup>5</sup> Lewis Lung Carcinoma (LLC) or CT26 colon carcinoma cells were implanted subcutaneously into the flanks of 8-week-old C57BL/6 or BALB/c



(WT or nude) female mice, respectively (Charles River). When tumors reached 100 mm<sup>3</sup>, mice were treated by daily intraperitoneal injections of vehicle or EI-52 at the indicated dose. Tumor volume was measured twice a week with an electronic caliper.

*Spontaneous model:* five-week-old K-ras<sup>LA2</sup> mice were treated intraperitoneally 5 times a week for 10 weeks with 25 mg/kg EI-52 or vehicle. Tumor load was evaluated at regular intervals on a Perkin Elmer Quantum FX microCT scan. Lung tumor load was quantified using the CALIPER software.

### **Statistical analysis**

Statistical tests were performed with an unpaired Student *t* test. Mann-Whitney test was used for comparison of animal groups. For all tests,  $P < 0.05$  was considered significant. Data were graphed and analyzed using GraphPad Prism v.9.

### **Ethics approvals**

Mouse experiments were conducted in agreement with the local ethics committee, (Comité d'Evaluation Commun au Centre Léon Bérard, à l'Animalerie de transit de l'ENS, au PBES et au laboratoire P4; CECCAP), authorization numbers #5681, #9283.

Ex-vivo and Patient-derived tumoroid experiments were conducted according to the French regulations on the protection of persons. For the BRC of CLB (n°BB-0033-00050) biological material collection and retention activity is declared to the Ministry of Research (DC-2008-99 and AC-2019-3426). Samples were used in the context of patient diagnosis. Non used part of the samples might be used for research if patient is not opposed to it (information notice transmitted to each patient).

The BRC is compliant to GDPR requirements and the CNIL (French National Commission for Computing and Liberties) law. The BRC is certified according to AFNOR NFS96900 (N° 2009/35884.2) and ISO 9001 (Certification N° 2013/56348.2).

### **Acknowledgement**

We thank the Research Pathology, P-PAC imaging, EX-VIVO, and Organoid 3D-ONCO platforms, Université de Lyon, Université Claude Bernard Lyon 1, INSERM 1052, CNRS 5286, Centre Léon Bérard, Centre de recherche en Cancérologie de Lyon (CRCL), Lyon, 69373, France

This work was supported by funding from La Ligue Nationale Contre le Cancer (EL2014-2), Institut National du Cancer PLBIO (2020-119), Fondation ARC pour la recherche sur le cancer (PJA20171206416), the Integrated Cancer Research Site LYriCAN (INCa-DGOS-Inserm\_12563), and the ANR (ANR -11-EQPX-0035).

### **Author contributions**

MB, LMag, LMar, SD, RJ, RF, TF, NH and VC performed experiments and analyzed data. BV performed docking studies. FV and PS performed and analyzed transcriptomic analysis. FV, SG, SM, TR, and IC analyzed data. FV, SG, TR, and IC wrote the manuscript. SL, SM, SA, VF, TR, and IC edited the manuscript. TR and IC conceived the project and managed all studies.

## References

1. Lavoie, H., Gagnon, J. & Therrien, M. ERK signalling: a master regulator of cell behaviour, life and fate. *Nat. Rev. Mol. Cell Biol.* **21**, 607–632 (2020).
2. Ünal, E. B., Uhlig, F. & Blüthgen, N. A compendium of ERK targets. *FEBS Lett.* **591**, 2607–2615 (2017).
3. Sharrocks, A. D., Yang, S.-H. & Galanis, A. Docking domains and substrate-specificity determination for MAP kinases. *Trends Biochem. Sci.* **25**, 448–453 (2000).
4. Hanahan, D. & Weinberg, R. A. Hallmarks of Cancer: The Next Generation. *Cell* **144**, 646–674 (2011).
5. Coste, I. *et al.* Dual function of MyD88 in RAS signaling and inflammation, leading to mouse and human cell transformation. *J. Clin. Invest.* **120**, 3663–3667 (2010).
6. Kfoury, A. *et al.* MyD88 in DNA Repair and Cancer Cell Resistance to Genotoxic Drugs. *JNCI J. Natl. Cancer Inst.* **105**, 937–946 (2013).
7. Krivák, R. & Hoksza, D. P2Rank: machine learning based tool for rapid and accurate prediction of ligand binding sites from protein structure. *J. Cheminformatics* **10**, 39 (2018).
8. Romero-Durana, M., Jiménez-García, B. & Fernández-Recio, J. pyDockEneRes: per-residue decomposition of protein-protein docking energy. *Bioinforma. Oxf. Engl.* **36**, 2284–2285 (2020).
9. Zhou, T., Sun, L., Humphreys, J. & Goldsmith, E. J. Docking Interactions Induce Exposure of Activation Loop in the MAP Kinase ERK2. *Structure* **14**, 1011–1019 (2006).
10. Garai, Á. *et al.* Specificity of Linear Motifs That Bind to a Common Mitogen-Activated Protein Kinase Docking Groove. *Sci. Signal.* **5**, (2012).
11. Kase, H. *et al.* K-252 compounds, novel and potent inhibitors of protein kinase C and cyclic nucleotide-dependent protein kinases. *Biochem. Biophys. Res. Commun.* **142**, 436–440 (1987).
12. Ohori, M. *et al.* Identification of a selective ERK inhibitor and structural determination of the inhibitor-ERK2 complex. *Biochem. Biophys. Res. Commun.* **336**, 357–363 (2005).
13. Robinson, F. L., Whitehurst, A. W., Raman, M. & Cobb, M. H. Identification of Novel Point Mutations in ERK2 That Selectively Disrupt Binding to MEK1. *J. Biol. Chem.* **277**, 14844–14852 (2002).
14. Dimitri, C. A., Dowdle, W., MacKeigan, J. P., Blenis, J. & Murphy, L. O. Spatially Separate Docking Sites on ERK2 Regulate Distinct Signaling Events In Vivo. *Curr. Biol.* **15**, 1319–1324 (2005).
15. Murphy, L. O. & Blenis, J. MAPK signal specificity: the right place at the right time. *Trends Biochem. Sci.* **31**, 268–275 (2006).
16. Bastola, P., Neums, L., Schoenen, F. J. & Chien, J. VCP inhibitors induce endoplasmic reticulum stress, cause cell cycle arrest, trigger caspase-mediated cell death and synergistically kill ovarian cancer cells in combination with Salubrinal. *Mol. Oncol.* **10**, 1559–1574 (2016).
17. Johnson, L. *et al.* Somatic activation of the K-ras oncogene causes early onset lung cancer in mice. *Nature* **410**, 1111–1116 (2001).
18. Kue, C. S., Tan, K. Y., Lam, M. L. & Lee, H. B. Chick embryo chorioallantoic membrane (CAM): an alternative predictive model in acute toxicological studies for anti-cancer drugs. *Exp. Anim.* **64**, 129–138 (2015).
19. Kepp, O. *et al.* Consensus guidelines for the detection of immunogenic cell death. *OncoImmunology* **3**, e955691 (2014).
20. Sukkurwala, A. Q. *et al.* Immunogenic calreticulin exposure occurs through a phylogenetically conserved stress pathway involving the chemokine CXCL8. *Cell Death*

*Differ.* **21**, 59–68 (2014).

21. Bartholomeusz, C. *et al.* PEA-15 Induces Autophagy in Human Ovarian Cancer Cells and Is Associated with Prolonged Overall Survival. *Cancer Res.* **68**, 9302–9310 (2008).
22. Cagnol, S. & Chambard, J.-C. ERK and cell death: Mechanisms of ERK-induced cell death - apoptosis, autophagy and senescence: ERK and cell death. *FEBS J.* **277**, 2–21 (2010).
23. Hancock, C. N. *et al.* Identification of Novel Extracellular Signal-Regulated Kinase Docking Domain Inhibitors. *J. Med. Chem.* **48**, 4586–4595 (2005).
24. Kaoud, T. S. *et al.* Modulating multi-functional ERK complexes by covalent targeting of a recruitment site in vivo. *Nat. Commun.* **10**, 5232 (2019).
25. Herrero, A. *et al.* Small Molecule Inhibition of ERK Dimerization Prevents Tumorigenesis by RAS-ERK Pathway Oncogenes. *Cancer Cell* **28**, 170–182 (2015).
26. Miteva, M. A., Tufféry, P. & Villoutreix, B. O. PCE: web tools to compute protein continuum electrostatics. *Nucleic Acids Res.* **33**, W372-375 (2005).
27. Spitzer, R. & Jain, A. N. Surflex-Dock: Docking benchmarks and real-world application. *J. Comput. Aided Mol. Des.* **26**, 687–699 (2012).
28. Lagarde, N. *et al.* Online structure-based screening of purchasable approved drugs and natural compounds: retrospective examples of drug repositioning on cancer targets. *Oncotarget* **9**, 32346–32361 (2018).
29. Labbé, C. M. *et al.* MTiOpenScreen: a web server for structure-based virtual screening. *Nucleic Acids Res.* **43**, W448-454 (2015).
30. Forli, S. *et al.* Computational protein-ligand docking and virtual drug screening with the AutoDock suite. *Nat. Protoc.* **11**, 905–919 (2016).
31. Koes, D. R., Baumgartner, M. P. & Camacho, C. J. Lessons learned in empirical scoring with smina from the CSAR 2011 benchmarking exercise. *J. Chem. Inf. Model.* **53**, 1893–1904 (2013).
32. Quiroga, R. & Villarreal, M. A. Vinardo: A Scoring Function Based on Autodock Vina Improves Scoring, Docking, and Virtual Screening. *PloS One* **11**, e0155183 (2016).
33. Kerppola, T. K. Visualization of molecular interactions using bimolecular fluorescence complementation analysis: characteristics of protein fragment complementation. *Chem. Soc. Rev.* **38**, 2876–2886 (2009).
34. Söderberg, O. *et al.* Direct observation of individual endogenous protein complexes in situ by proximity ligation. *Nat. Methods* **3**, 995–1000 (2006).

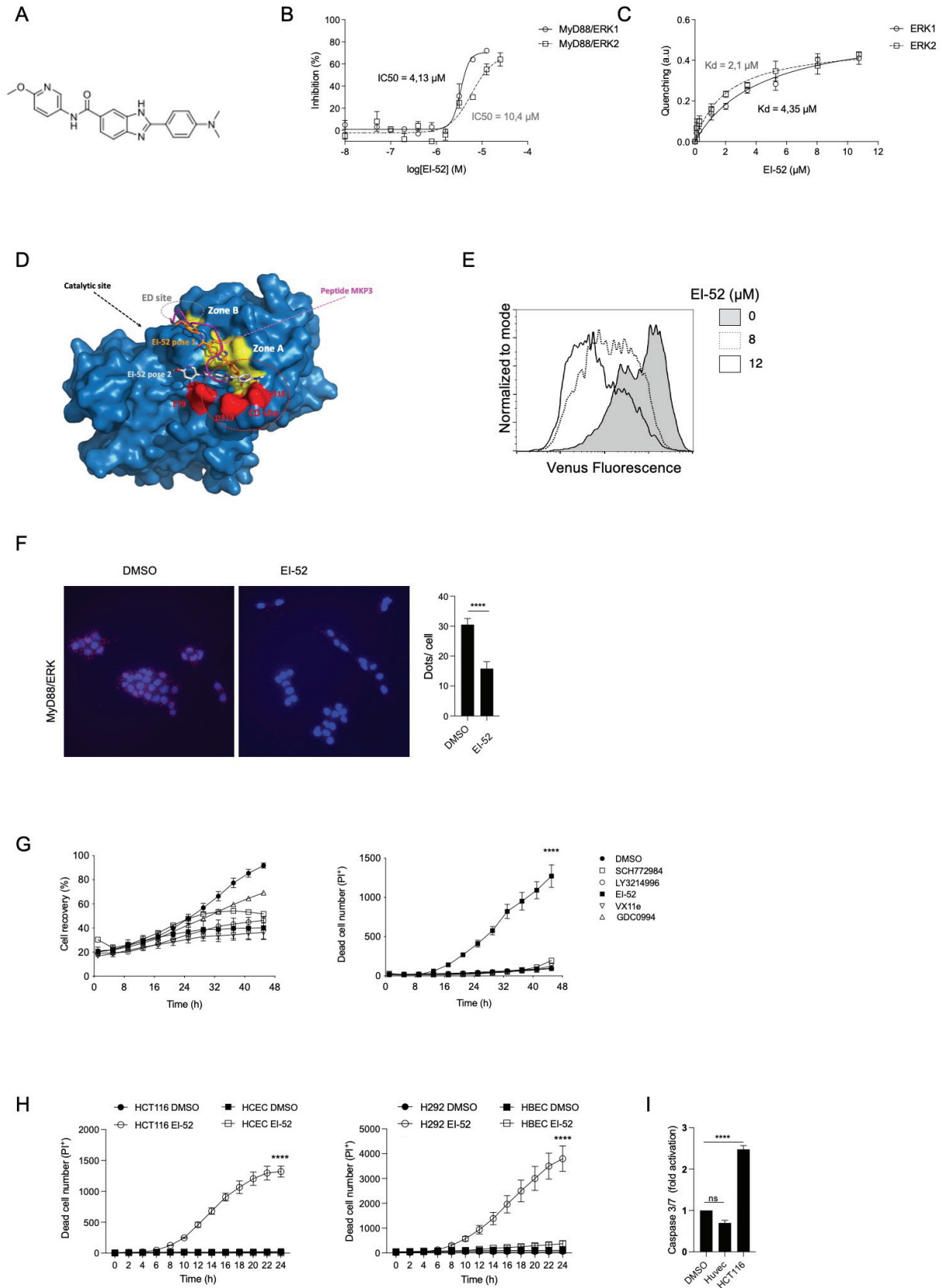


**Figure 1: EI-52 inhibits ERK-MyD88 protein-protein interaction and induces cancer cell death. (A)** EI-52 chemical structure. **(B)** ERK1/2-MyD88 interaction inhibition by EI-

52 in HTRF assay. The experiment was performed at least 3 times. **(C)** Fluorescence quenching assay showing that EI-52 directly binds to ERK1 and ERK2. Representative of 2 experiments. **(D)** *In silico* docking of EI-52 on ERK's DRS. The ERK molecular surface is shown in blue, three negatively charged residues are represented in red. The predicted binding Zone A includes the so-called Common Docking (CD) domain (red dotted circle). The co-crystallized MKP3 peptide is shown in magenta (PDB: 2FYS). Key hydrophobic/aromatic residues in the ERK binding groove are painted in yellow. The two proposed orientations of the docked EI-52 compound are shown (stick representation). **(E)** Flow cytometry analysis of BiFC, showing that EI-52 (8  $\mu$ M) is able to prevent MyD88-ERK1 interaction in transfected HEK293T cells. Representative of 2 experiments. **(F)** PLA was conducted in HCT116 cells to analyze the interaction of endogenous MyD88 and ERK. Cells were treated with EI-52 (8  $\mu$ M) or the equivalent volume of vehicle (DMSO) for 3h. After cell fixation, PLA with antibodies against MyD88 and ERK was performed. The detected interactions are indicated by red dots. The nuclei were counterstained with DAPI (blue). The number of interactions detected by ImageJ analysis is shown as the mean  $\pm$  SEM of three independent experiments. \*\*\*\*,  $P < 0,0001$ , unpaired two-tailed Student *t* test. **(G)** Cell recovery was evaluated by measuring confluence (Left panel) and cell death quantification by measuring number of propidium iodide positive cells (Right panel) after treatment with EI-52 or ERK kinase inhibitors over 48h at 8  $\mu$ M. The experiment was performed 2 times, with similar results, and data from a representative experiment are shown. Cell death after EI-52 treatment compared with the control group (DMSO) \*\*\*\*,  $P < 0.0001$  Two-way ANOVA. **(H)** Cell death quantification by measuring number of propidium iodide positive cells after treatment of transformed or untransformed cell lines with control (DMSO) or EI-52 over 48h at 8  $\mu$ M (n=3). EI-52 treatment compared with the control group (DMSO) in transformed cells. \*\*\*\*,  $P < 0.0001$

Two-way ANOVA. (I) Caspase 3/7 activity after 16h treatment of HCT116 cells or HUVEC with EI-52 (8 $\mu$ M). Results are expressed as EI-52 treatment/DMSO ratio. Pool of 3 donors HUVEC EI-52/DMSO ratio non-significant, HCT116 EI-52/DMSO ratio \*\*\*\*, P<0.0001, One-way ANOVA.

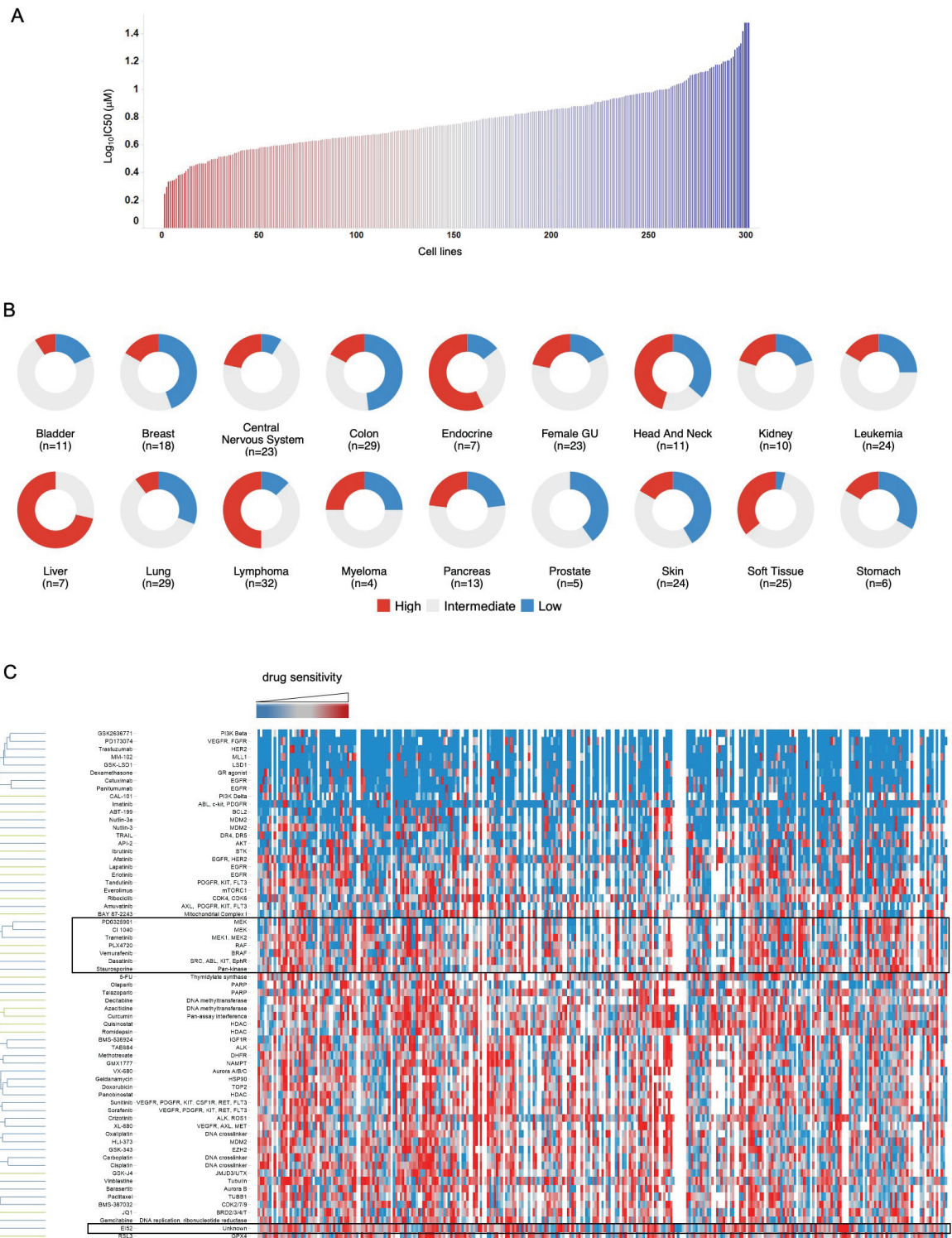


**Figure 2: EI-52 activity is mechanistically distinctive and tumor-type agnostic**

(A) Waterfall plot of IC50 values of 301 cell lines of the OncoPanel™ collection. Each bar represents one cell line, colored by relative drug response. (B) Classification of response to EI-52 according to the origin of the cancer cell lines. Pie charts showing the distribution



of cell lines classified as sensitive (red), relatively resistant (blue), or intermediate (gray) within each cancer type represented in OncoPanel™. The number of cell lines for each tissue/tumor type is indicated in parentheses. (C) Dendrogram with EI-52 and 63 anti-tumour reference compounds clustered by drug sensitivity in 301 cell lines.

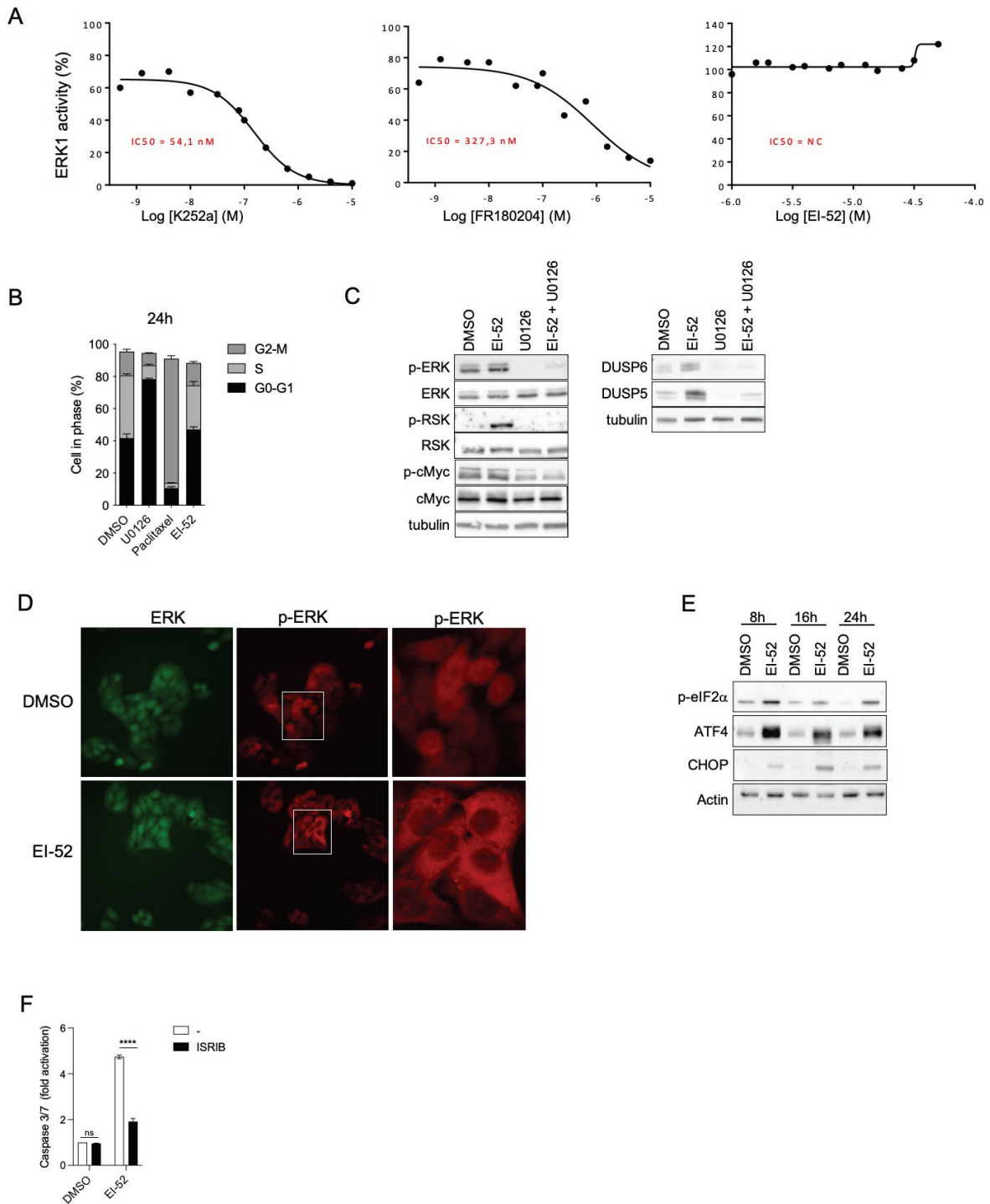


**Figure 3: EI-52 modifies ERK activity and localization, leading to integrated stress response and apoptosis in cancer cells.** (A) *In vitro* ERK1 kinase assay was performed with the pan-serine/threonine protein kinase inhibitor (K252a), the selective ERK inhibitor (FR180204), or EI-52. The experiment was performed 2 times, with similar results, and data from a representative experiment are shown. (B) HCT116 cells treated

with vehicle (DMSO), MEK inhibitor (U0126) 10 $\mu$ M, paclitaxel 25nM, or EI-52 8 $\mu$ M for 24h. Fixed cells were collected and the cell cycle was measured by flow cytometry using BrdU/PI staining. The representative data of two independent experiments are shown. (C) Serum starved-HeLa cells were treated for 8 hours with EI-52 8  $\mu$ M, U0126 10  $\mu$ M or a combination of EI-52 and U0126 and ERK targets were analyzed by western blot. The representative data of two independent experiments are shown. (D) Immunofluorescence staining of phosphorylated-ERK and total ERK after treatment of serum starved-HeLa cells with EI-52 8  $\mu$ M for 6 hours. The representative data of three independent experiments are shown. (E) HCT116 cells were treated for the indicated times with 8  $\mu$ M of EI-52 and ISR markers were analyzed by western blot. The representative data of three independent experiments are shown. (F) HCT116 cells were incubated in the absence or presence of ISRIB 400 nM for 1h and then treated with EI-52 8  $\mu$ M for 16h. Bar graph represents the fold change of caspase 3/7 activity. The experiment was performed 3 times. Result expressed as treatment/DMSO ratio mean  $\pm$  SEM of three independent experiments. ns: non-significant, \*\*\*\*, P<0.0001, One-way ANOVA.

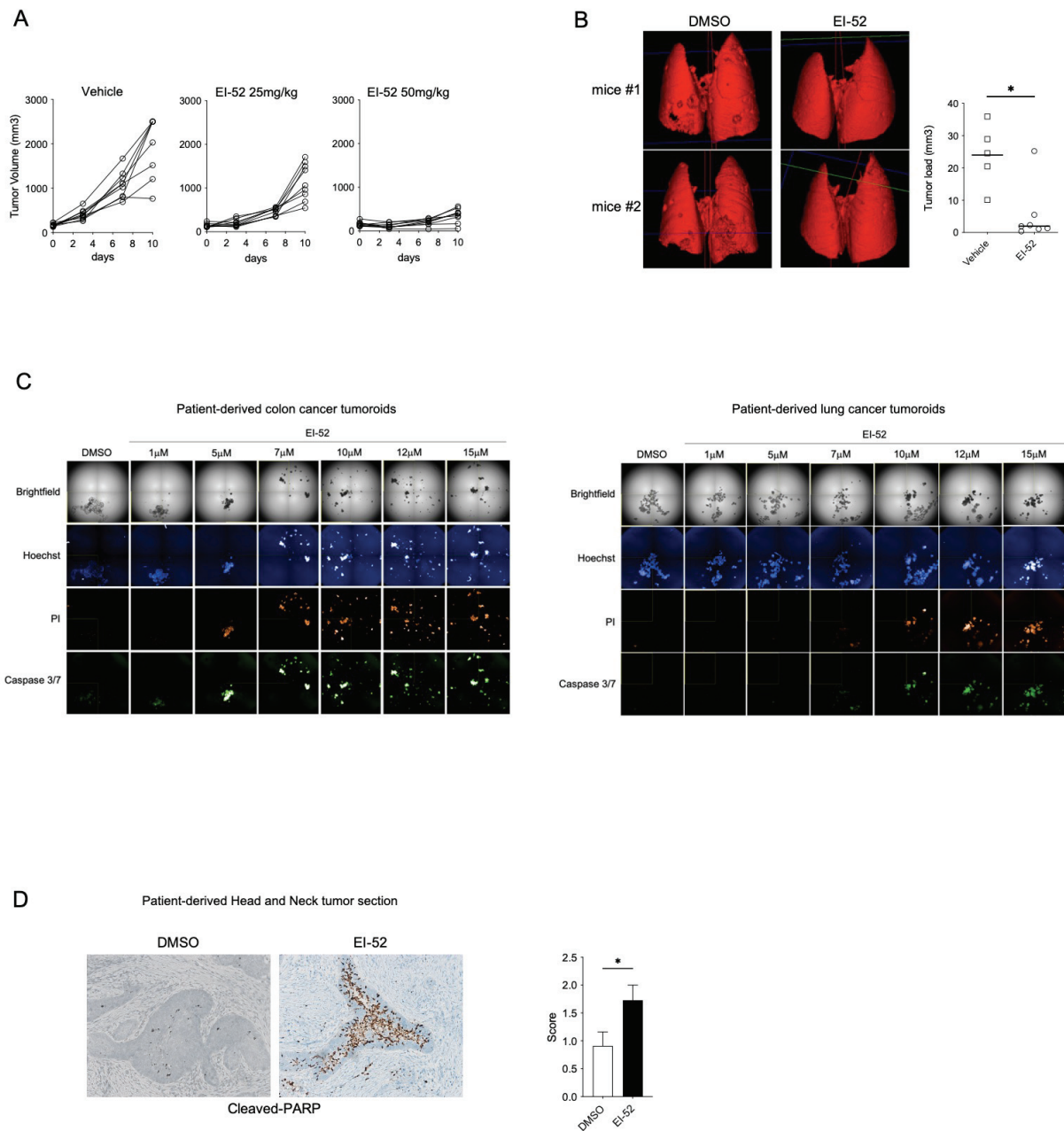


**Figure 4: EI-52 inhibits tumor growth in mouse tumor models and induces cell death of patient-derived tumoroids and ex-vivo tumors.** (A) C57BL/6 mice (n =9/group) injected subcutaneously with Lewis Lung Carcinoma cells were treated daily by intraperitoneal injection with vehicle (PBS, 40% PEG 400, 20% DMSO) or with 25 or 50 mg/kg EI-52. Tumor volume was measured twice a week with an electronic caliper. (B) Five-week-old K-ras<sup>LA2</sup> mice (WT n= 5, K-Ras mutant n=7) were treated intraperitoneally 5 times a week for 10 weeks with 25 mg/kg EI-52. Tumor load was

evaluated on a Perkin Elmer Quantum FX microCT scan. Left panel: example of image reconstitution of lungs from 2 mice treated for 10 weeks with vehicle or with EI-52. Right panel: tumor load in the lungs of vehicle- or EI-52-treated mice at 10 weeks. \*,  $P < 0.05$ , Mann-Whitney Test. (C) Patient-derived cancer tumoroids from colon and lung were treated for 48h with DMSO or indicated concentrations of EI-52. Cell death (PI-positive) and apoptosis (caspase 3/7 cleavage) were observed by OPERA imaging. (D) Thick (250  $\mu\text{m}$ ) sections of surgical pieces from head and neck cancers were cultured in optimized medium in presence of DMSO or EI-52 (8  $\mu\text{M}$ ). 24h later, thin sections were sliced and stained for the apoptotic marker cleaved-PARP (left panel). IHC scoring allows a semi-quantitative analysis of apoptosis (right panel), H&N  $n=11$ , \*,  $P < 0.05$  paired, two-side Student  $t$  test.

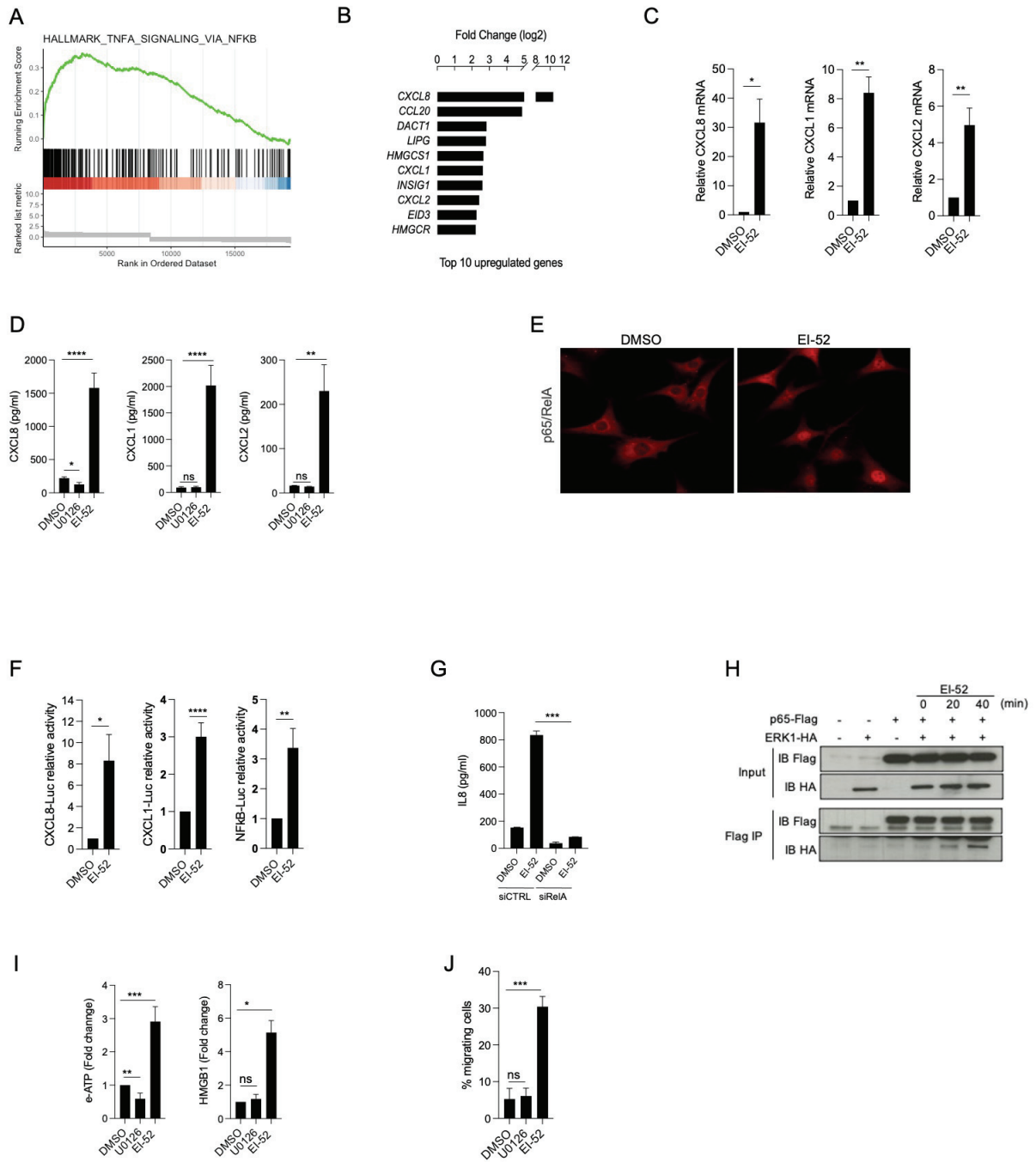


**Figure 5: EI-52 induces immunogenic cancer cell death *in vitro*** (A) GSEA plot for enrichment of the Hallmark TNFA signaling via NFkB gene set in HCT116 cells treated for 18h with EI-52 (6  $\mu$ M) compared to DMSO. (B) Top ten genes upregulated in HCT116 cells treated for 18h with EI-52 (6  $\mu$ M) compared to DMSO. (C) Quantitative PCR of chemokine mRNA from HCT116 cells treated for 16h with either DMSO or EI-52 (8  $\mu$ M).

Mean  $\pm$  SEM of three independent experiments \*,  $p < 0.05$ ; \*\*,  $p < 0.01$ , One sample *t*-test.

**(D)** CXCL8, CXCL1, and CXCL2 protein quantification in culture supernatants of HCT116 cells treated with DMSO, with the MEK inhibitor U0126 (10  $\mu$ M), or with EI-52 (8  $\mu$ M) for 24 hours. Mean  $\pm$  SEM of at least three independent experiments. ns, non-significant, \*,  $p < 0.05$ ; \*\*,  $p < 0.001$ , \*\*\*\*,  $p < 0.0001$  unpaired two-tailed Student *t* test. **(E)** Immunofluorescence staining of p65/RelA after treatment of HCT116 cells with EI-52 8 $\mu$ M for 1 hour. Image representative of three independent experiments. **(F)** Luciferase reporter activity of NF- $\kappa$ B, CXCL1 and CXCL8 was measured with Dual-Luciferase Reporter assay (Promega) after reporter transfection in HEK293T cells and 16h of treatment with DMSO or EI-52 (8  $\mu$ M). Results are expressed as mean of treatment /DMSO ratio  $\pm$  SEM of at least three independent experiments. ns, non-significant, \*,  $p < 0.05$ ; \*\*,  $p < 0.001$ , \*\*\*,  $p < 0.005$  one sample-*t* test. **(G)** IL8 secretion was measured in supernatant of HCT116 cells transfected with control or RelA RNAi for twenty-four hours and treated 16h with DMSO or EI-52 (8  $\mu$ M). Mean  $\pm$  SEM representative of two experiments. \*\*\*,  $p < 0.005$  unpaired two-tailed Student *t* test **(H)** Co-immunoprecipitation of ERK1 with P65-Flag after treatment of transfected HEK293T cells with EI-52 (8  $\mu$ M). Immunoprecipitation were performed with anti-Flag antibody. **(I)** Measure of extracellular ATP (e-ATP) and HMGB1 released in culture supernatants of HCT116 cells treated for 24h with DMSO, MEK inhibitor U0126 (10  $\mu$ M), or EI-52 (8  $\mu$ M). Results are expressed as mean of treatment /DMSO ratio  $\pm$  SEM of at least three independent experiments. ns, non-significant, \*,  $p < 0.05$ ; \*\*,  $p < 0.001$ , \*\*\*,  $p < 0.005$  one sample-*t* test. **(J)** Chemotaxis was evaluated by counting THP1 cells migrating from the upper to lower Boyden chamber containing supernatant of HCT116 cells treated twenty-four hours with control, U0126 (10  $\mu$ M), or EI-52 (8  $\mu$ M). Results are expressed as mean  $\pm$  SEM of three independent experiments. ns, non-significant, \*\*\*,  $p < 0.005$ .

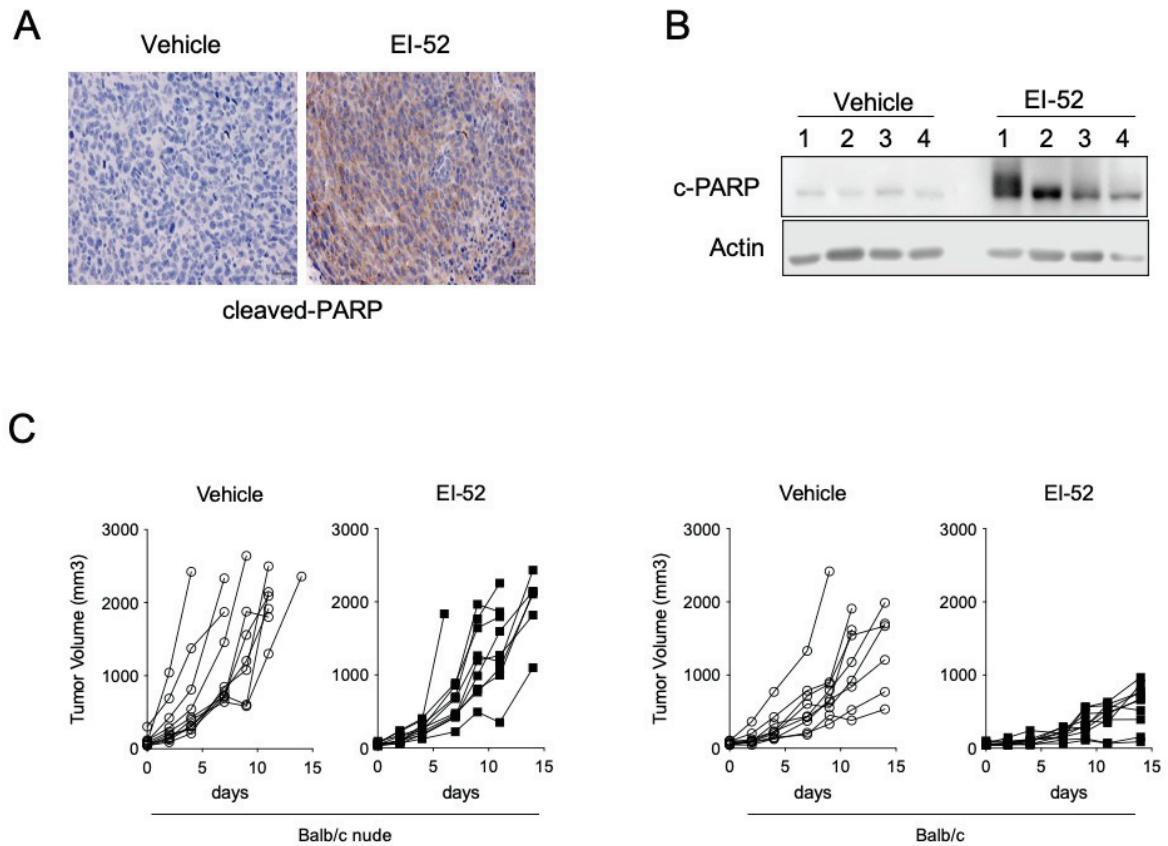


**Figure 6: ERK-MyD88 interaction inhibition by EI-52 induces cancer cell death and immune T-cell response *in vivo*.** Following s.c. implantation of syngeneic CT26 cells, BALB/c mice were treated intraperitoneally for 24 hours with vehicle or EI-52 50mg/kg and tumors were collected. **(A)** Cleaved-PARP was observed by IHC staining or **(B)** by western Blot of tumor cell lysates recovered from 4 mice per treatment (Left panel). **(C)** Following s.c. implantation of CT26 cells, syngeneic wild-type and nude BALB/c mice (n=10/group) were treated daily with vehicle or with 25 mg/kg EI-52 intraperitoneally. Tumor volume was measured twice a week with an electronic caliper.



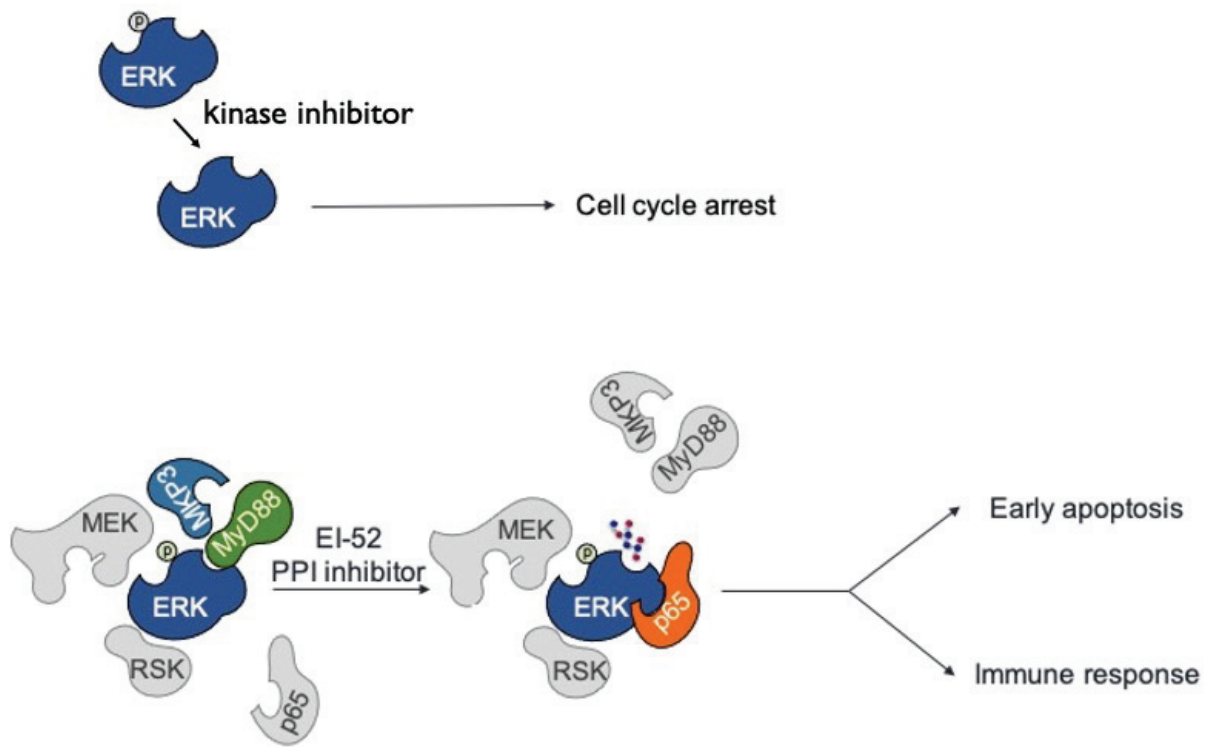
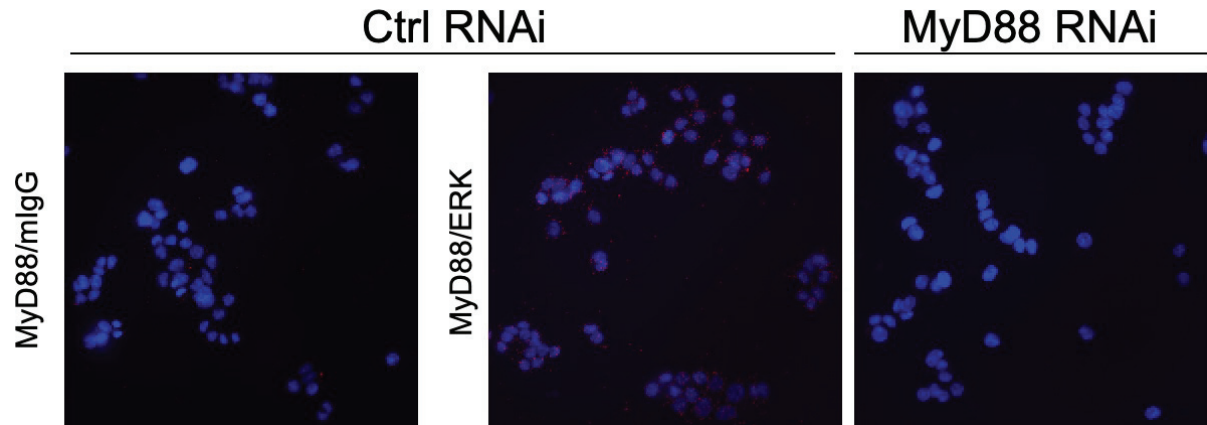


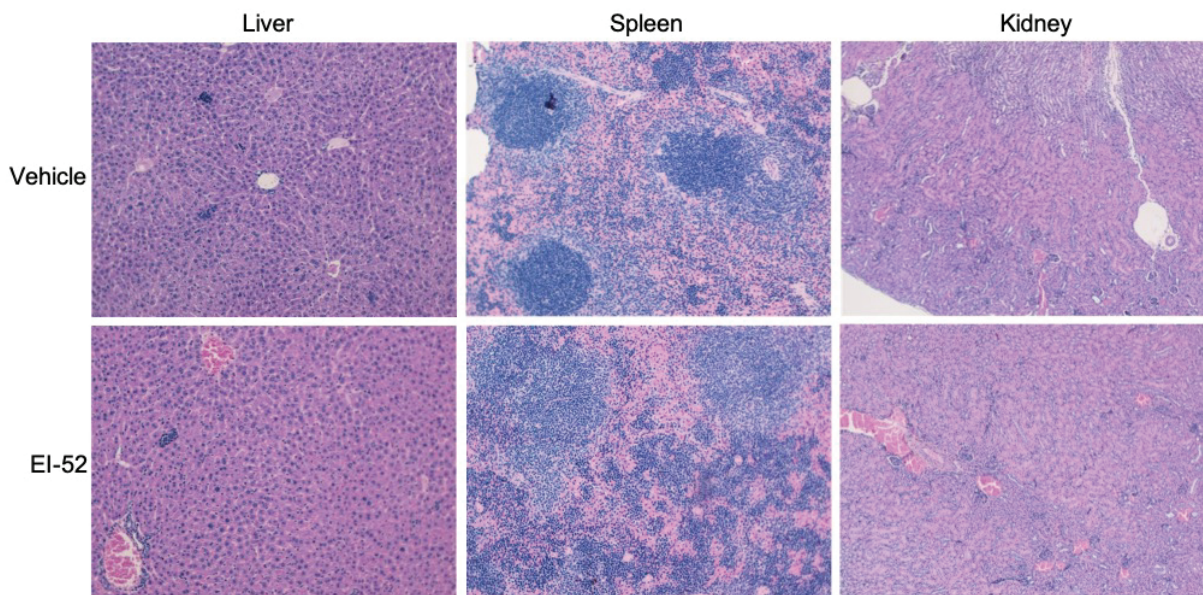
**Figure 7: Illustration.**

Biological outcome of ERK kinase vs ERK-MyD88 PPI inhibition.



### Supplemental figure 1

Specificity control experiment related to Figure 1F. Knockdown of MyD88 with siRNA abolishes the MyD88-ERK PLA signal.



### Supplemental figure 2

Histology (HPS staining) of organs from mice treated intraperitoneally five times per week with 25 mg/kg of EI-52 for 10 consecutive weeks.



**3. Article 2, submitted, in review.**

Available on bioRxiv preprint, doi: <https://doi.org/10.1101/2022.12.16.520736>;

**AB668, a novel highly selective protein kinase CK2 inhibitor with a distinct anti-tumor mechanism as compared to CX-4945 and SGC-CK2-1**

Alexandre Bancet<sup>1</sup>, **Rita Frem**<sup>2,#</sup>, Florian Jeanneret<sup>4,#</sup>, Angélique Mularoni<sup>1</sup>, Pauline Bazelle<sup>4</sup>, Caroline Roelants<sup>4</sup>, Jean-Guy Delcros<sup>1</sup>, Jean-François Guichou<sup>3</sup>, Catherine Pillet<sup>4</sup>, Isabelle Coste<sup>2</sup>, Renno Toufic<sup>2</sup>, Christophe Battail<sup>4</sup>, Claude Cochet<sup>4</sup>, Thierry Lomberget<sup>5</sup>, Odile Filhol<sup>4</sup>, Isabelle Krimm<sup>1</sup>

## **AB668, a novel highly selective protein kinase CK2 inhibitor with a distinct anti-tumor mechanism as compared to CX-4945 and SGC-CK2-1**

**Alexandre Bancet<sup>1</sup>, Rita Frem<sup>2,#</sup>, Florian Jeanneret<sup>3,#</sup>, Angélique Mularoni<sup>1</sup>, Pauline Bazelle<sup>3</sup>, Caroline Roelants<sup>3</sup>, Jean-Guy Delcros<sup>1</sup>, Jean-François Guichou<sup>4</sup>, Catherine Pillet<sup>3</sup>, Isabelle Coste<sup>2</sup>, Toufic Renno<sup>2</sup>, Christophe Battail<sup>3</sup>, Claude Cochet<sup>3</sup>, Thierry Lomberget<sup>5</sup>, Odile Filhol<sup>3,\*</sup>, Isabelle Krimm<sup>1,\*</sup>**

<sup>1</sup> Univ Lyon, Université Claude Bernard Lyon 1, INSERM 1052, CNRS 5286, Centre Léon Bérard, Centre de recherche en cancérologie de Lyon, Institut Convergence Plascan, Team « Small Molecules for Biological Targets », Lyon, 69373, France

<sup>2</sup> Univ Lyon, Université Claude Bernard Lyon 1, INSERM 1052, CNRS 5286, Centre Léon Bérard, Centre de recherche en cancérologie de Lyon, Institut Convergence Plascan, Team Targeting non-canonical protein functions in cancer, Lyon, 69373, France

<sup>3</sup> Univ. Grenoble Alpes, INSERM 1292, CEA, UMR Biosanté, Grenoble, 38000, France

<sup>4</sup> Centre de Biologie Structurale, CNRS, INSERM, Univ. Montpellier, Montpellier 34090, France

<sup>5</sup> Univ Lyon, Université Claude Bernard Lyon 1, CNRS UMR 5246, Institut de Chimie et Biochimie Moléculaires et Supramoléculaires (ICBMS), COSSBA Team, Faculté de Pharmacie-ISPB, 8 Avenue Rockefeller, FR-69373 Lyon Cedex 08, France

# Contributed equally to this work

\*Corresponding authors

## Abstract

Although the involvement of protein kinase CK2 in cancer is well-documented, there is a need for selective CK2 inhibitors suitable for investigating CK2 specific roles in cancer-related biological pathways and further explore its therapeutic potential. Here we have discovered AB668, a new bivalent inhibitor that binds both at the ATP site and an allosteric  $\alpha$ D pocket unique to CK2. The molecule inhibits CK2 activity with an outstanding selectivity over other kinases. Using caspase activation assay, live-cell imaging and transcriptomic analysis, we have compared the effects of this bivalent inhibitor to the non-selective ATP-competitive inhibitor CX-4945 that reached clinic and to the selective ATP-competitive SGC-CK2-1 molecule. Our results show that in contrast to CX-4945 or SGC-CK2-1, AB668 has a distinct mechanism of action regarding its anti-cancer activity, inducing apoptotic cell death and stimulating distinct biological pathways in several cancer cell lines while sparing healthy cells. Our data suggest that targeting a cryptic CK2  $\alpha$ D pocket validates an allosteric approach to targeting CK2 and provides a starting point for creating drug-like CK2 inhibitors for aggressive cancers.

## Acknowledgment

We thank Institut Convergence PLAsCAN (ANR-17-CONV-002), as well as ANR-21-CE18-0014-01 for project ANR-CK2COV, Ligue contre le Cancer (Comité de l'Isère), ITMO Cancer of Aviesan on funds administered by Inserm, Commissariat à l'Energie Atomique et aux Energies Alternatives (CEA), Université Grenoble-Alpes (UGA) and SATT PULSALYS for financial supports. We acknowledge both the European Union's Horizon 2020 research and innovation program which funded P.B. and F.J. through the KATY project (grant agreement No 101017453) and the contribution of SFR Biosciences (UAR3444/CNRS, US8/Inserm, ENS de Lyon, UCBL): Protein Science Facilities. We are grateful to Dr David Knapp and Dr Andreas Krämer for the gift of the CK2 $\alpha$  plasmid and their advice for CK2 $\alpha$  crystallization. FJ and PB are supported by the KATY EU program Horizon 2020/H2020-SCI-FA-DTS-2020-1 (contract number 101017453).

We acknowledge the staff of the ID30B beamline at the ESRF. The CBS is a member of the French Infrastructure for Integrated Structural Biology (FRISBI), a national infrastructure supported by the French National Research Agency (ANR-10-INBS-05).

We thank Muriel Gelin for technical help for the treatment of the x-ray diffraction data.

## Introduction

CK2 is a constitutively active protein kinase ubiquitously expressed in eukaryotes and particularly well conserved among species. CK2 phosphorylates serine or threonine residues within an acidic context (S/TXXD/E/pS/pT/pY) and is responsible for the generation of a large proportion of the human phosphoproteome (Franchin et al., 2015). One of the distinctive features of CK2 is to exist in cells as a catalytic subunit CK2 $\alpha$  and as a holoenzyme CK2 $\alpha_2\beta_2$ , which consists of two catalytic subunits CK2 $\alpha$  that interact with a dimer of two regulatory subunits CK2 $\beta$  (Niefind 2001). Although the so-called regulatory CK2 $\beta$  subunits are not essential per se for CK2 $\alpha$  kinase activity as the catalytic subunit is constitutively active (Niefind et al., 2009), several reports showed that CK2 $\beta$  influences significantly CK2 substrate preference as well as CK2 $\alpha$  localization (Núñez de Villavicencio-Díaz et al., 2015; Bibby et al., 2005). Up to now, several hundreds of proteins have been shown to be CK2 substrates in cells (Meggio and Pinna et al., 2003; Bian 2016; Borgo et al., 2017). CK2 is involved in important physiological functions, such as embryonic development, differentiation, immunity, cell survival, epithelial homeostasis and circadian rhythms. CK2 is also implicated in numerous human diseases such as cancer, neurodegenerative diseases, viral and parasite infections, cystic fibrosis, psychiatric disorders, diabetes, inflammatory and cardiovascular diseases (Borgo et al., 2021; Dominguez et al., 2009). In cancer, CK2 promotes cell proliferation and survival (Chua et al., 2017a; Trembley et al., 2009). CK2 might also be involved in immune cell development and function in cancer (Husain et al., 2021), in cancer metabolism (Silva-Pavez et al., 2020) as well as in antitumor drug resistance (Borgo et al., 2019). For example, proliferation, migration, invasion, and survival of cholangiocarcinoma cells exposed to cytostatic drugs are markedly reduced when cells are depleted in CK2 $\alpha$  subunit (Di Maira et al., 2019). Globally, CK2 is overexpressed in a very large number of human tumors (e.g., breast, ovarian, prostate, lung, colon, kidney, skin and pancreatic cancers) and its over-expression correlates with poor prognosis (Laramas et al., 2007; Chua et al., 2017b; Roelants et al., 2015). The higher sensitivity of cancer cells to CK2 inhibition, as compared to their healthy counterparts, led to the hypothesis of a “non-oncogenic” CK2 addiction of cancer cells (Luo et al., 2009; Ruzzene et al., 2010). Compiling evidence from the literature suggests that CK2 modulates all hallmarks of cancer (Firnau et al., 2022). Consequently, CK2 is considered as a “master regulator” and a promising therapeutic target to treat different human tumors (Roffey et al., 2021).

Many CK2 inhibitors that target the CK2 catalytic site have been proposed (Atkinson et al., 2021). The most advanced molecule silmitasertib (CX-4945) inhibits CK2 $\alpha$  catalytic activity with a  $K_i$  of 0.38 nM (Pierre et al., 2011) and the compound has entered several clinical trials. Notably, silmitasertib received an orphan drug designation for the treatment of cholangiocarcinoma in 2016, medulloblastoma in 2020, recurrent Sonic Hedgehog-driven medulloblastoma in 2021 and biliary tract cancer in 2022 (Lee et al., 2022). Although described as highly selective, CX-4945 inhibits several kinases with nanomolar IC<sub>50</sub> values (CLK1, CLK2, CLK3, DYRK1A, DYRK1B, DAPK3, HIPK3...) (Pierre et al., 2011). For example, CX-4945 was reported to regulate splicing in mammalian cells in a CK2-independent manner through the inhibition of Clk1, Clk2 and Clk3 (Kim et al., 2016). Therefore, despite its therapeutic efficacy, CX-4945 cannot be used to probe the cellular functions of CK2. Recently, a newly developed ATP-competitive CK2 inhibitor, SGC-CK2-1, was reported (Wells et al., 2021). SGC-CK2-1 (IC<sub>50</sub> 2.3 nM on CK2 $\alpha$ ) is much more selective than CX-4945 and was consequently described as a genuine chemical probe to assess the consequences of the pharmacological inhibition of CK2 kinase activity (Wells et al., 2021). When tested on a panel of 140 cancer cell lines, SGC-CK2-1 reduced cell growth in blood, head/neck, brain, breast, skin, stomach and duodenum cell lines with a micromolar range efficacy. This poor antiproliferative effect led the authors to question the inhibition of CK2 as a strategy for cancer therapy (Wells et al., 2021; Licciardello et al., 2021).

To further decipher the role of CK2 in cancer biology, we considered the opportunity of targeting allosteric sites of the protein. Allosteric compounds have the advantage to bind to less conserved pockets of the kinase. Conceptually, such compounds would be more selective chemical tools. Also, as therapeutics, they would generate less side effects due to off-target kinase inhibition (Lu et al., 2020). Regarding CK2, the CK2 $\alpha$ /CK2 $\beta$  interface and the so-called  $\alpha$ D pocket have both been targeted by small-molecule inhibitors (Figure S1) (Iegre et al., 2021). We previously reported a small-molecule that binds at the CK2 $\alpha$ /CK2 $\beta$  interface and disrupts the holoenzyme in cells, inhibiting cell growth and migration (Kufareva et al., 2019). However, the affinity of the inhibitor was rather weak ( $K_D$  30  $\mu$ M) for further characterization. Bivalent CK2 inhibitors targeting simultaneously the ATP-binding site and the  $\alpha$ D pocket have also been reported (Brear et al., 2016, De Fusco et al., 2017, Lindenblatt et al., 2022). The bivalent inhibitor CAM4066 ( $K_D$  of 0.32  $\mu$ M) reduced cell viability in HCT116, Jurkat and A549 cells with GI<sub>50</sub> of 9, 6 and 20  $\mu$ M, respectively (Brear et al., 2016). The bivalent inhibitor KN2 ( $K_i$  6 nM for holoenzyme CK2) proved to be cytotoxic in HeLa cells (6  $\mu$ M) but also displayed



cytotoxicity in nontumor HEK293 cell line (16  $\mu$ M). None of those bivalent compounds were used to explore CK2 function in cancer cells. Here, we report a highly selective CK2 bivalent inhibitor, AB668, that binds simultaneously the ATP site and the  $\alpha$ D pocket of CK2 $\alpha$ . AB668 displays an outstanding selectivity measured against a panel of 468 kinases, inhibits the activity of the holoenzyme CK2 with a  $K_i$  of 41 nM and induces apoptotic cell death on various cancer cell lines, while being non-cytotoxic for healthy cells. AB668 therefore represents a valuable chemical tool to explore CK2 mechanisms in cancer and to decipher the specific function of this particular pocket of the kinase. Here we compared the impact on cancer cells of AB668 and the two ATP-competitive CK2 inhibitors CX-4945 and SGC-CK2-1 on various cancer cells, using live cell imaging and transcriptomic analysis. Our results highlight that, by targeting both the ATP site and the  $\alpha$ D pocket, AB668 discloses a distinct mode of action compared to canonical ATP-competitive inhibitors, suggesting that targeting the  $\alpha$ D pocket of CK2 may represent a valuable pharmacological tool and therapeutic strategy in cancer.

## Results

### Binding mode, activity, and selectivity profile of AB668.

During our efforts to optimize the CK2 $\alpha$ /CK2 $\beta$  interface inhibitor that we previously reported (Kufareva et al., 2019, Figure S1), one of the chemical series led to the discovery of AB668, a compound that simultaneously binds at the ATP site and the  $\alpha$ D allosteric pocket of CK2 (Figure 1a and Figure S2). A Thermal Shift Assay experiment was used to confirm direct binding of AB668 with CK2 $\alpha$ . CK2 $\alpha$  alone displayed a  $T_m$  of  $43.6 \pm 0.4^\circ\text{C}$ . At saturating inhibitor concentration, AB668 induced a significant increase of the  $T_m$  value ( $\Delta T_m = 5.2 \pm 0.4^\circ\text{C}$ ). By comparison, the ATP-competitive inhibitors CX-4945 and SGC-CK2-1 induced a substantial increase of the  $T_m$  value ( $\Delta T_m = 13.8 \pm 0.4^\circ\text{C}$ ,  $\Delta T_m = 11.0 \pm 0.3^\circ\text{C}$ , respectively) (Figure S3). The lower magnitude of the change in  $T_m$  induced by AB668 may be related to its different binding site and to its lower affinity, as described below. The 3D X-ray structure of AB668 bound to CK2 $\alpha$  was resolved using crystallization conditions reported for the X-ray structure of the CK2 $\alpha$ -SGC-CK2-1 complex (Wells et al., 2021). The indole moiety of the bivalent inhibitor AB668 binds in the ATP site and interacts with the side chain of Lys68 through a hydrogen bond mediated by a water molecule, and the carbonyl group directly interacts with Lys68 through a weak hydrogen bond (Figure 1b). The aromatic moiety of indole

is sandwiched between Val53, Val66, Ile95, Phe113, Met163 and Ile174. On the other side of the bivalent inhibitor, the substituted phenyl binds in the highly hydrophobic  $\alpha$ D-pocket of CK2 (Tyr125, Leu128, Ile133, Met137, Tyr136, Ile140, Pro159, Val162, Ile164, Met221 and Met225). Regarding the linker part between the indole moiety and the substituted phenyl, the sulfonamide group interacts with the peptide chain of Ile164, while the nitrogen of piperidine interacts with Asn118 side chain. As illustrated in Figure 1c, the  $\alpha$ D-helix position is shifted together with the side chains of residues Phe121 and Tyr125 upon AB668 binding and remains flexible in the crystal, with large B-factors values observed from residues Asn118 to Thr127. Modification of the conformation of the  $\beta$ 4- $\beta$ 5 loop is observed in one monomer but not in the second one, suggesting that the loop conformation is highly dynamic, which is corroborated by large B-factors values for the loop.

The affinity of AB668 for CK2 $\alpha$  was  $86 \pm 20$  nM, as determined by the KINOMEscan<sup>TM</sup> profiling service (Eurofins) (Figure 1d). AB668 also inhibited the CK2 holoenzyme with an inhibitory constant  $K_i$  of 41 nM, as determined using a canonical radiometric assay with a CK2 $\beta$ -dependent peptide substrate (Figure S4a). We also showed that AB668 inhibits the phosphorylation of a CK2 protein substrate. The phosphorylation of SIX1, a transcription factor that is specifically phosphorylated by the CK2 holoenzyme (Wu et al., 2016) was inhibited by about 90% in the presence of 0.5  $\mu$ M AB668 (Figure S4b).

The selectivity of AB668 was profiled against 468 kinases, using an active site-directed competition binding assay and  $IC_{50}$  validation with the screening platform from Eurofins DiscoverX. For this, AB668 was tested at a concentration of 2  $\mu$ M (25 times its  $K_d$  value). As shown in Figure 1e, besides CK2 $\alpha$  and CK2 $\alpha'$ , only one kinase (RPS6KA5) displayed a percent inhibition larger than 50%. A value of 0.01 was obtained for the selectivity score ( $S_{10}(2 \mu M)$ ) (Bosc et al., 2017), showing that, by targeting the ligandable  $\alpha$ D pocket, AB668 displays an outstanding selectivity against a large kinase panel.

### **Cellular activity of AB668 in cancerous cells.**

We next evaluated whether this allosteric inhibitor was capable of engaging and inhibiting CK2 in living cells. As we previously reported that the CK2 subunits are overexpressed at the protein level in renal carcinoma compared to normal renal tissues (Roelants et al., 2015), we tested the effects of AB668, CX-4945 and SGC-CK2-1 in clear cell renal cell carcinoma (ccRCC) 786-O cells. Like staurosporine, AB668 and CX-4945 induced caspase-3 activation in 786-O cells, as shown after 72 h treatment using a quantitative fluorometric assay (Figure 2a). In contrast, and

as previously reported (Wells et al., 2021), SGC-CK2-1 did not activate caspase-3 (Figure 2a). Caspase-3 activation induced by AB668 was confirmed by Western blot experiments (Figure 2b), showing the cleavage of PARP, a known target of caspase-3 (Duncan et al., 2011; Boulares et al., 1999). Similarly, AB668 reduced the expression of survivin, a member of the Inhibitor of Apoptosis Protein family that inhibits caspases and blocks cell death (Figure 2b) (Barrett et al., 2011). These observations encouraged us to further characterize the potential functional impact of AB668 and the ATP-competitive inhibitors in living cancer cells.

For this, Incucyte Live cell analysis was used to analyze the effect of the various CK2 inhibitors in 786-O cells (Figure 2c). We also performed the same experiments for a melanoma cell line (A375), for which few information is available regarding the effect of CK2 inhibition (Parker et al., 2014; Zhou et al., 2016). As illustrated in Figure 2c, AB668 induced significant cell proliferation arrest associated with cell death and apoptosis in both cancer cell lines. By comparison, CX-4945 had only a moderate effect on 786-O cell growth and was a poor apoptosis inducer. Similarly, A375 cells were almost completely insensitive to CX-4945 and SGC-CK2-1 showing that these inhibitors had no impact on the survival of both cell lines (Figure 2c). CK2 has been shown to be involved in apoptotic pathway protecting substrates from caspase-3-mediated proteolysis (Duncan et al., 2011; Turowec et al., 2013), and CX-4945 was previously reported to induce apoptotic cell death in cancer cells lines such as PC3 prostatic adenocarcinoma (Pierre et al., 2011), B-ALL, T-ALL (Richter et al., 2019; Buontempo et al., 2014), H1299, Calu-1 and H358 (So 2015). Our data suggest that the selective CK2 inhibition by SGC-CK2-1 is not sufficient to induce caspase-3-mediated apoptosis and that apoptotic cell death induced by CX-4945 may be related to its activity on other kinases.

We then evaluated the efficacy of AB668 on an *ex-vivo* culture model of renal carcinoma that we previously used to study individual responses to targeted therapies (Roelants et al., 2018; Roelants et al., 2020). As shown in Figure 2d, 10  $\mu$ M CX-4945 had no effect on tumor slices of renal carcinoma, while 5  $\mu$ M AB668 significantly reduced cell viability after 24h of treatment, showing its higher efficacy in this drug sensitivity prediction model. This study suggests that AB668-mediated CK2 inhibition could prove a viable therapeutic strategy in renal carcinoma and highlights that treatment of tumor tissue slice culture best predicts CK2 dependency.

Importantly, no cytotoxicity of AB668 was observed in normal human cell lines such as RPTEC (Renal Proximal Tubule Epithelial Cells) and primary hepatocytes (Figure 2e).

## **Target engagement of AB668 in cancer and healthy cells.**

We next evaluated the effects of AB668 in 786-O cells on CK2-mediated downstream phosphorylation events by western blot analysis. Notably, CK2 is known to phosphorylate AKT at Ser129 (Di Maira et al., 2005; Zanin et al., 2012). As expected, AB668 decreased, in a dose-dependent manner, the phosphorylation of S129AKT (Figure 3a). AB668 also induced a dose-dependent inhibition of the activated forms of mTOR and STAT3, two proteins that regulate proliferation and apoptosis in cancer cells (Sabatini et al., 2006; Yuan et al., 2004). It was reported that inhibition of CK2 hinders STAT3 signaling and decreases aggressive phenotypes in multiple cancer types (Gray et al., 2014; Aparicio-Siegmund S. et al., 2014). AB668 activated p38MAPK, a tumor suppressor well known for its role in transducing stress signals from the environment (Figure 3a). Interestingly, mouse modeling studies showed that mTOR activation in combination with inactivation of the p38MAPK initiates renal cell carcinoma (Wu et al., 2021).

Although p53 is rarely mutated in ccRCC, its overexpression has been linked to poor prognosis (Noon et al., 2010; Diesing et al., 2021). Similarly, it has been reported that irradiation of ccRCC cell lines including 786-O cells, induced p53 phosphorylation without detectable activation indicating a functional inhibition in ccRCC (Diesing et al., 2021). As illustrated in Figure 3a, AB668 led to a weak increase of p53 phosphorylation only at high concentrations, ruling out its implication in the regulation of 786-O cell viability.

Previous work has demonstrated the anti-apoptotic role of the cyclin-dependent kinase inhibitor p21 in RCC as a potential mechanism for their drug resistance (Weiss et al., 2003). p21 binds to and inhibits the activity of proteins involved in apoptosis, including pro-Caspase-3 (Karimian et al., 2016; Abbas, et al., 2009). Phosphorylation of p21 at Thr145 by AKT1 induces its cytoplasmic accumulation (Rossig et al., 2001; Zhou et al., 2001) and propels its anti-apoptotic functions (Karimian et al., 2016; Abbas, et al., 2009). Interestingly, Sorafenib, as one of the few available effective therapeutic options for metastatic RCC, was shown to attenuate the anti-apoptotic role of p21 in kidney cancer cells (Inoue et al., 2011). We have previously shown that CX-4945 inhibits the AKT1-dependent phosphorylation of p21 in 786-O cells (Roelants et al., 2015). As shown in Figure 3a, this phosphorylation was also strongly downregulated by low concentrations of AB668 in accordance with its inhibitory effect on AKT phosphorylation in 786-O cells. Finally, we have also evaluated the effects of AB668 in the triple-negative breast

cancer cell line MDA-MB231 by western blot analysis. In comparison with 786-O cells, AB668 led to similar effects on CK2-mediated downstream phosphorylation events (Figure S5).

Motivated by the striking difference in sensitivity to AB668 between cancer versus normal cells, we evaluated its target engagement by assaying the CK2 activity in extracts of 786-O cancer cells and human embryonic kidney HEK293 cells after treatment with increasing concentrations of AB668. Inhibition constants  $IC_{50}$  were  $0.34 \pm 0.07 \mu\text{M}$  and  $0.60 \pm 0.11 \mu\text{M}$  for 786-O cells and HEK293 cells, respectively (Figure 3c). These results show that AB668 inhibited CK2 activity with a similar potency in both cell types although it did not induce cytotoxicity in normal cells (Figure 2e and Figure S5b). The comparison of downstream phosphorylation events mediated by CK2 in 786-O and HEK293 cells in response to CX-4945 or AB668 indicates that p21 phosphorylation was impaired in 786-O cells but unaffected in HEK293 cells in response to AB668 (Figure 3b).

### **Deregulations of the transcriptome in response to AB668 or CX-4945.**

To assess the impact of AB668 and CX-4945 at the transcriptomic level, molecular profiling of 786-O cells treated with these CK2 inhibitors was performed by BRB-seq, followed by differential gene expression analysis (Figure 4a – left and center plot). Only 48 genes were significantly differentially expressed (Benjamini-Hochberg corrected p-value  $< 0.05$  and  $|\log_2(\text{Fold change})| > 0.5$ ) in response to AB668 when compared to cells treated with DMSO. In contrast, 102 genes were deregulated by CX-4945 compared to DMSO. This might be related to the lower specificity of this CK2 inhibitor. Moreover, 341 genes were significantly differentially expressed in cells exposed either to AB668 or CX-4945, revealing strong differences in transcriptome perturbations associated to these two CK2 inhibitors (Figure 4a – right plot). Interestingly, SERPINE1, also known as Plasminogen Activator Inhibitor type-1 (PAI-1) a protein with a growth and migration stimulatory functions and an anti-apoptotic activity (Planus et al., 1997; Kubala and DeClerck, 2019) was found significantly down-regulated by AB668, when compared to CX-4945 or DMSO. In ccRCC tumor tissues, the expression level of PAI-1 is higher than in normal tissues and has been proven to be a reliable biological and prognostic marker associated with poor prognosis (Sui et al., 2021). Metabolic enzymes such as PSAT1, the phosphoserine aminotransferase (PSAT1), UDP-N-acetylglucosamine pyrophosphorylase 1 (UAP1) the UDP-N-acetylglucosamine pyrophosphorylase 1 and methylenetetrahydrofolate deshydrogenase/cyclohydrolase (MTHFD2), the methylenetetrahydrofolate deshydrogenase/cyclohydrolase that are highly

expressed in a wide range of tumors and associated with poor prognosis in tumor progression (Itkonen, Engedal et al., 2015; Puttamallesh et al., 2020; Reina-Campos et al., 2020; Huang et al., 2021; Zhu et al., 2022) were significantly down regulated by AB668 when compared to CX-4945.

In addition, we specifically identified, among the genes differentially expressed compared to the DMSO control, those whose expression was deregulated in an opposite way between AB668 and CX-4549 (Figure 4b). For example, SERPINE1 is down-regulated by CX-4945 but up-regulated by AB668 compared to DMSO-exposed cells. Interestingly, genes involved in fatty acid, cholesterol and steroid metabolisms like, Farnesyl-diphosphate farnesyltransferase 1 (FDFT1), 3-hydroxy-3-methylglutaryl-CoA synthase 1 (HMGCS1) and Isopentenyl-diphosphate delta isomerase 1 (IDI1) were all up-regulated by AB668 while down-regulated by CX-4945. Other fatty acid metabolism related genes 3-Hydroxy-3-Methylglutaryl-CoA Reductase (HMGCR) and Squalene Epoxidase (SQLE) were also up-regulated in response to AB668 compared to CX-4945 or DMSO (Figure 4a). This can be related to the recently pointed out role of CK2 in lipid homeostasis and its deregulation in cancer cells (Guerra et al., 2020). In particular, HIF expression drives lipid deposition in ccRCC *via* the repression of fatty acid metabolism (Du et al., 2017). Importantly, it was previously shown that low expression of FDPS, FDFT1, HMGCS1, HMGCR and IDI1 genes and high expression of SQLE were associated with patients with high-risk of ccRCC (Qi et al., 2021). Thus, by up-regulating 5 out of 6 genes in this prognostic signature, AB668 could represent a therapeutic option to counteract ccRCC tumor progression.

An identification of the biological pathways over-represented in genes deregulated in expression, in response to either AB668 or CX-4945 compared to DMSO, was then carried out using the Gene Set Enrichment Analysis (GSEA) method and the Reactome database. Among the 17 significantly altered pathways, 5 were related to the metabolism of steroids and lipids and 12 were connected to cell cycle and mitotic processes (Figure 4d). While pathways related to steroids and lipids metabolism were up-regulated in response to ABB668, cell cycle and mitotic processes-based pathways were down-regulated by AB668. This down-regulation of cell cycle is consistent with the strong inhibition of cell proliferation observed in cell lines treated with AB668. Furthermore, among the pathways identified as significantly deregulated in response to AB668 compared to DMSO, we found that all but two (transferin endocytosis and recycling and sphingolipid metabolism) have opposite deregulations in response to CX-

4945 (Figure 4c), illustrating the strongly different effects of these CK2 inhibitors on these cellular processes.

In summary, our transcriptomic analysis clearly demonstrates that the inhibition of CK2 by the dual inhibitor AB668 or by a pure ATP-competitive CX-4945 inhibitor that reached clinical trials differentially affect biological pathways in 786-O cancer cells. More specifically, AB668 induces a deep alteration of antiapoptotic pathways, cell cycle and mitotic processes, as well as steroids and lipids metabolism, which all are involved in renal cancer tumorigenicity.

## Discussion

The key role of CK2-dependent pathways in cancer has motivated the development of CK2 inhibitors. While most of these inhibitors act by an orthosteric mechanism, meaning that they bind to the highly conserved ATP binding-pocket of the kinase (Cozza et al., 2012), small molecules that act outside the ATP site have been also described (Iegre et al., 2021). Here, we have disclosed a new bivalent CK2 inhibitor that binds at both the ATP site and the allosteric  $\alpha$ D pocket, a feature that accounts for its high selectivity profile in the human kinome. The presence of this ligandable allosteric pocket on CK2 was previously revealed during a crystallographic fragment screening campaign (Brear et al., 2016), in agreement with the high mobility of the  $\alpha$ D helix in CK2. The flexibility of this  $\alpha$ D helix was experimentally observed in various crystallographic structures of the kinase and was also reported in metadynamic studies of CK2 structure (Gouron et al., 2014). Two bivalent CK2 inhibitors targeting this pocket, in addition to the ATP site, have been previously published (Brear et al., 2016; Lindenblatt et al., 2022). While their impact on cell cytotoxicity has been reported, the effect of such inhibitors on cellular CK2 functions has not been explored.

Here, we have compared the effects of the bivalent CK2 inhibitor AB668 to CX-4945 and SGC-CK2-1 using caspase activation assay, live-cell imaging and transcriptomic analysis. Our data highlight that AB668 has a distinct mechanism of action regarding its anti-cancer activity. Treatment with AB668 strongly impacted cancer cell viability resulting in apoptotic cell death, while sparing healthy cells. A long-held view has suggested that malignant cells are dependent upon sustained CK2 signaling for survival thereby exhibiting an exquisite sensitivity to CK2 inhibition (Ruzzene et al, 2010; Roffey et al, 2021; Firnau et al, 2022). Conversely, non-cancer cells are more resistant to induction of cell death on downregulation of CK2 activity, which is the expected basis for safely using a pharmacological chemical inhibitor. By contrast, although

CX-4945 or SGC-CK2-1 reduced cell proliferation, both compounds were inefficient to induce cell death. These observations suggest that targeting the allosteric CK2  $\alpha$ D pocket has a distinct cellular impact as compared to targeting only the CK2 ATP binding site. These results also indicate that CK2 is a key player in cancer biology and that targeting CK2 is a valuable strategy (Salvi et al., 2021).

Transcriptomic analysis further supports this hypothesis, as we could highlight striking differences in biological pathways induced by cell treatment with either AB668 or the ATP-competitive inhibitor CX-4945. AB668 acts by an unconventional mechanism and induces strong apoptotic cell death. Thus, this strong pharmacological effect observed in various functional assays indicates that AB668 is an important novel investigational probe for exploiting apoptotic vulnerabilities in cancer as well as a promising lead for the next generation of drug-like CK2 inhibitors with improved potency and optimal drug properties. Future experiments will need to define further the mechanisms by which AB668, by occupying the allosteric  $\alpha$ D pocket, induces apoptotic cell death in cancer cells, while sparing healthy cells. Taken together, our results strongly suggest that CK2 inhibition using small molecules that target binding sites outside the ATP pocket could be a valuable strategy in treating various aggressive cancers and disease-relevant contexts.



## Figure Legends

**Figure 1. Binding mode, affinity for CK2 $\alpha$  and kinase selectivity profile of AB668.** **a)** Chemical structure of AB668 and CK2 $\alpha$ /AB668 complex crystal 3D structure showing the binding site of AB668: the inhibitor binds both the ATP pocket and the  $\alpha$ D pocket of CK2 $\alpha$ . **b)** Stick representation of AB668 bound to CK2 $\alpha$ : side chains in interaction with the inhibitor are shown, and hydrogen bonds are displayed. **c)** Conformational rearrangement of CK2 $\alpha$  upon AB668 binding: the helix is shifted to allow the binding of AB668 in the  $\alpha$ D pocket. The structure of CK2 $\alpha$  bound to AB668 is superimposed to the structure of the holoenzyme (pdb code 1JWH), and to the apo structure of CK2 $\alpha$  (pdb code 3QAO) **d)** Binding affinity of AB668 as determined by the KINOMEscan<sup>TM</sup> profiling service (Eurofins). **e)** Selectivity profile of AB668, profiled against 468 kinases, using the screening platform from Eurofins DiscoverX. AB668 concentration was 2  $\mu$ M (25 times its  $K_d$  value).

**Figure 2. Cellular activity of AB668 and comparison to CX-4945 and SGC-CK2-1.** **a)** Quantitative fluorometric assay showing caspase-3 activation in 786-O cells treated with staurosporine, AB668, SGC-CK2-1 or CX-4945. Assays were performed after 72 h treatment with the compounds at 20  $\mu$ M. **b)** Western blot experiments on 786-O cells treated with AB668 (2.5, 5, 7.5, 10 and 15  $\mu$ M) for 48h showing the cleavage of PARP as well as the expression level of survivin. **c)** Live cell imaging showing proliferation arrest, cell death and apoptosis in 786-O and A375 cells treated with AB668, CX-4945 or SGC-CK2-1 (4  $\mu$ M) for 48h. **d)** Effect of AB668 and CX-4945 on *ex vivo* culture of intact tumor slices of clear cell renal carcinoma. Tumors were extracted from renal carcinoma xenografted mice that were directly processed into 300  $\mu$ m slices and treated for 48 h as described in Methods. Cell viability was evaluated by luciferin measurement of treated tumor-slice cultures as described in Methods. **e)** Cell viability of primary hepatocytes and RPTEC (Renal Proximal Tubule Epithelial Cells) treated with AB668.

**Figure 3. Target engagement of AB668 in 786-O cells and HEK293 cells.** **a)** Western blot analysis in response to AB668 in 786-O cells. The inhibition of phosphorylated mTOR (S2448), STAT3 (S727), p53 (S15), p38 MAPK (T180/Y182) and AKT (S129) and p21 (T145) was analyzed after 48 h of inhibitor AB668 treatment. **b)** The inhibition of phosphorylated AKT

(S129), p53 (S15), p38 MAPK (T180/Y182) and p21 (T145) was analyzed after 48 h of AB668 (1  $\mu$ M) or CX-4945 (5  $\mu$ M) treatment in 786-O cancer cells or HEK293 cells. Glyceraldehyde-3-phosphate dehydrogenase (GAPDH) was used as a loading control. **c)** CK2 activity measured in cell extracts of 786-O cells (upper panel) or HEK293 cells (lower panel) after treatment with AB668. Inhibition constants  $IC_{50}$  are  $0.34 \pm 0.07 \mu\text{M}$  for 786-O cells and  $0.60 \pm 0.11 \mu\text{M}$  for HEK293 cells.

**Figure 4. Deregulations of the transcriptome in response to AB668 or CX-4945. a-**

**c)** Volcano plots based upon differential gene expression analysis of the transcriptomes of 786-O cells exposed to the different CK2 inhibitors: **a)** AB668 vs DMSO **b)** CX-4945 vs DMSO and **c)** AB668 vs CX-4945. **d)** Differences of  $\text{Log}_2(\text{Fold Changes})$  of gene expression values for AB668 and CX-4945 treated cells compared to DMSO treated cells. **e)** Normalized Enrichment Scores (NES), calculated by the Gene Set Enrichment Analysis (GSEA) method, for significantly deregulated pathways obtained from AB668 vs DMSO analysis in comparison to the NES scores generated from CX-4945 vs DMSO analysis. **f)** Histograms of  $\text{Log}_2(\text{Fold Changes})$  of gene expression values for AB668 vs CX-4945 comparison for significantly deregulated pathways found by GSEA analysis, using REACTOME pathway database.

## Methods

### Recombinant proteins for enzymatic measurements

Both human recombinant CK2 $\alpha$  subunit and chicken recombinant MBP (maltose-binding protein)-CK2 $\beta$  were expressed in *Escherichia coli* and purified as previously reported (Hériché et al., 1997; Chantalat et al., 1999). Proteins were quantified using a Bradford assay and the quality of the purification was asserted by SDS-PAGE analysis.

### CK2 activity assays in vitro

Radiometric kinase assays were performed as previously reported (Kufareva et al., 2019). Briefly, in a final volume of 20  $\mu$ L at 4°C, 3.0  $\mu$ L of CK2 $\alpha$  protein (36 ng) was incubated in the reaction mixture (20 mM Tris-HCl, pH 7.5, 150 mM NaCl, 1.0 mM DTT) with 1.0 mM of the synthetic substrate peptide, 20 mM of MgCl<sub>2</sub>, 1.0  $\mu$ Ci of [<sup>32</sup>P]-ATP and 2.0  $\mu$ L of different concentrations of the inhibitor, diluted in Tris-HCl-glycerol, 0.05% Tween 20. Final ATP concentration was 10  $\mu$ M when not stated otherwise. The kinase reactions were performed under linear kinetic conditions for 5 min at room temperature followed by quenching with the addition of 60  $\mu$ L of 4% TCA. <sup>32</sup>P incorporation in peptide substrate was determined by spotting the supernatant onto phospho-cellulose paper disks (Whatman P81, 4 cm<sup>2</sup>). The disks were washed three times in cold 0.5% phosphoric acid, 5 min on a rocking platform per wash, dried and finally the radioactivity was measured. Percentage inhibition was calculated relative to a DMSO control and all measurements were performed in duplicate. A canonical CK2 peptide substrate (Seq. RRREDEESDDE) phosphorylated equally by CK2 $\alpha_2\beta_2$  (CK2 $\beta$ -independent) and a 22-residue long *N*-terminal fragment of the eukaryotic translation initiation factor 2 (eIF2) (.MSGDEMIFDPTMSKKKKKKKKP), exclusively phosphorylated by CK2 $\alpha_2\beta_2$  (CK2 $\beta$ -dependent) were used for the radiometric kinase assays. Phosphorylation assay using GST-SIX1 (3.7  $\mu$ g) were performed in the same buffer. Final concentration of ATP was 100  $\mu$ M. Samples were analyzed by SDS-PAGE and subjected to autoradiography. Phosphoproteins were quantified by densitometry scanning using ImageJ (National Institutes of Health software v1.52).

### X-ray crystallography

Recombinant protein for X-ray studies was produced as published in Wells et al. (2021). Protein concentration was 9 mg/ml. Crystals of human CK2 $\alpha$  were grown at 20 °C using the hanging-drop vapor-diffusion method with a reservoir solution containing 33% polyethylene glycol

methyl ether 5000, 0.2 M ammonium sulfate, 0.1 M MES pH 6.5. The drops contained 1  $\mu$ L of the reservoir solution and 1  $\mu$ L of the protein. The crystals were soaked by adding 0.2  $\mu$ L of ligand solution at 100 mM in DMSO. The crystals were cryo-protected with reservoir solution supplemented with 20% glycerol and then flash-cooled in liquid nitrogen. X-ray diffraction data were collected at the ESRF Synchrotron in Grenoble, France, on beamline IB30B. Data were integrated and processed using XDS (Kabsch et al., 2010). The crystals belong to the space group P43212 with two monomers in the asymmetric unit. The structures were solved by molecular replacement using PDB entry 6Z84 as the search model. Bound ligands were manually identified and fitted into  $F_o - F_c$  electron density using Coot (Emsley & Cowtan, 2004). Files in CIF format for ligand were generated using Grade Server (<http://grade.globalphasing.org/cgi-bin/grade/server.cgi>). The structure was refined by rounds of rebuilding in Coot and refinement using Phenix (Adams et al., 2010). Data collection and refinement statistics for crystal structure is presented in Table S1.

### **Thermal Shift Assay**

The thermal shift assay was performed on a LightCycler 480 Real-Time PCR System (Roche) in 96-well white plates (Armadillo plate, Thermo Scientific) using an integration time of 120ms. Each well contained 10  $\mu$ L of 5  $\mu$ g CK2 $\alpha$  (purified as described by Hériché et al., 1997; Chantalat et al., 1999) and 2.5 $\times$  SYPRO Orange (Life Technologies) in PBS-0.9% glycerol, with ligands added to a final concentration of 0.1  $\mu$ M to 500  $\mu$ M in 5% (v/v) DMSO. All assays were carried out in triplicate. Each plate was sealed with an optically clear foil and centrifuged for 1 min at 300 rpm before performing the assay. The plates were heated from 20 to 80°C at a heating rate 0.01°C/s. The fluorescence intensity was measured with  $\lambda_{ex}$  = 483 nm and  $\lambda_{em}$  = 568 nm. The melting temperature ( $T_m$ ) was determined using the TSA-CRAFT software that enables automatic analysis of TSA data exported from the Roche Lightcycler 480 software (Lee et al., 2019).

### **Kinase screening**

Profiling of 468 recombinant protein kinases was performed by Eurofins Discovery (KINOMEscan™ Profiling Service, San Diego, USA) at 10  $\mu$ M of ATP in the presence of 2  $\mu$ M AB668. Inhibition, expressed as the percent of activity, was calculated from the residual activity measured in the presence of the inhibitor.

### **Cell lines**

All cell lines were purchased from American Type Culture Collection (ATCC) and grown on standard tissue culture plastic in a 5% CO<sub>2</sub> humidified incubator at 37°C. 786-O were maintained in RPMI 1640 medium (Gibco), containing 10% of FBS, penicillin (24 U/mL), and streptomycin (25 µg/mL). A549, A375 and MDA-MB231 were cultured in DMEM + GlutaMAX medium (Gibco) supplemented with 10% of FBS. HEK293T were grown in EMEM supplemented with 10% of FBS and RPTEC were maintained in ProXup (Evercyte). MCF10A were cultured as described (Debnath et al., 2003).

### **Caspase-3 assay**

The Caspase-3 Fluorometric Assay Kit II from Biovision was used to determine caspase-3 activity in cells following manufacturer's instructions. Briefly, cultured cells collected by scraping were lysed and Bradford reagent was used to quantify proteins in the cell lysate. Fifty micrograms of proteins were added in a 96-well white plate. Reaction was started by adding the caspase-3 substrate, DEVD-AFC. Fluorescence measurements (excitation: 405 nm; emission: 520 nm) were made at 37°C in a FLUOstar OPTIMA microplate reader (BMG Labtech) every 5 min over an hour. Cells treated with 500 nM staurosporine, a potent apoptotic inducer, were used as positive controls.

### **Cell death & proliferation**

786-O (2 x 10<sup>4</sup> cells per well), HEK293 (2 x 10<sup>4</sup> cells per well), MCF10A (2 x 10<sup>4</sup> cells per well), MDA-MB231 (2 x 10<sup>4</sup> cells per well) and RPTEC (7 x 10<sup>3</sup> cells per well) cells were seeded into 96-well flat-bottom cell culture plates. After 24 h, compounds dissolved in DMSO were diluted in the culture medium containing 0.5 µg/mL propidium iodide (PI, Sigma-Aldrich) and were added to the cell culture media such as the final DMSO concentrations is equal to 0.2% (v/v). Experiments were conducted at 37°C in a 5% CO<sub>2</sub> atmosphere and the plates were tracked using an Essen IncuCyte Zoom live-cell microscopy instrument. For cell death, PI-stained red fluorescent cells images were captured every 3 h for the entire duration of the experiment and normalized to the DMSO standard control. For cell proliferation, the software incorporated into the IncuCyte Zoom was specifically calibrated to ensure accurate distinction of cells from the empty spaces. Cell proliferation was monitored by analyzing the occupied area (% confluence) of cell images over time.

### **Real-time proliferation, cell death and apoptosis assay on A375 cells**

A375 melanoma cells ( $2.5 \times 10^4$  cells per well) were plated in 48-well plates. After 24 hours, cells were treated with various doses of AB668, CX4945, or SGC-CK2-1. Treatment medium contained 0.3  $\mu\text{g}/\text{mL}$  propidium iodide (Sigma-Aldrich) and 2  $\mu\text{M}$  CellEvent™ Caspase-3/7 Green Detection Reagent (ThermoFisher Scientific). Images were captured automatically every two hours for 48 hours using the IncuCyte™ S3 Live-Cell Analysis Instrument (Essen BioScience). Image analysis was performed using IncuCyte software. Data was plotted as mean  $\pm$  SD using GraphPad Prism 9.

### **Preparation of cell extracts**

786-O ( $3 \times 10^5$  cells per well), HEK 293 ( $2 \times 10^5$  cells per well), MDA-MB231 ( $3 \times 10^5$  cells per well), and RPTEC ( $3 \times 10^5$  cells per well) cells were seeded into 6-well tissue and cultured for 24 h prior to the addition of inhibitors (as described above). After incubation, medium was removed, cells were washed with cold PBS and frozen at  $-80^\circ\text{C}$ . Cells were lysed using a RIPA buffer (10 mM Tris-HCl, pH 7.4, 150 mM NaCl, 1% Triton X-100, 0.1% SDS, 0.5% DOC and 1.0 mM EDTA) with the addition of protease and phosphatase inhibitor cocktail (Sigma-Aldrich, P8340, P2850, P5726) at the recommended concentrations. Cell pellets were incubated in RIPA buffer on ice for 30 min, then centrifuged for 15 min at  $4^\circ\text{C}$  at 13000 rpm and the supernatants collected. Proteins were quantified using the Pierce BCA protein assay kit (Pierce, ThermoFisher Scientific).

### **CK2 activity in cells**

Cell homogenates were assayed for CK2 activity with radiometric assays as described above.

### **Immunoblotting**

Equal amounts of lysates (20-35  $\mu\text{g}$ ) were loaded onto a precast 4-12% gradient gel (Bio-Rad) and submitted to electrophoresis in NuPAGE buffer (150 V for 1.5 h). The gels were transferred onto PVDF membrane (100 V for 1 h). Membranes were blocked during 1 h at room temperature with saturation buffer (5% BSA in Tris-buffered saline with 0.1% Tween 20 (TBST) and then incubated with primary antibody diluted in saturation buffer for 2 h or overnight on a rocking platform shaker. Primary antibodies were GAPDH antibody (#AM4300) from Invitrogen, ThermoFisher, P-AKT-phospho-Ser129 (#AP3020a) from Interchim, AKT (#9272), PARP (#9542), mTOR (#2972), mTOR-phospho-Ser2448 (#2971), p38MAPK (#9212), p38MAPK-phospho-Thr180/Tyr182 (#9211), p53 (#9282), p53-phospho-Ser15 (#9286), STAT3 (#6139), STAT3-phospho-Ser727 (#9134) antibodies from Cell Signaling,

survivin (#NB500201) antibody from Novus biologicals, p21 antibody (#sc-397) from Santa Cruz Biotechnologies, p21-phospho-Thr145(#ab-47300) antibody from Abcam. After washing three times with TBST, secondary antibody (peroxidase-conjugated affinity pure Goat anti-rabbit IgG (#111035003) or peroxidase-conjugated affinity pure goat anti-mouse IgG (#115035003) from Jackson Immuno Research) was added for 1 h followed by three more washes with TBST. Immobilon Forte Western HRP substrate (Millipore) was added and detection was achieved by using Fusion FX acquisition system (Vilbert). Anti-GAPDH was used as loading control and images were analyzed and band intensities were quantified using ImageJ (National Institutes of Health software v1.52).

### ***In vivo* orthotopic tumor xenograft models.**

All animal studies were approved by the institutional guidelines and those formulated by the European Community for the Use of Experimental Animals. Six week-old BALB/c Female nude mice (Charles River Laboratories) with a mean body weight of 18-20 g were used to establish orthotopic xenograft tumor models. The mice were housed and fed under specific pathogen-free conditions. To produce tumors, renal cancer cells 786-O-luc were harvested from subconfluent cultures by a brief exposure to 0.25 % trypsin-EDTA. Trypsinization was stopped with medium containing 10 % FBS, and the cells were washed once in serum-free medium and resuspended in 500 µl PBS. Renal orthotopic implantation was carried out by injection of  $3 \times 10^6$  786-O luc cells into the right kidney of athymic nude mice. Mice were weighed once a week to monitor their health and tumor growth was measured by imaging luminescence of 786-O-luc cells (IVIS).

### **Fresh tissue sectioning.**

A Vibratome VT1200 (Leica Microsystems) was used to cut thin (300 µm) slices from fresh tissue. Samples were soaked in ice-cold sterile balanced salt solution (HBSS), orientated, mounted, and immobilized using cyanoacrylate glue. Slicing speed was optimized according to tissue density and type; in general, slower slicing speed was used on the softer tissues and vice versa (0.08-0.12 mm/s neoplastic tissue; 0.01-0.08 mm/s normal tissue). Vibration amplitude was set at 2.95-3.0 mm.

### **Organotypic tissue cultures.**

Tissue slices were cultured on organotypic inserts for 48 h (one slice per insert; Millipore). Organotypic inserts are Teflon membranes with 0.4 µm pores that allow preservation of 3D

tissue structure in culture. Tissue culture was performed at 37°C in a 5 % CO<sub>2</sub> humidified incubator using 1 ml of DMEM media supplemented with 20 % FBS (GIBCO), 100 U/ml penicillin (Invitrogen) and place in a rotor agitator to allow gas and fluids exchanges with the medium. The tissue slices were incubated with the CX-4945 (10 µM) or AB668 (5 µM) until 68 hours. Tumor slice viability was monitored at indicated time points, by luminescence imaging of 786-O-luc cells after luciferin addition (IVIS) as previously described (Roelants et al., 2018; Roelants et al., 2020).

### **BRB-seq library preparation and sequencing**

786-O cells (150, 000) were treated for 24h with DMSO, 5 µM of CX4945 or AB668. Total RNA was extracted from treated cells using the MirVana PARIS kit (Thermofisher). The 3' Bulk RNA Barcoding and sequencing (BRB-seq) experiments were performed at the Research Institute for Environmental and Occupational Health (Irset, Rennes, France) according to the published protocol (Alpern et al., 2019). Briefly, the reverse transcription and the template switching reactions were performed using 4 µl total RNA at 2.5 ng/µl. RNA were first mixed with 1 µl barcoded oligo-dT (10 µM BU3 primers, Microsynth), 1 µL dNTP (0.2 mM) in a PCR plate, incubated at 65 °C for 5 min and then put on ice. The first-strand synthesis reactions were performed in 10 µl total volume with 5 µl of RT Buffer and 0.125 µl of Maxima H minus Reverse Transcriptase (Thermofisher Scientific, #EP0753) and 1 µl of 10 µM template switch oligo (TSO, IDT). The plates were then incubated at 42°C for 90 min and then put on ice.

After Reverse Transcription (RT), decorated cDNA from multiple samples were pooled together and purified using the DNA Clean & concentrator-5 Kit (Zymo research, #D4014). After elution with 20 µl of nuclease free water, the samples were incubated with 1 µl Exonuclease I (NEB, #M0293) and 2 µl of 10X reaction buffer at 37°C for 30 min, followed by enzyme inactivation at 80°C for 20 min.

Double-strand (ds) cDNAs were generated by PCR amplification in 50 µl-total reaction volume using the Advantage 2 PCR Enzyme System (Clontech, #639206). PCR reaction was performed using 20 µl cDNA from previous step, 5 µl of 10X Advantage 2 PCR buffer, 1 µl of dNTPs 50X, 1 µl of 10 µM LA-oligo (Microsynt), 1 µl of Advantage 2 Polymerase and 22 µl of nuclease-free water following the program (95°C-1 min; 11 cycles: 95°C-15 s, 65°C-30 s, 68°C-6 min; 72°C-10 min). Full-length double-stranded cDNA was purified with 30 µl of AMPure XP magnetic beads (Beckman Coulter, #A63881), eluted in 12 µl of nuclease free water and quantify using the dsDNA QuantiFluor Dye System (Promega, #E2670).



The sequencing libraries were built by tagmentation using 50 ng of ds cDNA with Illumina Nextera XT Kit (Illumina, #FC-131-1024) following the manufacturer's recommendations. The reaction was incubated 5 min at 55°C, immediately purified with DNA Clean & concentrator-5 Kit (Zymo research) and eluted with 21 µl of nuclease free water. Tagmented library was PCR amplified using 20 µl eluted cDNA, 2.5 µl of i7 Illumina Index, 2.5 µl of 5 µM P5-BRB primer (IDT) using the following program (72°C-3 min; 98°C-30 s; 13 cycles: 98°C-10 s, 63°C-30 s, 72°C-5 min). The fragments ranging 300-800 base pair (bp) were size-selected using SPRIselect (Bekman Coulter, #) (first round 0.65x beads, second 0.56x) with a final elution of 12 µl nuclease-free water. The resulting library was sequenced on Illumina HiSeq 4000 sequencer as Paired-End 100 base reads following Illumina's instructions. Image analysis and base calling were performed using RTA 2.7.7 and bcl2fastq 2.17.1.14. Adapter dimer reads were removed using DimerRemover (<https://sourceforge.net/projects/dimerremover/>).

### **BRB-seq raw data preprocessing**

The first read contains 16 bases that must have a quality score higher than 10. The first 6 bp correspond to a unique sample-specific barcode and the following 10 bp to a unique molecular identifier (UMI). The second reads were aligned to the human reference transcriptome from the UCSC website (release hg38) using BWA version 0.7.4.4 with the non-default parameter “-1 24”. Reads mapping to several positions in the genome were filtered out from the analysis. The pipeline is described in Draskau (2021). After quality control and data preprocessing, a gene count matrix was generated by counting the number of unique UMIs associated with each gene (lines) for each sample (columns). The resulting UMI matrix was further normalized by using the rlog transformation implemented in the DeSeq2 package (Love et al., 2014).

### **Bioinformatics analysis**

Differential Gene Expression (DGE) analyses were performed using DeSeq2 R package (version 1.34.0, R 4.1) for each pairwise comparison of AB668, CX-4945 and DMSO conditions (Table S2). For these 3 DGE results, p-values were corrected by the Benjamini-Hochberg method. Only genes with corrected P-values < 0.05 and  $|\text{Log}_2(\text{Fold Change})| > 0.5$  were considered as significantly differentially expressed. The first sample label in a comparison (e.g. AB668 for "AB668 vs DMSO") means that it is the numerator in the calculation of the fold change (Fold Change = AB668/DMSO). The top 15 of significant genes based on FDR values and apoptotic and lipid & steroid

metabolism related genes (if not overlapping with the top 15) are displayed in volcano plots. All DGE values for each selected genes in three comparisons can be retrieved in the supp-data (volcanoPlots3\_AB668\_CX\_DMSO.ods). Gene Set Enrichment Analysis (GSEA) of Reactome pathway database (reactome.db version 1.82.0) was carried out using the Bioconductor/R package clusterProfiler (version 4.6.0). Pathways are considered significantly enriched whether related corrected P-value (Benjamini-Hochberg correction) is lower than 0.05.

## References

Abbas, T. & Dutta, A. p21 in cancer: intricate networks and multiple activities. *Nat. Rev. Cancer*. **9**, 400-414 (2009).

Aparicio-Siegmund, S., Sommer, J., Monhasery, N., Schwanbeck, R., Keil, E., Finkenstädt, D., Pfeffer, K., Rose-John, S., Scheller, J. & Garbers, C. Inhibition of protein kinase II (CK2) prevents induced signal transducer and activator of transcription (STAT) 1/3 and constitutive STAT3 activation. *Oncotarget* **5**, 2131-48. doi: 10.18632/oncotarget.1852. 2014

Atkinson, E.L., Iegre, J., Brear, P.D., Zhabina, E.A., Hyvönen, M. & Spring, D.R. Downfalls of Chemical Probes Acting at the Kinase ATP-Site: CK2 as a Case Study. *Molecules* **26**, 1977 (2021).

Barrett, R.M., Colnaghi, R. & Wheatley, S.P. Threonine 48 in the BIR domain of survivin is critical to its mitotic and anti-apoptotic activities and can be phosphorylated by CK2 in vitro. *Cell Cycle* **10**, 538-548 (2011).

Bian, Y., Ye M., Wang, C., Cheng, K., Song, C., Dong, M., Pan, Y., Qin H. & Zou, H. Global screening of CK2 kinase substrates by an integrated phosphoproteomics workflow. *Sci Rep*. **3**, 3460. (2013).

Bibby, A.C. & Litchfield, D.W. The multiple personalities of the regulatory subunit of protein kinase CK2: CK2 dependent and CK2 independent roles reveal a secret identity for CK2beta. *Int. J. Biol. Sci.* **1**, 67-79 (2005).

Bosc, N., Meyer, C. & Bonnet, P. The use of novel selectivity metrics in kinase research. *BMC Bioinformatics* **18**, 17 (2017).

Boulares, A.H., Yakovlev, A.G., Ivanova, V., Stoica, B.A., Wang, G., Iyer, S., Smulson, M. Role of poly(ADP-ribose) polymerase (PARP) cleavage in apoptosis. Caspase 3-resistant PARP mutant increases rates of apoptosis in transfected cells. *J. Biol. Chem.* **274**, 22932-22940 (1999).

Borgo, C., Franchin, C., Scalco, S., Bosello-Travain, V., Donella-Deana, A., Arrigoni, G., Salvi, M. & Pinna, L.A. Generation and quantitative proteomics analysis of CK2 $\alpha$ / $\alpha^{(-/-)}$  cells. *Sci Rep.* **7**, 42409 (2017).

Borgo, C. & Ruzzene, M. Role of protein kinase CK2 in antitumor drug resistance. *J. Exp. Clin. Cancer Res.* **38**, 287 (2019).

Brear, P., De Fusco, C., Hadje Georgiou, K., Francis-Newton, N.J., Stubbs, C.J., Sore, H.F., Venkitaraman, A.R., Abell, C., Spring, D.R., Hyvönen, M. Specific inhibition of CK2 $\alpha$  from an anchor outside the active site. *Chem Sci.* **7**, 6839-6845 (2016). doi: 10.1039/c6sc02335e.

Borgo, C., D'Amore, C., Sarno, S., Salvi, M. & Ruzzene, M. Protein kinase CK2: a potential therapeutic target for diverse human diseases. *Signal Transduct. Target. Ther.* **6**, 183 (2021).

Buontempo, F., Orsini, E., Martins, L.R., Antunes, I., Lonetti, A., Chiarini, F., Tabellini, G., Evangelisti, C., Evangelisti, C., Melchionda, F., Pession, A., Bertaina, A., Locatelli, F., McCubrey, J.A., Cappellini, A., Barata, J.T., Martelli, A.M. Cytotoxic activity of the casein kinase 2 inhibitor CX-4945 against T-cell acute lymphoblastic leukemia: targeting the unfolded protein response signaling. *Leukemia* **28**, 543-553 (2014).

Chua, M.M., Ortega, C.E., Sheikh, A., Lee, M., Abdul-Rassoul, H., Hartshorn, K.L. & Dominguez, I. CK2 in Cancer: Cellular and Biochemical Mechanisms and Potential Therapeutic Target. *Pharmaceuticals (Basel)* **10**, 8 (2017a).

Chua, M.M., Lee, M. & Dominguez, I. Cancer-type dependent expression of CK2 transcripts. *PLoS One* **12**, e0188854 (2017b).

Cozza, G., Pinna, L.A. & Moro, S. Protein kinase CK2 inhibitors: a patent review. *Expert Opin. Ther. Pat.* **22**, 1081-1097 (2012).

De Fusco, C., Brear, P., Iegre, J., Georgiou, K.H., Sore, H.F., Hyvönen, M. & Spring, D.R. A fragment-based approach leading to the discovery of a novel binding site and the selective CK2 inhibitor CAM4066. *Bioorg. Med. Chem.* **25**, 3471-3482 (2017).

Diesing, K., Ribback, S., Winter, S., Gellert, M., Oster, A.M., Stühler, V., Gläser, E., Adler, F., Hartwig, C., Scharpf, M., Bedke, J., Burchardt, M., Schwab, M., Lillig, C.H. & Kroeger, N. p53 is functionally inhibited in clear cell renal cell carcinoma (ccRCC): a mechanistic and correlative investigation into genetic and molecular characteristics. *J. Cancer Res. Clin. Oncol.* **147**, 3565-3576 (2021).

Di Maira, G., Salvi, M., Arrigoni, G., Marin, O., Sarno, S., Brustolon, F., Pinna, L.A & Ruzzene M. Protein kinase CK2 phosphorylates and upregulates Akt/PKB. *Cell Death Differ.* **12**, 668-677 (2005).

Di Maira, G., Gentilini, A., Pastore, M., Caligiuri, A., Piombanti, B., Raggi, C., Rovida, E., Lewinska, M., Andersen, J.B., Borgo, C., Salvi, M., Ottaviani, D., Ruzzene, M. & Marra, F. The protein kinase CK2 contributes to the malignant phenotype of cholangiocarcinoma cells. *Oncogenesis* **8**, 61 (2019).

Dominguez, I., Sonenshein, G.E. & Seldin, D.C. Protein kinase CK2 in health and disease: CK2 and its role in Wnt and NF-kappaB signaling: linking development and cancer. *Cell. Mol. Life Sci.* **66**, 1850-7 (2009).

Du, W., Zhang L., Brett-Morris, A., Aguila, B., Kerner, J., Hoppel, C.L., Puchowicz, M., Serra, D., Herrero, L., Rini, B.I., Campbell, S. & Welford, S.M. HIF drives lipid deposition and cancer in ccRCC via repression of fatty acid metabolism. *Nat Commun.* **8**, 1769 (2017).

Duncan, J.S., Turowec, J.P., Duncan, K.E, Vilc, G., Wu, C., Lüscher, B., Li, S.S., Gloor, G.B & Litchfield, D.W. A peptide-based target screen implicates the protein kinase CK2 in the global regulation of caspase signaling. *Sci. Signal.* **4**, ra30 (2011).

Firna, M.B. & Brieger, A. CK2 and the Hallmarks of Cancer. *Biomedicines* **10**, 1987. (2022).

Franchin, C., Salvi, M., Arrigoni, G. & Pinna, L.A. Proteomics perturbations promoted by the protein kinase CK2 inhibitor quinalizarin. *Biochim Biophys Acta*. 1854(10 Pt B):1676-1686 (2015).

Gouron, A., Milet, A. & Jamet, H. Conformational flexibility of human casein kinase catalytic subunit explored by metadynamics. *Biophys J.*, 106(5):1134-1141 (2014) doi: 10.1016/j.bpj.2014.01.031.

Gray, G.K., McFarland, B.C., Rowse, A.L., Gibson, S.A., Benveniste, E.N. Therapeutic CK2 inhibition attenuates diverse prosurvival signaling cascades and decreases cell viability in human breast cancer cells. *Oncotarget*, **5**, 6484-96 (2014). doi: 10.18632/oncotarget.2248.

Guerra, B. & Issinger, O.G. Role of Protein Kinase CK2 in Aberrant Lipid Metabolism in Cancer. *Pharmaceuticals (Basel)* **13**, 292 (2020).

Huang, J., Y. Qin, C. Lin, X. Huang and F. Zhang (2021). MTHFD2 facilitates breast cancer cell proliferation via the AKT signaling pathway. *Exp Ther Med* **22**(1): 703.

Husain, K., Williamson, T.T., Nelson, N. & Ghansah, T. Protein kinase 2 (CK2): a potential regulator of immune cell development and function in cancer. *Immunol. Med.* **44**, 159-174. (2021).

Iegre, J., Atkinson, E.L., Brear, P.D., Cooper, B.M., Hyvönen, M & Spring D.R.. Chemical probes targeting the kinase CK2: a journey outside the catalytic box. *Org. Biomol. Chem.* **19**, 4380-4396 (2021). doi: 10.1039/d1ob00257k.

Inoue, H., Hwang, S.H., Wecksler, A.T., Hammock, B.D. & Weiss, R.H. Sorafenib attenuates p21 in kidney cancer cells and augments cell death in combination with DNA-damaging chemotherapy. *Cancer Biol. Ther.* **12**, 827-836 (2011).

Itkonen, H. M., N. Engedal, E. Babaie, M. Luhr, I. J. Guldvik, S. Minner, J. Hohloch, M. C. Tsourlakis, T. Schlomm & I. G. Mills. UAP1 is overexpressed in prostate cancer and is protective against inhibitors of N-linked glycosylation. *Oncogene* **34**(28): 3744-3750 (2015)

Karimian, A., Ahmadi, Y. & Yousefi, B. Multiple functions of p21 in cell cycle, apoptosis and transcriptional regulation after DNA damage. *DNA Repair (Amst)*. **42**, 63-71 (2016).

Kim H, Choi K, Kang H, Lee SY, Chi SW, Lee MS, Song J, Im D, Choi Y, Cho S. Identification of a novel function of CX-4945 as a splicing regulator. *PLoS One* **9**:e94978. (2014) doi: 10.1371/journal.pone.0094978.

Kubala, M.H., DeClerck, Y.A. The plasminogen activator inhibitor-1 paradox in cancer: a mechanistic understanding. *Cancer Metastasis Rev.* **38**, 483-492 (2019).

Kufareva, I., Bestgen, B., Brear, P., Prudent, R., Laudet, B., Moucadel, V., Ettaoussi, M., Sautel, C.F., Krimm, I., Engel, M., Filhol, O., Le Borgne, M., Lomberget, T., Cochet, C. & Abagyan, R. Discovery of holoenzyme-disrupting chemicals as substrate-selective CK2 inhibitors. *Sci Rep.*, **9**, 15893 (2019).

Laramas, M., Pasquier, D., Filhol, O., Ringeisen, F., Descotes, J.L., & Cochet, C. Nuclear localization of protein kinase CK2 catalytic subunit (CK2alpha) is associated with poor prognostic factors in human prostate cancer. *Eur. J. Cancer.* **43**(5), 928-934 (2007).

Lee, D.S., Lee, S., Kim, C., Kim, D, Kim, KP, Yoo, C. The Casein Kinase 2 Inhibitor CX-4945 Promotes Cholangiocarcinoma Cell Death Through PLK1. *Anticancer Res.* **42**, 3435-3443 (2022).

Licciardello, M.P. & Workman, P. A. New Chemical Probe Challenges the Broad Cancer Essentiality of CK2. *Trends Pharmacol. Sci.* **42**, 313-315 (2021).

Lindenblatt, D., Applegate, V., Nickelsen, A., Klußmann, M., Neundorf, I., Götz, C., Jose, J. & Niefind, K. Molecular Plasticity of Crystalline CK2 $\alpha'$  Leads to KN2, a Bivalent Inhibitor of Protein Kinase CK2 with Extraordinary Selectivity. *J. Med. Chem.* **65**, 1302-1312 (2022).

Lu, X., Smail, J.B., Ding, K. New Promise and Opportunities for Allosteric Kinase Inhibitors. *Angew. Chem. Int. Ed. Engl.* **59**, 13764-13776 (2020).

Luo, J., Solimini, N.L., Elledge, S.J. Principles of cancer therapy: oncogene and non-oncogene addiction. *Cell* **136**, 823-837 (2009).

Meggio, F. & Pinna, L.A. One-thousand-and-one substrates of protein kinase CK2? *FASEB J.* **17**, 349-368 (2003).

Niefind, K., Guerra, B., Ermakowa, I. & Issinger, O.G. Crystal structure of human protein kinase CK2: insights into basic properties of the CK2 holoenzyme. *EMBO J.* **20**, 5320-5331 (2001).

Niefind, K., Raaf, J. & Issinger, O.G. Protein kinase CK2 in health and disease: Protein kinase CK2: from structures to insights. *Cell Mol. Life Sci.* **66**, 1800-1816 (2009).

Noon, A.P., Vlatković, N., Polański, R., Maguire, M., Shawki, H., Parsons, K. & Boyd, M.T. p53 and MDM2 in renal cell carcinoma: biomarkers for disease progression and future therapeutic targets? *Cancer* **116**, 780-790 (2010).

Núñez de Villavicencio-Díaz, T., Mazola, Y., Perera Negrín, Y., Cruz García, Y., Guirola Cruz, O. & Perea Rodríguez, S.E. Predicting CK2 beta-dependent substrates using linear patterns. *Biochem Biophys. Rep.* **4**, 20-27 (2015).

Parker, R., Clifton-Bligh, R. & Molloy, M.P. Phosphoproteomics of MAPK inhibition in BRAF-mutated cells and a role for the lethal synergism of dual BRAF and CK2 inhibition. *Mol. Cancer Ther.* **13**, 1894-1906 (2014).

Pierre, F. et al. Pre-clinical characterization of CX-4945, a potent and selective small molecule inhibitor of CK2 for the treatment of cancer. *Mol. Cell. Biochem.* **356**, 37-43 (2011).

Planus, E., Barlovatz-Meimon, G., Rogers, R.A., Bonavaud, S., Ingber, D.E., Wang, N. Binding of urokinase to plasminogen activator inhibitor type-1 mediates cell adhesion and spreading. *J. Cell. Sci.* **110**, 1091-1098 (1997).



Puttamallesh, V. N., B. Deb, K. Gondkar, A. Jain, B. Nair, A. Pandey, A. Chatterjee, H. Gowda & P. Kumar. Quantitative Proteomics of Urinary Bladder Cancer Cell Lines Identify UAP1 as a Potential Therapeutic Target. *Genes (Basel)* **11**(7) (2020)

Qi, X., Lv, X., Wang, X., Ruan, Z., Zhang, P., Wang, Q., Xu, Y. & Wu, G. A New Survival Model Based on Cholesterol Biosynthesis-Related Genes for Prognostic Prediction in Clear Cell Renal Cell Carcinoma. *Biomed. Res.* **2021**, 9972968 (2021).

Reina-Campos, M., M. T. Diaz-Meco & J. Moscat. The complexity of the serine glycine one-carbon pathway in cancer. *J Cell Biol* **219**(1) 2020)

Richter, A., Roof, C., Hamed, M., Gladbach, Y.S., Sender, S., Konkolefski, C., Knübel, G., Sekora, A., Fuellen, G., Vollmar, B., Murua Escobar, H. & Junghanss, C. Combined Casein Kinase II inhibition and epigenetic modulation in acute B-lymphoblastic leukemia. *BMC Cancer* **19**, 202 (2019).

Roelants, C. *et al.* (2015). Dysregulated Expression of Protein Kinase CK2 in Renal Cancer. In: Ahmed, K., Issinger, OG., Szyszka, R. (eds) Protein Kinase CK2 Cellular Function in Normal and Disease States. *Advances in Biochemistry in Health and Disease*, vol 12. Springer

Roelants, C., Giacosa, S., Pillet, C., Bussat, R., Champelovier, P., Bastien, O., Guyon, L., Arnoux, V., Cochet, C., Filhol, O. Combined inhibition of PI3K and Src kinases demonstrates synergistic therapeutic efficacy in clear-cell renal carcinoma. *Oncotarget* **9**, 30066-30078 (2018).

Roelants, C., Pillet, C., Franquet, Q., Sarrazin, C., Peilleron, N., Giacosa, S., Guyon, L., Fontanell, A., Fiard, G., Long, J.A., Descotes, J.L., Cochet, C., Filhol, O. Ex-Vivo Treatment of Tumor Tissue Slices as a Predictive Preclinical Method to Evaluate Targeted Therapies for Patients with Renal Carcinoma. *Cancers (Basel)* **12**, 232 (2020).

Roffey, S.E. & Litchfield, D.W. CK2 Regulation: Perspectives in 2021. *Biomedicines* **9**, 1361 (2021).

Rössig, L., Jadidi, A.S., Urbich, C., Badorff, C., Zeiher, A.M. & Dimmeler S. Akt-dependent phosphorylation of p21(Cip1) regulates PCNA binding and proliferation of endothelial cells. *Mol. Cell. Biol.* **2**, 5644-5657 (2001).

Ruzzene, M. & Pinna, L.A. Addiction to protein kinase CK2: a common denominator of diverse cancer cells? *Biochim. Biophys. Acta* **1804**, 499-504 (2010).

Sabatini, D.M. mTOR and cancer: insights into a complex relationship. *Nat. Rev. Cancer* **6**, 729-734 (2006).

Salvi, M., Borgo, C., Pinna, L.A., Ruzzene, M. Targeting CK2 in cancer: a valuable strategy or a waste of time? *Cell Death Discov.* **7**, 325 (2021).

Silva-Pavez, E., Tapia, J.C. Protein Kinase CK2 in Cancer Energetics. *Front Oncol.* **10**, 893 (2020).

So, K.S., Rho, J.K., Choi, Y.J., Kim, S.Y., Choi, C. M., Chun, Y.J. & Lee, J.C. AKT/mTOR down-regulation by CX-4945, a CK2 inhibitor, promotes apoptosis in chemorefractory non-small cell lung cancer cells. *Anticancer Res.* **35**, 1537-1542 (2015).

Sui, Y., Lu, K. & Fu, L. Prediction and analysis of novel key genes ITGAX, LAPTM5, SERPINE1 in clear cell renal cell carcinoma through bioinformatics analysis. *PeerJ.* **9**, e11272 (2021).

Trembley, J.H., Wang, G., Unger, G., Slaton, J. & Ahmed, K. Protein kinase CK2 in health and disease: CK2: a key player in cancer biology. *Cell. Mol. Life Sci.* **66**, 1858-1867 (2009).

Turowec, J.P., Vilks, G., Gabriel, M., Litchfield, D.W. Characterizing the convergence of protein kinase CK2 and caspase-3 reveals isoform-specific phosphorylation of caspase-3 by CK2 $\alpha$ : implications for pathological roles of CK2 in promoting cancer cell survival. *Oncotarget* **4**, 560-571 (2013).

Weiss, R.H. p21Waf1/Cip1 as a therapeutic target in breast and other cancers. *Cancer Cell* **4**, 425-429 (2003).

Wells, C.I., Drewry, D.H., Pickett, J.E., Tjaden, A., Krämer, A., Müller, S., Gyenis, L., Menyhart, D., Litchfield, D.W., Knapp, S. & Axtman, A.D. Development of a potent and selective chemical probe for the pleiotropic kinase CK2. *Cell. Chem. Biol.* **28**, 546-558 (2021).

Wu, W., Ren, Z., Li, P., Yu, D., Chen, J., Huang, R. & Liu, H. Six1: a critical transcription factor in tumorigenesis. *Int J Cancer.*, **136**, 1245-53 (2015).

Wu H, He D, Biswas S, Shafiquzzaman M, Zhou X, Charron J, Wang Y, Nayak BK, Habib SL, Liu H, Li B. mTOR Activation Initiates Renal Cell Carcinoma Development by Coordinating ERK and p38MAPK. *Cancer Res.*, **81**, 3174-3186 (2021). doi: 10.1158/0008-5472.CAN-20-3979.

Yuan, Z.L., Guan, Y.J., Wang, L., Wei, W., Kane, A.B. & Chin, Y.E. Central role of the threonine residue within the p+1 loop of receptor tyrosine kinase in STAT3 constitutive phosphorylation in metastatic cancer cells. *Mol. Cell. Biol.* **24**, 9390-9400 (2004).

Zanin, S., Borgo, C., Girardi, C., O'Brien, S.E., Miyata, Y., Pinna, L.A., Donella-Deana, A. & Ruzzene, M. Effects of the CK2 inhibitors CX-4945 and CX-5011 on drug-resistant cells. *PLoS One* **7**, e49193 (2012).

Zhou, B.P., Liao, Y., Xia, W., Spohn, B., Lee, M.H., Hung, M.C. Cytoplasmic localization of p21Cip1/WAF1 by Akt-induced phosphorylation in HER-2/neu-overexpressing cells. *Nat. Cell. Biol.* **3**, 245-252 (2001).

Zhou, B., Ritt, D.A., Morrison, D.K., Der, C.J. & Cox, A.D. Protein Kinase CK2 $\alpha$  Maintains Extracellular Signal-regulated Kinase (ERK) Activity in a CK2 $\alpha$  Kinase-independent Manner to Promote Resistance to Inhibitors of RAF and MEK but Not ERK in BRAF Mutant Melanoma. *J. Biol. Chem.* **291**, 17804-17815 (2016).

Zhu, L., X. Liu, W. Zhang, H. Hu, Q. Wang & K. Xu. MTHFD2 is a potential oncogene for its strong association with poor prognosis and high level of immune infiltrates in urothelial carcinomas of bladder. *BMC Cancer*, **22**(1): 556 (2022).

## References for Methods

Adams, P.D., Afonin, P.V., Bunkóczi, G., Chen, V.B., Davis, I.W., Echols, N., Headd, J.J., Hung, L.W., Kapral., G.J., Grosse-Kunstleve, R.W., McCoy, A.J., Moriarty, N.W., Oeffner, R., Read, R.J., Richardson, D.C., Richardson, J.S., Terwilliger, T.C., Zwart, P.H. PHENIX: a comprehensive Python-based system for macromolecular structure solution. *Acta Crystallogr. D Biol. Crystallogr.* **66**, 213-221 (2010).

Alpern, D., Gardeux, V., Russeil, J., Mangeat, B., Meireles-Filho, A.C.A., Breyse, R., Hacker, D.; Deplancke, B. BRB-seq: Ultra-affordable high-throughput transcriptomics enabled by bulk RNA barcoding and sequencing. *Genome Biol.* **20**, 71 (2019).

Chantalat, L., Leroy, D., Filhol, O., Nueda, A., Benitez, M.J., Chambaz, E.M., Cochet, C. & Dideberg, O. Crystal structure of the human protein kinase CK2 regulatory subunit reveals its zinc finger-mediated dimerization. *EMBO J.* **18**, 2930-2940 (1999).

Debnath, J., Muthuswamy, S. K. & Brugge, J. S.. Morphogenesis and Oncogenesis of MCF-10A Mammary Epithelial Acini Grown in Three-Dimensional Basement Membrane Cultures. *Methods* **30**, 256–268 (2003).

Draskau, M.K., Lardenois, A., Evrard, B., Boberg, J., Chalmel, F. & Svingen, T. Transcriptome analysis of fetal rat testis following intrauterine exposure to the azole fungicides triticonazole and flusilazole reveals subtle changes despite adverse endocrine effects. *Chemosphere* **264**, 128468 (2021). doi: 10.1016/j.chemosphere.2020.128468.

Emsley, P. & Cowtan, K. Coot: model-building tools for molecular graphics. *Acta Crystallogr. D Biol. Crystallogr.* **60**, 2126-2132 (2004).

Hériché, J.K., Lebrin, F., Rabilloud, T., Leroy, D., Chambaz, E.M., Goldberg, Y. Regulation of protein phosphatase 2A by direct interaction with casein kinase 2alpha. *Science*, **276**, 952-955 (1997).

Kabsch, W. XDS. *Acta Crystallogr. D Biol. Crystallogr.* **66**, 125-132 (2010).

Kufareva, I., Bestgen, B., Brear, P., Prudent, R., Laudet, B., Moucadel, V., Ettaoussi, M., Sautel, C.F., Krimm, I., Engel, M., Filhol, O., Le Borgne, M., Lomberget, T., Cochet, C. & Abagyan, R. Discovery of holoenzyme-disrupting chemicals as substrate-selective CK2 inhibitors. *Sci Rep.*, **9**, 15893 (2019).

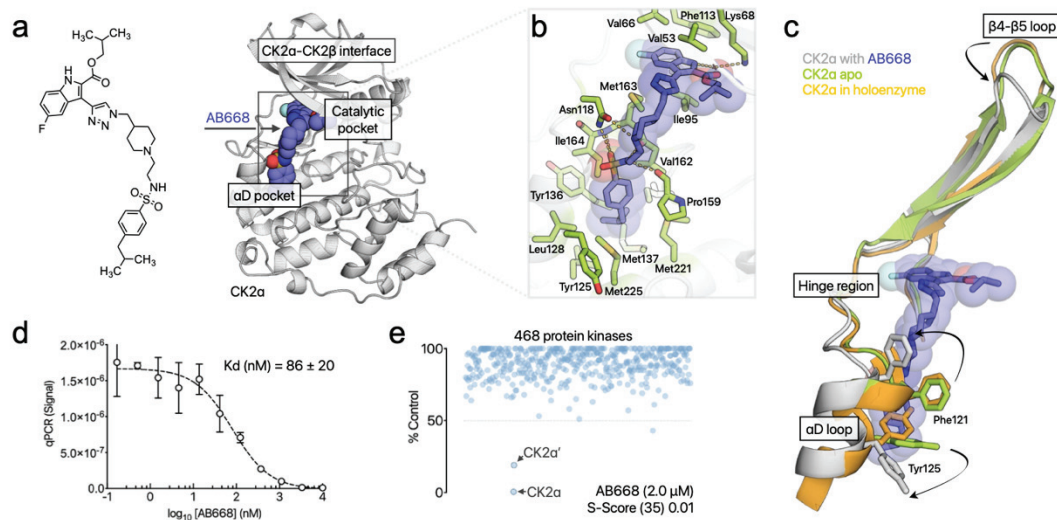
Lee, P.-H., Huang, X.X., The, B.T., Ng, L.-M. TSA-CRAFT: A free software for automatic and robust thermal shift assay data analysis. *SLAS Discovery* **24**, 606-612 (2019).

Love, M.I., Huber, W. & Anders, S. Moderated estimation of fold change and dispersion for RNA-seq data with DESeq2. *Genome Biol.* **15**, 550 (2014). doi: 10.1186/s13059-014-0550-8.

Roelants, C., Giacosa, S., Pillet, C., Bussat, R., Champelovier, P., Bastien, O., Guyon, L., Arnoux, V., Cochet, C., Filhol, O. Combined inhibition of PI3K and Src kinases demonstrates synergistic therapeutic efficacy in clear-cell renal carcinoma. *Oncotarget* **9**, 30066-30078 (2018).

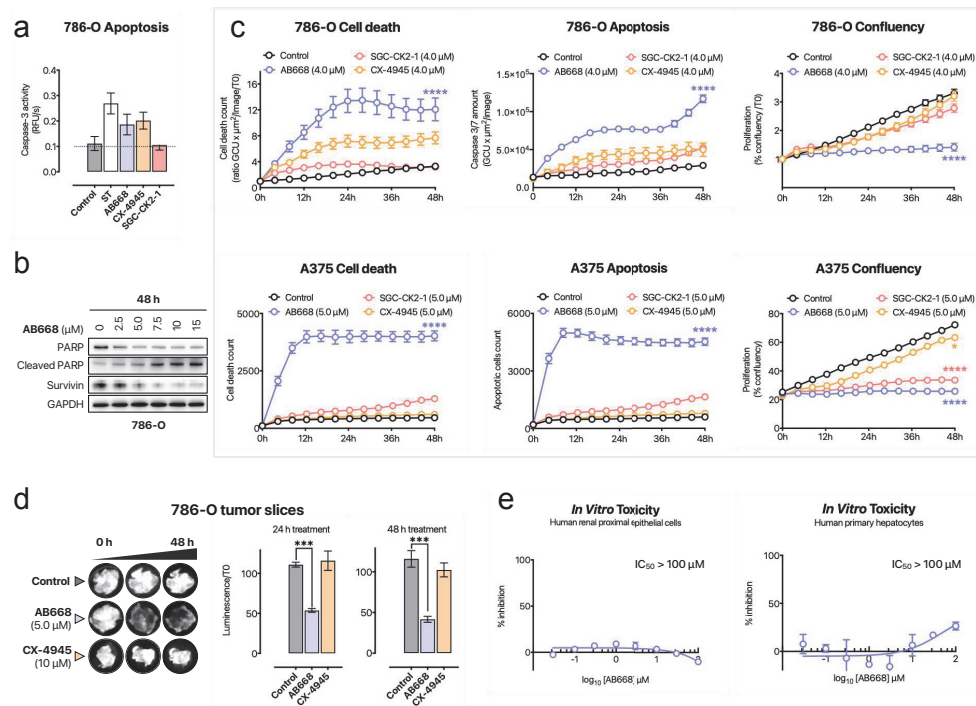
Roelants, C., Pillet, C., Franquet, Q., Sarrazin, C., Peilleron, N., Giacosa, S., Guyon, L., Fontanell, A., Fiard, G., Long, J.A., Descotes, J.L., Cochet, C., Filhol, O. Ex-Vivo Treatment of Tumor Tissue Slices as a Predictive Preclinical Method to Evaluate Targeted Therapies for Patients with Renal Carcinoma. *Cancers (Basel)* **12**, 232 (2020).

**Figure 1**



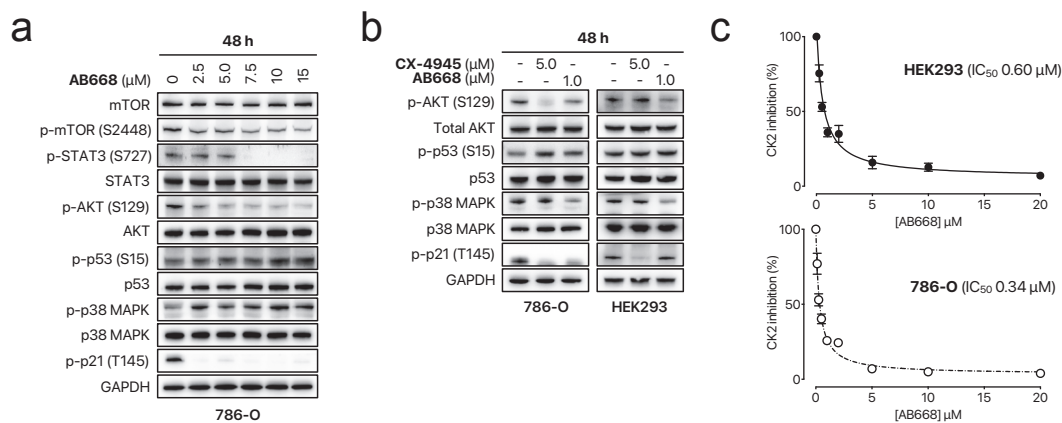
**Binding mode, affinity for CK2 $\alpha$  and kinase selectivity profile of AB668.** **a)** Chemical structure of AB668 and CK2 $\alpha$ /AB668 complex crystal 3D structure (pdb code 8C5Q) showing the binding site of AB668: the inhibitor binds both the ATP pocket and the  $\alpha$ D pocket of CK2 $\alpha$ . **b)** Stick representation of AB668 bound to CK2 $\alpha$ : side chains in interaction with the inhibitor are shown, and hydrogen bonds are displayed. **c)** Conformational rearrangement of CK2 $\alpha$  upon AB668 binding: the helix is shifted to allow the binding of AB668 in the  $\alpha$ D pocket. The structure of CK2 $\alpha$  bound to AB668 is superimposed to the structure of the holoenzyme (pdb code 1JWH), and to the apo structure of CK2 $\alpha$  (pdb code 3QAO) **d)** Binding affinity of AB668 as determined by the KINOMEscan<sup>TM</sup> profiling service (Eurofins). **e)** Selectivity profile of AB668, profiled against 468 kinases, using the screening platform from Eurofins DiscoverX. AB668 concentration was 2  $\mu$ M (25 times its  $K_d$  value).

**Figure 2**



**Cellular activity of AB668 and comparison to CX-4945 and SGC-CK2-1.** **a)** Quantitative fluorometric assay showing caspase-3 activation in 786-O cells treated with staurosporine, AB668, SGC-CK2-1 or CX-4945. Assays were performed after 72 h treatment with the compounds at 20 μM. **b)** Western blot experiments on 786-O cells treated with AB668 (2.5, 5, 7.5, 10 and 15 μM) for 48h showing the cleavage of PARP as well as the expression level of survivin. **c)** Live cell imaging showing proliferation arrest, cell death and apoptosis in 786-O and A375 cells treated with AB668, CX-4945 or SGC-CK2-1 (4 μM) for 48h. **d)** Effect of AB668 and CX-4945 on *ex vivo* culture of intact tumor slices of clear cell renal carcinoma. Tumors were extracted from renal carcinoma xenografted mice that were directly processed into 300 μm slices and treated for 48 h as described in Methods. Cell viability was evaluated by luciferin measurement of treated tumor-slice cultures as described in Methods. **e)** Cell viability of primary hepatocytes and RPTEC (Renal Proximal Tubule Epithelial Cells) treated with AB668.

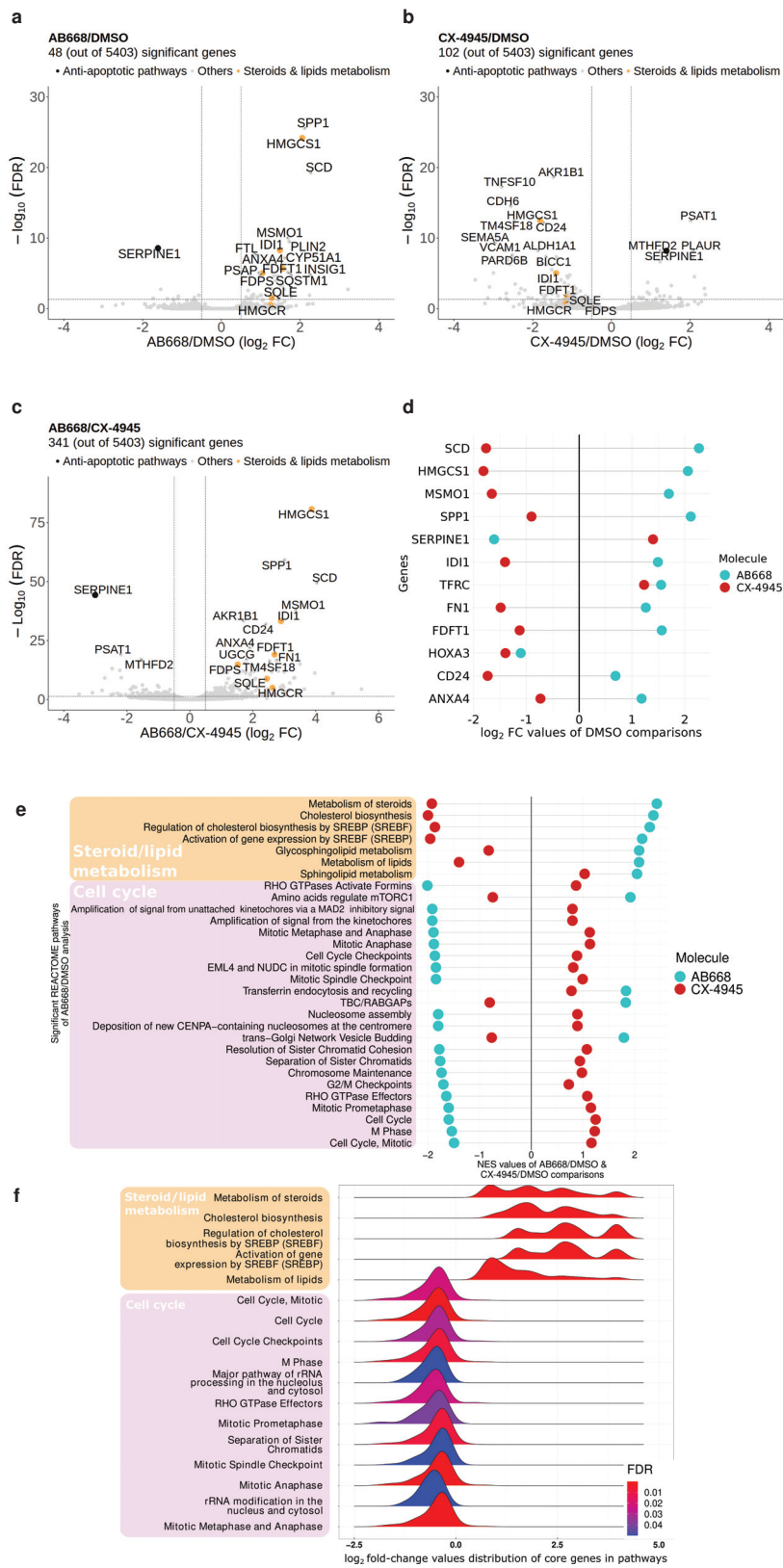
**Figure 3**



**Target engagement of AB668 in 786-O cells and HEK293 cells.** **a)** Western blot analysis in response to AB668 in 786-O cells. The inhibition of phosphorylated mTOR (S2448), STAT3 (S727), p53 (S15), p38 MAPK (T180/Y182) and AKT (S129) and p21 (T145) was analyzed after 48 h of inhibitor AB668 treatment. **b)** The inhibition of phosphorylated AKT (S129), p53 (S15), p38 MAPK (T180/Y182) and p21 (T145) was analyzed after 48 h of AB668 (1 μM) or CX-4945 (5 μM) treatment in 786-O cancer cells or HEK293 cells. Glyceraldehyde-3-phosphate dehydrogenase (GAPDH) was used as a loading control. **c)** CK2 activity measured in cell extracts of 786-O cells (upper panel) or HEK293 cells (lower panel) after treatment with AB668. Inhibition constants IC<sub>50</sub> are 0.34 ± 0.07 μM for 786-O cells and 0.60 ± 0.11 μM for HEK293 cells.



**Figure 4**



**Deregulations of the transcriptome in response to AB668 or CX-4945. a-c) Volcano plots based upon differential gene expression analysis of the transcriptomes of 786-O cells exposed**

to the different CK2 inhibitors: **a)** AB668 vs DMSO **b)** CX-4945 vs DMSO and **c)** AB668 vs CX-4945. **d)** Differences of Log<sub>2</sub>(Fold Changes) of gene expression values for AB668 and CX-4945 treated cells compared to DMSO treated cells. **e)** Normalized Enrichment Scores (NES), calculated by the Gene Set Enrichment Analysis (GSEA) method, for significantly deregulated pathways obtained from AB668 vs DMSO analysis in comparison to the NES scores generated from CX-4945 vs DMSO analysis. **f)** Histograms of Log<sub>2</sub>(Fold Changes) of gene expression values for AB668 vs CX-4945 comparison for significantly deregulated pathways found by GSEA analysis, using REACTOME pathway database.

## Bibliography

- [1] W. Zhang, H. T. Liu, and H. Tu, "MAPK signal pathways in the regulation of cell proliferation in mammalian cells," *Cell Res*, 2002, [Online]. Available: <http://www.cell-research.com>
- [2] Y. Sun, W. Z. Liu, T. Liu, X. Feng, N. Yang, and H. F. Zhou, "Signaling pathway of MAPK/ERK in cell proliferation, differentiation, migration, senescence and apoptosis," *Journal of Receptors and Signal Transduction*, vol. 35, no. 6. Taylor and Francis Ltd, pp. 600–604, Nov. 02, 2015. doi: 10.3109/10799893.2015.1030412.
- [3] E. F. Wagner and Á. R. Nebreda, "Signal integration by JNK and p38 MAPK pathways in cancer development," *Nature Reviews Cancer*, vol. 9, no. 8. pp. 537–549, Aug. 2009. doi: 10.1038/nrc2694.
- [4] G. N. Nithianandarajah-Jones, B. Wilm, C. E. P. Goldring, J. Müller, and M. J. Cross, "The role of ERK5 in endothelial cell function," *Biochemical Society Transactions*, vol. 42, no. 6. Portland Press Ltd, pp. 1584–1589, Dec. 01, 2014. doi: 10.1042/BST20140276.
- [5] R. Roskoski, "ERK1/2 MAP kinases: Structure, function, and regulation," *Pharmacological Research*, vol. 66, no. 2. pp. 105–143, Aug. 2012. doi: 10.1016/j.phrs.2012.04.005.
- [6] Z. Lu and S. Xu, "ERK1/2 MAP kinases in cell survival and apoptosis," *IUBMB Life (International Union of Biochemistry and Molecular Biology: Life)*, vol. 58, no. 11, pp. 621–631, Nov. 2006, doi: 10.1080/15216540600957438.
- [7] M. Cargnello and P. P. Roux, "Activation and Function of the MAPKs and Their Substrates, the MAPK-Activated Protein Kinases," *Microbiology and Molecular Biology Reviews*, vol. 75, no. 1, pp. 50–83, Mar. 2011, doi: 10.1128/mnbr.00031-10.
- [8] Y. Pylayeva-Gupta, E. Grabocka, and D. Bar-Sagi, "RAS oncogenes: Weaving a tumorigenic web," *Nature Reviews Cancer*, vol. 11, no. 11. pp. 761–774, Nov. 2011. doi: 10.1038/nrc3106.
- [9] R. Roskoski, "RAF protein-serine/threonine kinases: Structure and regulation," *Biochemical and Biophysical Research Communications*, vol. 399, no. 3. pp. 313–317, Aug. 2010. doi: 10.1016/j.bbrc.2010.07.092.
- [10] R. Roskoski, "MEK1/2 dual-specificity protein kinases: Structure and regulation," *Biochemical and Biophysical Research Communications*, vol. 417, no. 1. pp. 5–10, Jan. 06, 2012. doi: 10.1016/j.bbrc.2011.11.145.
- [11] A. C. Lloyd, "Distinct functions for ERKs?," *Journal of Biology*, vol. 5, no. 13, 2006, [Online]. Available: <http://jbiol.com/content/5/5/13>
- [12] S. Yoon and R. Seger, "The extracellular signal-regulated kinase: Multiple substrates regulate diverse cellular functions," *Growth Factors*, vol. 24, no. 1, pp. 21–44, Jan. 2006, doi: 10.1080/02699050500284218.
- [13] A. Herrero and P. Crespo, "Ras dimers: The novice couple at the ras-erk pathway ball," *Genes*, vol. 12, no. 10. MDPI, Oct. 01, 2021. doi: 10.3390/genes12101556.
- [14] M. Zhang, R. Maloney, H. Jang, and R. Nussinov, "The mechanism of Raf activation through dimerization," *Chem Sci*, vol. 12, no. 47, pp. 15609–15619, Dec. 2021, doi: 10.1039/d1sc03444h.
- [15] J. Yuan *et al.*, "Activating mutations in MEK1 enhance homodimerization and promote tumorigenesis," *Sci. Signal*, vol. 11, p. 6795, 2018, [Online]. Available: <https://www.science.org>
- [16] B. Casar, A. Pinto, and P. Crespo, "ERK dimers and scaffold proteins: Unexpected partners for a forgotten (cytoplasmic) task," *Cell Cycle*, vol. 8, no. 7. Taylor and Francis Inc., pp. 1007–1013, Apr. 01, 2009. doi: 10.4161/cc.8.7.8078.
- [17] M. A. Lemmon and J. Schlessinger, "Cell signaling by receptor tyrosine kinases," *Cell*, vol. 141, no. 7. Elsevier B.V., pp. 1117–1134, 2010. doi: 10.1016/j.cell.2010.06.011.
- [18] N. Tuteja, "Signaling through G protein coupled receptors," *Plant Signaling and Behavior*, vol. 4, no. 10. pp. 942–947, 2009. doi: 10.4161/psb.4.10.9530.

- [19] Y. Guo, W. Pan, S. Liu, Z. Shen, Y. Xu, and L. Hu, "ERK/MAPK signalling pathway and tumorigenesis (Review)," *Exp Ther Med*, Jan. 2020, doi: 10.3892/etm.2020.8454.
- [20] E. B. Ünal, F. Uhlitz, and N. Blüthgen, "A compendium of ERK targets," *FEBS Letters*, vol. 591, no. 17. Wiley Blackwell, pp. 2607–2615, Sep. 01, 2017. doi: 10.1002/1873-3468.12740.
- [21] G. Maik-Rachline, A. Hacoheh-Lev-Ran, and R. Seger, "Nuclear erk: Mechanism of translocation, substrates, and role in cancer," *International Journal of Molecular Sciences*, vol. 20, no. 5. MDPI AG, Mar. 01, 2019. doi: 10.3390/ijms20051194.
- [22] S. Bahrami and F. Drabløs, "Gene regulation in the immediate-early response process," *Advances in Biological Regulation*, vol. 62. Elsevier Ltd, pp. 37–49, Sep. 01, 2016. doi: 10.1016/j.jbior.2016.05.001.
- [23] Y. Romeo, X. Zhang, and P. P. Roux, "Regulation and function of the RSK family of protein kinases," *Biochemical Journal*, vol. 441, no. 2. pp. 553–569, Jan. 15, 2012. doi: 10.1042/BJ20110289.
- [24] M. C. Brown and C. E. Turner, "Paxillin: Adapting to Change," *Physiol Rev*, vol. 84, 2004, doi: 10.1152/physrev.00002.2004.-Molecular.
- [25] Z. X. Liu, C. F. Yu, C. Nickel, S. Thomas, and L. G. Cantley, "Hepatocyte growth factor induces ERK-dependent paxillin phosphorylation and regulates paxillin-focal adhesion kinase association," *Journal of Biological Chemistry*, vol. 277, no. 12, pp. 10452–10458, Mar. 2002, doi: 10.1074/jbc.M107551200.
- [26] H. Lavoie, J. Gagnon, and M. Therrien, "ERK signalling: a master regulator of cell behaviour, life and fate," *Nat Rev Mol Cell Biol*, doi: 10.1038/s41580-020-0255-7.
- [27] R. Anjum and J. Blenis, "The RSK family of kinases: Emerging roles in cellular signalling," *Nature Reviews Molecular Cell Biology*, vol. 9, no. 10. pp. 747–758, Oct. 2008. doi: 10.1038/nrm2509.
- [28] K. A. Rauen, "The RASopathies," *Annual Review of Genomics and Human Genetics*, vol. 14. pp. 355–369, Aug. 2013. doi: 10.1146/annurev-genom-091212-153523.
- [29] D. Lake, S. A. L. Corrêa, and J. Müller, "Negative feedback regulation of the ERK1/2 MAPK pathway," *Cellular and Molecular Life Sciences*, vol. 73, no. 23. Birkhauser Verlag AG, pp. 4397–4413, Jun. 24, 2016. doi: 10.1007/s00018-016-2297-8.
- [30] S. S. Taylor and A. P. Kornev, "Protein kinases: Evolution of dynamic regulatory proteins," *Trends in Biochemical Sciences*, vol. 36, no. 2. pp. 65–77, Feb. 2011. doi: 10.1016/j.tibs.2010.09.006.
- [31] S. K. Hanks, A. M. Quinn, and T. Hunter, "The Protein Kinase Family: Conserved Features and Deduced Phylogeny of the Catalytic Domains," *Science (1979)*, vol. 241, no. 4861, pp. 42–52, Jul. 1988, doi: 10.1126/science.3291115.
- [32] R. J. Davis, "The Mitogen-activated Protein Kinase Signal Transduction Pathway\*," *J Biol Chem*, vol. 268, no. 20, pp. 14553–14556, 1993.
- [33] D. Jacobs, D. Glossip, H. Xing, A. J. Muslin, and K. Kornfeld, "Multiple docking sites on substrate proteins form a modular system that mediates recognition by ERK MAP kinase," *Genes Dev*, vol. 163, no. 13, 1999, [Online]. Available: [www.genesdev.org](http://www.genesdev.org)
- [34] A. Herrero *et al.*, "Small Molecule Inhibition of ERK Dimerization Prevents Tumorigenesis by RAS-ERK Pathway Oncogenes," *Cancer Cell*, vol. 28, no. 2, pp. 170–182, Aug. 2015, doi: 10.1016/j.ccell.2015.07.001.
- [35] B. Casar, A. Pinto, and P. Crespo, "Essential Role of ERK Dimers in the Activation of Cytoplasmic but Not Nuclear Substrates by ERK-Scaffold Complexes," *Mol Cell*, vol. 31, no. 5, pp. 708–721, Sep. 2008, doi: 10.1016/j.molcel.2008.07.024.
- [36] D. S. Lidke *et al.*, "ERK nuclear translocation is dimerization-independent but controlled by the rate of phosphorylation," *Journal of Biological Chemistry*, vol. 285, no. 5, pp. 3092–3102, Jan. 2010, doi: 10.1074/jbc.M109.064972.

- [37] R. Buscà, J. Pouysségur, and P. Lenormand, "ERK1 and ERK2 map kinases: Specific roles or functional redundancy?," *Frontiers in Cell and Developmental Biology*, vol. 4, no. JUN. Frontiers Media S.A., Jun. 08, 2016. doi: 10.3389/fcell.2016.00053.
- [38] I. Wortzel and R. Seger, "The ERK cascade: Distinct functions within various subcellular organelles," *Genes and Cancer*, vol. 2, no. 3. SAGE Publications Inc., pp. 195–209, Mar. 01, 2011. doi: 10.1177/1947601911407328.
- [39] R. García-Gómez, X. R. Bustelo, and P. Crespo, "Protein-Protein Interactions: Emerging Oncotargets in the RAS-ERK Pathway.," *Trends Cancer*, vol. 4, no. 9, pp. 616–633, Sep. 2018, doi: 10.1016/j.trecan.2018.07.002.
- [40] F. Liu, X. Yang, M. Geng, and M. Huang, "Targeting ERK, an Achilles' Heel of the MAPK pathway, in cancer therapy," *Acta Pharmaceutica Sinica B*, vol. 8, no. 4. Chinese Academy of Medical Sciences, pp. 552–562, Jul. 01, 2018. doi: 10.1016/j.apsb.2018.01.008.
- [41] R. Kannaiyan and D. Mahadevan, "A comprehensive review of protein kinase inhibitors for cancer therapy," *Expert Review of Anticancer Therapy*, vol. 18, no. 12. Taylor and Francis Ltd, pp. 1249–1270, Dec. 02, 2018. doi: 10.1080/14737140.2018.1527688.
- [42] F. Skoulidis *et al.*, "Sotorasib for Lung Cancers with KRAS p.G12C Mutation ," *New England Journal of Medicine*, vol. 384, no. 25, pp. 2371–2381, Jun. 2021, doi: 10.1056/nejmoa2103695.
- [43] X. Pan *et al.*, "Development of small molecule extracellular signal-regulated kinases (ERKs) inhibitors for cancer therapy," *Acta Pharmaceutica Sinica B*, vol. 12, no. 5. Chinese Academy of Medical Sciences, pp. 2171–2192, May 01, 2022. doi: 10.1016/j.apsb.2021.12.022.
- [44] S. Liu, J.-P. Sun, B. Zhou, and Z.-Y. Zhang, "Structural basis of docking interactions between ERK2 and MAP kinase phosphatase 3," *PNAS*, vol. 103, no. 14, pp. 5326–5331, 2006, [Online]. Available: [www.pnas.org/cgi/doi/10.1073/pnas.0510506103](http://www.pnas.org/cgi/doi/10.1073/pnas.0510506103)
- [45] R. Samadani *et al.*, "Small-molecule inhibitors of ERK-mediated immediate early gene expression and proliferation of melanoma cells expressing mutated BRAf," *Biochemical Journal*, vol. 467, no. 3, pp. 425–438, May 2015, doi: 10.1042/BJ20131571.
- [46] M. Morante, A. Pandiella, P. Crespo, and A. Herrero, "Immune Checkpoint Inhibitors and RAS–ERK Pathway-Targeted Drugs as Combined Therapy for the Treatment of Melanoma," *Biomolecules*, vol. 12, no. 11. MDPI, Nov. 01, 2022. doi: 10.3390/biom12111562.
- [47] M. A. Zaballos, A. Acuña-Ruiz, M. Morante, G. Riesco-Eizaguirre, P. Crespo, and P. Santisteban, "Inhibiting ERK dimerization ameliorates BRAF-driven anaplastic thyroid cancer," *Cellular and Molecular Life Sciences*, vol. 79, no. 9, Sep. 2022, doi: 10.1007/s00018-022-04530-9.
- [48] M. Najafi, A. Ahmadi, and K. Mortezaee, "Extracellular-signal-regulated kinase/mitogen-activated protein kinase signaling as a target for cancer therapy: an updated review," *Cell Biology International*, vol. 43, no. 11. Wiley-Blackwell Publishing Ltd, pp. 1206–1222, Nov. 01, 2019. doi: 10.1002/cbin.11187.
- [49] C. Braicu *et al.*, "A comprehensive review on MAPK: A promising therapeutic target in cancer," *Cancers*, vol. 11, no. 10. MDPI AG, Oct. 01, 2019. doi: 10.3390/cancers11101618.
- [50] A. Kfoury, F. Virard, T. Renno, and I. Coste, "Dual function of MyD88 in inflammation and oncogenesis: implications for therapeutic intervention.," *Curr Opin Oncol*, vol. 26, no. 1, pp. 86–91, Jan. 2014, doi: 10.1097/CCO.0000000000000037.
- [51] I. Coste *et al.*, "Dual function of MyD88 in RAS signaling and inflammation, leading to mouse and human cell transformation," *J Clin Invest*, vol. 120, no. 10, Oct. 2010, doi: 10.1172/JCI42771DS1.
- [52] F. di Sole and A. C. C. Girardi, "Uncovering the pathway of sepsis-induced renal tubular dysfunction. Focus on 'Basolateral LPS inhibits NHE3 and HCO<sup>3-</sup> absorption through TLR4/MyD88-dependent ERK activation in medullary thick ascending limb,'" *American Journal of Physiology - Cell Physiology*, vol. 301, no. 6. Dec. 2011. doi: 10.1152/ajpcell.00350.2011.

- [53] S. H. Lee *et al.*, “ERK activation drives intestinal tumorigenesis in Apc min/+ mice,” *Nat Med*, vol. 16, no. 6, pp. 665–670, Jun. 2010, doi: 10.1038/nm.2143.
- [54] M. Y. Peroval, A. C. Boyd, J. R. Young, and A. L. Smith, “A Critical Role for MAPK Signalling Pathways in the Transcriptional Regulation of Toll Like Receptors,” *PLoS One*, vol. 8, no. 2, Feb. 2013, doi: 10.1371/journal.pone.0051243.
- [55] L. Wang, K. Yu, X. Zhang, and S. Yu, “Dual functional roles of the MyD88 signaling in colorectal cancer development,” *Biomedicine and Pharmacotherapy*, vol. 107. Elsevier Masson SAS, pp. 177–184, Nov. 01, 2018. doi: 10.1016/j.biopha.2018.07.139.
- [56] R. Salcedo, C. Cataisson, U. Hasan, S. H. Yuspa, and G. Trinchieri, “MyD88 and its divergent toll in carcinogenesis,” *Trends in Immunology*, vol. 34, no. 8. pp. 379–389, Aug. 2013. doi: 10.1016/j.it.2013.03.008.
- [57] P. Cohen, “The TLR and IL-1 signalling network at a glance,” *J Cell Sci*, vol. 127, no. 11, pp. 2383–2390, 2014, doi: 10.1242/jcs.149831.
- [58] L. Chen, L. Zheng, P. Chen, and G. Liang, “Myeloid Differentiation Primary Response Protein 88 (MyD88): The Central Hub of TLR/IL-1R Signaling,” *Journal of Medicinal Chemistry*, vol. 63, no. 22. American Chemical Society, pp. 13316–13329, Nov. 25, 2020. doi: 10.1021/acs.jmedchem.0c00884.
- [59] J. Deguine and G. M. Barton, “MyD88: A central player in innate immune signaling,” *F1000Prime Rep*, vol. 6, Nov. 2014, doi: 10.12703/P6-97.
- [60] T. Kawasaki and T. Kawai, “Toll-like receptor signaling pathways,” *Frontiers in Immunology*, vol. 5, no. SEP. Frontiers Media S.A., 2014. doi: 10.3389/fimmu.2014.00461.
- [61] K. U. Saikh, “MyD88 and beyond: a perspective on MyD88-targeted therapeutic approach for modulation of host immunity,” *Immunologic Research*, vol. 69, no. 2. Springer, pp. 117–128, Apr. 01, 2021. doi: 10.1007/s12026-021-09188-2.
- [62] S. Agarwal and Karthik. Krishnamurthy, *Histology, Skin*. StatPearls, 2022.
- [63] W. Lopez-Ojeda, A. Pandey, M. Alhajj, and A. M. Oakley, *Anatomy, Skin (Integument)*. StatPearls, 2022.
- [64] H. Yousef, M. Alhajj, and S. Sharma, *Anatomy, Skin (Integument), Epidermis*. StatPearls, 2022. Accessed: Mar. 17, 2023. [Online]. Available: <https://www.ncbi.nlm.nih.gov/books/NBK470464/>
- [65] PDQ Adult Treatment Editorial Board., “Skin Cancer Treatment (PDQ®): Health Professional Version. 2023 Mar 2.,” in *PDQ Cancer Information Summaries*, Bethesda (MD): National Cancer Institute (US), 2023. Accessed: Mar. 17, 2023. [Online]. Available: [https://www.ncbi.nlm.nih.gov/books/NBK65928/#\\_NBK65928\\_pubdet\\_](https://www.ncbi.nlm.nih.gov/books/NBK65928/#_NBK65928_pubdet_)
- [66] D. Ramadon, M. T. C. McCrudden, A. J. Courtenay, and R. F. Donnelly, “Enhancement strategies for transdermal drug delivery systems: current trends and applications.,” *Drug Deliv Transl Res*, vol. 12, no. 4, pp. 758–791, Apr. 2022, doi: 10.1007/s13346-021-00909-6.
- [67] M. Cichorek, M. Wachulska, A. Stasiewicz, and A. Tymińska, “Skin melanocytes: Biology and development,” *Postepy Dermatol Alergol*, vol. 30, no. 1, pp. 30–41, 2013, doi: 10.5114/pdia.2013.33376.
- [68] J. Y. Lin and D. E. Fisher, “Melanocyte biology and skin pigmentation,” *Nature*, vol. 445, no. 7130. Nature Publishing Group, pp. 843–850, Feb. 22, 2007. doi: 10.1038/nature05660.
- [69] T. H. Nasti and L. Timares, “MC1R, eumelanin and pheomelanin: Their role in determining the susceptibility to skin cancer,” *Photochem Photobiol*, vol. 91, no. 1, pp. 188–200, 2015, doi: 10.1111/php.12335.
- [70] S. Pavel, “Dynamics of melanogenesis intermediates.,” *J Invest Dermatol*, vol. 100, no. 2 Suppl, pp. 162S-165S, Feb. 1993.

- [71] J. Borovanský, P. Mirejovský, and P. A. Riley, "Possible relationship between abnormal melanosome structure and cytotoxic phenomena in malignant melanoma.," *Neoplasma*, vol. 38, no. 4, pp. 393–400, 1991.
- [72] A. M. Morgan, J. Lo, and D. E. Fisher, "How does pheomelanin synthesis contribute to melanomagenesis?: Two distinct mechanisms could explain the carcinogenicity of pheomelanin synthesis," *BioEssays*, vol. 35, no. 8, pp. 672–676, Aug. 2013, doi: 10.1002/bies.201300020.
- [73] E. Le Pape, K. Wakamatsu, S. Ito, R. Wolber, and V. J. Hearing, "Regulation of eumelanin/pheomelanin synthesis and visible pigmentation in melanocytes by ligands of the melanocortin 1 receptor," *Pigment Cell Melanoma Res*, vol. 21, no. 4, pp. 477–486, Aug. 2008, doi: 10.1111/j.1755-148X.2008.00479.x.
- [74] S. Corre *et al.*, "UV-induced expression of key component of the tanning process, the POMC and MC1R genes, is dependent on the p-38-activated upstream stimulating factor-1 (USF-1)," *Journal of Biological Chemistry*, vol. 279, no. 49, pp. 51226–51233, Dec. 2004, doi: 10.1074/jbc.M409768200.
- [75] C. Bertolotto *et al.*, "Microphthalmia Gene Product as a Signal Transducer in cAMP-Induced Differentiation of Melanocytes," *J Cell Biol*, vol. 142, no. 3, pp. 827–835, 1998, [Online]. Available: <http://www.jcb.org>
- [76] N. K. Haass and M. Herlyn, "Normal Human Melanocyte Homeostasis as a Paradigm for Understanding Melanoma," *J Invest Dermatol Symp Proc*, vol. 10, pp. 153–163, 2005.
- [77] N. K. Haass, K. S. M. Smalley, L. Li, and M. Herlyn, "Adhesion, migration and communication in melanocytes and melanoma," *Pigment Cell Research*, vol. 18, no. 3, pp. 150–159, Jun. 2005. doi: 10.1111/j.1600-0749.2005.00235.x.
- [78] G.-E. Costin and V. J. Hearing, "Human skin pigmentation: melanocytes modulate skin color in response to stress," *The FASEB Journal*, vol. 21, no. 4, pp. 976–994, Apr. 2007, doi: 10.1096/fj.06-6649rev.
- [79] J. P. Johnson, "Cell adhesion molecules in the development and progression of malignant melanoma.," *Cancer Metastasis Rev*, vol. 18, no. 3, pp. 345–57, 1999, doi: 10.1023/a:1006304806799.
- [80] J. Tímár and A. Ladányi, "Molecular Pathology of Skin Melanoma: Epidemiology, Differential Diagnostics, Prognosis and Therapy Prediction," *International Journal of Molecular Sciences*, vol. 23, no. 10, MDPI, May 01, 2022. doi: 10.3390/ijms23105384.
- [81] M. G. Davey, N. Miller, and N. M. McInerney, "A Review of Epidemiology and Cancer Biology of Malignant Melanoma," *Cureus*, May 2021, doi: 10.7759/cureus.15087.
- [82] L. E. Davis, S. C. Shalin, and A. J. Tackett, "Current state of melanoma diagnosis and treatment.," *Cancer Biol Ther*, vol. 20, no. 11, pp. 1366–1379, Nov. 2019, doi: 10.1080/15384047.2019.1640032.
- [83] R. L. Siegel, K. D. Miller, and A. Jemal, "Cancer statistics, 2020," *CA Cancer J Clin*, vol. 70, no. 1, pp. 7–30, Jan. 2020, doi: 10.3322/caac.21590.
- [84] N. H. Matthews, W.-Q. Li, A. A. Qureshi, M. A. Weinstock, and E. Cho, "Epidemiology of Melanoma," in *Cutaneous Melanoma: Etiology and Therapy*, Codon Publications, 2017, pp. 3–22. doi: 10.15586/codon.cutaneousmelanoma.2017.ch1.
- [85] Y. Wang, N. Freemantle, I. Nazareth, and K. Hunt, "Gender differences in survival and the use of primary care prior to diagnosis of three cancers: an analysis of routinely collected UK general practice data.," *PLoS One*, vol. 9, no. 7, p. e101562, 2014, doi: 10.1371/journal.pone.0101562.
- [86] T. Randic, I. Kozar, C. Margue, J. Utikal, and S. Kreis, "NRAS mutant melanoma: Towards better therapies," *Cancer Treatment Reviews*, vol. 99, W.B. Saunders Ltd, Sep. 01, 2021. doi: 10.1016/j.ctrv.2021.102238.

- [87] J. Paluncic *et al.*, “Roads to melanoma: Key pathways and emerging players in melanoma progression and oncogenic signaling,” *Biochimica et Biophysica Acta - Molecular Cell Research*, vol. 1863, no. 4. Elsevier B.V., pp. 770–784, Apr. 01, 2016. doi: 10.1016/j.bbamcr.2016.01.025.
- [88] Y. Qin, Q. Zuo, L. Huang, L. Huang, G. Merlino, and Y. Yu, “PERK mediates resistance to BRAF inhibition in melanoma with impaired PTEN,” *NPJ Precis Oncol*, vol. 5, no. 1, Dec. 2021, doi: 10.1038/s41698-021-00207-x.
- [89] D. Dankort *et al.*, “BrafV600E cooperates with Pten loss to induce metastatic melanoma,” *Nat Genet*, vol. 41, no. 5, pp. 544–552, May 2009, doi: 10.1038/ng.356.
- [90] E. Pérez-Guijarro, C. P. Day, G. Merlino, and M. R. Zaidi, “Genetically engineered mouse models of melanoma,” *Cancer*, vol. 123. John Wiley and Sons Inc., pp. 2089–2103, Jun. 01, 2017. doi: 10.1002/cncr.30684.
- [91] L. Vidarsdottir *et al.*, “PTENP1-AS contributes to BRAF inhibitor resistance and is associated with adverse clinical outcome in stage III melanoma,” *Sci Rep*, vol. 11, no. 1, Dec. 2021, doi: 10.1038/s41598-021-89389-9.
- [92] R. Cabrita *et al.*, “The role of PTEN loss in immune escape, melanoma prognosis and therapy response,” *Cancers (Basel)*, vol. 12, no. 3, Mar. 2020, doi: 10.3390/cancers12030742.
- [93] M. Ottaviano *et al.*, “BRAF gene and melanoma: Back to the future,” *International Journal of Molecular Sciences*, vol. 22, no. 7. MDPI AG, Apr. 01, 2021. doi: 10.3390/ijms22073474.
- [94] A. Garcia-Alvarez, C. Ortiz, and E. Muñoz-Couselo, “Current perspectives and novel strategies of nras-mutant melanoma,” *OncoTargets and Therapy*, vol. 14. Dove Medical Press Ltd, pp. 3709–3719, 2021. doi: 10.2147/OTT.S278095.
- [95] A. Popovic and S. Tartare-Deckert, “Role of extracellular matrix architecture and signaling in melanoma therapeutic resistance,” *Frontiers in Oncology*, vol. 12. Frontiers Media S.A., Sep. 02, 2022. doi: 10.3389/fonc.2022.924553.
- [96] S. M. Hossain and M. R. Eccles, “Phenotype Switching and the Melanoma Microenvironment; Impact on Immunotherapy and Drug Resistance,” *International Journal of Molecular Sciences*, vol. 24, no. 2. MDPI, Jan. 01, 2023. doi: 10.3390/ijms24021601.
- [97] F. Z. Li, A. S. Dhillon, R. L. Anderson, G. McArthur, and P. T. Ferrao, “Phenotype switching in melanoma: Implications for progression and therapy,” *Frontiers in Oncology*, vol. 5, no. FEB. Frontiers Research Foundation, 2015. doi: 10.3389/fonc.2015.00031.
- [98] C. Pagliuca, L. Di Leo, and D. De Zio, “New Insights into the Phenotype Switching of Melanoma,” *Cancers*, vol. 14, no. 24. MDPI, Dec. 01, 2022. doi: 10.3390/cancers14246118.
- [99] J. Caramel *et al.*, “A Switch in the Expression of Embryonic EMT-Inducers Drives the Development of Malignant Melanoma,” *Cancer Cell*, vol. 24, no. 4, pp. 466–480, Oct. 2013, doi: 10.1016/j.ccr.2013.08.018.
- [100] F. Rambow, J.-C. Marine, and C. R. Goding, “Melanoma plasticity and phenotypic diversity: therapeutic barriers and opportunities,” 2019, doi: 10.1101/gad.329771.
- [101] I. Yeh and B. C. Bastian, “Melanoma pathology: new approaches and classification\*,” *British Journal of Dermatology*, vol. 185, no. 2, pp. 282–293, Aug. 2021, doi: 10.1111/bjd.20427.
- [102] Y. Puckett, A. M. Wilson, F. Farci, and C. Thevenin, “Melanoma Pathology,” in *StatPearls*, StatPearls, Ed., Treasure Island (FL), 2023. Accessed: Mar. 21, 2023. [Online]. Available: [https://www.ncbi.nlm.nih.gov/books/NBK459367/#\\_NBK459367\\_pubdet\\_](https://www.ncbi.nlm.nih.gov/books/NBK459367/#_NBK459367_pubdet_)
- [103] R. A. Scolyer, R. V. Rawson, J. E. Gershenwald, P. M. Ferguson, and V. G. Prieto, “Melanoma pathology reporting and staging,” *Modern Pathology*, vol. 33, pp. 15–24, Jan. 2020, doi: 10.1038/s41379-019-0402-x.



- [104] L. E. Haydu *et al.*, “Conditional Survival: An Assessment of the Prognosis of Patients at Time Points After Initial Diagnosis and Treatment of Locoregional Melanoma Metastasis.,” *J Clin Oncol*, vol. 35, no. 15, pp. 1721–1729, May 2017, doi: 10.1200/JCO.2016.71.9393.
- [105] E. Z. Keung and J. E. Gershenwald, “The eighth edition American Joint Committee on Cancer (AJCC) melanoma staging system: implications for melanoma treatment and care,” *Expert Rev Anticancer Ther*, vol. 18, no. 8, pp. 775–784, Aug. 2018, doi: 10.1080/14737140.2018.1489246.
- [106] Brendan D. Curti and Mark B. Faries, “Recent advances in the treatment of melanoma.,” *The New England Journal of Medicine*, vol. 89, pp. 73–74, Feb. 2021, doi: 10.1056/NEJMra2034861.
- [107] S. Sood, R. Jayachandiran, and S. Pandey, “Current Advancements and Novel Strategies in the Treatment of Metastatic Melanoma,” *Integrative Cancer Therapies*, vol. 20. SAGE Publications Inc., 2021. doi: 10.1177/1534735421990078.
- [108] A. Villani, L. Potestio, G. Fabbrocini, G. Troncone, U. Malapelle, and M. Scalvenzi, “The Treatment of Advanced Melanoma: Therapeutic Update,” *International Journal of Molecular Sciences*, vol. 23, no. 12. MDPI, Jun. 01, 2022. doi: 10.3390/ijms23126388.
- [109] R. W. Jenkins and D. E. Fisher, “Treatment of Advanced Melanoma in 2020 and Beyond,” *Journal of Investigative Dermatology*, vol. 141, no. 1. Elsevier B.V., pp. 23–31, Jan. 01, 2021. doi: 10.1016/j.jid.2020.03.943.
- [110] M. Patel *et al.*, “Resistance to molecularly targeted therapies in melanoma,” *Cancers*, vol. 13, no. 5. MDPI AG, pp. 1–26, Mar. 01, 2021. doi: 10.3390/cancers13051115.
- [111] M. Karasarides *et al.*, “Hallmarks of Resistance to Immune-Checkpoint Inhibitors,” *Cancer Immunol Res*, vol. 10, no. 4, pp. 372–383, Apr. 2022, doi: 10.1158/2326-6066.CIR-20-0586.
- [112] H. Davies *et al.*, “Mutations of the BRAF gene in human cancer.,” *Nature*, vol. 417, no. 6892, pp. 949–54, Jun. 2002, doi: 10.1038/nature00766.
- [113] B. Switzer, I. Puzanov, J. J. Skitzki, L. Hamad, and M. S. Ernstoff, “Managing Metastatic Melanoma in 2022: A Clinical Review,” *JCO Oncol Pract*, vol. 18, pp. 335–351, 2022, doi: 10.1200/OP.21.
- [114] T. Randic, I. Kozar, C. Margue, J. Utikal, and S. Kreis, “NRAS mutant melanoma: Towards better therapies,” *Cancer Treatment Reviews*, vol. 99. W.B. Saunders Ltd, Sep. 01, 2021. doi: 10.1016/j.ctrv.2021.102238.
- [115] W. R. Montor, A. R. O. S. E. Salas, and F. H. M. de Melo, “Receptor tyrosine kinases and downstream pathways as druggable targets for cancer treatment: The current arsenal of inhibitors,” *Molecular Cancer*, vol. 17, no. 1. BioMed Central Ltd., Feb. 19, 2018. doi: 10.1186/s12943-018-0792-2.
- [116] S. Caksa, U. Baqai, and A. E. Aplin, “The future of targeted kinase inhibitors in melanoma,” *Pharmacology and Therapeutics*, vol. 239. Elsevier Inc., Nov. 01, 2022. doi: 10.1016/j.pharmthera.2022.108200.
- [117] A. M. Czarnecka, E. Bartnik, M. Fiedorowicz, and P. Rutkowski, “Targeted therapy in melanoma and mechanisms of resistance,” *International Journal of Molecular Sciences*, vol. 21, no. 13. MDPI AG, pp. 1–21, Jul. 01, 2020. doi: 10.3390/ijms21134576.
- [118] M. P. Smith and C. Wellbrock, “Molecular pathways: Maintaining MAPK inhibitor sensitivity by targeting nonmutational tolerance,” *Clinical Cancer Research*, vol. 22, no. 24, pp. 5966–5970, Dec. 2016, doi: 10.1158/1078-0432.CCR-16-0954.
- [119] S. Vafaei *et al.*, “Combination therapy with immune checkpoint inhibitors (ICIs); a new frontier,” *Cancer Cell International*, vol. 22, no. 1. BioMed Central Ltd, Jan. 01, 2022. doi: 10.1186/s12935-021-02407-8.
- [120] M. Morante, A. Pandiella, P. Crespo, and A. Herrero, “Immune Checkpoint Inhibitors and RAS–ERK Pathway-Targeted Drugs as Combined Therapy for the Treatment of Melanoma,” *Biomolecules*, vol. 12, no. 11. MDPI, Nov. 01, 2022. doi: 10.3390/biom12111562.

- [121] J. A. Marin-Acevedo, E. M. O. Kimbrough, and Y. Lou, "Next generation of immune checkpoint inhibitors and beyond," *Journal of Hematology and Oncology*, vol. 14, no. 1. BioMed Central Ltd, Dec. 01, 2021. doi: 10.1186/s13045-021-01056-8.
- [122] J. Larkin *et al.*, "Five-Year Survival with Combined Nivolumab and Ipilimumab in Advanced Melanoma," *New England Journal of Medicine*, vol. 381, no. 16, pp. 1535–1546, Oct. 2019, doi: 10.1056/nejmoa1910836.
- [123] S. Das and D. B. Johnson, "Immune-related adverse events and anti-tumor efficacy of immune checkpoint inhibitors," *Journal for ImmunoTherapy of Cancer*, vol. 7, no. 1. BioMed Central Ltd., Nov. 15, 2019. doi: 10.1186/s40425-019-0805-8.
- [124] S. M. Hossain *et al.*, "Innate immune checkpoint inhibitor resistance is associated with melanoma sub-types exhibiting invasive and de-differentiated gene expression signatures," *Front Immunol*, vol. 13, Sep. 2022, doi: 10.3389/fimmu.2022.955063.
- [125] S. Diazzi, S. Tartare-Deckert, and M. Deckert, "Bad neighborhood: Fibrotic stroma as a new player in melanoma resistance to targeted therapies," *Cancers*, vol. 12, no. 6. MDPI AG, Jun. 01, 2020. doi: 10.3390/cancers12061364.
- [126] S. Diazzi, S. Tartare-Deckert, and M. Deckert, "The mechanical phenotypic plasticity of melanoma cell: an emerging driver of therapy cross-resistance," *Oncogenesis*, vol. 12, no. 1. Springer Nature, Dec. 01, 2023. doi: 10.1038/s41389-023-00452-8.
- [127] M. Bidram *et al.*, "Mrna-based cancer vaccines: A therapeutic strategy for the treatment of melanoma patients," *Vaccines*, vol. 9, no. 10. MDPI, Oct. 01, 2021. doi: 10.3390/vaccines9101060.
- [128] J. B. Swann *et al.*, "Demonstration of inflammation-induced cancer and cancer immunoediting during primary tumorigenesis.," *Proc Natl Acad Sci U S A*, vol. 105, no. 2, pp. 652–6, Jan. 2008, doi: 10.1073/pnas.0708594105.
- [129] S. Rakoff-Nahoum and R. Medzhitov, "Regulation of spontaneous intestinal tumorigenesis through the adaptor protein MyD88.," *Science*, vol. 317, no. 5834, pp. 124–7, Jul. 2007, doi: 10.1126/science.1140488.
- [130] F. L. Robinson, A. W. Whitehurst, M. Raman, and M. H. Cobb, "Identification of novel point mutations in ERK2 that selectively disrupt binding to MEK1.," *J Biol Chem*, vol. 277, no. 17, pp. 14844–52, Apr. 2002, doi: 10.1074/jbc.M107776200.
- [131] S. Aida *et al.*, "MITF suppression improves the sensitivity of melanoma cells to a BRAF inhibitor," *Cancer Lett*, vol. 409, pp. 116–124, Nov. 2017, doi: 10.1016/j.canlet.2017.09.008.
- [132] L. E. Davis, S. C. Shalin, and A. J. Tackett, "Current state of melanoma diagnosis and treatment," *Cancer Biology and Therapy*, vol. 20, no. 11. Taylor and Francis Inc., pp. 1366–1379, Nov. 02, 2019. doi: 10.1080/15384047.2019.1640032.
- [133] Z. Apalla, D. Nashan, R. B. Weller, and X. Castellsagué, "Skin Cancer: Epidemiology, Disease Burden, Pathophysiology, Diagnosis, and Therapeutic Approaches," *Dermatology and Therapy*, vol. 7. Springer Healthcare, pp. 5–19, Jan. 01, 2017. doi: 10.1007/s13555-016-0165-y.
- [134] National Cancer Institute : [www.cancer.org](http://www.cancer.org), "Melanoma Treatment," <https://www.cancer.org/cancer/melanoma-skin-cancer/treating.html>.
- [135] A. Garcia-Alvarez, C. Ortiz, and E. Muñoz-Couselo, "Current perspectives and novel strategies of nras-mutant melanoma," *OncoTargets and Therapy*, vol. 14. Dove Medical Press Ltd, pp. 3709–3719, 2021. doi: 10.2147/OTT.S278095.
- [136] Z. J. Jaeger *et al.*, "Objective response to immune checkpoint inhibitor therapy in NRAS-mutant melanoma: A systematic review and meta-analysis," *Frontiers in Medicine*, vol. 10. Frontiers Media S.A., 2023. doi: 10.3389/fmed.2023.1090737.

- [137] L. Zhou *et al.*, “Association of NRAS Mutation With Clinical Outcomes of Anti-PD-1 Monotherapy in Advanced Melanoma: A Pooled Analysis of Four Asian Clinical Trials,” *Front Immunol*, vol. 12, Jul. 2021, doi: 10.3389/fimmu.2021.691032.
- [138] A. Vennepureddy, N. Thumallapally, V. M. Nehru, J.-P. Atallah, and T. Terjanian, “Novel Drugs and Combination Therapies for the Treatment of Metastatic Melanoma,” *J Clin Med Res*, vol. 8, no. 2, pp. 63–75, 2016, doi: 10.14740/jocmr2424w.
- [139] I. Márquez-Rodas *et al.*, “Immune checkpoint inhibitors: Therapeutic advances in melanoma,” *Annals of Translational Medicine*, vol. 3, no. 18. AME Publishing Company, Oct. 01, 2015. doi: 10.3978/j.issn.2305-5839.2015.10.27.
- [140] M. L. Hartman and M. Czyz, “MITF in melanoma: mechanisms behind its expression and activity,” *Cellular and Molecular Life Sciences*, pp. 1249–1260, 2015, doi: 10.1007/s00018-014-1791-0.
- [141] P. Cohen, D. Cross, and P. A. Jänne, “Kinase drug discovery 20 years after imatinib: progress and future directions,” *Nature Reviews Drug Discovery*, vol. 20, no. 7. Nature Research, pp. 551–569, Jul. 01, 2021. doi: 10.1038/s41573-021-00195-4.
- [142] P. B. Chapman *et al.*, “Vemurafenib in patients with BRAFV600 mutation-positive metastatic melanoma: Final overall survival results of the randomized BRIM-3 study,” *Annals of Oncology*, vol. 28, no. 10, pp. 2581–2587, Oct. 2017, doi: 10.1093/annonc/mdx339.
- [143] L. Dary Gutiérrez-Castañeda, J. A. Nova, J. D. Tovar-Parra, and F. L. Acosta, “Frequency of mutations in BRAF, NRAS, and KIT in different populations and histological subtypes of melanoma: a systemic review,” 2020, doi: 10.1097/CMR.0000000000000628.
- [144] A. M. Czarnecka, E. Bartnik, M. Fiedorowicz, and P. Rutkowski, “Targeted therapy in melanoma and mechanisms of resistance,” *International Journal of Molecular Sciences*, vol. 21, no. 13. MDPI AG, pp. 1–21, Jul. 01, 2020. doi: 10.3390/ijms21134576.
- [145] M. B. Atkins *et al.*, “The state of Melanoma: Emergent challenges and opportunities,” *Clinical Cancer Research*, vol. 27, no. 10, pp. 2678–2697, May 2021, doi: 10.1158/1078-0432.CCR-20-4092.
- [146] C. J. Hui Goh *et al.*, “Identification of pathways modulating vemurafenib resistance in melanoma cells via a genome-wide CRISPR/Cas9 screen,” *G3: Genes, Genomes, Genetics*, vol. 11, no. 2, Feb. 2021, doi: 10.1093/g3journal/jkaa069.
- [147] I. Proietti *et al.*, “Mechanisms of acquired BRAF inhibitor resistance in melanoma: A systematic review,” *Cancers*, vol. 12, no. 10. MDPI AG, pp. 1–29, Oct. 01, 2020. doi: 10.3390/cancers12102801.
- [148] H. Zecena *et al.*, “Systems biology analysis of mitogen activated protein kinase inhibitor resistance in malignant melanoma,” *BMC Syst Biol*, vol. 12, no. 1, Apr. 2018, doi: 10.1186/s12918-018-0554-1.
- [149] S. Y. Lim, A. M. Menzies, and H. Rizos, “Mechanisms and strategies to overcome resistance to molecularly targeted therapy for melanoma,” *Cancer*, vol. 123. John Wiley and Sons Inc., pp. 2118–2129, Jun. 01, 2017. doi: 10.1002/cncr.30435.
- [150] V. E. Wang *et al.*, “Adaptive Resistance to Dual BRAF/MEK Inhibition in BRAF-Driven Tumors through Autocrine FGFR Pathway Activation.,” *Clin Cancer Res*, vol. 25, no. 23, pp. 7202–7217, Dec. 2019, doi: 10.1158/1078-0432.CCR-18-2779.
- [151] N. Selvarajoo and J. Stanslas, “Assessment of Growth Inhibitory, Cell Cycle Arrest, and Apoptosis Inducing Potential of RAS-MAPK Inhibitors in Gemcitabine-Sensitive Pancreatic Cancer Cells,” *Front Pharmacol*, vol. 9, 2018, doi: 10.3389/conf.fphar.2018.63.00145.
- [152] A. X. Toress-Collado, R. Nazarian, and A. R. Jazirehi, “Rescue of cell cycle progression in BRAFV600E inhibitor-resistant human melanoma by a chromatin modifier.,” *Tumour Biol*, vol. 39, no. 9, p. 1010428317721620, Sep. 2017, doi: 10.1177/1010428317721620.
- [153] S. Haferkamp *et al.*, “Vemurafenib induces senescence features in melanoma cells,” *Journal of Investigative Dermatology*, vol. 133, no. 6, pp. 1601–1609, 2013, doi: 10.1038/jid.2013.6.

- [154] S. A. Luebker and S. A. Koepsell, "Diverse mechanisms of BRAF inhibitor resistance in melanoma identified in clinical and preclinical studies," *Frontiers in Oncology*, vol. 9, no. MAR. Frontiers Media S.A., 2019. doi: 10.3389/fonc.2019.00268.
- [155] Á. P. Hernández *et al.*, "Restoring the immunity in the tumor microenvironment: Insights into immunogenic cell death in onco-therapies," *Cancers*, vol. 13, no. 11. MDPI AG, Jun. 01, 2021. doi: 10.3390/cancers13112821.
- [156] Y. Fang *et al.*, "Pyroptosis: A new frontier in cancer," *Biomedicine & Pharmacotherapy*, vol. 121, p. 109595, Jan. 2020, doi: 10.1016/J.BIOPHA.2019.109595.
- [157] H. Lu *et al.*, "Recent advances in the development of protein–protein interactions modulators: mechanisms and clinical trials," *Signal Transduction and Targeted Therapy*, vol. 5, no. 1. Springer Nature, Dec. 01, 2020. doi: 10.1038/s41392-020-00315-3.
- [158] T. Maculins *et al.*, "Discovery of Protein-Protein Interaction Inhibitors by Integrating Protein Engineering and Chemical Screening Platforms," *Cell Chem Biol*, vol. 27, no. 11, pp. 1441-1451.e7, Nov. 2020, doi: 10.1016/j.chembiol.2020.07.010.
- [159] A. P. Higuero, H. Jubb, and T. L. Blundell, "Protein-protein interactions as druggable targets: Recent technological advances," *Current Opinion in Pharmacology*, vol. 13, no. 5. Elsevier Ltd, pp. 791–796, 2013. doi: 10.1016/j.coph.2013.05.009.
- [160] L. Haas *et al.*, "Acquired resistance to anti-MAPK targeted therapy confers an immune-evasive tumor microenvironment and cross-resistance to immunotherapy in melanoma," *Nat Cancer*, vol. 2, no. 7, pp. 693–708, Jul. 2021, doi: 10.1038/s43018-021-00221-9.
- [161] A. L. Furfaro *et al.*, "HO-1 downregulation favors BRAF V600 melanoma cell death induced by Vemurafenib/PLX4032 and increases NK recognition," *Int J Cancer*, vol. 146, no. 7, pp. 1950–1962, Apr. 2020, doi: 10.1002/ijc.32611.
- [162] S. Haferkamp *et al.*, "Vemurafenib Induces Senescence Features in Melanoma Cells," *Journal of Investigative Dermatology*, vol. 133, no. 6, pp. 1601–1609, Jun. 2013, doi: 10.1038/jid.2013.6.
- [163] G. Jelena, S.-R. Tatjana, F. S. Juan, P. Marijana, Č. Milena, and R. Siniša, "Telmisartan induces melanoma cell apoptosis and synergizes with vemurafenib *in vitro* by altering cell bioenergetics," *Cancer Biol Med*, vol. 16, no. 2, p. 247, 2019, doi: 10.20892/j.issn.2095-3941.2018.0375.
- [164] D. Bauer, F. Werth, H. A. Nguyen, F. Kiecker, and J. Eberle, "Critical role of reactive oxygen species (ROS) for synergistic enhancement of apoptosis by vemurafenib and the potassium channel inhibitor TRAM-34 in melanoma cells," *Cell Death Dis*, vol. 8, no. 2, pp. e2594–e2594, Feb. 2017, doi: 10.1038/cddis.2017.6.
- [165] J. Peh, T. M. Fan, K. L. Wycislo, H. S. Roth, and P. J. Hergenrother, "The Combination of Vemurafenib and Pro-caspase-3 Activation Is Synergistic in Mutant BRAF Melanomas.," *Mol Cancer Ther*, vol. 15, no. 8, pp. 1859–69, Aug. 2016, doi: 10.1158/1535-7163.MCT-16-0025.
- [166] P. Uehuei *et al.*, "ACY-1215 accelerates vemurafenib induced cell death of BRAF-mutant melanoma cells via induction of ER stress and inhibition of ERK activation," *Oncol Rep*, vol. 37, no. 2, pp. 1270–1276, Feb. 2017, doi: 10.3892/or.2016.5340.
- [167] L. Lin, D. Ding, Y. Jiang, Y. Li, and S. Li, "MEK inhibitors induce apoptosis via FoxO3a-dependent PUMA induction in colorectal cancer cells.," *Oncogenesis*, vol. 7, no. 9, p. 67, Sep. 2018, doi: 10.1038/s41389-018-0078-y.
- [168] C. Gianna Hoffman-Luca *et al.*, "Elucidation of acquired resistance to Bcl-2 and MDM2 inhibitors in acute Leukemia in Vitro and in Vivo," *Clinical Cancer Research*, vol. 21, no. 11, pp. 2558–2568, Jun. 2015, doi: 10.1158/1078-0432.CCR-14-2506.
- [169] M. Winder and A. Virós, "Mechanisms of Drug Resistance in Melanoma.," *Handb Exp Pharmacol*, vol. 249, pp. 91–108, 2018, doi: 10.1007/164\_2017\_17.

- [170] L. Croce, F. Coperchini, F. Magri, L. Chiovato, and M. Rotondi, "The multifaceted anti-cancer effects of BRAF-inhibitors The wild type BRAF gene," *Oncotarget*, vol. 10, no. 61, pp. 6623–6640, 2019, [Online]. Available: [www.oncotarget.com](http://www.oncotarget.com)
- [171] F. Coperchini *et al.*, "The BRAF-inhibitor PLX4720 inhibits CXCL8 secretion in BRAFV600E mutated and normal thyroid cells: a further anti-cancer effect of BRAF-inhibitors," *Sci Rep*, vol. 9, no. 1, Dec. 2019, doi: 10.1038/s41598-019-40818-w.
- [172] A. Showalter *et al.*, "Cytokines in immunogenic cell death: Applications for cancer immunotherapy," *Cytokine*, vol. 97, Academic Press, pp. 123–132, Sep. 01, 2017. doi: 10.1016/j.cyto.2017.05.024.
- [173] A. Q. Sukkurwala *et al.*, "Immunogenic calreticulin exposure occurs through a phylogenetically conserved stress pathway involving the chemokine CXCL8," *Cell Death Differ*, vol. 21, no. 1, pp. 59–68, Jan. 2014, doi: 10.1038/cdd.2013.73.
- [174] M. Kuske *et al.*, "Immunomodulatory effects of BRAF and MEK inhibitors: Implications for Melanoma therapy," *Pharmacological Research*, vol. 136, Academic Press, pp. 151–159, Oct. 01, 2018. doi: 10.1016/j.phrs.2018.08.019.
- [175] D. Wang *et al.*, "Immunogenic chemotherapy effectively inhibits KRAS-Driven lung cancer," *Cancer Lett*, vol. 492, pp. 31–43, Nov. 2020, doi: 10.1016/J.CANLET.2020.07.043.
- [176] J. Xu, Y. Xiong, Z. Xu, H. Xing, L. Zhou, and X. Zhang, "From targeted therapy to a novel way: Immunogenic cell death in lung cancer," *Front Med (Lausanne)*, vol. 9, Dec. 2022, doi: 10.3389/fmed.2022.1102550.
- [177] A. Petrazzuolo, M. Perez-Lanzon, P. Liu, M. C. Maiuri, and G. Kroemer, "Crizotinib and ceritinib trigger immunogenic cell death via on-target effects," *Oncoimmunology*, vol. 10, no. 1, Jan. 2021, doi: 10.1080/2162402X.2021.1973197.
- [178] J. Zhou, Q. Yang, L. Lu, Z. Tuo, Z. Shou, and J. Cheng, "PLK1 Inhibition Induces Immunogenic Cell Death and Enhances Immunity against NSCLC.," *Int J Med Sci*, vol. 18, no. 15, pp. 3516–3525, 2021, doi: 10.7150/ijms.60135.
- [179] B. L. Rapoport and R. Anderson, "Realizing the clinical potential of immunogenic cell death in cancer chemotherapy and radiotherapy," *International Journal of Molecular Sciences*, vol. 20, no. 4, MDPI AG, Feb. 02, 2019. doi: 10.3390/ijms20040959.
- [180] P. K. Bommareddy, S. Aspromonte, A. Zloza, S. D. Rabkin, and H. L. Kaufman, "MEK inhibition enhances oncolytic virus immunotherapy through increased tumor cell killing and T cell activation," *Sci Transl Med*, vol. 10, no. 471, Dec. 2018, doi: 10.1126/scitranslmed.aau0417.
- [181] D. A. Erkes *et al.*, "Mutant BRAF and MEK inhibitors regulate the tumor immune microenvironment via pyroptosis," *Cancer Discov*, vol. 10, no. 2, pp. 255–269, Feb. 2020, doi: 10.1158/2159-8290.CD-19-0672.
- [182] R. Ahn and J. Ursini-Siegel, "Clinical potential of kinase inhibitors in combination with immune checkpoint inhibitors for the treatment of solid tumors," *International Journal of Molecular Sciences*, vol. 22, no. 5, MDPI AG, pp. 1–23, Mar. 01, 2021. doi: 10.3390/ijms22052608.
- [183] A. Kulkarni, S. K. Natarajan, V. Chandrasekar, P. R. Pandey, and S. Sengupta, "Combining Immune Checkpoint Inhibitors and Kinase-Inhibiting Supramolecular Therapeutics for Enhanced Anticancer Efficacy.," *ACS Nano*, vol. 10, no. 10, pp. 9227–9242, Oct. 2016, doi: 10.1021/acs.nano.6b01600.
- [184] S. Vafaei *et al.*, "Combination therapy with immune checkpoint inhibitors (ICIs); a new frontier," *Cancer Cell International*, vol. 22, no. 1, BioMed Central Ltd, Jan. 01, 2022. doi: 10.1186/s12935-021-02407-8.
- [185] W. Fu and G. Ma, "Significance of immunogenic cell death-related genes in prognosis prediction and immune microenvironment landscape of patients with cutaneous melanoma," *Front Genet*, vol. 13, Sep. 2022, doi: 10.3389/fgene.2022.988821.

- [186] R. Rosa, F. Monteleone, N. Zambrano, and R. Bianco, "In Vitro and In Vivo Models for Analysis of Resistance to Anticancer Molecular Therapies," *Curr Med Chem*, vol. 21, pp. 1595–1606, 2014, [Online]. Available: [www.broadinstitute.org/ccle](http://www.broadinstitute.org/ccle)
- [187] M. Denis *et al.*, "In Vivo Syngeneic Tumor Models with Acquired Resistance to Anti-PD-1/PD-L1 Therapies," *Cancer Immunol Res*, vol. 10, no. 8, pp. 1013–1027, Aug. 2022, doi: 10.1158/2326-6066.CIR-21-0802.
- [188] P. Bastola, L. Neums, F. J. Schoenen, and J. Chien, "VCP inhibitors induce endoplasmic reticulum stress, cause cell cycle arrest, trigger caspase-mediated cell death and synergistically kill ovarian cancer cells in combination with Salubrinal.," *Mol Oncol*, vol. 10, no. 10, pp. 1559–1574, Dec. 2016, doi: 10.1016/j.molonc.2016.09.005.
- [189] T. G. Boulton *et al.*, "ERKs: a family of protein-serine/threonine kinases that are activated and tyrosine phosphorylated in response to insulin and NGF.," *Cell*, vol. 65, no. 4, pp. 663–75, May 1991, doi: 10.1016/0092-8674(91)90098-j.
- [190] C. Wang *et al.*, "Extracellular signal-regulated kinases associate with and phosphorylate DHPS to promote cell proliferation," *Oncogenesis*, vol. 9, no. 9, Sep. 2020, doi: 10.1038/s41389-020-00271-1.
- [191] T. S. Kaoud *et al.*, "Modulating multi-functional ERK complexes by covalent targeting of a recruitment site in vivo," *Nat Commun*, vol. 10, no. 1, Dec. 2019, doi: 10.1038/s41467-019-12996-8.
- [192] C. N. Hancock, A. Macias, E. K. Lee, S. Y. Yu, A. D. Mackerell, and P. Shapiro, "Identification of novel extracellular signal-regulated kinase docking domain inhibitors.," *J Med Chem*, vol. 48, no. 14, pp. 4586–95, Jul. 2005, doi: 10.1021/jm0501174.
- [193] R. García-Gómez, X. R. Bustelo, and P. Crespo, "Protein–Protein Interactions: Emerging Oncotargets in the RAS-ERK Pathway," *Trends in Cancer*, vol. 4, no. 9. Cell Press, pp. 616–633, Sep. 01, 2018. doi: 10.1016/j.trecan.2018.07.002.
- [194] P. P. Roux, S. A. Richards, and J. Blenis, "Phosphorylation of p90 ribosomal S6 kinase (RSK) regulates extracellular signal-regulated kinase docking and RSK activity.," *Mol Cell Biol*, vol. 23, no. 14, pp. 4796–804, Jul. 2003, doi: 10.1128/MCB.23.14.4796-4804.2003.
- [195] S. Vetterkind, R. H. Poythress, Q. Q. Lin, and K. G. Morgan, "Hierarchical scaffolding of an ERK1/2 activation pathway," *Cell Communication and Signaling*, vol. 11, no. 1, 2013, doi: 10.1186/1478-811X-11-65.
- [196] J. A. Smith, C. E. Poteet-Smith, K. Malarkey, and T. W. Sturgill, "Identification of an extracellular signal-regulated kinase (ERK) docking site in ribosomal S6 kinase, a sequence critical for activation by ERK in vivo," *Journal of Biological Chemistry*, vol. 274, no. 5, pp. 2893–2898, Jan. 1999, doi: 10.1074/jbc.274.5.2893.
- [197] M. McCormick *et al.*, "Distinct signalling particles containing ERK/MEK and B-Raf in PC12 cells," *Biochem. J*, vol. 387, pp. 155–164, 2005.
- [198] A. S. Futran, A. J. Link, R. Seger, and S. Y. Shvartsman, "ERK as a model for systems biology of enzyme kinetics in cells," *Current Biology*, vol. 23, no. 21. Nov. 04, 2013. doi: 10.1016/j.cub.2013.09.033.
- [199] F. L. Robinson, A. W. Whitehurst, M. Raman, and M. H. Cobb, "Identification of novel point mutations in ERK2 that selectively disrupt binding to MEK1.," *J Biol Chem*, vol. 277, no. 17, pp. 14844–52, Apr. 2002, doi: 10.1074/jbc.M107776200.
- [200] A. M. Kidger and S. J. Cook, "De-RSKing ERK – regulation of ERK1/2-RSK dissociation by phosphorylation within a disordered motif," *FEBS Journal*, vol. 285, no. 1. Blackwell Publishing Ltd, pp. 42–45, Jan. 01, 2018. doi: 10.1111/febs.14344.